

Rugby Union Scrum Physics

Benjamin Lallemand

▶ **To cite this version:**

Benjamin Lallemand. Rugby Union Scrum Physics. Solid mechanics [physics.class-ph]. Institut Polytechnique de Paris, 2022. English. ⟨NNT : 2022IPPAX090⟩. ⟨tel-04105570⟩

HAL Id: tel-04105570

https://theses.hal.science/tel-04105570v1

Submitted on 24 May 2023

HAL is a multi-disciplinary open access archive for the deposit and dissemination of scientific research documents, whether they are published or not. The documents may come from teaching and research institutions in France or abroad, or from public or private research centers.

L'archive ouverte pluridisciplinaire **HAL**, est destinée au dépôt et à la diffusion de documents scientifiques de niveau recherche, publiés ou non, émanant des établissements d'enseignement et de recherche français ou étrangers, des laboratoires publics ou privés.



HAL Authorization

INSTITUT POLYTECHNIQUE DE PARIS

NNT : 2022IPPAX090

Thèse de doctorat

Physique de la mêlée

Thèse de doctorat de l'Institut Polytechnique de Paris
préparée à École polytechnique

École doctorale n°626 École doctorale de l'Institut Polytechnique de Paris (EDIPP)
Spécialité de doctorat : Mécanique des fluides et des solides

Thèse présentée et soutenue à Palaiseau, le 19 Octobre 2022, par

MONSIEUR BENJAMIN LALLEMAND

Composition du Jury :

Jean-Christophe Géminard Directeur de Recherche, ENS de Lyon (Laboratoire de Physique)	Président et rapporteur
Ezio Preatoni FHEA Senior Lecturer, University of Bath (Department for Health)	Rapporteur
Frédérique Hintzi Professeure associée, Université Savoie Mont-Blanc (LIBM)	Examinatrice
Jean Boisson Professeur Assistant, ENSTA Paris (Unité de Mécanique)	Examinateur
Christophe Clanet Directeur de Recherche, École polytechnique (LadHyX)	Directeur de thèse
Caroline Cohen Professeure Assistante, École polytechnique (LadHyX)	Directrice de thèse
Sylvain Blanchard Directeur Médical et Scientifique, Racing 92	Invité

Abstract

The scrum is a key element of a Rugby Union game. It consists of the ball being put back into play in opposition of strength between two packs of 8 forwards each. Each pack is organized in a 3-4-1 configuration with the three players of the first row in direct contact with the opponents, the two players of the second row that push behind the first row and the three players of the third row who complete the configuration. The scrum is orchestrated by the referee's calls which have changed over the history of Rugby to protect the physical integrity of the players. We can divide the scrum into two distinct phases in force production: an impact phase during which each pack accelerates and collides with the other, followed by a continuous pushing phase after the throw-in of the ball under the scrum. During the sustained push phase, the players of each pack try to synchronize to produce the greatest collective force. This thesis, financed by the professional rugby club of Racing 92, focuses on these two phases with experimental studies conducted at the individual level in order to understand the mechanisms of force production. First, using a scrum training machine equipped with force sensors called the "Atelier de la mêlée" and belonging to the French Federation of Rugby, we characterize individual players in order to construct a pusher phase space that allows us to quantify the quality of a scrum impact. Then, thanks to an individual scrum machine that we developed in the laboratory -also equipped with force sensors- we conducted experimental studies to find the individual scrummaging posture that maximizes the force produced by a player. We have also led a study that looks at the influence of the size of the cleats under the shoes on the force produced by a player on synthetic turf. Finally, we study the scrum at the collective scale to understand the mechanisms of force transmission in a professional pack thanks to the "Atelier de la mêlée". The objective is to improve the performance in scrums through the identification of physical variables translating the synchronization of a pack and its efficiency of pushing.

Résumé Substantiel

Le Rugby à XV est un sport d'affrontement entre deux équipes de 15 joueurs ou joueuses dans lequel il faut essayer de marquer le plus de points possibles. Lorsqu'une passe en avant intervient dans le jeu, le ballon est remis en jeu sous la forme d'une épreuve appelée la mêlée. La mêlée est une opposition de force entre deux packs de 8 joueurs, appelés les avants, qui cherchent à gagner ou à garder la possession du ballon. L'organisation du pack se fait en 3 rangées avec 3 joueurs en première ligne, 4 joueurs derrière eux en seconde ligne et un dernier joueur en troisième ligne. La mêlée est orchestrée par les commandements de l'arbitre qui ont changé au fil de ces vingt dernières années dans le but de protéger l'intégrité physique des joueurs qui devenaient de plus en plus athlétiques et massifs.
Après une phase de préparation, les joueurs s'arc-boutent à l'entente du commandement "Flexion", puis ils se lient au pack adverse après le commandement "Liez", pour enfin impacter le pack adverse à l'entente du commandement "Jeu".
En terme de production de force d'un pack, ce dernier commandement correspond à une première phase d'impact pendant laquelle chaque pack accélère et entre en collision avec l'autre, qui est ensuite suivie par une seconde phase de poussée continue intervenant après l'introduction du ballon sous l'édifice par le demi de mêlée.
Dans ce manuscrit, nous nous intéressons d'abord à la phase d'impact sous la forme d'une étude expérimentale menée sur une machine d'entraînement à la mêlée équipée de capteurs de force appartenant à la Fédération Française de Rugby et qui s'appelle l'Atelier de la mêlée. Nous avons caractérisé l'impact des joueurs en analysant les signaux de force mesurés à l'Atelier de la mêlée avec des joueurs professionnels du Racing 92 ainsi qu'avec un sujet non-pratiquant de l'activité Rugby. Les joueurs professionnels obtiennent des forces à l'impact plus élevées pour des vitesses équivalentes à celles du non-pratiquant et ils ont des qualités de gainage plus importantes, notamment au niveau des cervicales qui semblent être un point crucial de la protection des joueurs à l'impact.

Ensuite, nous étudions la phase de poussée continue grâce à un joug individuel que nous avons construit directement au laboratoire. Une première étude se concentre sur les angles optimaux permettant de maximiser les forces produites par un joueur en position de mêlée avec un support métallique au niveau des pieds. L'expérience réalisée sur deux joueurs espoirs du Racing 92 nous a montré que les deux joueurs obtenaient des forces maximales développées pour des angles de genoux autour de 130° et des angles de hanche de 150° dans le plan sagittal.
Dans une seconde étude, nous avons construit un gazon synthétique dans le laboratoire afin d'effectuer une nouvelle étude sur la position optimale de poussée avec des sujets portant des chaussures à crampons. En variant la distance entre leurs épaules et leurs pieds ainsi que la hauteur de poussée, nous mesurons les forces horizontales et verticales. Ainsi, nous expliquons l'importance de la force passive liée au poids dans les positions étendues (genou et hanche proches de la flexion) et nous montrons qu'il existe une élongation optimale pour la force active isométrique liée à l'activation des muscles.
Enfin, nous étudions l'influence de la taille des crampons sur les forces produites dans différentes postures et sur la position optimale de poussée. Pour le sujet étudié, plus la taille des crampons est longue, plus la position optimale est obtenue pour des épaules proches du sol et plus la force maximale horizontale développée est grande.

Finalement, nous finissons par étudier des problématiques à l'échelle collective. Nous avons conduit des expériences avec les joueurs professionnels du Racing 92 à l'Atelier de la mêlée afin de comprendre les mécanismes de transmission des forces dans un pack. L'objectif sportif étant d'améliorer les performances en mêlée grâce à l'identification des variables physiques traduisant la synchronisation d'un pack et son efficacité de poussée. Nous proposons un protocole expérimental supplémentaire dans lequel l'Atelier de la mêlée n'est plus passif lorsque les joueurs produisent leurs forces. Nous imposons des mouvements aux joueurs grâce à cette machine et ces déplacements sont représentatifs de déplacements caractéristiques directement mesurés sur des mêlées réelles. Cette dernière proposition permet un type d'expérience où les effets dynamiques sont présents et peut permettre de se rapprocher d'une situation de mêlée réelle.

Remerciements

Je veux commencer par remercier chaleureusement tous les membres du jury qui sont venus assister à ma soutenance. Ce fût une journée riche en émotions (et en salle d'attente virtuelle) où j'ai pu apprécier les multiples discussions que nous avons eu. Un grand merci aux rapporteurs Jean-Christophe et Ezio d'avoir relu, commenté, et discuté mon travail. A special thanks to Ezio who crossed the English Channel to listen to me speak in French for 45 minutes. Merci à Frédérique et Jean pour les échanges qui ont permis de mettre en perspective le travail en fonction des différents champs disciplinaires qu'il touche.

Merci à mes encadrants et encadrante qui ont supervisé cette thèse pendant ces trois années de doctorat.
Merci à toi Sylvain, pour avoir initié le travail de collaboration avec le LadHyX, et avoir participé à ma soutenance de thèse. La première moitié de ma thèse m'a permis de m'intégrer au sein du staff avec une position particulière et un nombre de surnoms incalculables. J'ai une pensée aussi pour Quentin, tu m'as permis de continuer à développer mon travail, toujours dans une bonne ambiance.
Merci à Caro, toujours une oreille pour discuter de sciences et autres. Grâce à toi, les moments les plus tortueux de la thèse sont passés plus facilement. Je resterai impressionné ton art de faire des manips aux résultats impressionnants avec deux bouts de ficelles et un capteur Futek.
Et enfin, merci à Christophe. En réfléchissant 5 minutes, vous avez le don de trouver toujours plus d'idées que moi en deux mois au début, et en deux semaines à la fin de la thèse. Merci pour la transmission de LA méthode et surtout, surtout, pour m'avoir expliquer une (ou deux fois) les règles de la belote et de Camel Up.

Ces trois années de doctorat se sont déroulées entre deux maisons: le Racing et le LadHyX. Deux maisons différentes qui ont fait de ces années une expérience innatendue et inoubliable. Tout d'abord, je remercie le Racing 92 pour m'avoir donné l'opportunité de faire ce travail original dans un monde que je ne connaissais pas de l'intérieur et que je suis heureux d'avoir rencontré.
Je remercie le Président, l'ensemble du staff, l'ensemble de l'équipe administrative qui fait tourner le club, et les joueurs. Le communiste, le ballon, la ventouse, Beji, Doyouwantacoffe ou encore l'homme bâton: je ne sais quel surnom retenir de toutes ces années passées.
Plus particulièrement, je remercie Laurent Travers pour les différents échanges qui nous ont permis de traduire ces travaux en réalités de terrain.
Un chaleureux merci à Pato, Philippe, et Dimitri.
Je profite de ce moment pour remercier la Fédération Française de Rugby et son pôle d'accompagnement à la performance. Grâce à Julien Piscione, Olivier Chaplain et Didier Retière nous avons eu le privilège d'effectuer des expériences de haut niveau avec les joueurs du Racing. Un grand merci pour l'accès à l'Atelier de la mêlée et pour les différents échanges qui ont fait avancer le travail.
Je tiens à remercier tous les joueurs du Racing qui ont pris part à des discussions et/ou des expériences (ou juste qui me chambraient). Ainsi, je remercie particulièrement Cedate, Donnacha, Jon, Fabien, Abel, GH, Gia, Guram, Luka, Teddy.
Puis, j'ai une pensée pour Teddy B., Romain, Jeanne, Alexandre, Franky, Hadj, Marco, Romain (aka le sanglier), Augustin, Lucile, Clément.
Un merci particulier au kinés et aux analystes vidéos: Antho, Damien, Pierre, Patrice et Baptiste.
Merci à Judith sans qui l'intégration au sein du Racing 92 n'aurait pas été la même. Enfin,

merci à l'équipe des préparateurs physiques qui m'ont accueilli sur leurs coins de bureaux pendant trois ans. Merci d'avoir écouté (subi) mes questionnements autour de la poussée en mêlée qui étaient souvent accompagnés d'hommes bâtons. Les anciens du gaz Michel et Gilbert, et les plus jeunes. Merci Fabien pour mes lombaires quand je piquais ton bureau et cette sortie vélo que j'attend toujours. Et enfin, un gros merci aux deux poulaches, avec qui on a pas révolutionné le rugby ou la matière noire, mais au moins on s'est bien marré. Merci à Briac, mon maître de stage et sacré zig. On aura rien compris aux GPS, mais on aura bien rigolé. Et enfin merci à Antoine, avec qui j'ai partagé l'aventure de la thèse (sauf que moi je n'avais pas multiple casquette). Merci de m'avoir donné l'occasion de crier "GoPro, enregistrer vidéo" et pour toutes ces séances de muscu (j'ai peut-être menti sur une partie ici).

Ensuite, merci à la maison du LadHyX avec presque 4 années passées. Je pars avec l'impression d'avoir fait partie des meubles de ce laboratoire. Un grand merci à tous les chercheurs et toutes les chercheuses, les ITA, les post-docs et les doctorantes et doctorants (comme ça personne n'est oublié).
Merci à Blaise, Sophie, Gabriel, Arezki, Lutz, Julie, Christophe, Avin, Julien pour toutes ces discussions autour d'un café. Merci pour l'aide précieuse et inestimable de Toaï (merci pour la passion mac), Daniel (merci pour les séries), Caro (merci pour l'arduino et la motivation) et Antoine (merci pour l'ovalie et les soudures de qualité). Un grand merci pour la gestion indispensable de Delphine, Sandrine, Magdalena, Patricia et Mélanie.
Merci à Tom le roi du baseball pour me permettre de garder des amis de droite. On se revoit à la fête de l'Huma. Merci à Pierre, l'ami des gouttes sur les fibres (une fois), avec qui j'ai partagé toutes ces années de thèse (ou de doctorat, j'ai déjà oublié ce qu'il fallait dire). Une pensée pour Mathilde, Nikhil, Kévin, Clara, Sara, Antoine, Rodolphe, Samy, Jérôme, Cécilia, Salma, Taha, Ursy, Francisco, Claire, Pierre Antoine, Valentin, Hassan, Rishabh, Prathmesh, Aude, Iman et tous les autres!
J'aimerais finir par remercier les physiciennes et physiciens du sport. L'ancienne génération du préfa, avec notamment Tom et Pierre (pas vraiment un physicien du sport mais ça passe), merci de nous avoir accueilli. Un merci particulier à Thibault sans qui je ne serais pas en train d'écrire ces remerciements. Puis, un grand merci aux trois stagiaires que j'ai eu la chance d'encadrer lors de leur premier passage dans le monde de la recherche: Awa, Baptiste et Simon.
Je souhaite un bon courage à la future génération (que j'embêterai à chacune des soutenances à venir). Je n'oublie pas Hector (cette fois) pour tout ces moments passés au préfa. Je souhaite bon courage à Thomas pour succéder à Charlie (et merci pour les essais très solides). Merci à Alice pour les précieux essais (et ce legging de chat). Ils auront pas sauver la planète, mais on aura bien rigolé. Merci au grande jugador Daniel (aka Le rouge, aka l'Argentino vero) pour toutes ces discussions passionnées de sciences (et surtout autres, sacré estafador).
Et enfin, je finis par remercier les compagnons et compagnonne de préfa de longue date. Merci Antoine (et surtout bravo) d'avoir supporté les choix musicaux de Charlie et Juliette (et d'avoir supporté le niveau de ski de Daniel aussi). Merci à mon voisin de tablée Charlie pour toutes ces heures partagées à refaire le monde sans dioxyde de carbone, à regarder des arrivées du Tour du Turkménistan, à admirer les jantes de nonante tout en étant concentréééé et bien sûr à se délecter de joyaux musicaux en bande organisée. Et enfin, merci à Juliette pour ces 4 annnées de longs brainstormings dans le préfa. Malgré tes goûts musicaux douteux (chacun son tour), les moments de manip et d'anlyse matlab intense resteront gravés dans ma mémoire (alors que rien ne marche jamais). Merci pour les trajets de l'ambiance, les astuces de manip, les pots à crayon 3D et chapeau pour ta thèse!

Après avoir remercier les collègues (surtout amies et amis), je tiens à remercier ici toutes les personnes croisées pendant ces quatre années qui m'ont permis - que ce soit l'espace de 5 secondes ou de journées entières- de penser à autre chose que ce travail. Je tiens ainsi à remercier toute la bande rencontrée pendant mon stage de M2 dans les résidences de l'X.
Un grand merci à la team des potes de prépa pour ces matchs incroyables et ces escapades nocturnes sur les plages du littoral Atlantique.
Merci aux musiciennes et musiciens rencontrés lors des soirées musicales parisiennes. Special thanks to the one and only Adeola, it is only the beginning.
Merci à Marie d'être venu tout droit de Lyon pour me voir parler de ton club de cœur. Merci à Louise pour ces innombrables fous rires et cette raclette (que j'attends toujours). Merci à Simon pour la chasse mémorable aux hyménoptères (et pour ton accent). Merci à Gatien pour toutes ces sorties vélo qui furent mes respirations du week-end (et surtour merci de m'avoir attendu). Merci à Lisa pour tous ces retours en bus à refaire le monde. Merci à Justine d'avoir été présente à la soutenance, je n'ai même pas envie de calculer les années qui se sont écoulées depuis qu'on se connait (ça rajeunit pas cette affaire).
Un grand merci aux colocataires qui ont survécu à la vie partagée avec un specimen comme le mien. Des bisous à Juliette, Olivia (et Thomas, colocataire de confinement) et Cindy. Et un merci à Simon pour toutes ces années de partage d'habitation, pour tes skills de maître maki et de constructeur de meuble en bois.
Deux familles de cœurs à remercier ensuite. Merci à la team de l'ENS de Lyon d'avoir partagé ces innombrables bières, repas, soirées, cours et encore repas. Merci à Léa de m'avoir hébergé des mois quand la thèse n'était pas encore lancée. Merci à Gab et Al pour les escapades lyonnaises des fêtes des lumières et ces parties de Mario Kart que vous me laissez probablement gagner. Merci à Alice pour tous les repas (plus légers que ceux d'Ulysse), les semaines au ski (où là les repas étaient moins légers pour le coup), les matchs de hand à Lyon (où je faisais semblant de servir à quelque chose sur votre banc) et surtout pour ce super film coréen où j'ai toujours rien compris de ce qu'il se passait. Merci à Joan pour tous ces instants de musiques et surtout de me montrer jour après jour que je reste un gauchiste de canapé. Merci enfin à Ulysse pour toutes tes réponses rapides, tes repas légers, tes 456 tonnes de houmous consommées en 7 ans et ces articles du Monde que je continuerai à te demander. Merci enfin à Docteur Romain pour tes cocktails toujours bien dosés, ton sens de la formule (j'ai pas encore tout compris ceci dit), pour nous avoir fait goûter une petite poire avec papy, pour tes découvertes musicales électro-chill et pour ces soirées à refaire le monde avec du rhum et un semblant de citron.
Merci à la seconde famille nantaise pour toutes ces années d'apéro, de soirées, de vacances et surtout de bêtises. Une bien belle rôtisserie que nous formons, même si on commence à se faire vieilles et vieux maintenant (je ne vous cite pas toutes et tous, sinon on y est dans 24 pages encore). Des bisous particuliers à Simon, tu m'as fait rencontrer ces énergumènes, et Flore, la pro de Linkedin. Une bise particulière à la partie du groupe exilée en Ile-de-France. Merci à Soso et Loulas pour les sorties vélos et votre aide pendant toutes ces années. Loulas, n'hésites pas si tu veux de l'aide pour appliquer le prochain article de JB Morin. Et merci à celles et ceux qui ont pu être là le jour J: Lisa, Margaux, Fabien (from Amsterdam yeeess), Clément (l'histoire retiendra que t'as toujours perdu à Fifa), Tiki et Laulau. Merci à Nicoach pour l'aide et on n'oubliera ce fameux déménagement de Lyon. Et un gros merci à Robin pour avoir fait le déplacement et toute l'aide apportée (alors que j'étais en parfait état le lendemain).

Un immense merci à la famille grâce à qui la vie loin de Nantes est possible. Merci à Julien, Christian, Ghislaine, Bernadette et Vanessa qui ont pu faire le déplacement, cela m'a énormément touché (et vous avez pu découvrir les bus parisiens, donc ça valait le coup). Des bisous particuliers à toute la famille avec qui j'ai d'innombrables souvenirs. J'ai une pensée pour mamie, qui nous manque toutes et tous, mais qui aurait aimé nous voir

encore toutes et tous ensemble.
Je voudrais finir cette partie de mes remerciements par une personne très importante à mes yeux aujourd'hui, et j'espère pour encore de nombreuses et innombrables années. Nora, merci pour toute l'aide que tu m'as apporté pour cette soutenance, merci pour tous ces week-ends inoubliables que l'on a partagés (que ce soit ceux où l'on observe des oiseaux à Bazouges-la-Pérouge ou ceux pendant lesquels tu m'as regardé écrire ce manuscrit). Quoi que l'on fasse, je veux juste qu'on le fasse ensemble.
Merci à toutes celles et ceux qui ont pu se déplacer pour la soutenance, cela m'a fait chaud au cœur et a permis de clôturer de la plus belle des manières qu'il soit ces trois années de travail.

Ce manuscrit a été écrit après plus de trois années de travail dans le monde du Rugby. Je n'ai pu m'empêcher de penser constamment à mon père devant tous ces matchs à la Paris Défense Arena. Je me rappelle de cette Coupe du Monde 2007 que l'on regardait, si seulement tu étais là. Imagine un peu, pendant trois ans, je suis allé au bureau rejoindre Szarzewski alors qu'on le regardait ensemble devant notre écran de télévision. Mais la vie c'est comme le rugby, même quand un joueur quitte le terrain, il faut continuer à se battre. Mon dernier remierciement s'adresse à ma maman, tu as tout donné et m'a toujours soutenu dans les études pour que je puisse en arriver là. Je t'en serai toujours redevable. Merci pour tout ce que tu as fait (en premier lieu me donner naissance), pour ton combat. On restera toujours une belle équipe.

Contents

Chapter 1 Introduction **1**
1.1 Basics of the Scrum . . . 2
1.2 Short History of the Scrum . . . 4

I Impact **13**

Chapter 2 Evolution of the Scrum Impact **17**
2.1 Evolution of the Players' Morphology . . . 18
2.2 History of Referee's Calls . . . 20

Chapter 3 Individual Player Characterization during Impact **25**
3.1 Individual Engagement Phase Experiment . . . 26
3.2 Mechanical Model . . . 33
3.3 Pusher Phase Space . . . 40
3.4 Discussion on Physiological Application . . . 42
3.5 Perspectives: Collective Force Signal . . . 44

Chapter 4 Influence of the Scrum Machine **47**
4.1 Evolution of the Scrum Machine used in Literature . . . 48
4.2 Scrum machine Characteristics . . . 49
4.3 Scrum Machine Influence on F_{peak} . . . 53
4.4 Scrum Machine Influence on the Determination of A . . . 56

II Individual Posture during Sustained Phase **61**

Chapter 5 Optimal Knee Angle for Individual Scrum Pushing **65**
5.1 Joint Angles . . . 66
5.2 Experimental Setup and Protocol . . . 69
5.3 Results . . . 73
5.4 Development of a Theoretical Model . . . 75
5.5 Isometric Torque of the Knee Extensors . . . 79
5.6 Discussion . . . 87

Chapter 6 Optimal Individual Scrum Posture on Grass **91**
6.1 Pushing Postures Observed in Other Sports . . . 92
6.2 Updated Experimental Setup . . . 95
6.3 Results . . . 99
6.4 Model of the Passive Force $\vec{F_p}$ . . . 112
6.5 Model of the Active Force $\vec{F_a}$ . . . 122
6.6 The Total Force: Comparison Experiments/Model . . . 125
6.7 Conclusion . . . 129

Chapter 7 Influence of Cleats Length on Optimal Posture **133**
7.1 The friction Coefficient . . . 134
7.2 Experimental Studies . . . 136
7.3 Results . . . 138

7.4 Comparison of the Total Force $\vec{F_x}$ 141

III Collective Effects and Dynamics **145**

Chapter 8 Transmission Losses in a Pack **149**
8.1 State of the Art 150
8.2 Experimental Study 151
8.3 Postures and Positions 156
8.4 1D Analogy: Tug of War 157
8.5 Passive and Active Components 160
8.6 Synchronization 163

Chapter 9 Scrum Instabilities **171**
9.1 An Instable Structure 172
9.2 Dynamics of the Contact Line of Scrums 175
9.3 Dynamical Experimental Study 179

Conclusion **187**

Bibliography **191**

1

Introduction

In this introduction Chapter, we are presenting scrum through Rugby Union history. It will lead us to modern scrum that could be split into two different phases: the impact phase and the pushing phase.

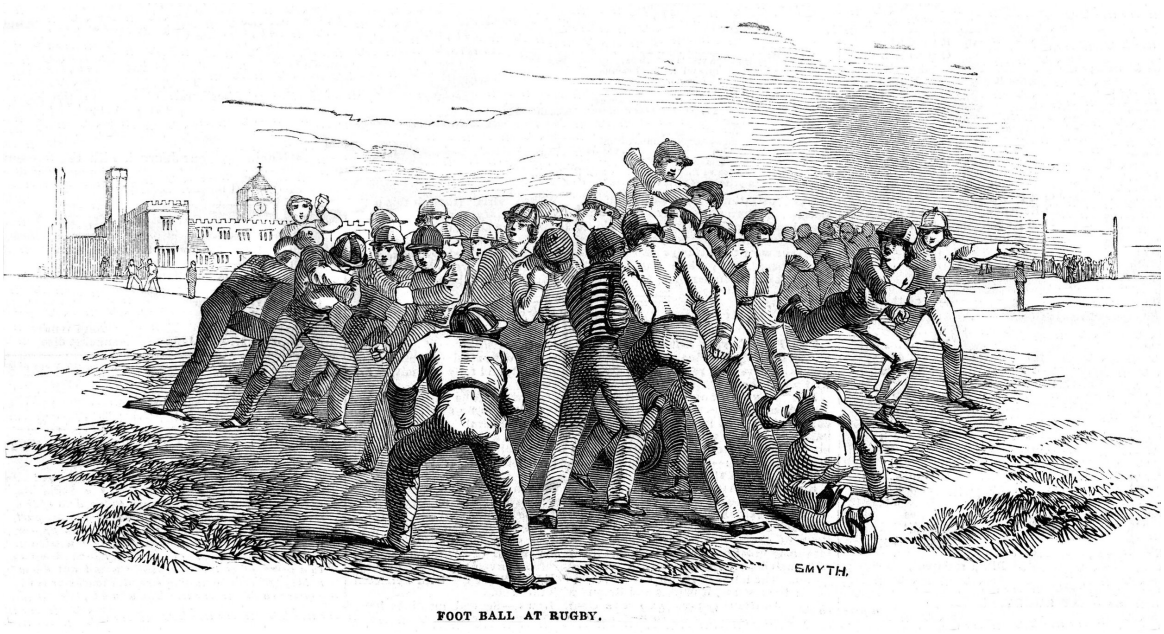


Figure 1.1: Smyth, *Football at Rugby* from **The Illustrated London News** of December 20, 1845.

Contents

1.1 Basics of the Scrum **2**
1.2 Short History of the Scrum **4**

1.1 Basics of the Scrum

1.1.1 Rugby Union

Rugby Union is a collective contact team sport that opposes two teams of fifteen players. The goal is to score as many points as possible by passing laterally or backward an oval-shaped ball to teammates on a playing field of 100×70 m. The points are scored with:

- a try. A player has to ground the ball behind the opponent's goal line (cf. Figure 1.2). It is worth 5 points.
- a conversion kick after a try or a penalty kick. A player kicks the ball with the foot between the uprights and above the crossbar of the goalposts (cf. Figure 1.2). The conversion kick is worth 2 points and the penalty kick scores 3 points.
- a drop goal. The player drop-kicks the ball with the foot between the uprights and above the crossbar of the goalposts. It is worth 3 points.

Modern Rugby Union is played with 15 players who have predefined roles according to the number on their jerseys. Each role and its associated number is presented in Figure 1.2. There is a distinction between two main groups of players: the forwards (from N°1 to N°8) and the backs (from N°9 to N°15).

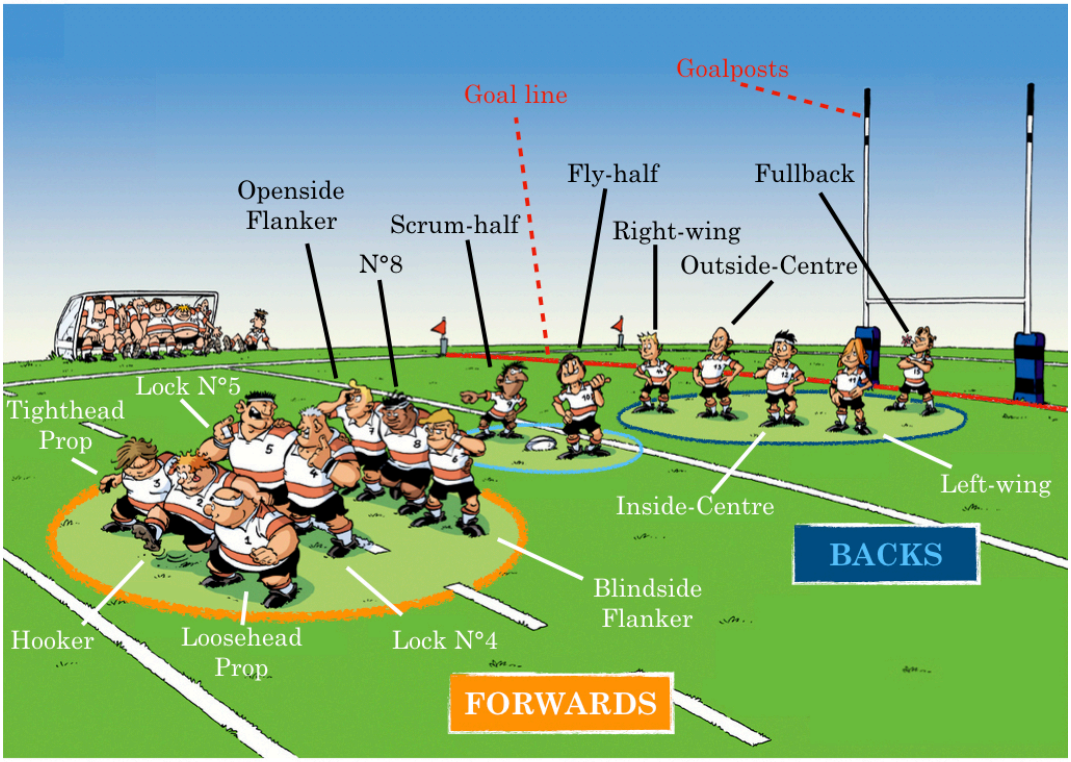


Figure 1.2: Positions of the player in Rugby Union extracted and modified from a sketch in [1]

Each position corresponds to different tasks to perform during a game. The back lines (highlighted in dark blue in Figure 1.2) are more likely to run to score tries (Wings N°11 and N°14), to create spaces in the defense of the opponent team (Centres N°12 and N°13),

and to be the last defense line (Fullback N°15). The half-backs (highlighted in light blue in Figure 1.2) organize the game plan by ordering the back lines (Fly-half N°10) and by being the link between the forwards and the backs (Scrum-half N°9).
The forwards (highlighted in orange in Figure 1.2) compete for the ball in two specific confrontations:

- the lineouts which intervene when the ball has to be put back into play when it has gone out of the limits of the playing field [2].
- the scrums which intervene to put the ball back into play after a knock-on, a throw forward, or a minor infringement [3].

They are composed of:

- the props (N°1 and N°3) who push in the first row of the scrum (cf. subsection 1.1.2) and are the first to protect the ball when a player of the team has been tackled.
- the hooker (N°2) is between the two props in the first row of the scrum and throws the ball into the lineouts.
- the locks (N°4 and N°5) who push in the second row of the scrum and are often the players who catch the ball in the lineouts.
- the flankers (N°6 and N°7) are positioned behind the props in the scrum.
- the Number-eight is the player behind the locks in the scrum.

In this thesis, we focus on the scrum which has been a part of the Rugby Union from the beginning in the XIX^{th} century but that has been importantly transformed over the decades as we will see in this introduction. Before going back in time, we start by describing how a scrum works today.

1.1.2 Configuration of a modern scrum

All the packs are using the same 3-4-1 configuration of players in three rows and each forward has a specific role in the scrum. We show a top-view picture of a modern scrum in Figure 1.3a and the equivalent scheme of the picture in Figure 1.3b.

Focusing on the light blue pack of Figure 1.3a, we can see that the first row (N° 1, 2, and 3) is composed of the loosehead prop, the hooker, and the tighthead prop. The loosehead prop only pushes against the tighthead prop of the opposite pack as we see in the scheme of Figure 1.3b. The tighthead prop has the head between two opponents with only the help of his/her hooker to push them while the loosehead prop has one opponent and the help from his/her hooker to push the opposite tighthead prop.
The second row (N° 4 and 5) is composed of the two locks (cf. Figure 1.2). The Number-4 lock and the Number-5 lock put their heads between the props and the hooker. Finally, the back row (N° 6, 7, and 8) is composed of the blindside flanker which is on the side of the scrum-half, and the openside flanker which is on the other side of the scrum. The two flankers are at the same level as the locks. They push with only one shoulder on their respective props. The Number-eight is putting his head between the two locks. He/she has a strategic role at the back of the scrum by controlling the ball and providing clean exits of the ball for the backs.
Although it is not mentioned in the rules that govern the scrum, the scrum-half always introduces the ball on the side of the tighthead prop of his/her team. The reason is that the

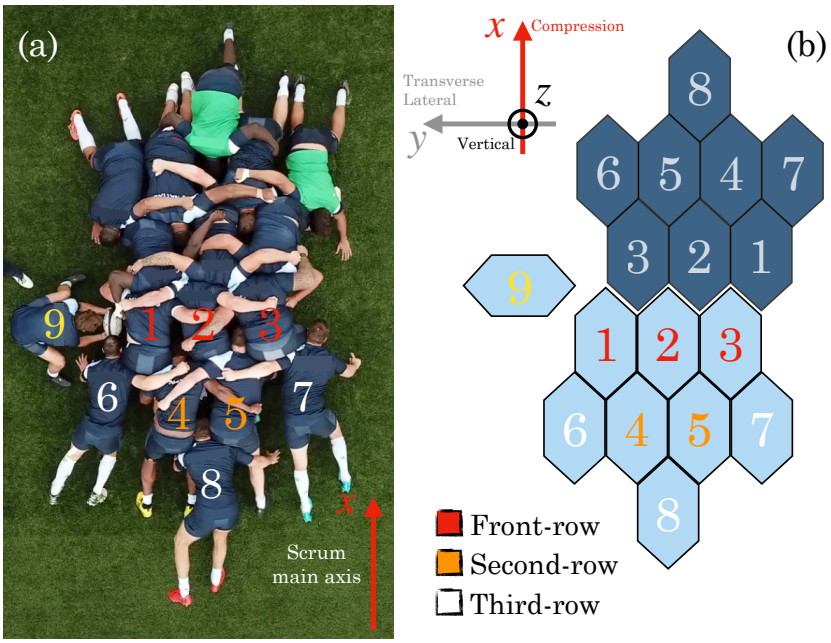


Figure 1.3: Top view picture and scheme of a modern scrum. (a) Scrum of the Racing 92 at practice. The scrum-half (9) throws in the ball under his loosehead prop (1). (b) Scheme of the 3-4-1 configurations adopted by each pack.

ball arrives faster at the hooker of his/her team with less road to travel and fewer players to pass under.
In Figure 1.3b, we define the x-axis along the pushes of the two packs. In the thesis, we will refer to this axis as the compression axis. The lateral axis is defined here as the y-axis and z corresponds to the vertical axis.

1.1.3 Height

In Figure 1.4a, we show a picture of another scrum of Racing 92 during a training session. The pack of the offensive team is the one that has the introduction of the ball. The offensive pack wins almost all the time the scrum and keeps possession of the ball. Since 1987, on average 90% of the scrums are won by the team that throws the ball in the scrum during the men's Rugby World Cup [4].

The side-view of this scrum is shown in Figure 1.4b. We measure the distance between the ground and the shoulders of the first-row players. We refer to this height as the height of the scrum or the pushing height. In a modern scrum, the typical pushing height is 60-70 cm.

1.2 Short History of the Scrum

When it emerged at Rugby School in the mid-1800s, Rugby football (ancestor of the Rugby Union) was played by schoolboys and was dominated by continual scrummaging [5]: players of both teams were gathering and starting an opposition of force for the possession of the ball. Passing the ball was very rare and the forwards were taking part in scrummage battles

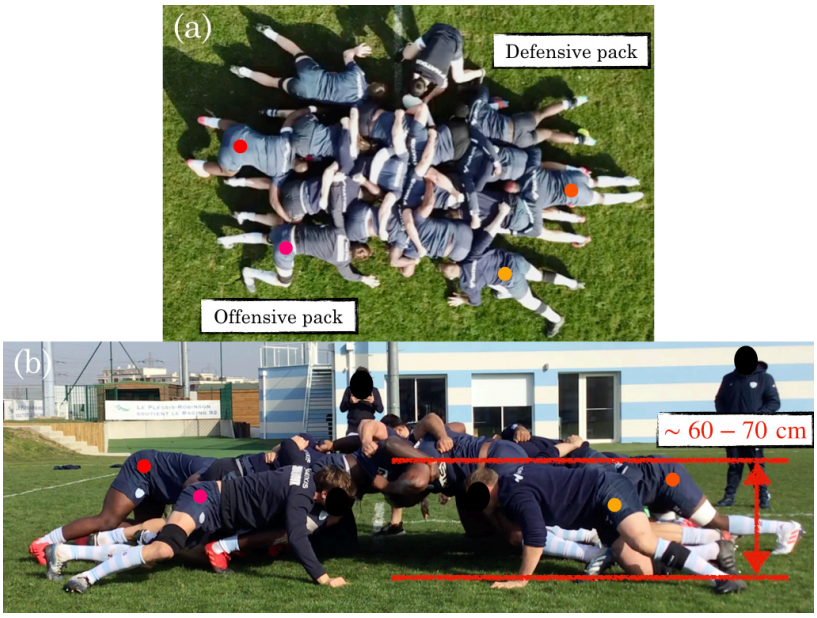


Figure 1.4: Scrum of Racing 92 during a training session. The colored points identify some of the players in both pictures. (a) Top-view picture. (b) Side-view picture.

by pushing the opponents towards their goal line and kicking the ball or the opponents' shins. They could be more than 30 players involved in these strength battles (cf. Figure 1.1).
In the 1870s, the first adult teams of Rugby Union appeared, at the same time, Rugby Union started to be played with 15 players on each team. Still, the aim of a scrum was to move the ball forward under a structure of men kicking the ball [6]. Some scrummages could last for minutes. In 1877, the secretary of the Rugby Football Union (FRU), Arthur Guillemard, described the progress of the scrums that occurs each time that the ball-carrying player was tackled [6]:

"the forwards of each side hurry up and a scrummage is instantly formed, each ten facing their opponents' goal, packed round the ball, shoulder to shoulder, leg to leg, as tight as they can stand, the twenty thus forming a round compact mass with the ball in the middle. Directly the holder of the ball has succeeded in forcing it down to the ground, he shouts "Down" and business may be commenced at once."

This period corresponds to the birth of the Racing Club de France (RCF) in Paris in 1882. It was one of the first Rugby-Football Clubs in France[1] and it still exists nowadays under the name of Racing 92. The RCF won the first French championship in 1892 against the Stade Français Paris Rugby (known as Stade Français nowadays) [7].

In the 1890s-1900s, the scrums started to be organized in several rows of players. The players in the first rows of each pack were the ones in direct contact with the opponents. However, there was no role specialization for each player as in modern Rugby Union (cf. subsection 1.1.2). For the forwards, the composition of each row was made on a "First come, first served" basis.

In Figure 1.5, we illustrate the organization of a scrum with a picture from 1904. We observe an opposition of two packs organized in three rows each. The number of forwards in each

[1] Le Havre Athletic Club was first one.

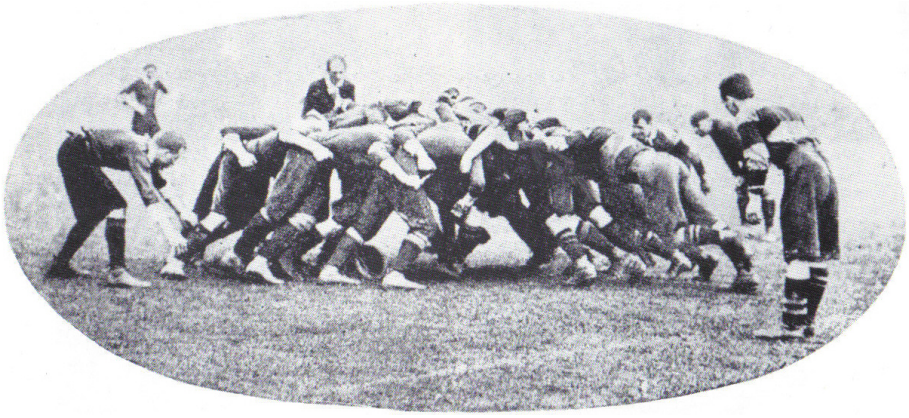


Figure 1.5: Picture of a Rugby union scrum in 1904, contested between Newport RFC (in hoops) and London Welsh (solids). Unknown author.

pack seems to be around six players and the player on the left seems to wait for the exit of the ball.

1.2.1 Configurations of the scrums before 1931

Thomas Elison was part of New Zealand's Native team in their 1888-1889 tour in Europe. He is known as one of the creators of the specialization of the role. The novelty came from that each forward knew which rows he belonged to. The three-row organization adopted was two players in the first row, three players in the second row, and two players in the back row. This configuration involved only seven forwards in the scrum: the eighth forward, the 'rover' or the wing forward, was situated outside of the pack and was free to harass the opponents, put the ball in the scrum, or protect his scrum-half [8]. This configuration is presented in Figure 1.6a. The two players of the first row can hook the ball with their feet after the throw-in of the ball by the scrum-half.

The packs were free to choose their own configuration between the 3-2-3 configuration (cf. Figure 1.6b) to the 3-4-1 configuration (cf. Figure 1.6c). In 1906, the national team of South Africa became the first international team to utilize the 3-4-1 configuration.
In 1931, the International Rugby Football Board (IRFB) imposed a new scrum law: after the trow-in by the half-scrum, the ball had to roll under three feet of the front row of each pack before being hooked. This rule signed the official death of the configurations with only two front-row players.

1.2.2 1950s to professionalization

In the XXth century, Rugby Union went from being a sport where the majority of playing time was dedicated to scrum and where the passes to the backs were rare, to a sport of movement and passes where the scrums became a way to restart the game after a throw-forward. The modifications of the rules by the IRFB encouraged the acceleration of the game and reformed the scrum, for example in 1954 a rule to stop the deliberate collapse of the scrum.

In Figure 1.7, we present the evolution of the scrum from the 1950s to the late 1990s. We present a picture of a scrum during a game between the British isles team and New Zealand in 1950 in Figure 1.7a. We show a scrum from 1971 in Figure 1.7b. In 1990, the scrum structure is closer to the ground as shown in the picture of a scrum during a Wales vs

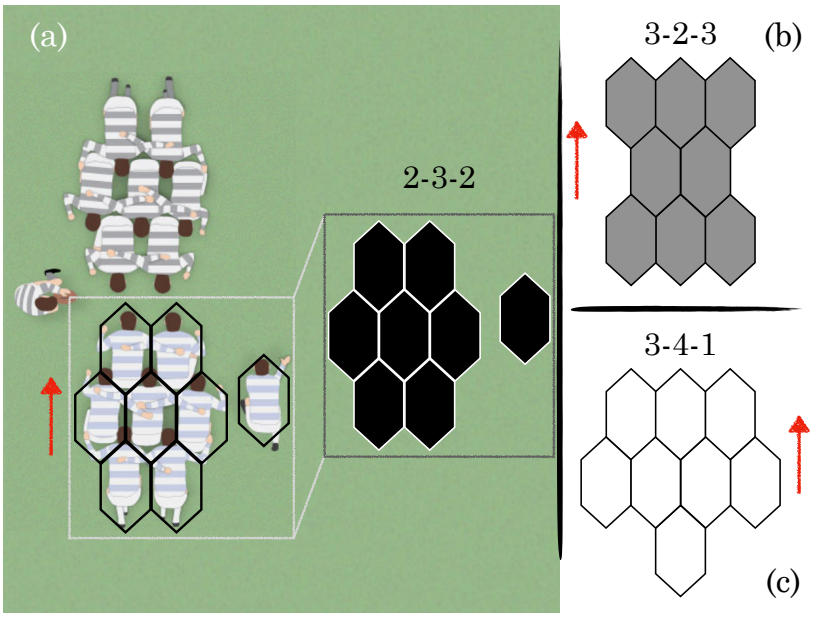


Figure 1.6: Some configurations of scrums observed in the History of Rugby Union. The red arrow identifies the direction of pushing for the attacking pack. (a) The 2-3-2 from New Zealand. (b) The 3-2-3 configuration. (c) The current 3-4-1 configuration was firstly used, at the international level, by the Springboks of South Africa in 1906.



Figure 1.7: Visual evolution of the scrum between 1950 and 1998. (a) Scrum in 1950. [9] (b) Scrum in 1971. [10] (c) Scrum in 1990. [11] (d) Scrum in 1998.[12]

Barbarians game in Figure 1.7c. In 1995, the IRFB removes from its statutes any mention of amateurism. The official professionalization of the Rugby Union started and in 1998 the

IRFB became the International Rugby Board (IRB). The same year, France won the Five Nations (England, Wales, Scotland, Ireland, France) Tournament with a Grand Slam[2], in particular, they beat the English team (24-17) (cf. Figure 1.7d).

We observe that the 3-4-1 formation was adopted by every team and that players adopted more crouched postures over the decades. In 1840, they were stood up (cf. Figure 1.1). In 1950, they had their legs straight with the trunk bent forward. In the late 1990s, the players are totally bent with their bodies really close to the ground.

Number of scrums in a game

During the XXth century, there is not only a visual evolution of the scrum through the decades, but there is also a decrease in the number of scrums during games due to the introduction of several rules that we previously evoked.
Quarrie *et al.* [13] counted the number of scrums that occurred in Bledisloe Cup games (New Zealand (NZ) versus Australia) from 1972 to 2004. In Figure 1.8, we present the number of scrums per game as a function of the year of the game. The blue dashed line marks the year of professionalization of the Rugby Union. We note a decrease in the number of scrums from 55 scrums in 1979 to 31 scrums in 2002.

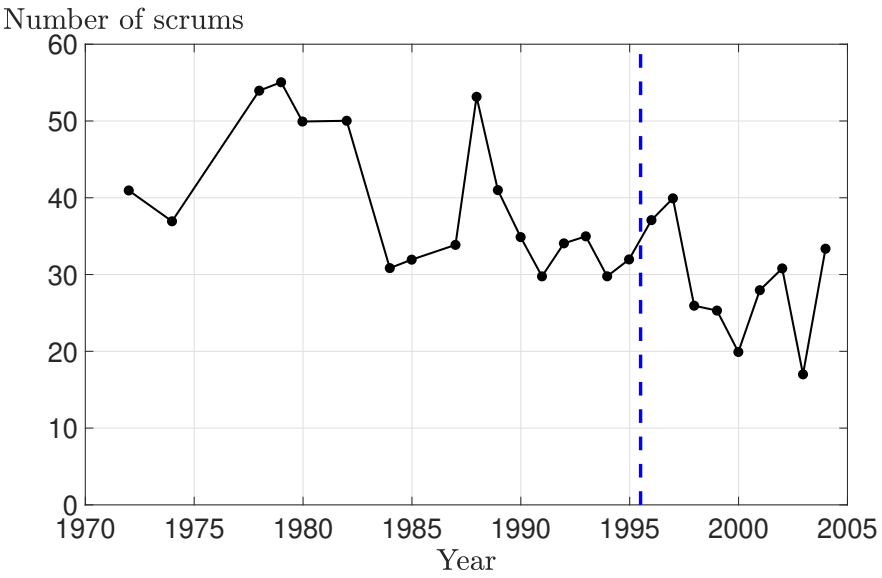


Figure 1.8: Number of scrums observed in the Bledisloe Cup games (NZ vs Australia) from 1972 to 2004. Extracted from [13].

Between 2000 and 2004, we observe in Figure 1.8 that the number of scrums is on average around 25. It corresponds to the number of scrums observed during the Six Nations (Five Nations + Italy) Tournament in 2005 and 2006 with 27 and 28 average number of scrums in a game respectively [14].
The same decrease in the number of scrums is observed in the average number of scrums per match during the mens' Rugby World Cup (RWC). In 1983, there were 31, in 1983, there were 27 and in 2011 there were 17 scrums on average [4].

In Table 1.1, the average number of scrums per match made by Racing 92 is presented. In the last column of this table, we specify the average number of scrums where the scrum-half

[2]They won all their games.

from Racing 92 throws the ball in the scrum. We note that the number of scrums seems

Season	N° of games	Average number of scrums per match	Racing 92 introduction
2019-2020	23	17 ± 3	7 ± 3
2020-2021	35	17 ± 5	8 ± 4
2021-2022	27	18 ± 4	9 ± 3

Table 1.1: Average number of scrums per match made by the Racing 92 between 2019 and May 2022 in official games.

to have diminished since the 2000s. This number is similar to the 17 scrums per match on average made by a Top 14[3] team during the 2016-2017 season [15].

Even if the number of scrums decreases, it remains a part of the battle for psychological and physical supremacy in Rugby Union games, it is probably linked to the historical importance of the scrum in this sport.

1.2.3 Phases of the modern scrum

Nowadays, the scrums are contests for the possession of the ball that occur after minor infringements, knock-ons, or throws forward in order to restart play during the games. The scrum-half of the team that suffered the infraction throws the ball under the tunnel formed by the two first rows of each pack (cf. Figure 1.3a). This action is called the throw-in. Then, the hooker of his/her team hooks the ball with one of his/her feet while the two packs are pushing for the contest of the ball along the main axis x (cf. Figure 1.3a).

Crouch, Bind, Set

With the professionalization of the Rugby Union, the way to begin a scrum became an issue of safety for players. To reduce the risk of injuries, scrum engagement is nowadays controlled by referee calls (cf. section 2.1). The referees shout "Crouch, Bind, Set" in order to organize each scrum. In Figure 1.9, we present the top-view chronophotography of a scrum during a practice of Racing 92.

When the referee blows the whistle to announce a scrum, the forwards of each team organize themselves in three rows and start to bind with their teammates of the same row (cf. Figure 1.9a). Then, in Figure 1.9b, the locks and the flankers place their heads in the spaces of the first rows (cf. Figure 1.3b) in order to set the two first rows of the 3-4-1 configuration (cf. Figure 1.9c). The 3-4-1 configuration is now part of the official rules of the scrum [3]. At this point, the first-row players are almost standing and the number-eights are not yet placed in the packs. The referee orders the first rows to crouch themselves, and by lowering their trunk towards the ground, the first rows of each pack bend over in Figure 1.9d.
After the "Bind" call, the props of each pack grab their direct opponent with their free arms (cf. Figure 1.9e). The players stabilize the structure, and when the referee shouts "Set", the two packs accelerate towards each other and impact (cf.Figure 1.9f). In this same figure, we note that the scrum-half is ready to throw the ball below his teammates. After that, the two packs are authorized to push the opponent along the compression force axis. In Figure 1.9g, the ball has been hooked by the hooker and is under the offensive pack. Finally, the Number-eight gets the ball at the feet of the Number-4 lock and passes it to a player outside of the frame to restart the game in Figure 1.9g.

[3]Rugby Union French championship

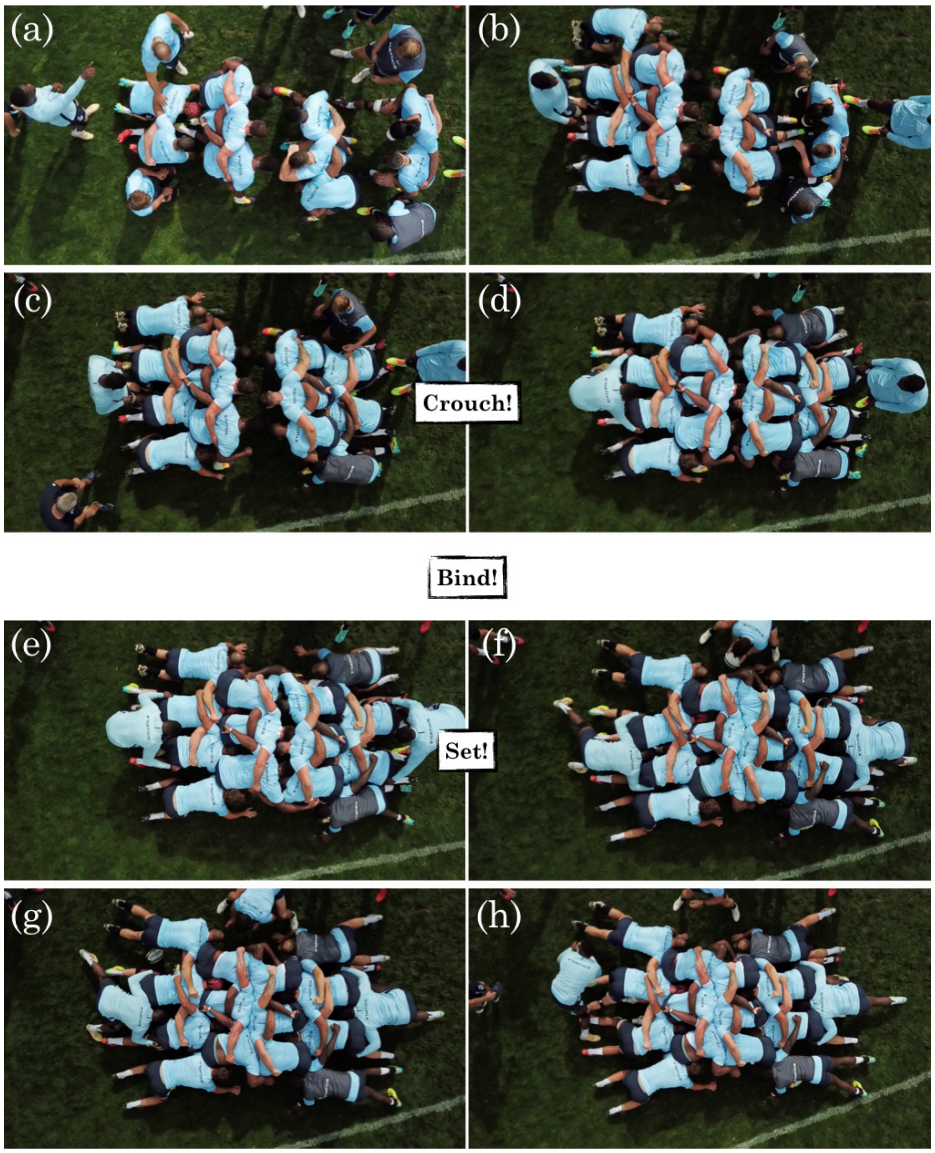


Figure 1.9: Chronophotography of a scrum. (a) The packs prepare the bindings between teammates. (b) The two first rows of each pack are constituted. (c) The players wait for the "Crouch" call. (d) The first rows put themselves in a crouched posture. (e) After the "Bind" call, the props of each pack bind to each other. (e) After the "Set" call, the first rows impact each other. (f) The throw-in of the ball. (h) The exit of the ball from the scrum.

Impact phase and sustained push phase

In the thesis, we study several issues about the transmission of force, the production of force, and the stability in scrums. To do so, we will deal with the same type of experimental tools in almost all the chapters: the instrumented scrum machines. A scrum machine is used during training sessions by Rugby Union teams to practice the packs of forwards. Contrary to an ordinary scrum, the first row players of a pack push against foams installed on the scrum machine. The scrum machines used in this thesis are instrumented meaning that they can measure the forces produced by the pack.
In section 3.1.3, we will introduce the dynamic instrumented scrum machine of the French Federation of Rugby which measures the forces in the three directions of space. In Figure 1.10, we present the signals of force measured along the compression axis (x-axis in Figure 1.10a) for a single player and a complete pack of professional players of Racing 92. The single player of Figure 1.10a is a professional lock of mass $m = 147$ kg and height 196

cm. He pushes on mannequins made of foams, and the force he produced is measured by force sensors. The corresponding signal of force is plotted in Figure 1.10b. The professional pack of mass $m_{pack} = 937$ kg is presented in Figure 1.10c and the corresponding signal of compression force in Figure 1.10d.
The red dashed lines in Figures 1.10b and d correspond to the "Set" call of the referee. Then, the impact of compression forces, represented in red, corresponds to the impact of the first rows in Figure 1.9f. After the rise of compression forces, the forces decrease and stabilize themselves. We observe variations of force between the impact phase in red and the blue dashed line that indicates the time corresponding to the throw-in of the ball by the scrum-half. Then, we observe the sustained pushing phase represented in blue with a new rise of the compression forces and a stabilization around a mean value that constitutes a plateau of force for a few seconds. This phase of constant pushing corresponds to the synchronized activation of the muscular forces of each pack.

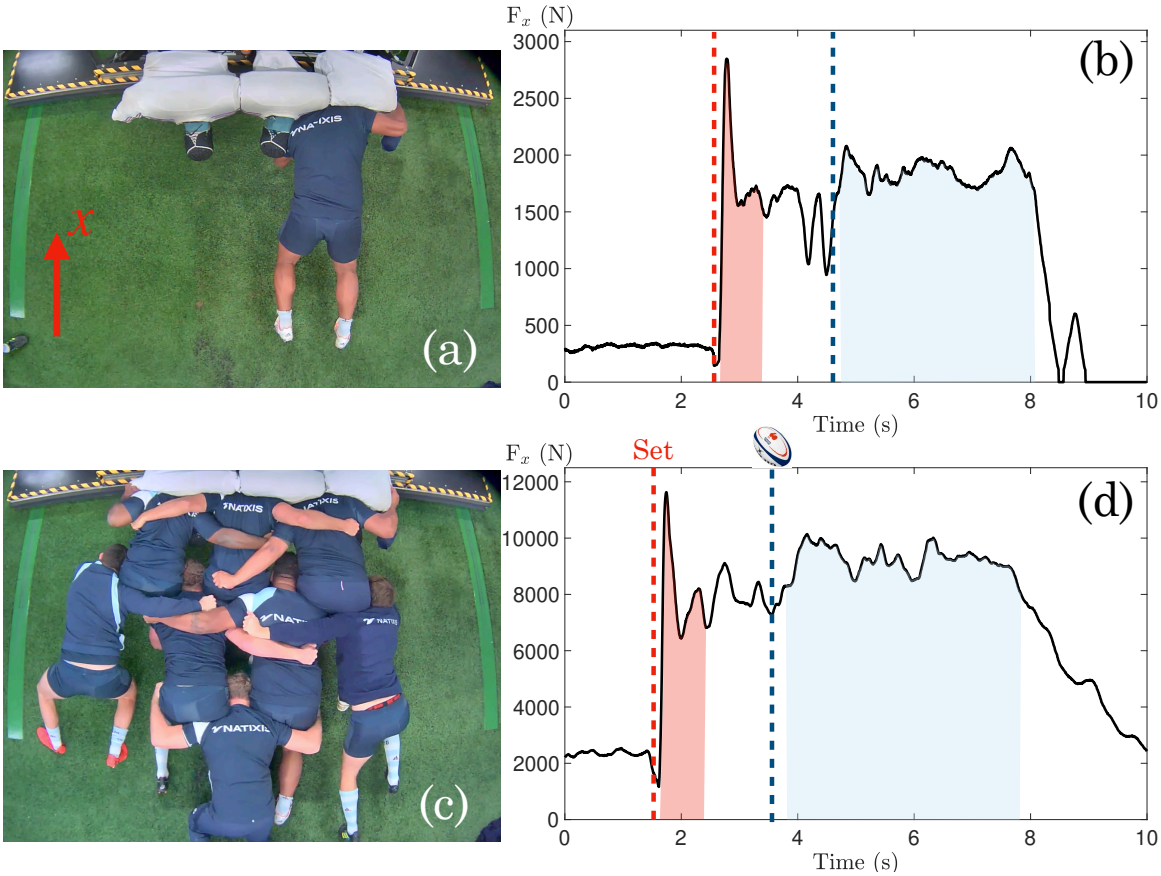


Figure 1.10: Time evolution of compression force signals for a professional lock and a complete pack pushing on a scrum machine. (a) Top-view picture of the professional lock of mass $m = 147$ kg. (b) Individual compression force signal with two distinct phases: the impact (in red) and the sustained push (in blue). (c) Top-view picture of the professional pack of mass $m_{pack} = 937$ kg. (d) Time evolution of the compression force produced by the professional pack. The red dashed line corresponds to the time of the "Set" call of the referee. The blue dashed line represents the time when the scrum-half throws in the ball.

We remark that both signals of force (individual and collective) have the same similar shape with the two distinct phases (cf. Figures 1.10b and d). The single player reaches smaller forces in each phase. During the impact phase in red, the maximum force is slightly above 3000 N which corresponds to twice the weight of the player ($2mg = 2 \times 147 \times 9.8 \simeq 2880N$). While the pack reaches an impact force slightly above 12 kN which represents 1.3 times

$m_{pack}g$. The red area in the single and collective single lasts for $\sim$ 0.5 s. Then, a professional single player can produce approximately 1500-2000 N for 3-4 seconds during the sustained phase (cf. Figure 1.10b), while a professional pack produces 8000-9000 N for the same amount of time in this phase (cf. Figure 1.10d).

This manuscript is divided into three parts. In Part I, we deal with studies about the impact phase. This phase We will start by describing the evolution of the referee's calls during these last 15 years in order to protect the players. We will then focus on an individual experimental study about the characterization of forwards thanks to the analysis of their force signal during the impact phase. Then, in Part II, we focus on the sustained push phase. Thanks to an individual scrum machine developed in the laboratory, we conducted experimental studies about the optimal scrummaging posture of a player. These two first parts mainly present experimental studies that we conducted at the individual scale about force production. Finally, we will look at issues about force transmission and dynamics on a collective scale in Part III. We will discuss the different physical parameters that influence the efficiency of transmission of the force in a pack.

PART I

IMPACT

We described the basics of the workings of the scrums and saw that they can be divided into two distinct phases in terms of the signal of force produced by a single player or a pack. In this part, we focus on the first phase of impact. We start with studying the link between the impact speed and the maximum force reached during the impact. We then conduct an experimental study about the determination of the characteristics of an individual player thanks to the analysis of the signal of compression force measured.

2

Evolution of the Scrum Impact

We present the history of the evolution of the scrum impact in the last 50 years.



During a France-England game in 1992, the French loosehead prop and hooker, Moscato and Tordo, stick their heads together before the impact. A certain idea of the french flair.

Contents

2.1 Evolution of the Players' Morphology **18**

2.2 History of Referee's Calls **20**

This work has been done with Caroline Cohen and Christophe Clanet thanks to a collaboration with Julien Piscione, Olivier Chaplain, and Didier Retière.
A special thanks to the professional and academy-level players of Racing 92 who participated in the tests.

2.1 Evolution of the Players' Morphology

During Union Rugby games, scrums are an important source of injuries for forwards. A two-season study made on 645 professional Rugby Union players from English Premiership concludes that scrums have a 60% higher risk of injury than tackles [14] and present the highest risk per event [14, 16].
The epidemiology of scrummaging shows that the most common injuries are neck, spine, [17, 18, 19, 20], and calf muscle ones [16]. It seems that the majority of spine injuries occur during engagement [18].

Milburn [21] described the engagement force as an impulsive force that becomes larger with higher front rows' engagement speed and larger player's weight. Figure 2.1 shows a typical force signal as a function of time for a professional pack of Racing 92 team with a mass of $m_{pack} = 937$ kg. This force signal is measured on a scrum machine we present in section 3.1.3. The compression force exhibits a first peak of maximum value $F_{peak} \simeq 11.5$ kN and a width τ, the typical impact time, of 0.3 s. The force drops to a value of 6 kN and then it fluctuates around a value of 8 kN under the maintained pressure of the scrum.

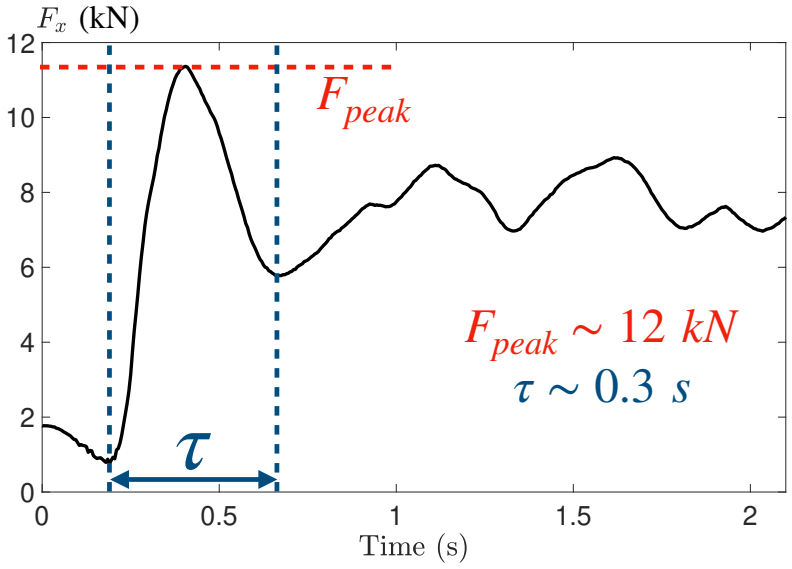


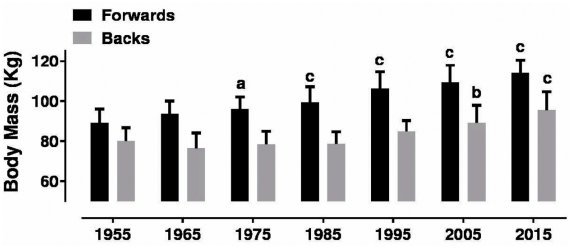
Figure 2.1: Scheme of a typical peak compression force signal F_x with the orders of magnitude for complete packs impacting on the scrum machine described in 3.1.3.

In 1990, Milburn *et al.* [21] made force measurements at a sampling frequency $f_e = 500$ Hz and obtained $F_{peak} = 8.0$ kN for an Australian University-level pack with a mean weight of the subjects of $m = 85.7$ kg, which means that the order of magnitude for the mass of the pack is $m_{pack} \sim 686$ kg. In 2013, Preatoni *et al.* [22] measured (with a sampling frequency of $f_e = 500$ Hz) an average peak force $F_{peak} = 16.5 \pm 1.4$ kN for six International-level packs of mean weight $m_{pack} = 893 \pm 17$ kg and $F_{peak} = 11.7 \pm 2.0$ kN for six Academy-level[1] packs of mean weight $m_{pack} = 793 \pm 20$ kg. A hypothesis to explain the observed increase of F_{peak} is the evolution of the mass of the packs.
Indeed, the morphology of rugby players changed in the last 40 years. Rugby player's masses

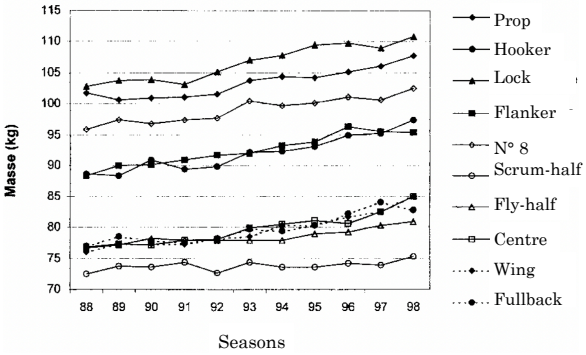
[1]Three Academy packs from full-time professional club or three academy packs from the first XV university packs.

have increased on average[23, 24, 25, 26]. This assertion is illustrated in Figure 2.2 through graphs and tables from the literature.
In Figure 2.2a, we show the body mass evolution of international rugby players taking part in the opening matches of the Five or Six nations tournament from 1955 to 2015 extracted from [25]. They are divided into two main groups of forwards and backs (cf. section 1.1.1). We can see that forwards are always heavier than backs but both groups had an increase in body mass. In 1955, the mean body mass of a player was 85 ± 8 kg and in 2015, it was 105 ± 12. The forwards of the 1955 Five Nations during the opening match had a mean weight of approximately 90 kg. Nowadays, the forwards of the 2015 Six Nations during the opening match have a mean weight close to 115 kg. Thus, the average weight of the pack increased by approximately 200 kg, which corresponds to an increase of 27 %.
In Figure 2.2b, we have a graph of the mass increase of french rugby players at the top level between 1988 and 1998 extracted from [26]. We can see that the most massive players were the locks followed by the props, which correspond to the results of Hill *et al.* [25] with international players at the Six Nations until 2015. Again, we observe that the mass of every position has increased.

(a)



(b)



(c)

Grouped playing position	Season; body mass, kg (standard deviation)								
	2002/3	2003/4	2005/6	2006/7	2007/8	2008/9	2009/10	2010/11	2011/12
All backs	88.7 (6.9)	90.1 (6.6)	92.1 (7.7)	91.9 (6.9)	91.7 (7.8)	91.8 (7.8)	91.4 (7.2)	91.9 (8.3)	91.4 (7.9)
Scrum half	83.0 (5.8)	85.5 (5.3)	87.0 (5.0)	87.1 (5.9)	85.3 (5.2)	85.0 (4.6)	85.4 (4.4)	84.5 (4.8)	84.9 (5.5)
Fly half	86.8 (4.1)	86.9 (5.2)	88.6 (5.5)	88.4 (3.9)	88.3 (5.2)	88.7 (4.5)	89.0 (5.6)	89.4 (5.8)	89.2 (5.5)
Centre	93.7 (5.6)	93.6 (5.3)	96.5 (6.2)	95.4 (5.8)	94.8 (6.6)	95.7 (6.7)	95.7 (5.6)	97.2 (6.6)	96.0 (6.7)
Back three	88.6 (6.7)	91.0 (6.7)	92.5 (8.4)	92.3 (7.4)	93.9 (8.2)	93.4 (8.3)	92.5 (7.5)	92.6 (8.7)	92.3 (8.0)
All forwards	109.0 (8.8)	108.3 (7.8)	109.8 (7.9)	111.0 (8.5)	110.7 (8.6)	109.3 (8.4)	109.8 (7.9)	110.7 (8.2)	110.6 (7.7)
Prop	114.2 (6.9)	113.9 (5.8)	114.4 (5.3)	116.7 (6.7)	117.4 (7.8)	115.6 (7.8)	115.3 (6.0)	117.1 (6.9)	116.7 (5.9)
Hooker	103.6 (8.4)	103.5 (6.6)	104.2 (6.3)	104.7 (6.2)	103.9 (6.1)	102.2 (6.5)	102.6 (6.0)	103.7 (6.7)	104.4 (5.6)
Second row	113.8 (7.1)	111.8 (6.5)	114.6 (7.0)	114.8 (6.1)	113.7 (5.9)	112.1 (5.7)	113.2 (6.5)	113.0 (5.6)	113.2 (6.2)
Back row	104.2 (7.2)	103.9 (6.5)	105.6 (6.9)	106.3 (7.7)	106.3 (6.6)	105.7 (6.3)	106.3 (6.2)	106.9 (6.3)	106.1 (5.9)

Figure 2.2: Evolution of masses of Rugby players during the last decades. (a) Extracted from [25]. (b) Extracted from [26]. (c) Extracted from [23].

We give another example in Figure 2.2c, with a table extracted from an article of Fuller *et al.* [23] where they gather measurements of anthropometrics of English professional rugby players[2] between 2002 and 2012. Props and locks remain the heavier players but we notice a stagnation in the average mass of locks during this 10-year study while the props have a 3 kg raise in 10 years.

[2]All players registered in first team squads of Premiership rugby clubs in England.

From Hill *et al.* [25], we see that the average mass of an international-level pack of Five/Six nations tournament goes from 796 kg to 912 kg between 1985 and 2015, which corresponds to a 15 % mass increase. Between the Academy-level packs of Milburn *et al.* [21] and the one of Preatoni *et al.* [22] 23 years later, we have a similar 16% mass increase.

The larger masses of players are not the only parameter that plays a key role in the increase of F_{peak}. While players increased in weight, they also developed physical qualities like speed abilities partly due to Rugby professionalization, which started in 1995. Higher masses and higher velocities induce higher impact energies and a higher risk of injuries. At the beginning of the 2000s, it was necessary to protect the physical integrity of the players, and the rules evolved in this way.

2.2 History of Referee's Calls

During the last two decades, official rules tend to protect forward players during the engagement phase by reducing the distance between the two opposite front rows [27].
Before 2007, there were no official referee calls to guide the player during the engagement phase. For example, in Figure 2.3, we present a 1973 scrum during a men's test game between Ireland and New Zealand. In Figure 2.3a, we observe that front-row players were starting to engage in a standing position really far from each other, approximately 2 meters. After the impact, the two packs directly push each other in Figure 2.3b. We remark that the scrum height is slightly higher than the one we measured on a modern scrum in Figure 1.4.

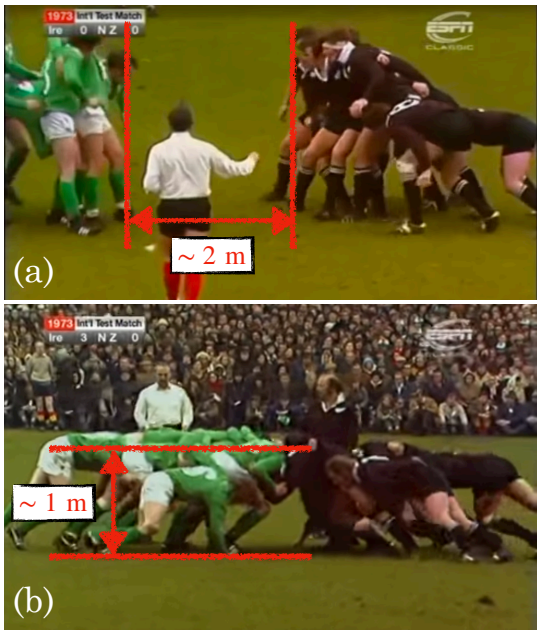


Figure 2.3: Example of a 1973 scrum during a men's international game between Ireland and New Zealand. Snapshots extracted from an ESPN video [28]. (a) Forward players quickly organized themselves in two packs separated by almost two meters. (b) Scrum after impact.

At the beginning of the 2000s, the idea to stabilize the front rows before the impact in order to reduce the number of collapsed scrums was introduced [29]. In some international games,

some referees started to shout "Crouch And Hold, Engage" to order the preparation of the players before the impact. The front rows started to crouch before engaging, but the space between these rows remained large (more than 1 meter) until the mid-2000s. In 2007, the International Rugby Board (IRB) implemented official oral commands from the referee to structure the scrum pre-impact phase. The sequence said by the referee was inspired by the informal "Crouch And Hold, Engage". The commands are organized in four steps that we illustrate with a scrum during the 2007 men's Rugby World Cup (RWC) game between France and Argentina in the small final (cf. Figure 2.4). The different steps are:

- "Crouch": the referee orders the two front rows to adopt a crouched position. In Figure 2.4a, before the "crouch" call, the eight players of each pack bind themselves to their teammates. Then, the referee says the "crouch" call. In Figure 2.4b, the first-row players get into the crouched position, while the locks and third-row players prepare their pushing postures by lifting their knees off the ground.
- "Touch": the referee asks props to touch their opponent with their free arms, it is a way to make sure that the gap is acceptable before impacting. In Figure 2.4c, we see the French loose-head arm coming back from touching the Argentinian tighthead prop after the referee's "touch" call.
- "Pause": the referee asks players to stabilize themselves before the next call that is coming quickly.
- "Engage": the referee orders the players to impact. Figure 2.4d represents the two packs just after the collision of the front rows.



(a) **(b)**

(c) **(d)**

Figure 2.4: Example of a scrum during the small final of 2007 men's RWC between France and Argentina. Snapshots extracted from a World Rugby video [30]. (a) Scrum before the "Crouch" call. (b) Scrum after the "Crouch" call. (c) Scrum after the "Touch" call. (d) Scrum after the "Engage" call.

This sequence of orders is called the CTPE sequence in the following. Directly after the apparition of these new calls, the number of neck and back injuries in New Zealand in 2007

diminished [31]. In 2012, the CTPE engagement phase became CTS for the "Crouch, Touch, Set" sequence. It was similar but the "Pause" call was removed and the order to impact was shortened from "Engage" to "Set", which helps for front rows impact synchronization. The actual referee's sequence appeared in the 2013-2014 season. This modification was going further in the desire to reduce the initial gap by ordering props to bind with their opponents before the "Set" call. The referee's call adopted is the "Crouch, Bind, Set" (CBS) sequence.

This historical evolution in referee's calls is interesting to develop in order to show the constant research in protecting the players from severe injuries. The effect of those modifications was to reduce the space between the front rows from two meters in 1973 to approximately 10 cm nowadays. The main effect of the evolution of these rules is to diminish the engagement speed v_0 and thus the value of the peak force F_{peak}.

This influence of impact speed is noticeable in Preatoni *et al.* [32] for a pack using different engagement techniques. In this article, the authors compare the value of F_{peak} depending on the engagement process for different playing levels. For the international and elite packs, mean F_{peak} values are reported in Table 2.1 depending on the engagement techniques. We already described the CTPE and CTS sequences. The Fold-In engagement process consists of a CTPE process with an instruction given to the players to generate no momentum before contact with the scrum machine. The engagement commands currently used in Rugby Union nowadays should be somewhere between CTS and Fold-In calls in terms of F_{peak}.
We also report the engagement speed v_0 that corresponds to "the front row center of mass maximum velocity during the initial engagement phase [...] defined as the weighted average of the centers of mass of the trunk of the three front row players" [32]. The front-row players reach this maximal speed just before the scrum machine slows them down. The mean values with their standard deviations are given in Table 2.1 in parentheses. We then understand that F_{peak} strongly decreases with the Fold-In techniques thanks to the reduction in impact speed v_0.

Playing-level (N° of packs)	CTPE		CTS		Fold-In	
	F_{peak} (kN)	v_0 (m.s^{-1})	F_{peak}	v_0	F_{peak}	v_0
International (6)	16.5 ± 1.4	2.7 ± 0.6	15.8 ± 1.6	2.9 ± 0.4	8.6 ± 2.0	1.8 ± 0.5
Elite (6)	16.5 ± 1.4	3.0 ± 0.6	15.9 ± 1.5	3.0 ± 0.6	8.6 ± 0.9	2.3 ± 0.2

Table 2.1: Average values F_{peak} and v_0 for packs of different playing-level. F_{peak} is expressed in kN and v_0 is expressed in m.s^{-1}. The data are extracted from [32]

The photographs in Figure 2.5 illustrate these changes in referee's calls by depicting the moment when the players lunge to impact. In Figure 2.5a, we present a scrum from 2011 where the CTS process imposed to the props to have the opposing front row within arm's reach. Thus, the pre-impact gap between the front rows was large, about 50 cm. Today, the front rows must link with their opponents before impacting thanks to CBS rules, as in the example presented in Figure 2.5b, thus reducing the pre-impact gap between front rows to about 15 cm. The reduction of this gap implies the reduction of the impact speed, and thus reduces the stresses on the players' necks.

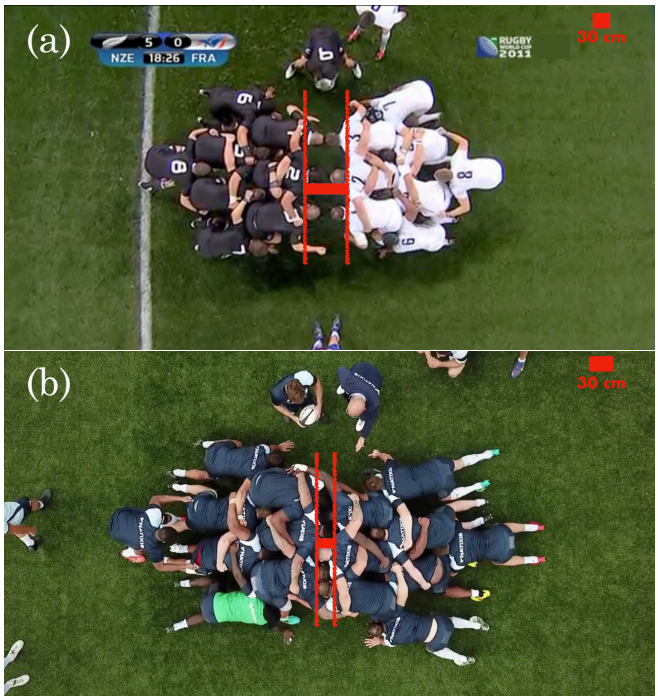


Figure 2.5: Pictures of scrums seen from above before the impact phase. (a) 2011 men's World Cup game during the final between New Zealand and France. (b) Scrum during a Racing 92 training session in 2018.

Take home message of Chapter 2

To understand the physics of scrum impacts, the important parameters to take into account are

1. Players and packs masses. In modern Union Rugby, players are athletic and massive. The masses of the packs increased during the last three decades but seemed to stabilize during the last years at a professional level.

2. Impact speed. With mass increasing, the way to reduce F_{peak} is to change scrum laws to diminish the front rows gap before the engagement phase.

3

Individual Player Characterization during Impact

Using individual experiments made at the "Atelier de la mêlée", the scrum machine of the French Federation of Rugby, we develop a model to characterize players and try to quantify the quality of an impact. We discuss the possible link with athletic qualities.



Picture of a Racing 92 professional player at "Atelier de la mêlée" by Antoine Garcia.

Contents

3.1	Individual Engagement Phase Experiment	**26**
3.2	Mechanical Model	**33**
3.3	Pusher Phase Space	**40**
3.4	Discussion on Physiological Application	**42**
3.5	Perspectives: Collective Force Signal	**44**

This work has been done with Sylvain Blanchard, Caroline Cohen, and Christophe Clanet thanks to a collaboration with Julien Piscione, Olivier Chaplain, and Didier Retière.
A special thanks to the professional and academy-level players of Racing 92 who participated in the tests.

3.1 Individual Engagement Phase Experiment

3.1.1 Observation of force signals

During the first session of experiments made with the professional players of Racing 92 at the "Atelier de la mêlée", we ask them to produce a maximal push individually and collectively on the scrum machine as if they were in a real scrum. We have already seen some examples of force signals we obtained (cf. Figures 1.10 and 3.3). In Figure 3.1, we show three examples of compression force signals at impact for three different subjects whose characteristics could be found in Table 3.1. The scrum machine mechanical parameters remain the same for all individual trials and we detail these experimental settings below in subsection 3.1.4.
The masses m_{tot} of participants A, B, and E are different (99 kg, 116 kg, and 147 kg respectively). Furthermore, these participants do not impact with the same engagement speed v_0 (2.2 m.s^{-1}, 1.0 m.s^{-1} and 1.1 m.s^{-1} respectively). So, we observe that they obtain different F_{peak} (cf. Chapter 2.2). We notice that the player with the highest v_0 (subject A) has the highest $F_{peak} \simeq 3550$ N. Then, subjects B and E have similar v_0, so the heaviest of the two players (subject E) is the one that obtains a greater F_{peak} ($F_{peak} \simeq 2990$ N and $F_{peak} \simeq 2850$ N for subjects B and E respectively).

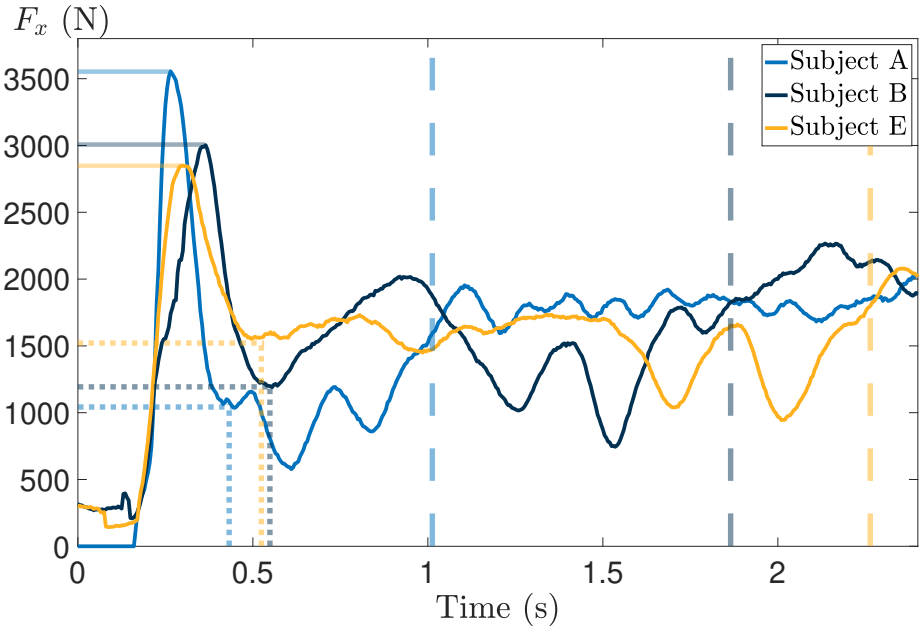


Figure 3.1: Examples of compression force signals measured on the M-Rex scrum machine for three different subjects A, B, and E.

One can evaluate the order of magnitude of each player's kinetic energy just before the impact:

$$E_{imp} \sim \frac{1}{2} m_{tot} v_0^2. \tag{3.1}$$

e obtain $E_{imp,A} \sim 2.4 \times 10^2$ J, $E_{imp,B} \sim 60$ J, and $E_{imp,E} \sim 90$ J. One can notice that the higher the kinetic energy E_{imp}, the higher the peak force F_{peak} is.
But there is more to discuss than just the F_{peak} value. Indeed, the shapes of the signals are different. After reaching F_{peak}, the signals do not drop at the same level and at the same

times as we see with the short dotted lines in Figure 3.1. Then, all the players are doing support recoveries of both feet which implies two consecutive drops in F_x, before they activate their muscles to enter the sustained pushing phase marked by the vertical dotted lines.

The question we raise here is: can we characterize physically a pack/a player thanks to the pushing force signal shape and knowing the engagement speed? And how can we physically define what is a good individual impact?

3.1.2 Participants

The participants of the experimental study are professional players of Racing 92 and Novice player who does not play Rugby Union. This last subject is here to compare the shapes of impact force signals regarding the playing level. Table 3.1 gathers the age, weight, playing level, height, mass, and engagement speed v_0 when impacting individually the scrum machine of all the subjects. Every participant provided informed consent before participating in the experimental session. All the experiments were conducted under the supervision of the Chief Medical Officer of Racing 92.

Player	Playing level	Position	Age	m_{tot} (kg)	Height (cm)	v_0 (m.s^{-1})
A	Professional	Hooker (H)	35	99	181	2.2
B	Professional	H	35	116	178	1.0
C	Professional	Loosehead Prop (LP)	28	116	183	4.0
D	Professional	Tighthead Prop (TP)	37	143	189	1.7
E	Professional	Lock (L)	29	147	196	1.1
F	Novice	[redacted]		75	175	2.6 (Imp. 1) 1.6 (Imp.2)

Table 3.1: Presentation of the subjects who take part in the individual impact force experimental study.

3.1.3 Experimental setup

"Atelier de la mêlée"

The "atelier de la mêlée" is an instrumented scrum machine that belongs to the French Federation of Rugby (FFR) which is located in Marcoussis, at the National Rugby Center (CNR). This is the place where all the French teams gather to prepare for the different competitions. In a closed room equipped with a synthetic turf, the "atelier de la mêlée" is composed of an instrumented scrum machine, called the M-Rex, surrounded by two side views cameras and one top view camera (cf. Figure 3.2).

The scrum machine M-Rex was designed by Thales [33]. Figure 3.2a exhibits the hexagonal structure (STEWART platform) attached to a ground triangular platform that can translate along the x-axis. This platform, delimited by yellow and black lines, is linked to the hexagonal one with six electric pistons that manage resistances along the x, y, and z axes. In Figure 3.2b, we feature the three mannequins made of foam which contain three triaxial force sensors. We note A, B, and C as the mannequins representing the opponent's tighthead, hooker, and loosehead respectively. Thus, sensor B measures the force that the opposing hooker endures during a scrum.
The scrum machine can be used in different modes:

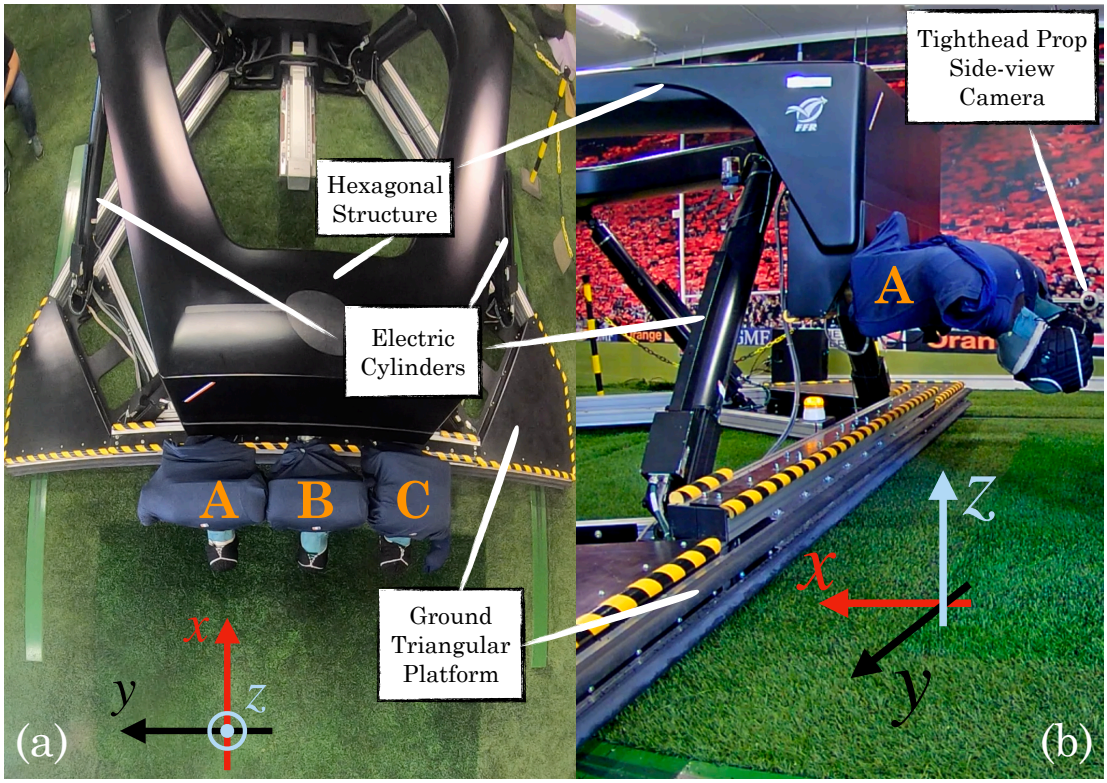


Figure 3.2: "Atelier de la mêlée" in CNR. (a) Top view of the collective scrum machine. We define the position of each force sensor located in the mannequins A, B, and C. The top black hexagonal platform is linked with the electric cylinders to the ground triangular platform. (b) Side-view from the loosehead prop camera of the M-Rex.

- Passive mode: the scrum machine does not apply any forces on the players (cf. Chapters 3 and 8). The platform is made of a system of different electric cylinders that allow the operator to choose different stiffnesses along the 3 different axes. Those stiffnesses are set thanks to a digital interface (cf. 4.2.2). It is also possible to block every cylinder and have an infinite stiffness along each space direction, only the mannequin foams will absorb impacts in this case.
- Active mode: the scrum machine can apply forces and displacements on the players (cf. Chapter 9). It is possible to set a position control or a force control thanks to the digital interface.

It is important to note that this machine is used by coaches to mimic complicated sequences of scrums to challenge their players. During the experiments we conducted, we used the scrum machine in simplified configurations: static, fixed stiffness along the x-axis, or simple dynamic movements (oscillations, constant velocity along the x-axis).

Force signal example

The sampling frequency we used in all our experiments with this setup is 200 Hz. In Figure 3.3, we show an example of the measurements made by the force sensors during the push of a professional pack of Racing 92.

In Figure 3.3b, we decompose the compression force F_x measured by each of the force sensors. We find that the opponent loose-head (sensor C) is the one experiencing the smaller forces.

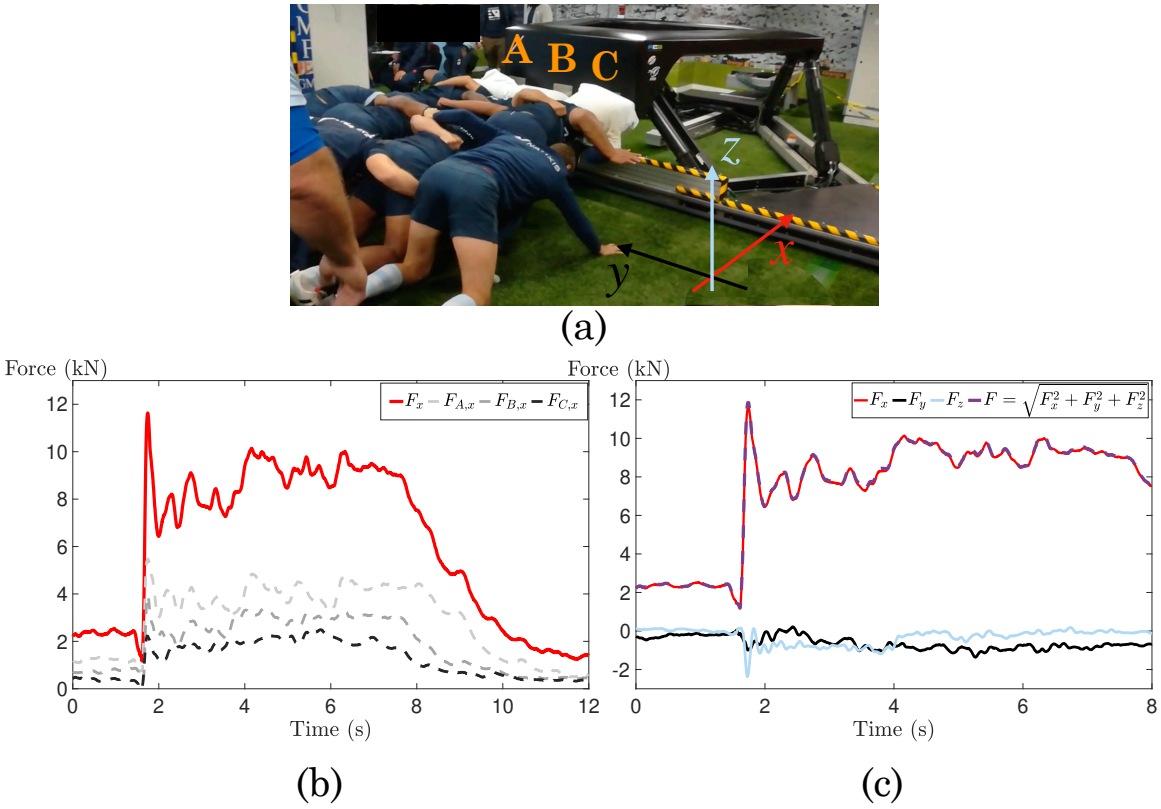


Figure 3.3: Force signal examples on a trial with a full pack. (a) The full pack of Racing 92 professional players pushing on the M-Rex. (b) Compression force F_x in full red line and distribution of compression forces on different force sensors A, B, and C featured in Figure 3.2. (c) Distribution of the total force F exerted by the pack along the 3 axes (x, y, z). The compression force is similar to the total force.

In the first row, this is the player that has only one opponent in front of him/her. In rugby, we often hear that the tighthead prop is the stronger player of the scrum, and it is verified with the highest amount of force measured on sensor A corresponding to the opponent tighthead prop.
About the direction of the force, it is described in Figure 3.3 where we notice the full pack applies a force $F(t)$ in (x,y,z) space. We have the relation

$$F^2 = F_x^2 + F_y^2 + F_z^2 \tag{3.2}$$

and we remark that for this trial we have $\frac{F_x^2}{F^2} > 0.95$. This remark remains true for all of our individual and collective trials on this scrum machine. So, when we need to simplify our physics studies, we can neglect F_y and F_z during the engagement phase in order to study the production of force. This remark corresponds to Milburn's description of the compression force during impact [21]. We would like to point out that F_y and F_z play a major role in injury prevention and stability of the scrums issues, where they cannot be neglected compared to the compression force.

For the experimental study, the scrum machine is used in passive mode with a finite stiffness with the same settings for all the subjects. During the impact, the scrum machine slightly moves during the experimental data collection. But during the impact, the position variation of the mannequin along the x-axis of typically $\Delta X \sim 2 - 4$ cm is negligible compared

to the heights of the players ($\sim$ 180 cm).

3.1.4 Protocol

We ask the professional participants (from A to E) to freely impact the scrum machine with their maximum force. The impact is followed by the sustained push phase (cf. Figure 1.10), without any particular instructions on the transition time.

The study is reduced to a 1D problem along the main compression axis. We work with F_x and the engagement speed considered in the problem is calculated along this axis. Indeed, thanks to the top view camera (f_e = 25 Hz) of the "Atelier de la mêlée", we estimate the subjects' speed during their acceleration in order to determine their impact velocity v_0. This operation is made by pointing manually a fixed point (thanks to the sponsor behind the jerseys of the players) of the upper body of the player with the software ImageJ. We then derived the displacement signal in order to obtain the speed signal on Matlab.
The chronophotography obtained with this camera of subject A impacting the scrum machine is shown in Figure 3.4. He is a professional hooker and usually binds his arms by grabbing his props around their trunks. We ask him to push between the sensors A and B (cf. section 3.1.3), as when he is in a full pack pushing on this scrum machine. In Figure 3.4a, we see that he first puts himself in a crouched position and stabilizes himself. Then, he accelerates his trunk along the x-axis towards mannequins in Figures 3.4b and 3.4c. Just after, he hits the scrum machine as fast as possible in Figure 3.4d. In this example, the player then regains his support, he starts by repositioning his left foot in Figure 3.4f and then his right foot in Figure 3.4g. Then, subject A enters the sustained pushing phase in Figure 3.4h and we notice that the scrum machine moves along the x-axis. The corresponding F_x signal is given in Figure 3.5 in solid blue line and we report the crucial times (t_b,t_0,t_1,t_{peak},t_2,t_3,t_4) on it.

In Figure 3.5, we observe that F_x reaches a maximum force F_{peak} after subject A hits the scrum machine. We call t_{peak} the corresponding time, after which the force drops until reaching its minimum value F_{reb} at t_{reb}. For this example, subject A is then moving his left foot at t_2 and his right foot at t_3. If we do not consider the forward steps, we can guess the force is stabilizing around 1100 N at a force we will call F_0. Some force signals like the Subject E one in yellow in Figure 3.1 stay constant after impact and the F_0 definition is clearer in this case ($F_{0,E}$ = 1700 N).

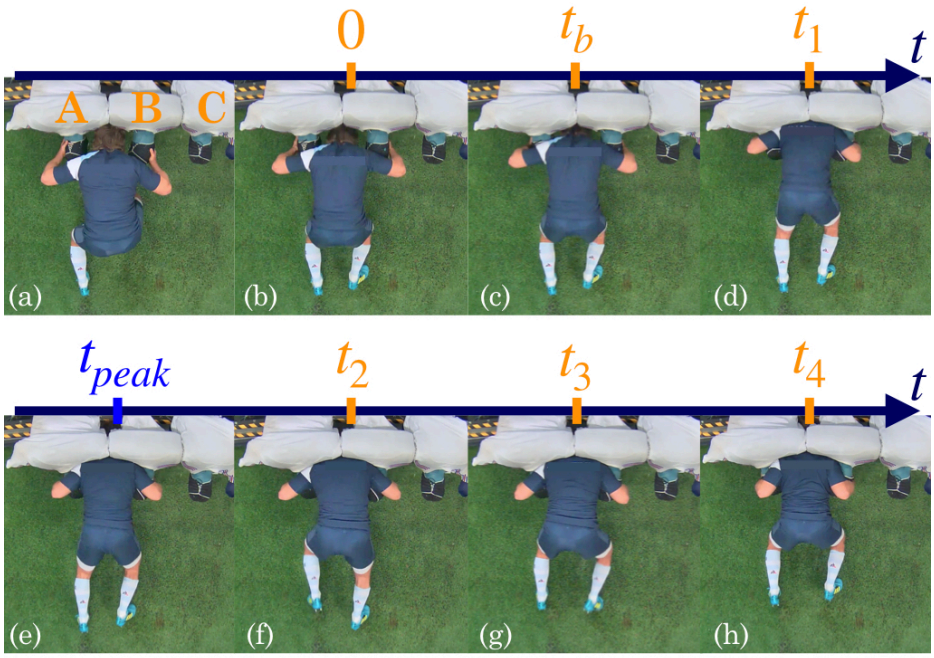


Figure 3.4: Top view chronophotography of subject A impacting FFR scrum machine. (a) Subject A is in a crouched position with shoulders at approximately 10 cm from the scrum machine. (b) Subject A is accelerating towards the scrum machine. (c) He keeps accelerating and this photography corresponds to the time t_b in the force curve of Figure 3.5. (d) Subject A hits the scrum machine at a velocity $v_0 = 2.2$ m.s^{-1}. It corresponds to t_1. (e) He reaches F_{peak} at t_{peak}. (f) After the impact, the player moves his left foot forward at time t_2. (g) He moves his right foot corresponding to time t_3. (h) He starts the sustained pushed phase at time t_4.

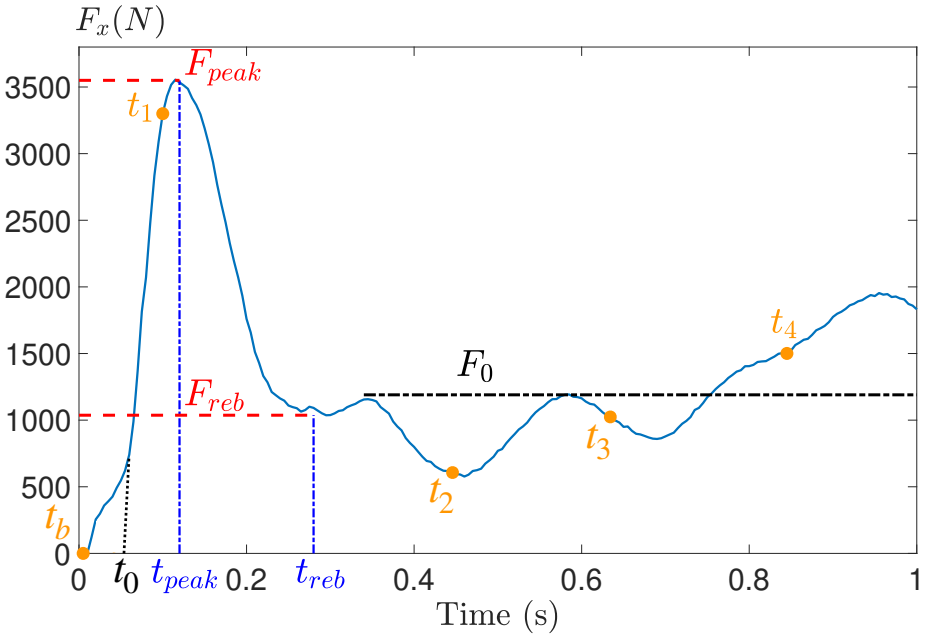


Figure 3.5: Compression force signal F_x obtained with subject A. This signal corresponds to the chronophotography of Figure 3.4.

3.1.5 Experimental results

Engagement speed influence

All the professional players impact the scrum machine once and chose their v_0. For comparison purposes, we ask subject F to impact on the scrum machine[1] at various speeds v_0 with the same impact protocol. We do not ask him to do the sustained push force phase, we only focus on the impact phase.
In Figure 3.6, we plot three experimental results on the M-Rex scrum machine with subject F for three different engagement speeds. We find the results of the previous Chapter, with an increase of F_{peak} with v_0 in Figure 3.6 for the novice player.

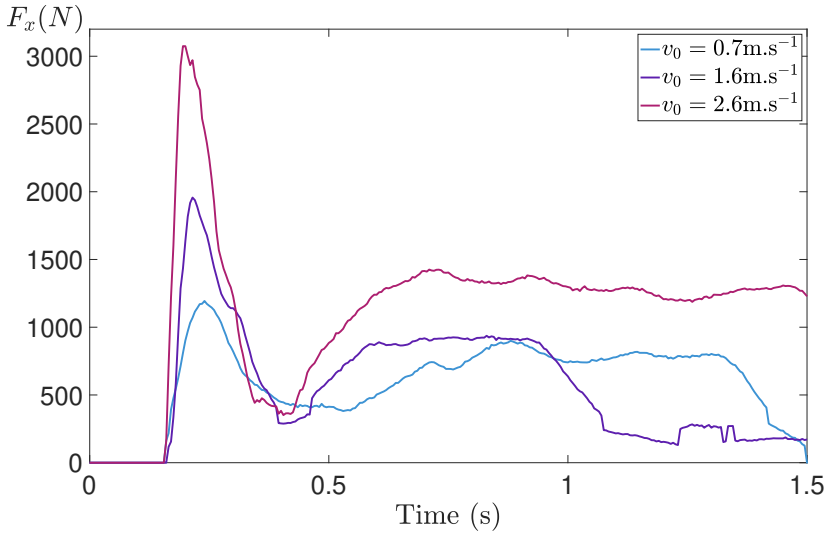


Figure 3.6: Force signals at different v_0 for subject F.

In Figure 3.6, we observe that the peak force F_{peak} increases with v_0. From $F_{peak} = 1370$ N for $v_0 = 0.7$ m.s^{-1}, the impact force reaches $F_{peak} = 3075$ N for $v_0 = 2.6$ m.s^{-1}.
Whatever the engagement speed, the compression force drops to approximately 500 N after F_{peak}.

Mass and playing-level influence

In Figure 3.7, we compare two force curves obtained for subject A (blue solid curve) and subject F (yellow solid line) at a similar engagement speed of $v_0 = 2.0 \pm 0.2$ m.s^{-1}. Their curves are different: especially in terms of peak compression force with a ratio of $\frac{F_{peak,A}}{F_{peak,F}} = 1.5$ between the professional and the novice. It is interesting to note that the masses ratio $\frac{m_A}{m_F}$ is equal to 1.3.
The signals of professional players on M-Rex also have one rebound before reaching F_0 (cf. Figure 3.1) disregarding the recovery of feet support. However, the rebound effect seems less important than for subject F with $F_{reb,pro} \sim 1000 - 1500$ N (cf. Figure 3.1) where $F_{reb,nov} \sim 300 - 500$ N. To explain F_{peak} difference at an equivalent v_0, mass is a part of the explanation. But, the difference in playing level may have an influence on damping performance. Subject F seems to bounce back a lot compared to professional players of Rugby Union.

[1]The settings of the M-Rex are fixed identical

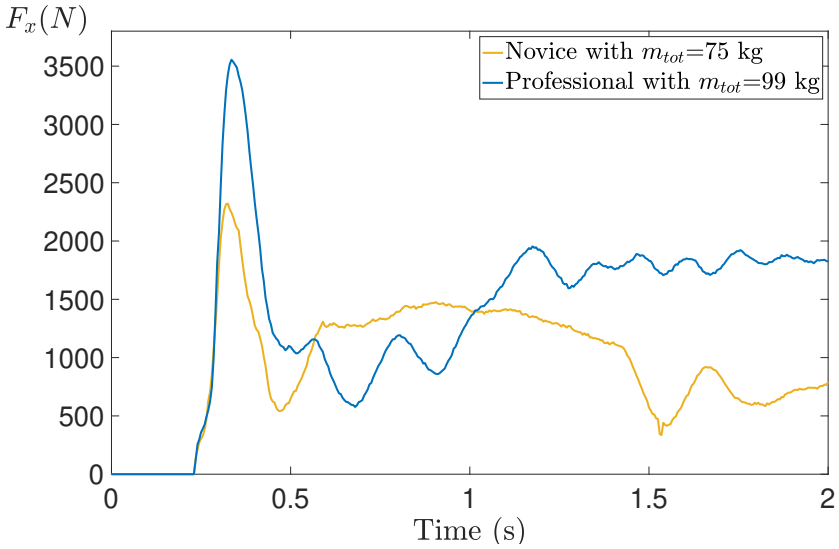


Figure 3.7: F_x at impact for subject A (blue solid line) and subject F (yellow solid line) with the same engagement speed of $v_0 = 2.0 \pm 0.2$ m.s^{-1}.

The playing level may also have an influence on F_{peak} values at equivalent engagement speed. Indeed, in Figure 3.6, subject F reaches high F_{peak} similar to the ones reached by the professionals in Figure 3.1. By calculating the impact energy E_{imp} (cf. equation 3.1) corresponding to the purple signal of Figure 3.6, we obtain $E_{imp,F} = \frac{1}{2} \times 75 \times 2.6^2 = 5.1 \times 10^2$ J. We notice that this energy is similar to $E_{imp,A}$ (cf. subsection 3.1.1) but the novice subject F does not reach the same F_{peak} than subject A ($F_{peak,F} \simeq 3075$ N and $F_{peak,A} \simeq 3550$ N). This quick calculation is just an order of magnitude and it quantifies kinetic energy by taking into account the total mass of the player. But as we can see in Figure 3.4, subject A mainly throws his trunk toward the scrum machine. So, for similar kinetic energies of impact, the conversion in force is better for the professional players than for the novice.

We experimentally observe differences between the players of different playing levels, but also among the professional players. We are going to develop a model that can explain those differences.

3.2 Mechanical Model

3.2.1 Model definition

We seek to characterize with a physical model the impact of a single player (cf. Figure 3.8a). We model the player as a spring of constant stiffness k in series with a damper of damping factor β placed in parallel with a generator of constant force F_0 that corresponds to the stabilizing force after impact and before muscle activation. We place an effective mass m between the spring and the damper-force generator cell. The mechanical analog of the player is presented in Figure 3.8b.

The compression force produced by the player is noted as $F(t)$. The total length $x(t)$ represents the distance from the feet to the shoulders of the player. We start by applying

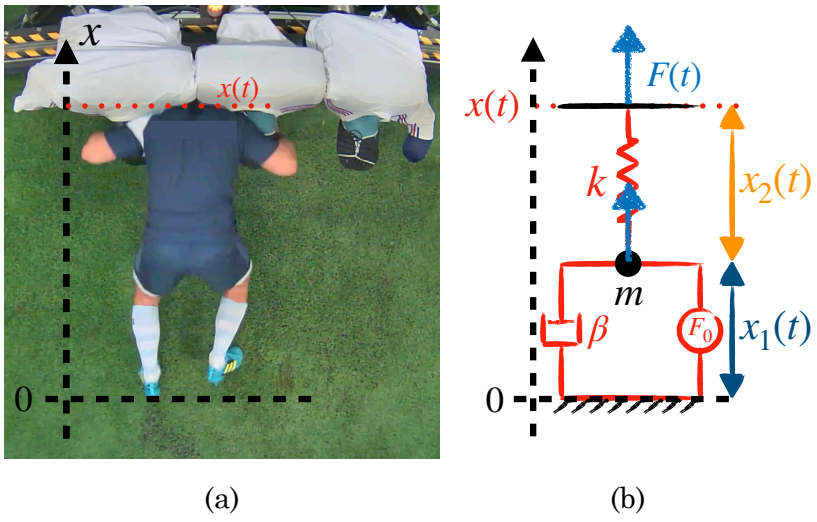


Figure 3.8: Model of a single player impacting the M-Rex scrum machine. (a) Top-view snapshot of subject A during the impact corresponding to Figure 3.5. (b) We consider a model composed of an effective mass m, a damper β, a spring of constant k, and a constant force generator F_0. We define x_1 and x_2 in relation to mass position, and the length x is given by $\forall t, x(t) = x_1(t) + x_2(t)$.

Newton's law of motion on the effective mass m, we obtain the following expression:

$$m\ddot{x_1}(t) = F_0 - \beta\dot{x_1}(t) - k(l_{20} - x_2(t)) \tag{3.3}$$

with l_{20} the resting length of the spring. We know that $\forall t, x(t) = x_1(t) + x_2(t)$ and that $\dot{x}_2(t) = -\dfrac{\dot{F}(t)}{k}$. Using these relations in equation (3.3), we obtain the differential equation that governs the behavior of F and x :

$$\frac{m}{k}\ddot{F}(t) + \frac{\beta}{k}\dot{F}(t) + F(t) = F_0 - \beta\dot{x}(t) - m\ddot{x}(t). \tag{3.4}$$

We use the assumption that the player keeps a constant length x. Indeed, as we can see in the example from Figure 3.4d to Figure 3.4f, the distance between feet and shoulders is almost the same for subject A during the impact. So, we have $\forall t, \dot{x}(t) = 0$. However, the mass m is free to move during the impact and we define its position with x_1 and x_2 (cf. Figure 3.8b).
We then use the scaling

$$\overline{F} = \frac{F}{F_0},\ \overline{x} = x\frac{k}{F_0}, \tag{3.5}$$

and use the dimensionless parameter

$$A = \frac{mk}{\beta^2}, \tag{3.6}$$

to rewrite the equation (3.4) as :

$$A\ddot{\overline{F}} + \dot{\overline{F}} + \overline{F} = 1. \tag{3.7}$$

Initial conditions are determined by noting that the force is null at the beginning (when the

player arrives on the scrum machine). We also know that the initial speed is v_0. Moreover, by looking at the model in Figure 3.8b, the force applied on the scrum machine is equal to the opposite of the restoring force of the spring k. The relationship between $F(t)$ and k is linked by the elongation of the spring. So, one can write the time derivative of the force F as $\dot{F}(t) = -k\dot{x}_2$. Therefore, the dimensionless initial conditions are:

$$\overline{F}(0) = 0, \quad \overline{\dot{F}}(0) = \frac{\beta v_0}{F_0}. \tag{3.8}$$

3.2.2 Model behavior and analytical solutions

Influence of A and v_0

The problem is reduced to a one-parameter dimensionless differential equation that we can solve numerically and analytically with the previous initial conditions. But the equation (3.7) hides a dependence to five parameters: k, m, β, F_0 and v_0. To get acquainted with this model, we show in Figure 3.9 the influence of mechanical parameters on force signals for a fixed v_0=2 m.s^{-1}.

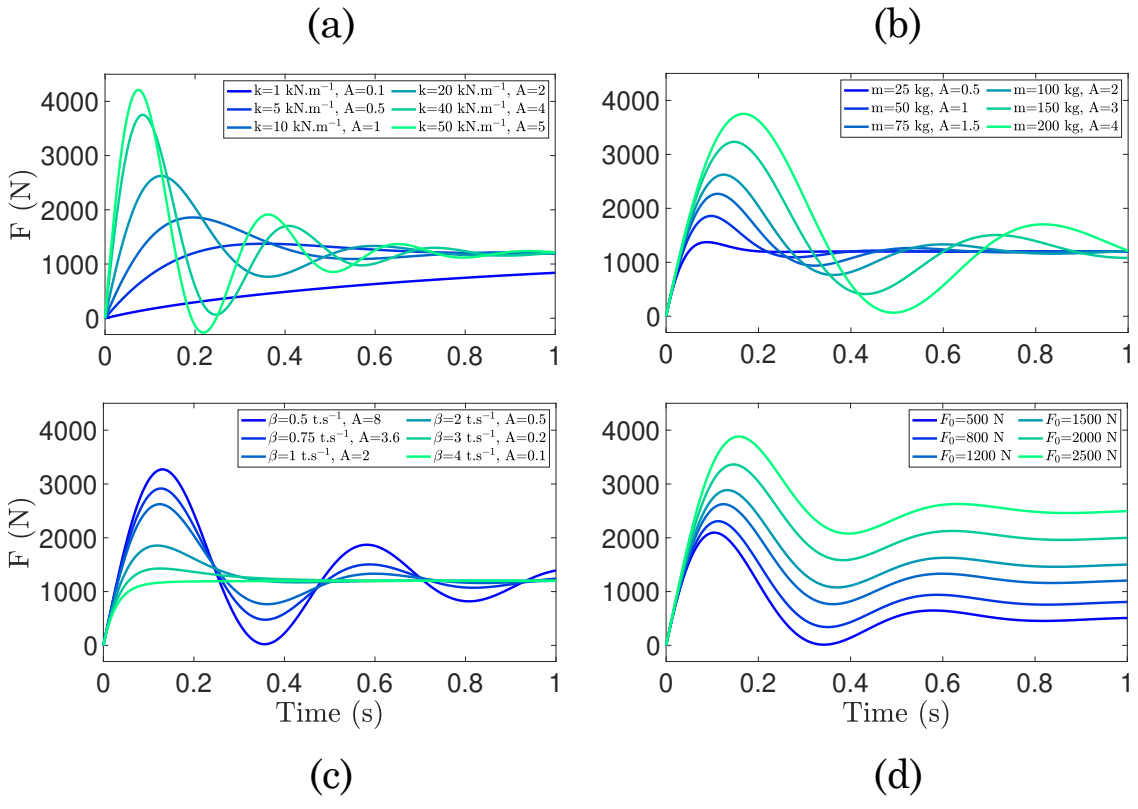


Figure 3.9: Influence of model parameters on force signals. Unless otherwise stated in legends, m =100 kg, k=2 $\times 10^4$ N.m^{-1}, β=1 $\times 10^3$ kg.s^{-1} and F_0= 1200 N. (a) Influence of k from 1 kN.m^{-1} to 50 kN.m^{-1}. (b) Influence of m from 25 kg to 200 kg. (c) Influence of β from 0.5 t.s^{-1} to 4 t.s^{-1}. 1 t= 10^3 kg. (d) Influence of F_0 from 500 N to 2500 N.

We notice in Figure 3.9a that when k increases, there is an increase in F_{peak} and a decrease in t_{peak} and t_{reb}. Increasing k means that A increases, and it implies more oscillations around F_0.
When the effective mass m increases in Figure 3.9b, F_{peak} is also increasing. t_{peak} and t_{reb}

are increasing not at the same speed because the peak becomes larger. The number of oscillations is kept constant and the amplitude increases with the mass. As for k, an increase in m implies an increase in parameter $A = \frac{mk}{\beta^2}$.
Increasing β (cf. Figure 3.9c) reduces F_{peak} while t_{peak} is slightly greater and t_{reb} is slightly lower. When β increases, A is diminished which implies larger damping of the oscillations. We note that the width of the peak remains constant.
Finally, when we increase F_0 in Figure 3.9d, F_{peak} increases and the peak becomes slightly larger. We do not change the value of A anymore and this is why the general aspect of the peak is quite the same. F_0 is the value of the stabilized force after impact, this is why we observe this shift in higher forces.
We see that for large A, the force signals show more instability in terms of oscillations. At fixed v_0, increasing A implies an increase in F_{peak}.

We now focus on the influence of the engagement speed v_0. We plot in Figure 3.10a the evolution of F for v_0 varying from 0.1 m.s^{-}1 to 4 m.s^{-}1 all other parameters remaining equal: m =100 kg, k=2 $\times 10^4$ N.m^{-1}, β=1 $\times 10^3$ kg.s^{-1} and F_0= 1200 N. It corresponds to an individual with $A = 2$.

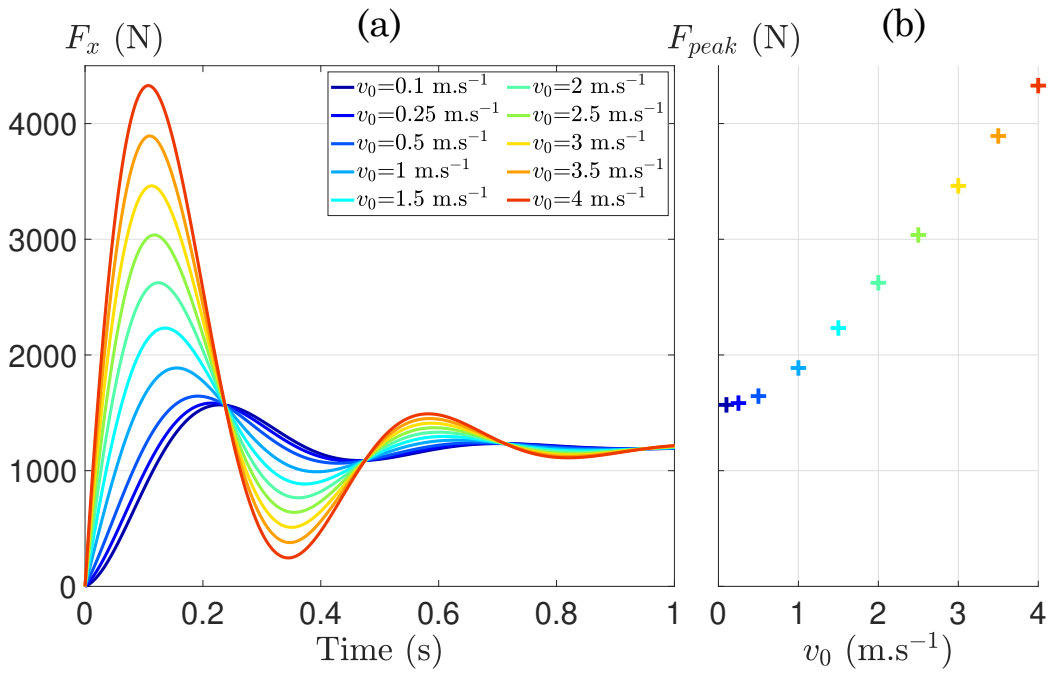


Figure 3.10: Influence of v_0 on the compression force determined with the mechanical model of Figure 3.8. The set of parameters used are m =100 kg, k=2 $\times 10^4$ N.m^{-1}, β=1 $\times 10^3$ kg.s^{-1} and F_0= 1200 N. (a) Evolution of the compression force signal for v_0 from 0.1 m.s^{-}1 to 4 m.s^{-}1. (b) F_{peak} as a function of v_0 corresponding to the force curves on the left.

In Figure 3.10b, for engagement speeds $v_0 > 1$ m.s^{-1}, we observe a linear behavior of F_{peak} with v_0 for an individual. With this set of parameters in the model, we obtain a plateau of F_{peak} at lower impact velocities that we did not see in Figure 4.6 because the subject did not impact the scrum machine for velocities lower than 1 m.s^{-}1.
We also see that v_0 influences the damping of oscillations: the larger v_0, the larger the number of oscillations is. So, referee's calls that tend to reduce the engagement speeds are

also reducing the rebound effect after impact and this probably helps to protect the front row players.

Analytical solutions

The equation (3.7) is analytically solvable and the analytical form changes with A. All the experimental data of impacts show a peak force and then the signal is stabilizing around F_0. This shape of the signal corresponds to a pseudo-periodic solution, and it is achieved for $A > 0.25$. The dimensionless compression force $\overline{F}$ is then written as:

$$\overline{F} = 1 + \exp\left(-\frac{\overline{t}}{2A}\right)\left(-\cos(\overline{\omega}\overline{t}) + \frac{2A\dot{\overline{F}}_0 - 1}{2A\overline{\omega}}\sin(\overline{\omega}\overline{t})\right) \tag{3.9}$$

with $\overline{\omega} = \frac{4A-1}{2A}$. We can write this expression with all the mechanical parameters and the initial speed v_0 and the expression of the compression force is

$$F(t) = F_0\left[\exp\left(-\frac{\beta}{2m}t\right)\left(-\cos(\omega t) + \frac{kv_0 - \frac{\beta F_0}{2m}}{F_0\omega}\sin(\omega t)\right) + 1\right] \tag{3.10}$$

with $\omega = \dfrac{\sqrt{4mk - \beta^2}}{2m}$.

3.2.3 Parameters determination

For the different parameters, we build an abacus in which exists a single path for a value of A (A and β identification), and then we determine the last parameters with knowing the A value (k and m identification). We are going to apply the methodology to the force signal of subject A presented in Figure 3.5.

Identification of A

The first step consists in searching A value in the plane $\left(\frac{t_{reb}-t_0}{t_{peak}-t_0}, \frac{F_{peak}}{F_{reb}}\right)$. This abacus is plotted thanks to numerical simulation in Figure 3.11.

For our example, we have F_0=1250 N, F_{peak}=3550 N, F_{reb}=1037 N, $t_{peak} - t_0$=0.065 s, $t_{reb} - t_0$=0.245 s. t_0 and all the other parameters are defined in Figure 3.5. In Figure 3.11, the graph enables us to determine the parameter A corresponding to $\frac{t_{reb}-t_0}{t_{peak}-t_0} = 3.77$ and $\frac{F_{peak}}{F_{reb}} = 3.42$. In this case, we obtain $A = 0.73$.

Identification of β, k and m

We then go in the plane $\left(\dot{\overline{F}}_0, \frac{F_{peak}}{F_0}\right)$ to determine the value of β. The abacus is presented in Figure 3.12. The intersection between the value of the ratio $\frac{F_{peak}}{F_0}$ and the curve corresponding to the previously determined value of A gives us the value of the initial derivative $\dot{\overline{F}}(0) = \dot{\overline{F}}_0$. In our example, we have $\frac{F_{peak}}{F_0} \simeq 2.8$.

Then, we obtain $\beta = \frac{F_0\dot{\overline{F}}(0)}{v_0}$ with $v_0 = 2.2$ m.s^{-1}. So, $\beta = 3.18 \times 10^3$ kg.s^{-1}.

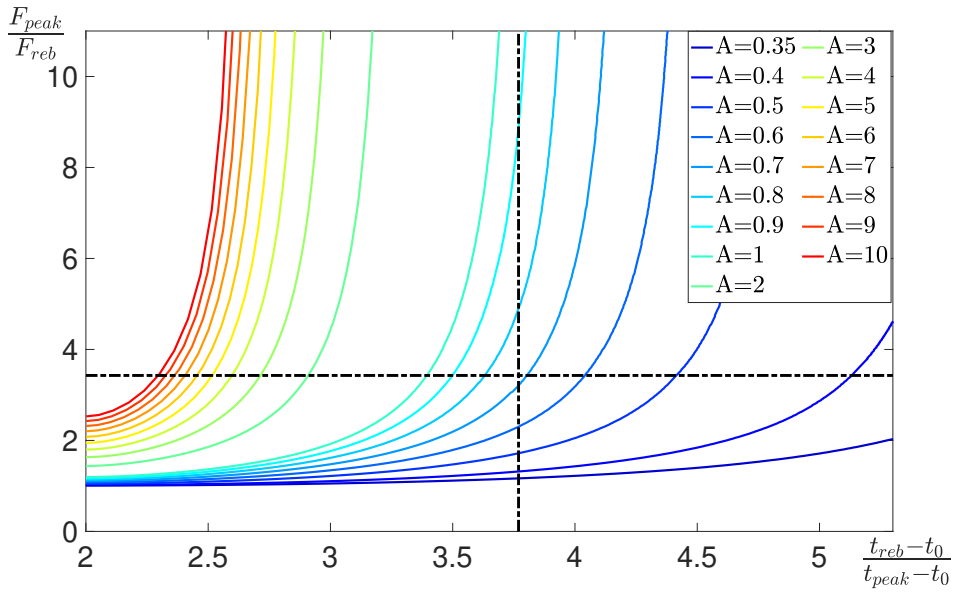


Figure 3.11: Abacus for the determination of A. For the example of Figure 3.5, we have $\frac{t_{reb}-t_0}{t_{peak}-t_0} \simeq 3.77$ and $\frac{F_{peak}}{F_{reb}} \simeq 3.42$. It gives us A=0.73.

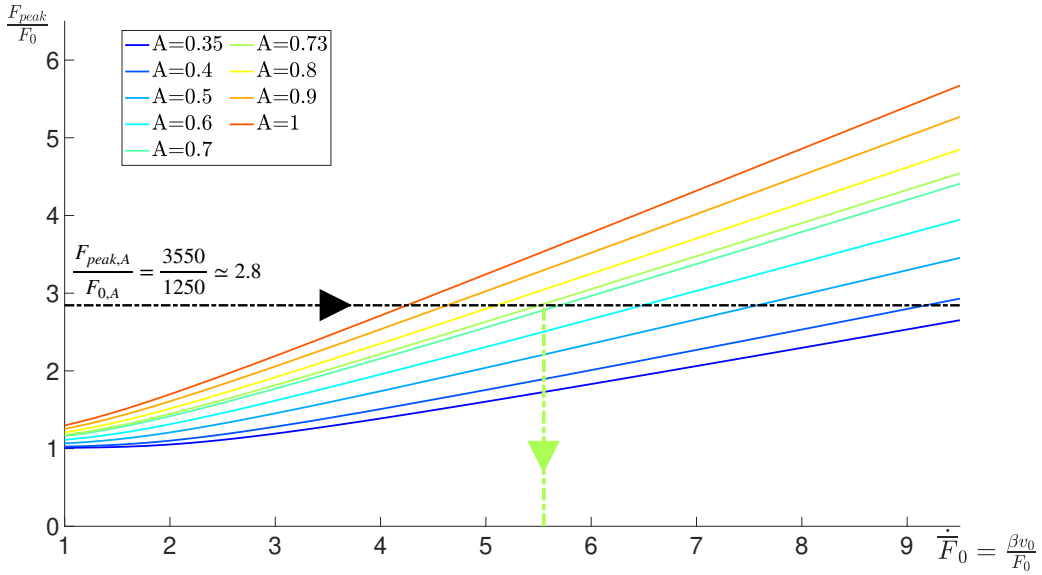


Figure 3.12: Abacus for the determination of β. We have $\frac{F_{peak}}{F_0} = 2.84$ and it intersects the curve $A = 0.73$ in $\dot{\overline{F}}(0) = 5.6$.

We identify k by searching in Figure 3.13 the intersection between the line at $\dot{\overline{F}}_0$ and the corresponding curve $\frac{kt_{reb}}{\beta}$ and $\frac{kt_{peak}}{\beta}$ for $A = 0.73$. The dashed colored lines correspond to the $\frac{kt_{reb}}{\beta}$ curves as a function of $\dot{\overline{F}}_0$. The solid colored lines correspond to the $\frac{kt_{peak}}{\beta}$ curves

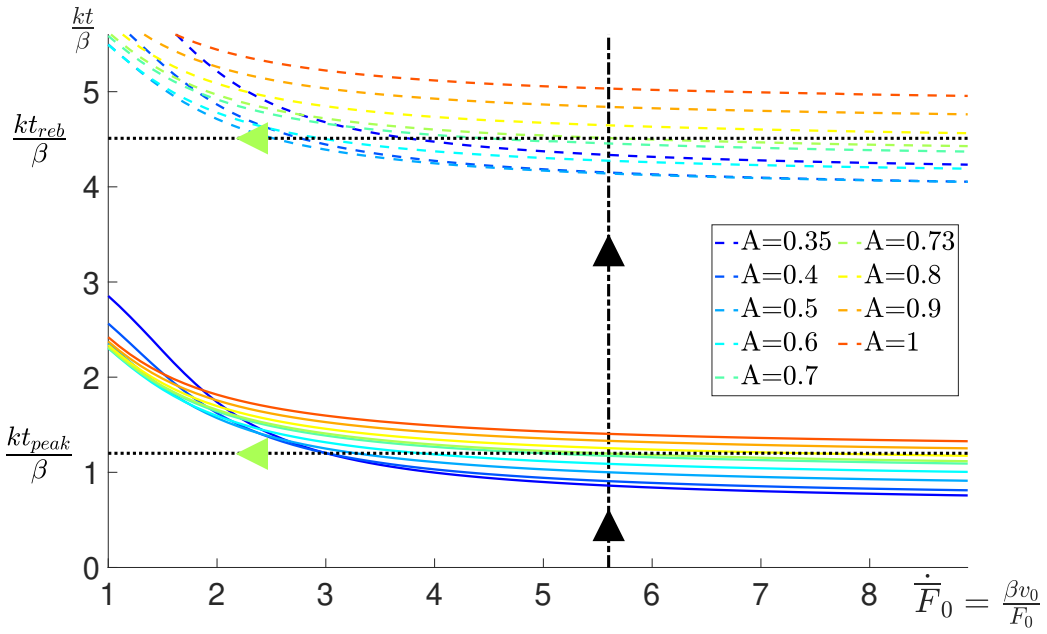


Figure 3.13: Graphic identification of k. With $\dot{\overline{F}}(0) = 5.6$, the intersection with the curves corresponding to $A = 0.73$ gives $\frac{kt_{reb}}{\beta} = 4.51$ and $\frac{kt_{peak}}{\beta} = 1.20$.

as a function of $\dot{\overline{F}}_0$. For subject A, we have $\dot{\overline{F}}_0 = 5.6$. The intersections are represented with dashed black lines. By following the green arrows, we determine $\frac{kt_{peak}}{\beta} \simeq 1.2$ and $\frac{kt_{reb}}{\beta} \simeq 4.51$. We finally obtain $k \simeq 5.9 \times 10^4$ N.m^{-1}.

The last step is to identify m using equation (3.6) where $m = \frac{\beta^2 A}{k}$. For our example we obtain $m = 125$ kg. This mass is an effective mass, it has to be understood as an equivalent mass that generates this peak force for all the set parameters determined before. For this example, it is higher than the player mass of $m_{tot} = 99$ kg.

3.2.4 Experimental and model comparison

In Figure 3.14a, we compare the experimental and model results for subject A. We use the set of parameters that we previously determined. The experimental curve is represented with a blue solid line and the model curve is represented with an orange solid line.

The result is quite satisfying with a good agreement for F_{peak} and F_{reb}. We notice that t_{reb} is slightly overestimated.
Figures 3.14b and c show the same results for subject B and subject E respectively. The parameters of the model obtained for these subjects can be found in Table 3.2. The agreement between the experiment and model is also good in terms of F_{peak} and F_{reb}. In Figure 3.14b, we see that the rise of force is quite different. t_0 is determined in order to have a good experiment/model agreement of F_{peak} and F_{reb}. We still note a little bump on the experimental curve before the t_0 model in Figures 3.14a and c. We believe that this phenomenon is related to the deformation of the M-Rex foams at the impact that we neglect in our mechanical model.

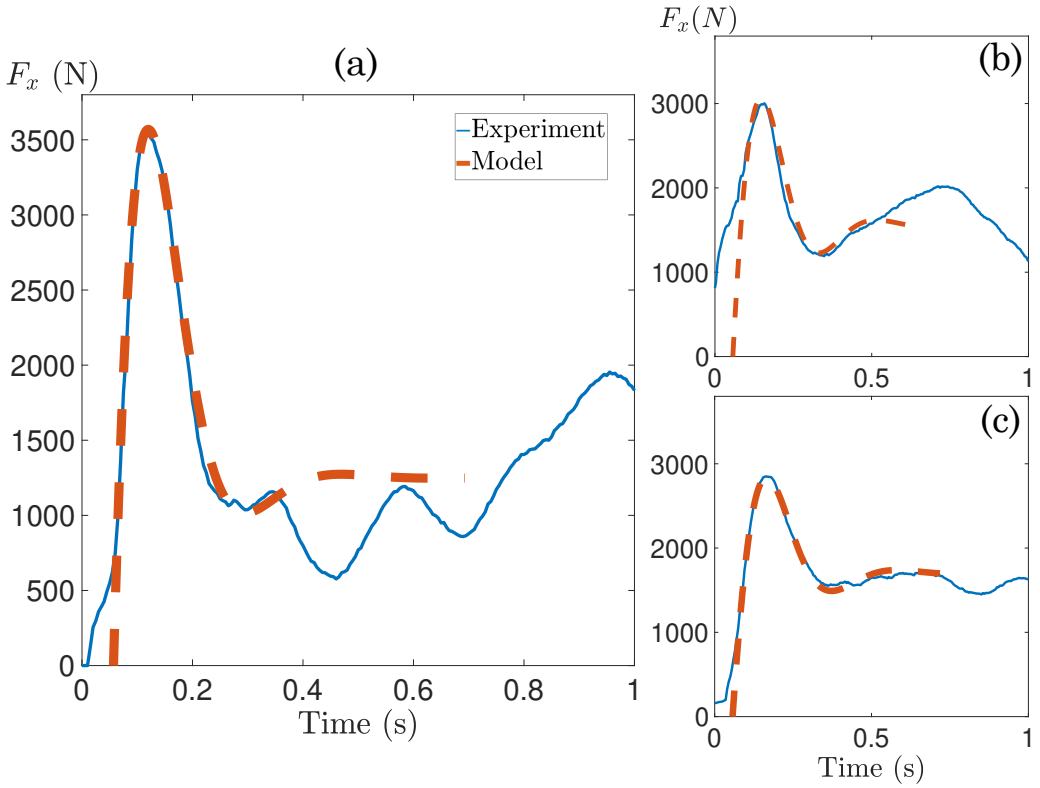


Figure 3.14: Experiment and model comparison for the curves of subjects A, B, and E presented in Figure 3.1. The experimental data is represented with a solid blue line and the model result is plotted in a dashed orange line. The parameters used in the model are collected in Table 3.2. The mass and the engagement speed corresponding to each trial could be found in Table 3.1. (a) Comparison for subject A. (b) Comparison for subject B. (c) Comparison for subject E.

3.3 Pusher Phase Space

3.3.1 Parameters identification for the different subjects

We apply the previous method to the different signals of subjects A to F. Table 3.2 gathers the values of the parameters identified on those signals.

Subject	Position	m_{tot} (kg)	F_0 (N)	m (kg)	k (N.m^{-1})	β (kg.s^{-1})	A
A	H	99	1250	125	5.9×10^4	3.2×10^3	0.73
B	H	116	1550	190	6.9×10^4	3.2×10^3	1.28
C	LP	116	1500	40	3.4×10^4	1.1×10^3	1.23
D	TP	143	1650	61	5.1×10^4	1.3×10^3	1.46
E	L	147	1700	166	4.9×10^4	2.7×10^3	1.11
F (Imp. 1)		75	1000	36	2.1×10^4	5.6×10^2	2.43
F (Imp. 2)		75	1050	34	1.8×10^4	4.0×10^2	3.74

Table 3.2: Model results for six professional players of Racing 92 and one novice player. The mass of the player is called m_{tot}.

In terms of order of magnitude, we note that all professional players have similar results for model parameters (F_0, m, k, β). We also note that for both novice trials, the order of magnitude of parameters is similar.

For professional players (from A to E), we have $\beta_{mean,pro} = (2.3 \pm 0.9) \times 10^3$ kg.s^{-1} which is five times higher than for subject F with $\beta_{mean,novice} = (4.8 \pm 1.1) \times 10^2$ kg.s^{-1}. We also have $\frac{k_{mean,pro}}{k_{mean,novice}} = 3$. Then, we notice that there are important variations in m values inside professional players (from 40 to 190 kg) but it is stable for both novice trials. Furthermore, we see that m_{tot} and F_0 seem linearly correlated (Pearson's correlation coefficient $R^2 = 0.83$, novice and professional data together): the heavier the player, the higher the mass m is.
Finally, it seems that professional players obtain values of the parameter A around 1. For subject F, both impacts give higher $A_{mean,F} \sim 2A_{mean,pro}$.

3.3.2 Phase plane

To characterize the players, we chose two parameters: A and $F_0 + mg$. The parameter A reflects the quality of the impact: a low A shows the ability to quickly damp the oscillations towards F_0.
The goal of an impact is also to produce maximum force in a scrum in order to win the position battle. The quantity $F_0 + mg$, where F_0 is linearly correlated to m_{tot} and mg is an equivalent weight engaged in the impact obtained with the mass of the model m, seems to reflect the force production of an impact.

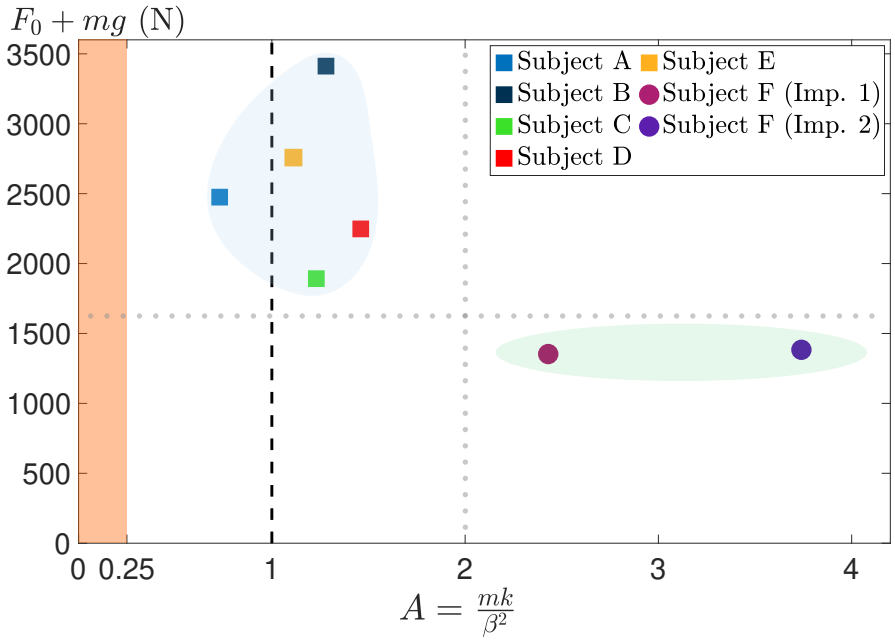


Figure 3.15: Pusher phase plane $(A, F_0 + mg)$. The orange zone is delimiting the aperiodic zone for $A < 0.25$. The professional results and the novice results form two distinct groups in the phase plane.

In Figure 3.15, we plot the different results of Table 3.2 in the plane $(A, F_0 + mg)$ with filled squares and circles. The squares correspond to the impact of subjects A to E. The circles correspond to the two impacts of subject F. The orange zone represents the values of $A < 0.25$ corresponding to the aperiodic regime.

We see that professional players form a group of low $A \sim 1$ and high forces $F0 + mg \sim 2000 - 3500$ N. The novice subject F has lower $F_0 + mg \sim 1400$ N and obtains higher values of $A \sim 3$. The gray dashed lines separate the phase plane into four zones. The

players can damp their oscillations of force better than the novice, but they also put more force in their impacts than the novice. It corresponds to the more significant F_{peak} reached by the professional players than the one reached by the novice at an equivalent speed (cf. subsection 3.1.5).
According to our model, it could be dangerous for a player to have high values of A: if $A \gg 1$, it implies that $mk \gg \beta$. In that case, it means that the player is not able to absorb the force engaged during the impact. This is why professional players train their core abilities, in particular the neck muscles, to improve their damping qualities.

3.4 Discussion on Physiological Application

3.4.1 Isometric neck force production

We have worked with the physical trainers of Racing 92 to link the physical parameters to physiological and athletic parameters that could explain the differences in performance. It seems that cervical rachis plays a predominant role in scrum force production [34, 35]. We thus decided to relate the parameter k, equivalent stiffness of the player, to core neck qualities.
To measure the cervical core, we have been inspired by studies on isometric[2] neck forces [36, 37, 38]. We develop our own experimental protocol (cf. Figure 3.16) to measure isometric forces in extension (cf. Figure 3.16a) and for lateral flexion (cf. Figure 3.16b). We chose to adopt a specific posture for the player close to the scrum posture. Then we chose to have a fixed dynamometer to measure our forces contrary to [36] where it is held by the physician.

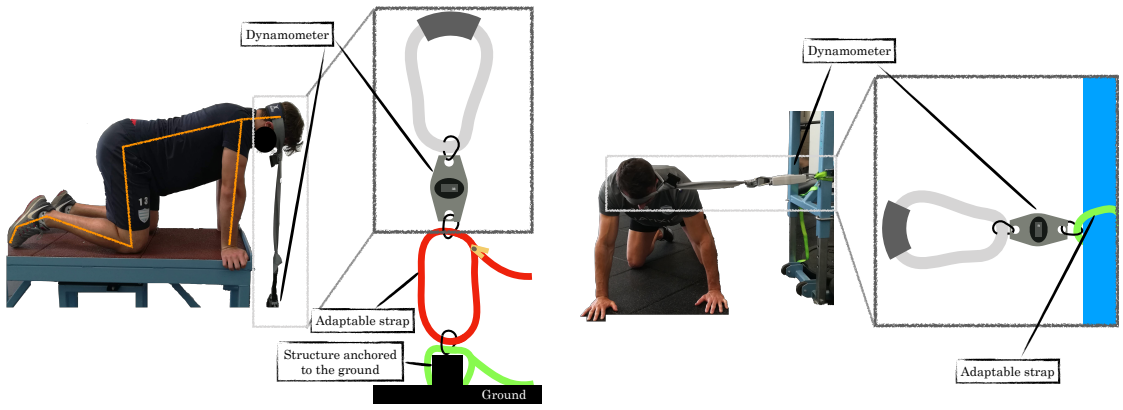
3.4.2 Experimental study

Protocol

We measure cervical forces of 48 professional players of Racing 92 (forwards and backs) with an average age of 24± 5 years.
The experimental setup is represented in Figure 3.16. For extension measurement, the dynamometer is linked to the ground and is stabilized by the force application of the player. We set the dynamometer height with straps in order that the player in a crouched posture can not move the head when he is applying maximal force. A picture and a scheme are presented in Figure 3.16a. In this position, players may be tempted to use their arms in order to produce force at the neck level. We specifically ask them to use their arms to stabilize themselves and not to produce force.
For lateral flexion measurements, we adapt the setup to fix it to a weight rack. The player is in a similar position but this time has to produce a force towards the right or left side of his head. The setup is built to adapt to the head height compared to the ground in Figure 3.16b.

On day one of the experiments, all the professional players do the extension experiments. During day two of the experiments, they do the right and left flexion measurements.
After a short warm-up, we ask the player to produce his maximal isometric force in extension and in right/left flexion for five seconds and we manually note the average maximal

[2]Length of the muscle does not change during the force production, it corresponds to a static situation



(a) **(b)**

Figure 3.16: Experimental setups for measuring neck isometric forces. (a) Neck extension force measurement setup. The player in a crouched position applies isometric extension force that we measure with a dynamometer. (b) Lateral flexion experimental setup.

force with a dynamometer whose precision is ±20 N. Each player does each measurement once. The experimental sessions are integrated into a weight-training session for the professional group. Unfortunately, these experimental sessions were realized two years after the experimental study previously presented in this Chapter. Subjects A, B, C, D, and E were no longer players of Racing 92 during the measurement of cervical forces.
The subject F introduced in subsection 3.1.4 also does this experimental protocol for comparison by playing level.

Results

In Table 3.3, we summarize results obtained with the setup of 3.16a for the different professional players of Racing 92 and also for the novice player.

	F_{up} (N)	N
All	392±69	48
Forwards	451±108	28
Backs	314±49	20
First row	510±98	14
Second/Third row	382±69	14
Novice	206	1

Table 3.3: Isometric neck force in extension. N is the number of players in the group.

Results for lateral flexion obtained with setup of Figure 3.16b are gathered in Table3.4. F_R stands for the right flexion and F_L stands for the left flexion.

3.4.3 Discussion

As expected, we observe forward players have a greater extension F_{up} and lateral flexion F_R, F_L forces than backs. Furthermore, first-row strengths are more important than second/third-row results. It is corroborated by the role they play in the scrum. Indeed, the work in cervical extension is omnipresent during the fight between the first lines of each pack. This could explain the huge difference of 130 N between the first rows and other forwards in extension.

	F_L (N)	F_R (N)	N
All	314±69	314±78	45
Forwards	353±59	363±59	28
Backs	255±29	255±39	17
First row	382±59	382±69	14
Second Row	363±10	372±20	4
Third Row	314±49	323±49	10
Second/Third Row	323±49	333±49	14
Novice	196	206	1

Table 3.4: Isometric neck force in lateral flexion.

Moreover, we would like to specify that on average tighthead props produced the highest neck forces (extension and lateral flexion). As we mentioned in Chapter 1.2.3, the tighthead props have to fight with two opponents in front of them, just with the help of a teammate on their left. Then, although the second rows have F_{up} that are on average lower than those of the first rows when we look at those measured in lateral flexion, we see that the values obtained are close to the first-row average because they are similar to those of the hookers and left-handed props, but lower than the tighthead props. Again, this may be related to the role in the scrum: second rows find their heads wedged between the buttocks of two front rows players. So, they have to endure significant transversal forces during a complete scrum.
All those results confirm tendencies observed in the literature [36, 37, 38]. But, we can not compare absolute values obtained in these articles because of the different experimental protocols (posture of the player, measuring device).

We can not conclude about impact model parameters results and isometric neck forces comparison between professional players due to a lack of common data. But, we can qualitatively compare the professional results of the first-row players and the novice. We notice in Table 3.16a that extension forces of the first rows are 2.5 higher than the novice performance. We remind that the k ratio between professional and novice obtained in 3.3.1 is equal to 3. The player's stiffness during impact and measurements of neck forces could be linked but we need further work to investigate this relationship and to see if these impact experiments could be a way to evaluate the core qualities of the cervicals.

3.5 Perspectives: Collective Force Signal

To simplify the study, we conducted experiments at the individual scale rather than the collective one in order to avoid the problems of synchronization between players and other collective effects which are complicated parameters to integrate into a simple mechanical model.

Nevertheless, it would be interesting to apply the method developed in this chapter on collective signals to quantify the quality of the impact of a pack. When we try to apply the same method to the pack, the results are not satisfying and do not fit correctly because a collective impact is far more complicated than an individual one.
Indeed, when we have collective trials, they are some problems with synchronization between players. As we see in Figure 3.17a, a complete pack applies a compression force on

the M-Rex scrum machine. In Figure 3.17b, we present the time evolution of the compression peak force F_x. We observe that $F_{peak} \sim 12$ kN, then the force drops to 6-7 kN. We decompose the forces measured by each force sensor (cf. subsection 3.1.3) and we notice the desynchronization of $F_{A,x}$, $F_{B,x}$ and $F_{C,x}$, as the maximum of force is not reached at the same moment on the three sensors.

The complexity of applying an equivalent model to this situation comes from the distribution of force sensors. Indeed, for individual cases, the forces measured on two forces sensors correspond to the forces produced by the single player. But, for collective trials, as we measure forces felt by each of the opponents, the force measured on one force sensor is not equivalent to the force produced-transmitted by one of the first-row players. For example, on sensor B, we do not know part of $F_{B,x}$ transmitted by the hooker and the one transmitted by the tighthead prop.

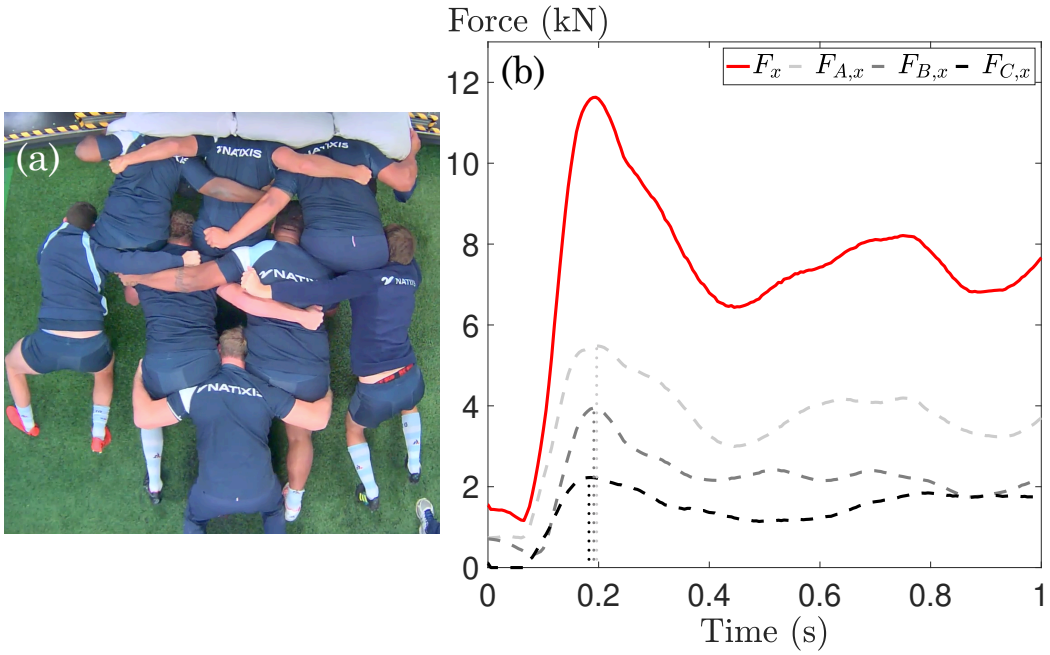


Figure 3.17: Example of a collective force signal for a professional pack of Racing 92 of mass m_{pack}=937 kg.

Nevertheless, it would be possible to develop a model with as many model cells (presented in Figure 3.8) as there are players in the pack. The challenge of developing such a model is to find how to link between them the different cells to account for inter-player bindings and random desynchronization. It would be possible then to construct an equivalent phase plane as Figure 3.15 but for collective trials and compare the results of professional players with amateur players.

Take home message of Chapter 3

1. Quality of a single player impact. On a known scrum machine, we built an experimental protocol to individually characterize players with a minimal physical model. A single parameter A reflects the stabilizing quality of an impact, and we build a phase plane to take into account the force level of this impact.

2. Isometric neck forces Cervical core qualities may be related to our parameter k. Further studies need to be conducted.

3. Extension of the model We can modify the model to adapt it to collective trials by disposing of several physical cells connected. In addition, we can imagine completing the Hill-modified model to simulate the second phase of a pushing force signal. It may be interesting to understand the muscles' activation time needed to reach the plateau force of the individual sustained force.

4

Influence of the Scrum Machine

Measuring the force impacts during scrums requires to use an instrumented scrum machine. In this chapter, we focus on the different properties of these scrum machines. we show that the peak force value at impact depends on the impactor but also the impacted.



Picture of a training session with a scrum machine in Milton High School (Bulawayo, Zimbabwe) in 1978. Extracted from [39].

Contents

4.1	Evolution of the Scrum Machine used in Literature	**48**
4.2	Scrum machine Characteristics	**49**
4.3	Scrum Machine Influence on F_{peak}	**53**
4.4	Scrum Machine Influence on the Determination of A	**56**

This work has been done with Caroline Cohen, and Christophe Clanet thanks to a collaboration with Julien Piscione and Olivier Chaplain.

4.1 Evolution of the Scrum Machine used in Literature

Through the history of impact evolution in Chapter 2.2, we saw that the two key parameters influencing F_{peak} are the mass m_{pack} and the engagement speed v_0. These parameters are related to the impactor, but we are going to see in this chapter that the scrum machine or the pack impacted also influences the values of the impact force F_{peak} and its width τ (cf. Figure 2.1).
In the literature, most of the studies use scrum machines instrumented with force sensors in order to measure the compression forces, and also the vertical and transverse components [40, 32, 21]. Previously, we gave F_{peak} values measured in two different studies (cf. Table 2.1) that used very different scrum machines.
Figure 4.1a presents the pictures of the scrum machine used by Milburn *et al.* in [21] viewed from the side (left) and the top (right). In Figure 4.1b, we have pictures (side-views and top-view) of the scrum machine used by Preatoni *et al.* in [32]. We specify the direction of the compression axis with a red arrow on each picture.

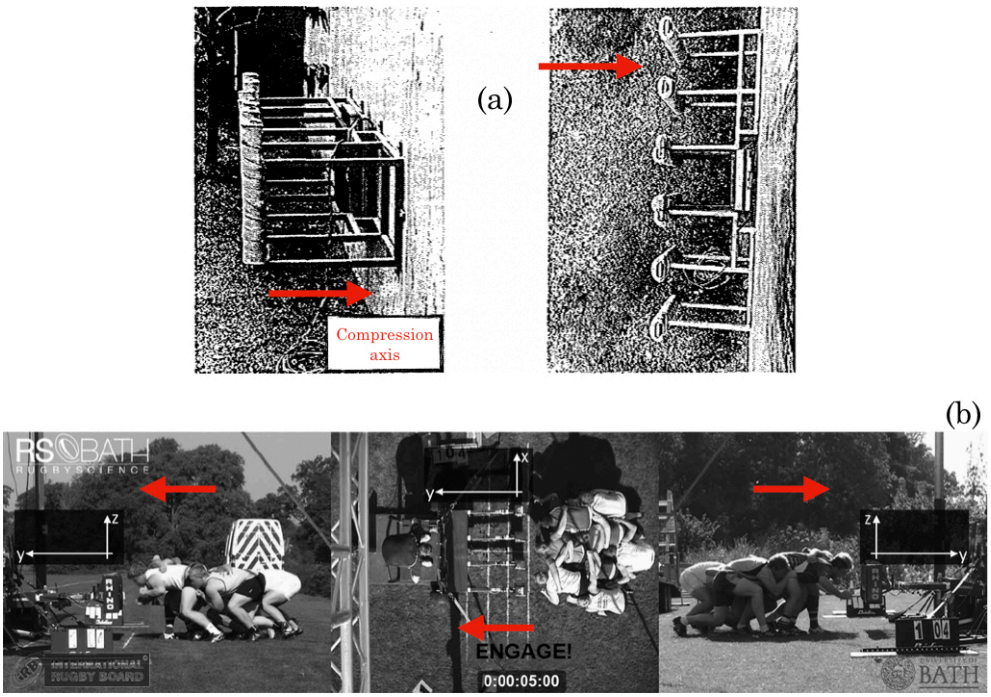


Figure 4.1: Evolution of scrum machine used in experimental studies. (a) Picture of the instrumented scrum machine of [21] in 1990. (b) Figure presenting the scrum machine used in [32] in 2013.

We clearly see that the scrum machines do not have the same geometry and that players were not pushing at the same heights. The scrum machine foams seem also different and more ergonomic in the modern version. The common point of these two experimental setups is the sampling frequency $f_e = 500$ Hz they used to measure the forces. We have based our previous comments on studies where this sampling frequency was high enough to study the impact force. For example, Quarrie *et al.* measured $F - peak$ values using a sampling frequency of 20 Hz to record the force. We saw in Figure 2.1 that the typical time τ of an impact is of the order of magnitude of 0.3 s, which means that they have approximately 6 points to describe the impact force signal. This is not enough to have a confident F_{peak} value.

4.2 Scrum machine Characteristics

In Chapter 3, we use the M-Rex scrum machine of the French Federation of Rugby (cf. Figure 3.2). We decide to characterize the scrum machine in order to understand the influence it has on the force measured during impact.

4.2.1 Foams Young Modulus

The first component to characterize is the one in direct contact with the players: the foams of the mannequins. We characterize them with a quasi-static force-deformation experiment. Foam mechanics is a complex domain. A lot of studies are focusing on quasi-static and dynamic stress-strain curves of polyurethane, which is the most common type of foam [41, 42, 43, 44]. Mane *et al.* [44] perform uni-axial compression experiments at quasi-static and dynamic rates on a cubic sample of polyurethane foam presented in Figure 4.2a. Del Piero *et al.* [41] perform similar experiments on a sample of polyurethane foam. In Figure 4.2c, we present the pictures of the load frame that applies the force on the sample of foam presented with chronophotography of the compression. Figures 4.2b and d show the stress-strain curves obtained experimentally. The stress is the force by the initial area of contact with the load frame, the strain is equal to the ratio between the length of compression and the resting length of the foam.

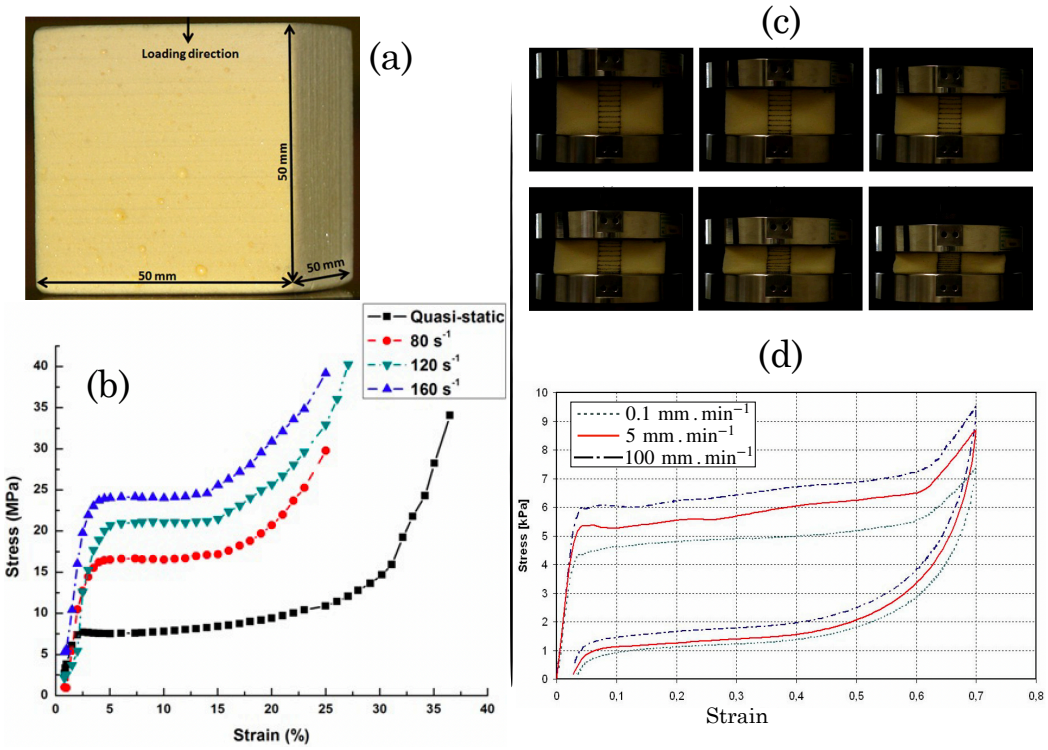


Figure 4.2: Stress-strain curves of polyurethane foams at quasi-static and dynamic rates of compression. (a) Sample of foam studied in [44]. (b) Stress-strain curves obtained at different speeds of compression. Extracted from [44]. (c) Experimental setup used in [41]. (b) Stress-strain curves obtained at different speeds of compression. Extracted from [41].

Thus, we extract two main results from these curves:

- the stress-strain curve depends on the speed of compression of the foam. At an equivalent strain, the stress increases with the speed of compression. So, polyurethane foams have viscoelastic behavior.
- the stress-strain curves always have a similar shape with a first elastic regime for small stresses ($< 4\%$) and then, the curves show a plateau of stress for higher strains.

The foam used in the M-Rex mannequins is likely to be polyurethane foam. And we focus here on their main elastic property.
Moreover, their behavior becomes even more complex when we study the dynamical response of foam to an impact [45, 46, 47]. And for the record, the excellent energy-absorbing properties of polyurethane foams are used to develop impact limiters [48], in particular, in Rugby Union, it is used to develop helmets to protect the players' heads during impacts [49, 50].

The experimental setup we use to quantify the elastic property of the M-Rex foam is presented with a top view picture in Figure 4.3b and a side view scheme in Figure 4.3c. We attach wooden plates (represented in brown) to an S-shape load cell (represented in gray and red) in order to apply manually a force F on mannequin B with a constant contact surface S. This force is applied perpendicularly. The rest length of the mannequin is called l_0 and is approximately equal to 20 cm. Thanks to a high-speed camera set at 50 frames per second (fps) we measure on a side-view video the displacement of the wooden plate Δl represented in Figure 4.3c. The sensor is placed in contact with the foam at its rest length l_0 without applying any force for the initial position. We select a line of pixels on the video capture along the force direction on Fiji [1] in order to determine the time evolution of Δl. We call this process a reslice. The reference length we used to calibrate images is the width of the wooden plate.

After data analysis, we plot the force measured by the sensor as a function of the displacement measured on the videos. This graph is shown in Figure 4.3a. It represents the force evolution during two cycles of compression-decompression of the foam with the experimental setup we described. It seems that exists a hysteresis, namely a different path followed by the curve when sinking and retracting from the foam.
We define the strain ϵ as the ratio of the variation of the size of the foam Δl and the resting length l_0:

$$\epsilon = \frac{\Delta l}{l_0}. \tag{4.1}$$

We see in Figure 4.3 that we reach a maximal deformation of $\Delta l \simeq 5$ cm, which means a maximal strain $\epsilon_{max} \simeq 0.25$. We will simplify the analysis of this result by assuming an elastic behavior of the foam in this regime. This is a strong hypothesis according to the literature [41, 42, 43, 44]. In other words, we imagine foams act like an effective spring characterized by a stiffness k_{foam}.
The link between force F needed to compress or extend the spring and its elongation Δl is the spring stiffness (in our case k_{foam}) and is described by Hooke's law:

$$F = k_{foam}\Delta l. \tag{4.2}$$

We observe in Figure 4.3 that the best linear fit leads to $k_{foam} \sim 1.1 \times 10^4$ N.m^{-1}. This strong approximation consists in neglecting the hysteresis and taking a mean value of F when sinking and retracting from the foam.

[1] `https://fiji.sc/`

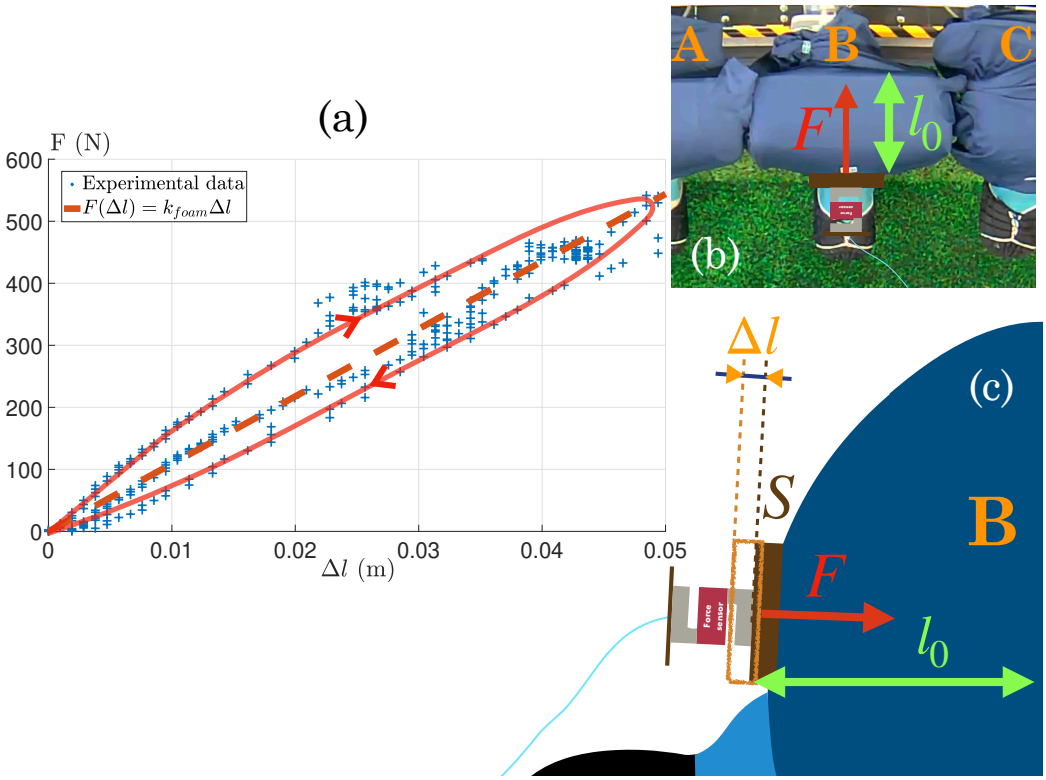


Figure 4.3: Determination of stress-strain curve of M-Rex foams. (a) Force as a function of the length of compression Δl. (b) Top-view of the experimental setup with the load cell with which we apply F on the mannequin B which has a rest length l_0. (c) Side-view scheme of the experimental setup with the red load cell of contact surface S (considered constant).

Hooke's law is often written in terms of stress $\sigma = \frac{F}{S}$- in Pascal with cross-sectional area S- and strain ϵ -we defined in the previous paragraph. With these notations, Hooke's law is expressed as

$$\sigma = E\epsilon, \tag{4.3}$$

with E the Young modulus in Pa. The Young modulus of an elastic solid reflects its ability to withstand compression or elongation with respect to its length.
Then, from equation (4.3), we obtain

$$E = \frac{k_{foam} l_0}{S} \tag{4.4}$$

to determine the Young modulus of the material of $E \simeq 0.22$ MPa. It is complicated to compare with an existing Young modulus of foams in their linear regimes because we made the strong assumption of linear behavior until a strain of 25%. But the order of magnitude of Young modulus for polyurethane foams varies from 0.1 MPa for a low-density foam ($d = 0.09$ g.cm^{-3}) to 15-150 MPa for higher density foams ($d = 0.16 - 0.32$ g.cm^{-3}) [51].

4.2.2 Force-displacement relationship depending on axial stiffnesses

In passive mode, it is possible to set the resistance of the M-Rex in the three directions of space. We decide to characterize the x-axis resistance, which corresponds to the compression axis. Here, the scrum machine is passive, and the resistances of y and z axes are fixed.
Thanks to the numerical control, we test three different stiffnesses- k_{10},k_{20} and k_{61}- along the x-axis and try to determine their physical values with a simple experimental protocol.

We manually push the central mannequin along the x-axis. We try to push with a constant force for 3 seconds and repeat the operation several times. We plot the measured force F_x (sensor B) and the displacement also measured by M-Rex along x and which we call ΔX. The results are plotted in Figure 4.4 increasing equivalent stiffness k from Figure 4.4a to c.

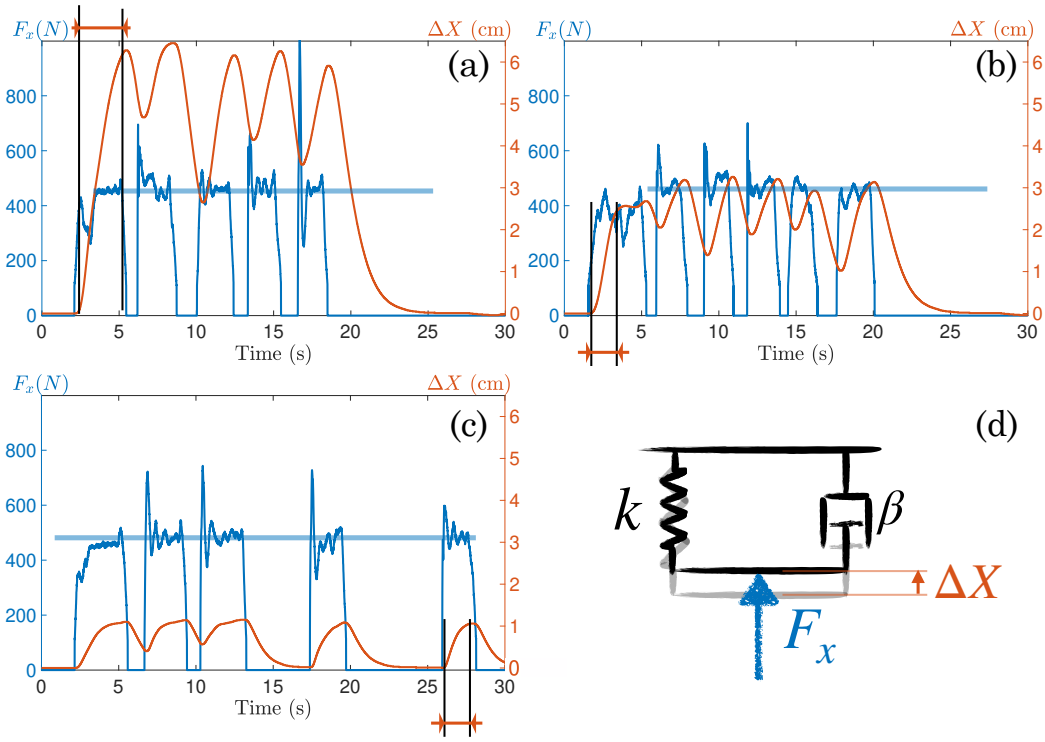


Figure 4.4: Force applied on the scrum machine in blue and corresponding displacement ΔX for different settings of stiffness. (a) Curves corresponding to k_{10}. (b) Curves corresponding to k_{20}. (c) Curves corresponding to k_{61}. (d) Minimal physical 1D model of the M-Rex scrum machine along the x-axis.

First, one can observe that the higher the stiffness, the lower the displacement in the plateau regime is. Secondly, it exists a time delay between the applied force and the displacement which corresponds to a damping effect. We thus learn that the scrum machine has a viscoelastic behavior and the force F_x could be written as

$$F_x = k\Delta X + \beta\Delta\dot{X} \tag{4.5}$$

with k the equivalent stiffness and β the equivalent viscosity.
In quasi-static approximation, we can approximate the different stiffness values by considering the mean plateau force and the displacement reached at the end of this plateau force. By using Hooke's relation introduced previously with equation (4.2), we obtain an equivalent stiffness k by dividing the plateau force by the maximum ΔX. We get respectively $k_{10} = 7.5 \times 10^3$ N.m^{-1}, $k_{20} = 1.5 \times 10^4$ N.m^{-1}, and $k_{61} = 4.4 \times 10^4$ N.m^{-1} for Figures 4.4a, b, and c. We used the equivalent quasi-static stiffness of $k_{61} = 4.4 \times 10^4$ N.m^{-1} in the experiments conducted in Chapter 3 (cf. subsection 4.2).
If we consider the complete viscoelastic behavior of the scrum machine as represented in Figure 4.4d, then we can approximate the β value by looking at the rise times represented with orange arrows and black lines in Figures 4.4a,b and c. Indeed, the displacement signals can be assimilated to a step response (constant force F_x) of a first-order system (cf. equation (4.5)). Then, the rise time T scales as $\frac{\beta}{k}$, and the displacement plateau is reached after $3T$.

For example, in Figure 4.4b, we have $3T \simeq 2.1$ s, which implies an order of magnitude of $\beta_{20} \sim 1 \times 10^4$ kg.s^{-1}. In the same way, we obtain $\beta_{10} \sim 8 \times 10^3$ kg.s^{-1} and $\beta_{61} \sim 2.5 \times 10^4$ kg.s^{-1}. The force signals are not optimal to determine the viscous coefficient, it would have been better to have a single push with a constant force F_x to have a clear rise time and a constant ΔX signal.

4.3 Scrum Machine Influence on F_{peak}

4.3.1 Relationship between v_0 and F_{peak} on M-Rex

We ask subject F of Chapter 3 to impact individually on the M-rex scrum machine as strongly as possible. The scrum machine is in passive mode with all the electric cylinders and the ground platform blocked (infinite stiffness). So, the impacts are only absorbed by the foams. The novice player has a mass of $m = 75$ kg (cf. Table 3.1) and does not practice Rugby Union at all.
The player is first adopting a crouched position, and he is asked to produce a maximal impact for different initial distances d_0 between his shoulders and the scrum machine. Thus, the engagement speed v_0 increases when d_0 increases: the player has more time to accelerate, and so he can reach higher velocities (cf. Chapter 2.2).
When a player hits the scrum machine -or the opponents- he undergoes a strong deceleration. Thus, the maximal speed before this deceleration is what we call the engagement speed v_0. We measure v_0 thanks to the top view camera set above the M-Rex. After some manual tracking comparisons, we saw that the speed of the shoulders and the speed of the center of mass of the trunk have similar dynamics and similar v_0. It was then easier to track the shoulder velocity with a reslice along the compression axis with the software Fiji. The sampling frequency of this fisheye camera is 25 fps, which is low to measure for high velocities.
In our experiments, the single-player engagement speed varies between 1 and 3 m.s^{-1}. Those values correspond to v_0 values measured in Milburn *et al.* [21] on a front-row impacting a scrum machine. They measured v_0 between 1 and 2 m.s^{-1}. In Preatoni *et al.*, they measured maximum engagement speed of 2.9 m.s^{-1} on their scrum machine for an international level pack in [32] (cf. Table 2.1).

For each trial, we measure F_{peak} the peak force on the pushing force signal $F_x(t)$ as defined in Figure 2.1. The results of F_{peak} in function of v_0 are presented in orange in Figure 4.7. We observe that the increase is almost linear with the engagement speed. The slope is approximately equal to 900 kg.s^{-1}.

4.3.2 Comparison with Racing 92 scrum machine

In this last part, we would like to highlight that impact force signals depend on the instrumented scrum machine used for the study.
We propose to compare the evolution of $F_{peak}(v_0)$ for the same player but on a different instrumented scrum machine.
We conduct the same experimental tests at the Racing 92 (R92) training center. We use a PREDATOR!® 65 Standard scrum machine[2] that has been instrumented by the start-up *Phyling*[3] with strain gauges to measure compression and vertical forces. In Figure 4.5a, we

[2] `https://www.rugbyscrummachines.co.uk/roller-machines/`
[3] `https://www.phyling.fr/`

detail the position of the four horizontal force sensors and the four vertical force sensors with a top-view scheme. We give a side-view scheme in Figure 4.5b where we see that this scrum machine is composed of two rollers that allow to be moved on the ground. To measure the forces, it is necessary to apply the brakes on each roller to prevent the machine from rolling on the ground.
F_x and F_z are acquired at a sampling frequency of 200 Hz. For each foams 1 and 2 of the scrum machine, we can measure compression and vertical forces. However, these measures are not independent due to the structure of the scrum machine which was not designed initially to measure pack efforts. Here, we ask the individual player to to his impact on the foam 1.

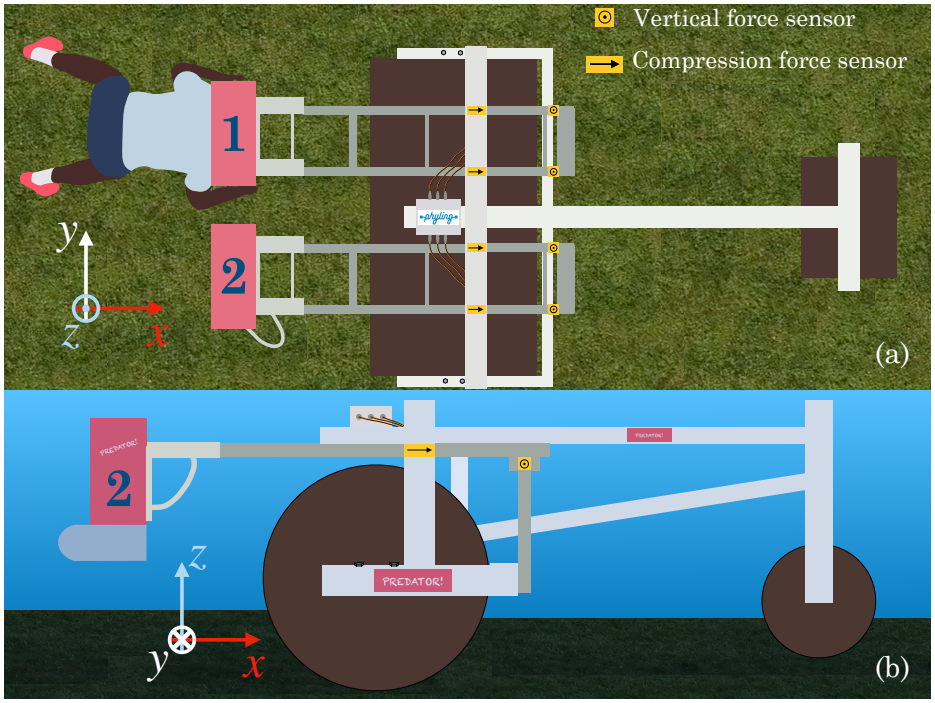


Figure 4.5: Racing 92 scrum machine instrumented by *Phyling*. The scrum machine is equipped with 4 horizontal force sensors that measure the horizontal pushing force F_x and 4 sensors that measure the vertical force F_z. (a) Top- view scheme. (b) Side-view scheme of the scrum machine.

Figure 4.6 shows a force signal measured with R92 scrum machine in blue. For the sake of comparison, we display on the same graph a force signal measured by the motionless M-Rex for the same player at a similar engagement speed v_0.

The shapes of the signals are unfortunately different. Force compression signals measured on the R92 scrum machine are thinner than impacts on the motionless "Atelier de la mêlée". In this example, we also observe that M-Rex foams seem to dampen more effectively with a pushing force that stabilize itself after 0.5 s and 0.7 s for M-Rex and R92 scrum machine respectively. The maximal forces are not the same with $F_{peak,R92}$ approximately equal to 2.5 kN with $v_0 = 1.5 \pm 0.1$ m.s^{-1} and $F_{peak,FFR} \simeq 1500$ N for an engagement speed of $v_0 = 1.3 \pm 0.1$ m.s^{-1}.
We finally notice that the stabilizing force value is similar for both measurement tools, around 1100 N.
With the same protocol as described at the beginning of this section, we obtain different values of F_{peak} (blue points) that are approximately 1.5 times higher than the one obtained with motionless M-Rex (orange points). The relation between v_0 and F_{peak}, shown in Figure 4.7, seems to be also linear but with a higher slope of approximately 2000 kg.s^{-1}.

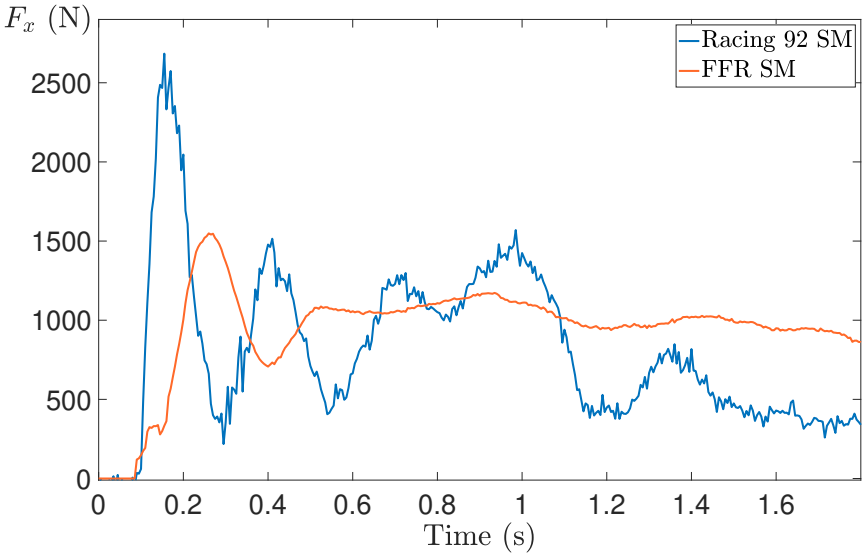


Figure 4.6: Two force signals examples with the same player at $v_0 = 1.3 \pm 0.1$ m.s^{-1} on FFR scrum machine and at $v_0 = 1.5 \pm 0.1$ m.s^{-1} on R92 scrum machine.

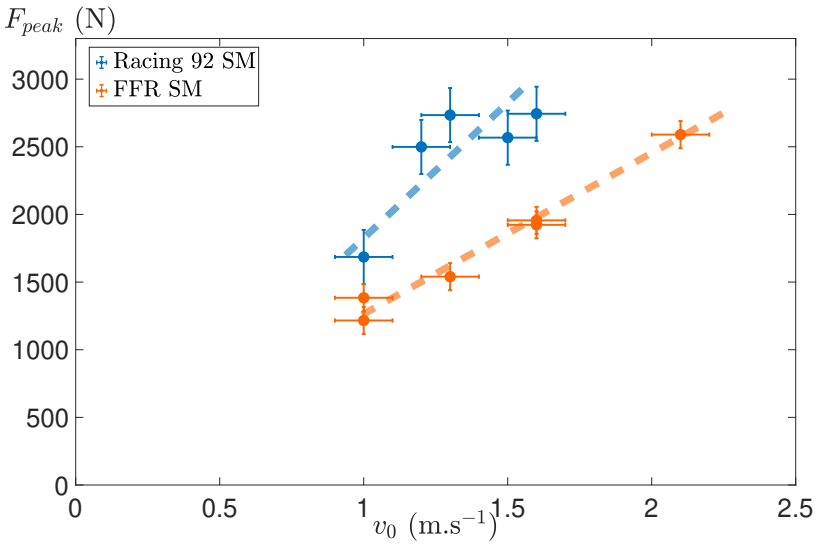


Figure 4.7: F_{peak} as a function of v_0 comparison between motionless M-Rex in Marcoussis and R92 scrum machine featured in figure 4.5.

We understand that the comparison between different studies about peak compression force using different scrum machine technologies and settings (foams, pistons, force sensor technology, sampling frequency) could be tricky. It is acceptable to see the evolution of the order of magnitude of impacts through the years because we know impact speeds are reduced with referee's calls change. But, we can not make fine deliveries of F_{peak} between two studies without considering the impact speed, the mass of the individual or pack, and knowing the characteristics of the measuring tool.

We finally observe that the impact depends also on the characteristics of what is impacted by the players. Thus, the peak compression force will certainly have different behavior on

live scrums compared to scrum machine experiments. In [27], the authors observe that peak compression forces from live scrummaging experiments do not have the same order of magnitudes as scrum machine experiments. For example, let us compare the peak compression forces for international-level packs studied in a live scrum experiment in Preatoni *et al.* [52]- where they measure the forces during impact with pressure mats sensors placed on the shoulders on the front rows of a pack- with another article of this team, but on a scrum machine in [32]. The mean masses of the packs, the engagement speed v_0 values, and the F_{peak} values are gathered in Table 4.1.

	Number of packs studied	Mean pack mass (kg)	Mean v_0 (m.s^{-1})	F_{peak} (kN)
Live scrum[52]	6	893 ± 17	2.7 ± 0.6	16.5 ± 1.4
Scrum machine [32]	5	887 ± 24	2.5 ± 0.3	9.3 ± 2.8

Table 4.1: Data comparison between two experiments with international level packs during engagement phase under CTPE referee's calls.

This table enhances the difference of magnitude in F_{peak} depending on the experimental setup. The differences can come from the sensors technology (pads on shoulders vs load cells behind foams), the difference in viscoelastic properties between humans and foams, and also from the difference in speed engagements processes. In one case, the pack is engaging against a motionless scrum machine. In the other one, two packs are engaging themselves towards each other with engagement speeds.

4.4 Scrum Machine Influence on the Determination of A

In this last section, we come back to the analysis of the signals of force during the impact that we made in Chapter 3 in order to see the influence of the settings of the scrum machine. Participant F did the same experimental protocol presented in subsection 3.1.4, but with different scrum machine settings. We ask him to impact the scrum machine at different v_0 and we block all the electric cylinders of the M-Rex. The foams are the only part of the scrum machine that absorb the impacts of subject F. We already presented in subsection 4.3.1 the relationship $F_{peak}(v_0)$ obtained for these experimental signals.
In Figure 4.8, we give three of the experimental curves obtained on the infinite scrum machine by subject F. The experimental curves are plotted in grayscale and the curves obtained with the mechanical model are represented with colored dashed lines. The results of the identification of the model parameters on the three experimental curves are gathered in Table 4.2.

Subject	v_0 (m.s^{-1})	m_{tot} (kg)	F_0 (N)	m (kg)	k (N.m^{-1})	β (kg.s^{-1})	A
F (Imp. 1)	1.3	75	550	40	1.3×10^4	2.6×10^2	7.38
F (Imp. 2)	1.5	75	1000	9.6	4.6×10^3	80	6.2
F (Imp. 3)	2	75	970	18	8.8×10^3	1.5×10^2	7.43

Table 4.2: Identification of parameters of the model for the subject F on infinite scrum machine.

In Figure 4.9, we add these new results in the pusher phase plane presented in Figure 3.15. We focus on the experiments of subject F. The points with k_{61} correspond to the results from Table 3.2 and the points with k_{inf} correspond to the results from Table 4.2.
We note that the new points are located in the same zone as in Figure 3.15. He obtains similar values of $F_0 + mg \sim 1000 - 1400$ N. However, the values of A are 3 times higher than the one he has with stiffness k_{61}. It corresponds to the force signals that oscillates more in

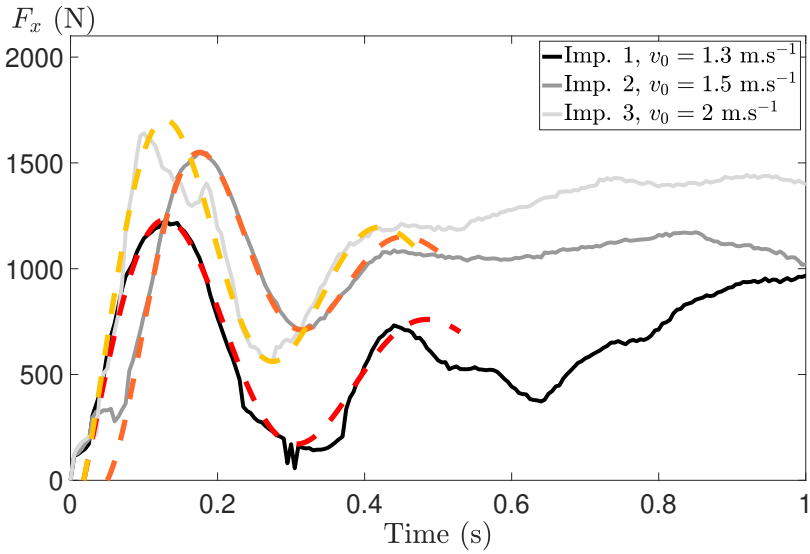


Figure 4.8: Comparison between experiments and the results of the model for the subject F on infinite scrum machine.

Figure 4.8 compared to Figure 3.6. We still notice, that for fixed scrum machine conditions, for different v_0, the player obtains the same order of magnitude of A.

We see that the stiffness of the scrum machine influences the rebound effect of a player impacting the foams. It is possible to implement a scrum machine model into the mechanical model of the impact presented in Figure 3.8. Thus, we are able to discriminate the influence of the scrum machine and the influence of the player impacting but it add more parameters in the model. This is why we prefer to compare the player on the same scrum machine with fixed settings.

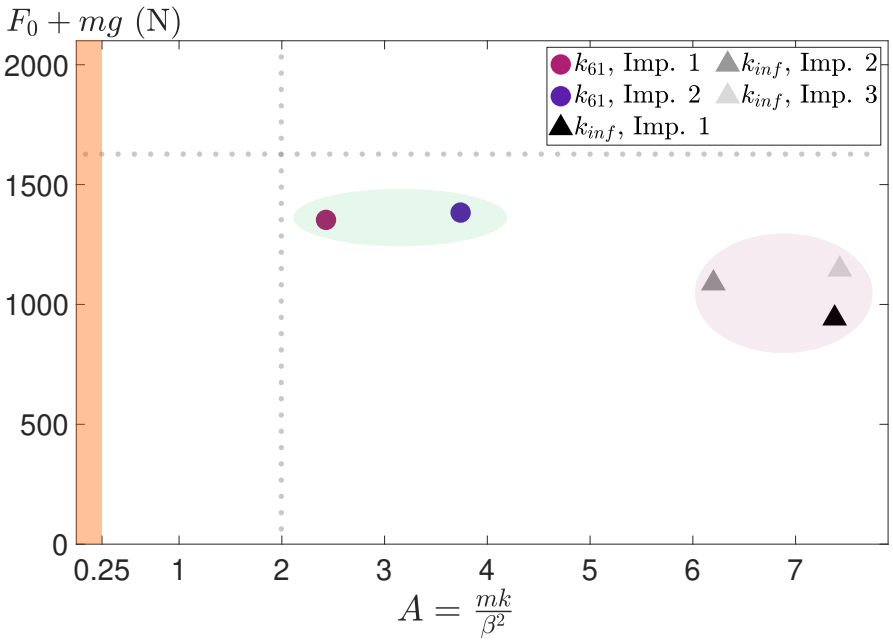


Figure 4.9: Phase plane $(A, F_0{+}mg)$. The orange zone is delimiting the aperiodic zone for $A < 0.25$.

Take home message of Chapter 4

1. Influence of the scrum machine: for the same player studied, we notice in a general way that the different scrum machines could give similar forces for the quasi-static studies (continuous pushing phase) but that impact studies are influenced by the mechanical characteristics scrum machine.

PART II

INDIVIDUAL POSTURE DURING SUSTAINED PHASE

In this part, we are going to discuss the second phase we identified during a scrum in Chapter 1.2.3: the sustained phase. After the scrum-half throw-in, two opponent packs are pushing each other in order to win the ball's possession. Each team needs to push as strongly as possible for a few seconds (cf. Figure 1.10). In those chapters, we will investigate individual scrum posture in order to maximize the pushing force of a player. If each player improves his pushing, one expects it will benefit the collective performance.

5

Optimal Knee Angle for Individual Scrum Pushing

We focus on the evolution of muscular force depending on the individual posture a player pushing on an individual scrum machine we developed in the laboratory.



Low X-ray images (EOS) of an academy-level hooker of Racing 92. Credit: Laura Valdes and Phillippe Rouch.

Contents

5.1	Joint Angles	**66**
5.2	Experimental Setup and Protocol	**69**
5.3	Results	**73**
5.4	Development of a Theoretical Model	**75**
5.5	Isometric Torque of the Knee Extensors	**79**
5.6	Discussion	**87**

This work has been done with Baptiste Loire, Awa Dimel Sy, Christophe Clanet, and Caroline Cohen thanks to a collaboration with Quentin Vincent, Baptiste Servat, Gilbert Gascou, and Michel Miro.
A special thanks to Briac Poussin, Antoine Kneblewski, Thomas Brunel, and the Racing 92 players who participated in the experiments.

In this chapter, we investigate the optimal position of an individual player in a scrummaging posture through the research of optimal knee angle during the sustained phase. By using the word optimal, we mean we want to find the angle that maximizes the player's pushing force developed on our scrum machine. In order to answer this question, we developed an instrumented scrum machine in the laboratory. The idea is to measure the player forces while capturing video footage in the sagittal plane. We thus develop an experimental setup that measures the compression forces: the ones that are useful to push opponents, to make them back off.

5.1 Joint Angles

5.1.1 State of the Art

A simple way to justify the existence of an optimal posture is to imagine pushing in a standing position or lying down. Between these two extreme postures, we want to know if it exists an intermediate posture that allows the player to produce and transmit the maximum pushing force, the one directed towards the x-axis in Figure 5.1, and how this optimum changes between people. In this figure, we present the way we quantify posture via joint angles. We define three joint angles in the sagittal plane of the player ψ_p, ψ_1, and ψ_2 which are the ankle, knee, and hip angles respectively. More precisely, these angles are defined thanks to anatomical points that are rotation centers of articulations (external malleolus, lateral femoral condyle, greater trochanter). The end of our foot segment is defined by the position of metatarsophalangeal joints in the sagittal plane. Shoulders penetrate into the foams, which implies that we can not see the position of vertebra C6 of the player (end of trunk segment) in Figure 5.1. So, the trunk segment is guided by the position of T6/T7 on the midaxillary line and by making the strong assumption that the trunk segment does not deform and keeps a constant length.
It is interesting to notice that for fixed anchor points with the ground and the scrum machine, the three joint angles are interdependent.

In [53], the authors study the individual scrummaging position of front-row forwards with electromyography (EMG) devices, and they mention in their introduction that to be efficient in horizontal force production, players need strength created by lower limb muscles (gluteal muscles, quadriceps, hamstrings) and a strong back to efficiently transfer the force to the opponents.
These notions are empirically used and transmitted by coaches in professional structures and could be read in coaching manuals like [54]. In this coaching manual of Rugby Union, one can read that for generating force and resisting, the "individual body shape" of players needs to have *a bend at the knees which provides an angle of approximately 110-115°"* and *"A straight, flat back to transmit force from the lower body, where it is generated"*. Or in [55] where the author gives similar advice to the players like having a low body height or having a knee angle between 100-120°, or finally in [56] with the advice of a knee angle between 110-120 °.
We understand individual posture is another key factor in scrum performance, this is why it has been already investigated by different research teams [57]. Although many studies have been conducted, there are still important questions unanswered due to a variety of experimental procedures and a lack of comparable data. As *E. Martin* and *G. Beckham* note in [58], most of the studies let the player free to adopt his/her posture while he/she is pushing [59, 60, 61]. Moreover, there is a wide range of experimental setups (foams, force sensors, live vs scrum machine, on-field/in the lab, motion capture, or video footage) which

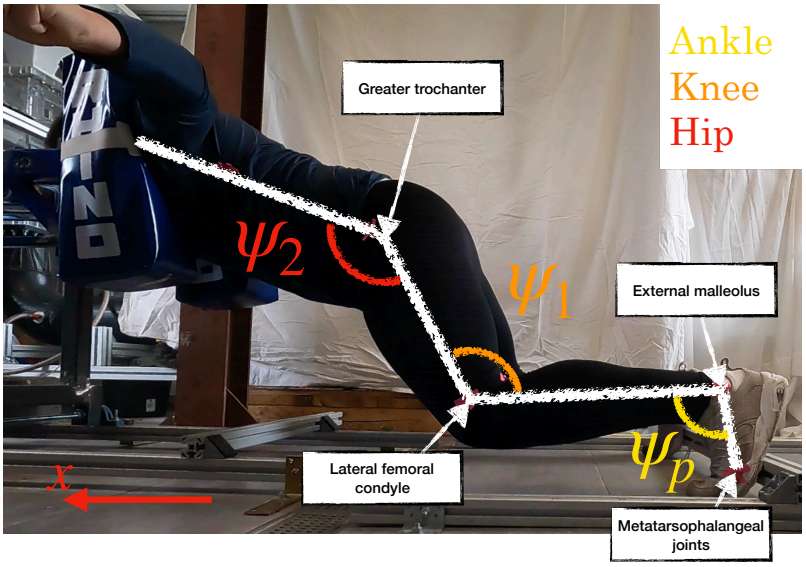


Figure 5.1: Example of a player in a scrummaging posture from a side view. We define the ankle angle ψ_p, the knee angle ψ_1 and the hip angle ψ_2. Anatomical landmarks are mentioned and are visible on the player thanks to pink crosses.

complicates experimental results comparison.
But we find back similar knee angle values in an article [62] where they constrain the pushing height of the player. Players could choose the foot distances to the scrum machine and they test parallel and cross feet positions. They find that players produce a significantly higher pushing force for a pushing height of 40% of the player's total height than for 36 and 38%. Moreover, there is no significant effect of foot positioning on force production. For a shoulder's height of 40% of the total player's height, with a parallel feet position, measured hip angles ψ_2 are around 119° and knee angles ψ_1 around 102°. In [60] players self-select their postures and they adopt ψ_2 of approximately 150±20° and ψ_1 of 145±20° during the sustained phase.
All those studies are conducted with scrum machines despite knowing that scrum machine work does not mimic the instability of a live situation. But live data are extremely difficult to obtain where scrum machine data are easier [63, 64, 34]. Again, we find in these articles the notions evoked in coaching manuals about leg force production and solid back as a vector of transmission toward the opponent. In [64] the notion of synchronization between players to maximize the horizontal force is also evoked. We will discuss this issue in Chapter 8.

The majority of the studies that investigate posture issues let the player be free to adopt one and only one posture. Then, the authors observe and measure the different biomechanical parameters. Furthermore, they only investigate the possible linear relation between parameters with Pearson's correlation coefficients. Moreover, some studies used footrest system [62, 65] allowing to adopt different postures than postures with cleat shoes [60, 53, 64]. Finally, except in [62], no constraint on the player's posture is imposed.
This is why we decided to build our own experimental setup in the laboratory environment in order to conduct individual compression force measurements controlling the variations of feet distance from the scrum machine. For each trial, we will measure joint angles in the sagittal plane of the player in order to link them with average force production in this posture. The first version of our setup is made of foot support that enables us to set this distance.

5.1.2 Measurements of joint angles on real scrums

Before presenting the experimental setup, let us add to the literature some angle measurements performed on side-view pictures of real scrums. In Figure 5.2, we have an example of a scrum during a practice of the Racing 92 team thanks to a view quasi-parallel to the ground. We represent in orange different knee angles ψ_1 of front-row players and flankers to have an idea of typical ψ_1 used in live scrums. In red, we represent the hip angles, and in yellow some ankle angles. The angles are manually measured with ImageJ.

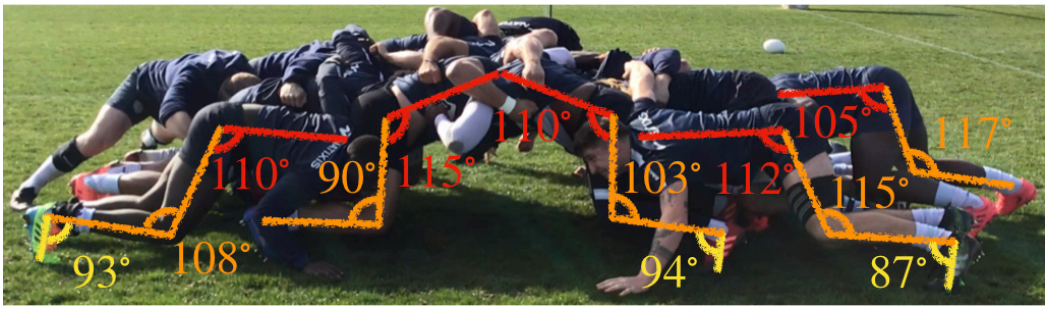


Figure 5.2: Scrum during a practice of professional rugby team of Racing 92. Front row players adopt $\psi_1 \sim 90 - 100°$ and flankers have larger $\psi_1 \sim 110 - 120°$. All the forwards seem to have $\psi_2 \sim 110°$.

We look at several practice scrums and make the following observations.
During the impact phase, all the forward players do an extension of hip and knee angles. Indeed, in Figure 5.2, after the "Set" call of the referee, the flankers extend their knee angle of 20° and 50° for the one of the left pack and the one of the right pack respectively. They increase their hip angle by 20° and 30°. The tighthead prop of the left pack and the loosehead prop of the right pack seems to have different strategy for their extension. Their knee angle remains similar before and after impact. All their extension seems to be made with the hip angle which increases by 15-20° during impact.
During the sustained phase, the ψ_1 of the front-row players stand in the range of $\psi_1 \sim 90 - 100°$ and are smaller than second and third-row players for whom $\psi_1 \sim 110 - 120°$. However, the hip angles ψ_2 seem to be similar for all the forwards in the scrum with values that stand in the range of $\psi_2 \sim 105 - 115°$. Finally, the ankle angle ψ_p as defined in Figure 5.1 is of the order of magnitude of 90°.
Even if the scrum is called stable (no collapse, no raised scrum, no retreating team: cf. Chapter 9), there are some movements of the contact line between the two front rows. This is an important difference between experiments in live scrums and experiments with a scrum machine.
During practice, if the front-row players are pushing alone (3 vs 3), they tend to adopt positions where they have ψ_1 slightly larger than the ones they have in a complete scrum. For example, in a 3vs3 scrum of the same training session, the loosehead prop of the right pack adopts a posture with $\psi_1 \simeq 119°$ and $\psi_2 \simeq 117°$ which is respectively 16° and 7° larger than in Figure 5.2. This is another important difference between individual posture situations and collective scrums: front-row players' postures are limited by the binding with the opponents and by the need to offer a support surface for the second rows and the flankers.

5.2 Experimental Setup and Protocol

We will start by introducing the experimental setup we designed, then we will detail the experimental protocol to change the player's position by moving only one parameter. Finally, we will discuss the results of two Academy players, and develop a theoretical model in order to understand the observations.

5.2.1 Material and Methods

Experimental Setup

From a training individual scrum machine, we designed a lab experimental tool. We modified and instrumented a Rhino® One Man Scrum Machine Sled[1] used during practice. The experimental scrum machine is presented with front-view and top-view pictures in Figure 5.3a and b respectively. It is then presented with side-view pictures and a scheme in Figures 5.3c,d, and e.
The shoulders of the pushing player are set on foams at a pushing height h compared to the ground. The force F_x produced by the player is measured thanks to Futek® S-beam load cells that can measure tension and compression along the x-direction (cf. Uniaxial Force sensors in Figure 5.3. On one side, they are fixed on the structure of the scrum machine which is itself anchored to the ground. On the other side, they are in plane contact with the free-moving part attached by a fixed pivot (PC) to the ground. Players push on this free moving part enabling the compression force measurement. The blue bungee cords with metal hooks are here to maintain the contact between the pivot free-moving part and the load cells (cf. Figure 5.3c) when the player is not pushing. This residual force is deduced from the force measurement on the player.

There are two hand holders independent from the structure on each part of the scrum machine (cf. Figure 5.3a) that are anchored to the ground. This setup allows to design experimental protocols where the player uses the arms to add pushing force: if the hand holders are integrated to the force measurement system, then when the player pulls on the hand holders with the arms this force is subtracted from the force produced by the player.

The scrum machine is installed in an indoor environment to be free of weather and light conditions. The ground of the lab is made of tiles, which explains why we designed a proper system to support the feet of the rugby player. In Figure 5.3a and 5.3d, we observe two parallel aluminum profile bars that are used as a rail to fix a transverse bar that serves as foot support (FS) (cf. Figures 5.3d and e).
During practice and games, the players wear cleat shoes on both natural and synthetic grass 5.4. Here, the experimental setup is made with this foot support. In Chapter 6, we will investigate the influence of synthetic grass and cleat shoes.

The Young Modulus of the blue foams is $E \sim 1.5 \times 10^4 Pa$ [66]. Foams are screwed to the metal plate linked to an L-shape metallic structure (cf. Figure 5.3e). All the structure is anchored to the ground.
The sampling frequency of the force acquisition is set to 600 Hz. The player is filmed by a top and side view taken with two GoPro® cameras recording at 60 fps. We post-process the data, and synchronize them with visual and sound cues.

[1] `https://rhino.direct/products/one-man-machine`

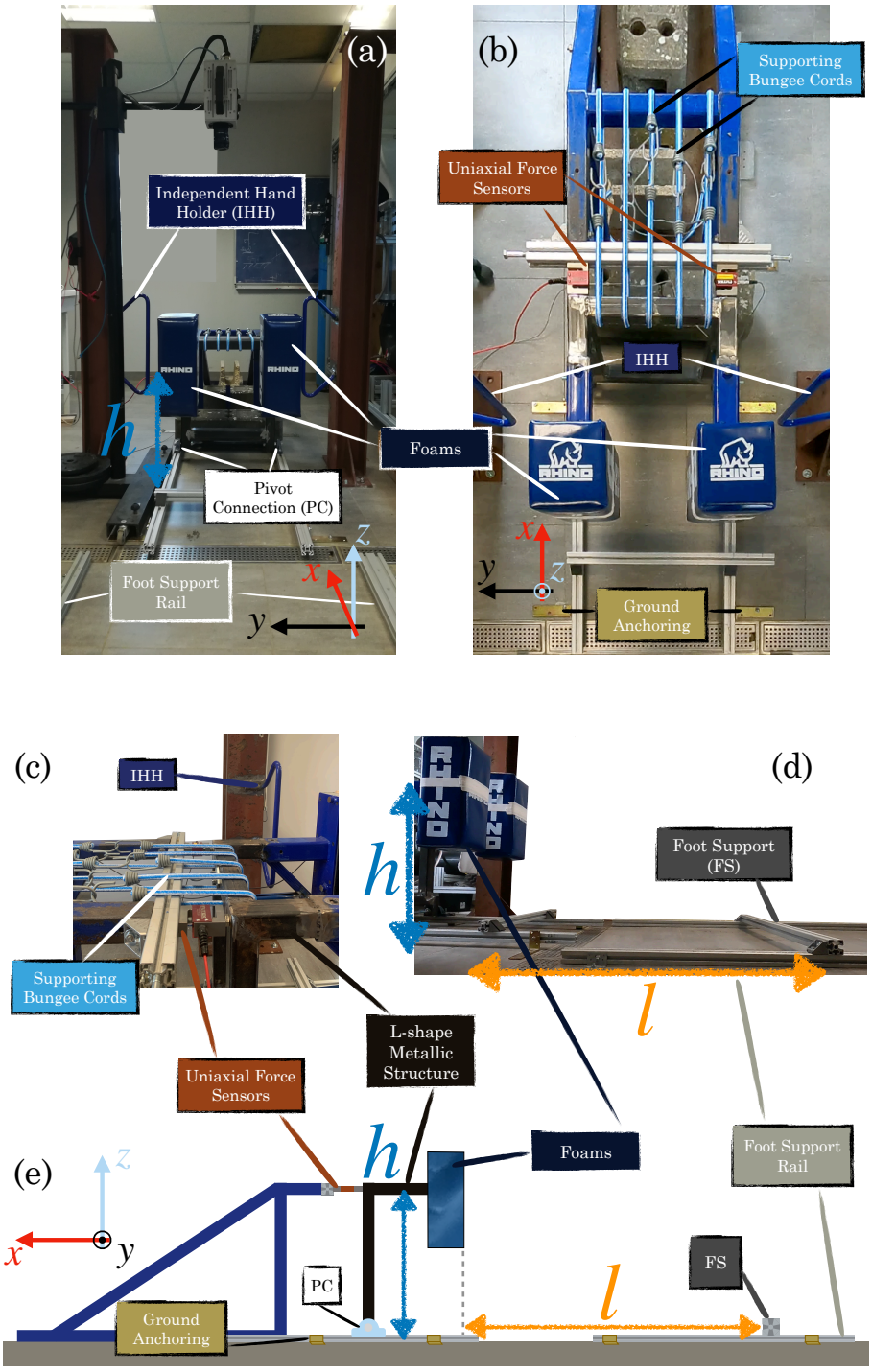


Figure 5.3: Presentation of the experimental setup. (a) Front-view picture of the instrumented scrum machine. We can see the blue foams on which the players are pushing with their shoulders. Handles are arc welded to two brown I-beams. (b) Top view of the scrum machine force measurement area. The two foams are screwed to metallic plates that are welded to an L-shape metallic structure. The load cells are screwed into an aluminum profile attached to the structure of the machine. And, they are in planar contact with the L-shape metallic structure. (c) Side view of the scrum machine force measurement area. The bungee cords are keeping the L-shape structure in contact with the force sensors. (d) Side-view picture of the player positioning area. The player has his/her feet on the foot support and his/her shoulders on the foams. (e) Scrum machine side view diagram with the definition of parameters l and h.



Figure 5.4: Difference in foot anchoring on synthetic turf with cleat shoes and on our experimental setup with the foot support.

Protocol

As we can see in Figures 5.3d and e, we define two control parameters l and h: the length and height of pushing. In this chapter, we ask the subject to have a constant pushing height h in each experiment. The height h we choose corresponds to the height of the metallic bars parallel to the ground of the initial scrum machine, and that height corresponds to the heights of real scrums we can observe in real games and training.
In this chapter, l will be the control parameter that enables us to browse different postures for the players. h is fixed ($h \sim 65$ cm) for all trials and is marked by a white strap visible in Figure 5.3d.

We ask the players to push on the scrum machine as hard as they can for a maximal effort of 4-5 seconds. We give an example of a snapshot of the player with a side view during this phase in Figure 5.5(a). The measured force is a maximal near-isometric force. From here on, the average plateau force reached during this phase is called F_x. After this maximal effort, we ask the subject to stay on the scrum machine without any muscular force production just by resting his body to stay in an equilibrium state. For the same length l and player, there is a snapshot taken during this phase in Figure 5.5(b). We call this force the passive force F_{p_x}.

We start by asking the player his natural scrum posture in order to set the first distance l we test. We call this natural length l_{nat}. Then, we change the length l around l_{nat} by using the support bar system by adding or subtracting 5 or 10 centimeters between each try.

Subjects

Two Academy players of Racing 92 performed the previously described protocol. Age, anthropometric data, and role of the players are summarized in Table 5.1.

Player	Age (Years)	Mass (kg)	Height (cm)	Player's Role
1	20	116	175	Hooker
2	19	120	186	Prop

Table 5.1: Age and anthropometrics of the two academy players tested in this Chapter.

Each player provided oral informed consent before participation. One medical officer of the team was there as well as a strength and conditioning coach.

5.2.2 Example of a force signal

For each trial, we know the compression force signal F_x by measuring the sum of the two forces measured by each force sensor. We plot an example of a force signal obtained with player 1 in Figure 5.5c.

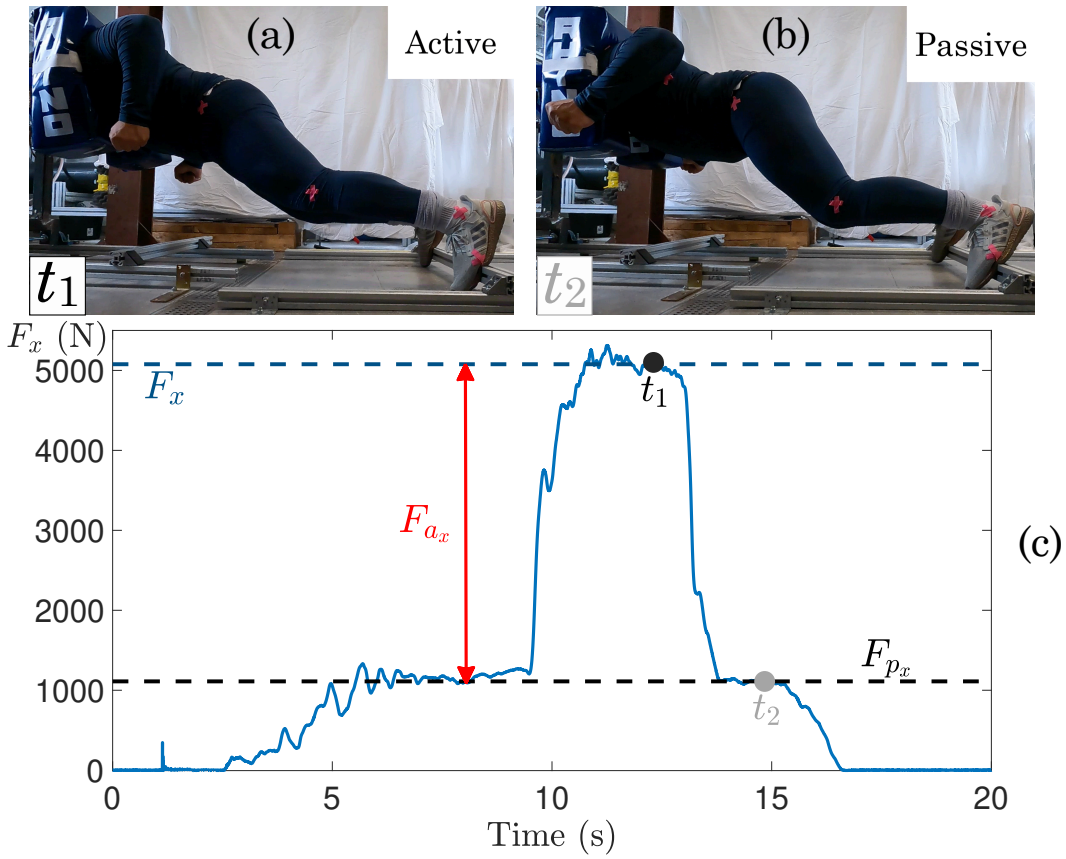


Figure 5.5: Snapshots of the experiment and signal of compression force of the player 1 with l= 113 cm. (a) The player is in the active phase, he is applying his maximal isometric force during 4-5 seconds. (b) The player is in the passive phase, the force measured is only due to his weight. (c) Compression force signal obtained with player 1 for $l = 113$ cm. The passive force is $F_{p_x} = 1110$ N, and the total force is $F_x = 5077$ N, which gives an active force of $F_{a_x} = 3967$ N.

At the beginning of the trial, at time $t = 1$ s, we apply a short blow to the scrum machine. At $t = 2.5$ s, the player starts to set his shoulders on the scrum machine. At $t = 9.5$ s, player 1 is activating his muscles to apply the plateau force F_x for 4 seconds. We point out $t = t_1$ that corresponds to the snapshot of Figure 5.5a. Finally, between $t = 14$ s and $t = 15$ s, the player adopts the passive posture of Figure 5.5(b) with a horizontal force measured on the scrum machine called F_{p_x}. Thus, we define the active force as:

$$F_{a_x} = F_x - F_{p_x}. \tag{5.1}$$

For each trial, we calculate the mean forces F_x, F_{p_x} and F_{a_x} on forces signals. We measure ψ_1, ψ_2 on side-view videos. We will not study the effect of ψ_p on the pushing force because the foot support imposes positions of ankles that are not similar to what we observe on synthetic or natural grass.

5.3 Results

5.3.1 Optimal length

For each length l, the postures of the players are obviously different. We observe in figure 5.6 that when l increases, ψ_1 and ψ_2 increase too. We plot the measured values of the joint angles (ψ_p, ψ_1, ψ_2) as a function of l for player 2. The angles obtained during the active phase are represented with circles and the angles during the passive phase are represented with triangles. We note that the active ψ_1 and ψ_2 increase linearly with l. We also observe that the passive angles are smaller than the active angles for a given l because during the active phase the shoulders of the players sink in the foams and slightly change l.

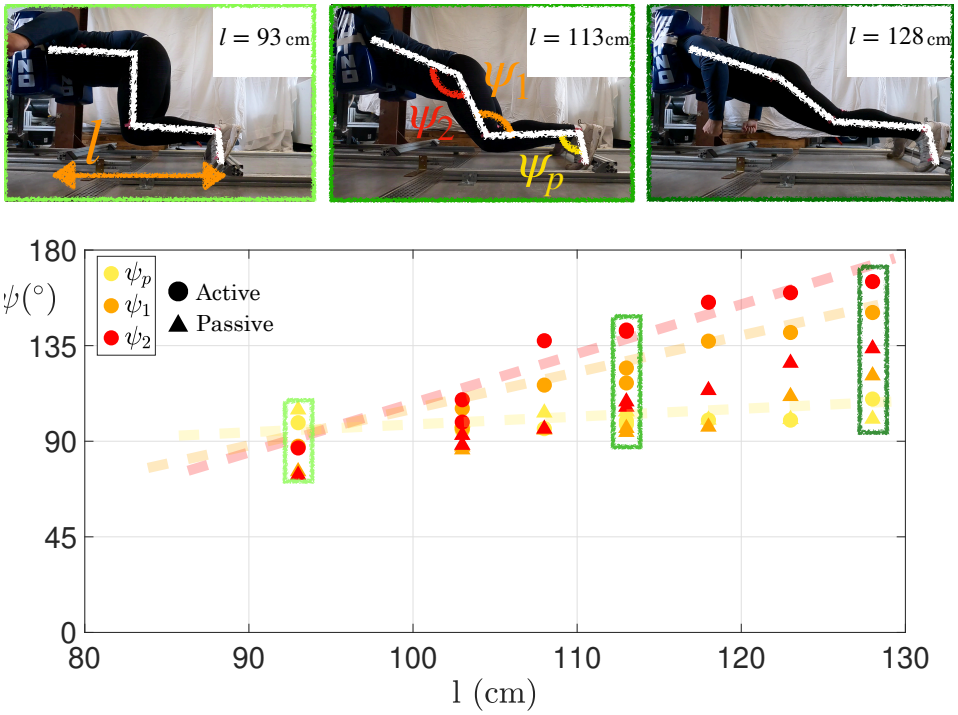


Figure 5.6: Evolution of the posture of player 2 with l. For each trial, we measure the active and passive joint angles ψ_1, ψ_2, and ψ_p. We plot them as a function of l for player 2.

In Figure 5.7, we plot F_x for each trial. Each point corresponds to a single push, and y-error bars correspond to the force variations (standard deviation σ_{F_x}) on the plateau force F_x. The x-error bars are equal to ± 2 cm and are of the order of magnitude of the displacement of the foams by the shoulders of the player. The shapes of the curves $F_x(l)$ are slightly different for our two players. Player 1 has a flatter curve than player 2, but both of them present a maximum.

Player 2 curve is sharped around $l_{opt,p} = 118 \pm 1$ cm while hooker's curve is almost flat between l =103 (mean of the two experiments at $l = 103 \pm 1$ cm) and l =188 cm, but slightly higher values are reached between $l_{opt,h} = 103 - 108$ cm. Both players reached similar force values around 5000 N which are extremely high for individual performance and will be discussed in 5.6.2. This amount of force corresponds to approximately 4.5 times their weight.
In Table 5.1, we note that players have similar masses, however, there is an 11 centimeters difference in height between them. It is interesting to notice that $l_{opt,h}$ and $l_{opt,p}$ are approximately separated by 10-15 cm, with the higher player having the higher l_{opt}.
One hypothesis to explain the difference in curves between these two players could be their

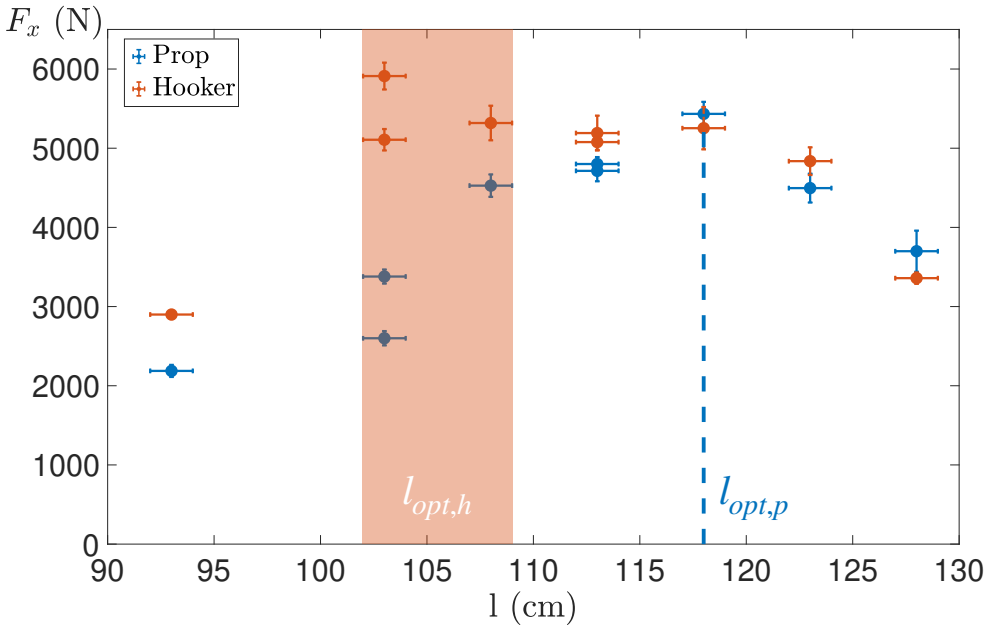


Figure 5.7: F_x as a function of l for the two academy-level players. The shapes of the two curves are different but both of them present an optimal distance l_{opt} different for each player.

difference in position in complete scrums. Indeed, the hooker needs to adapt his posture to push with his props, and with two-second rows behind him. This adaptability could be translated by the ability to produce the same level of force on a larger range of positions where props are a little bit more specific and efficient around one selected position. Further experimental studies with different professional players need to be done in order to confirm this point.

It seems that each player should have an optimal posture in which he/she can develop a maximal isometric force. At a constant pushing height h, the posture could be quantified by the distance l between shoulders and feet position projected on the ground, and this length seems to be directly linked to the height of the player. The passive forces observed are of the order of magnitude of the weight of the players (we will give more details about this passive force in Chapter 6). The active forces could reach 4000 N with this experimental setup with foot support.

5.3.2 Optimal joint angles

Now, we want to know if those differences in l_{opt} between players could hide a universal posture that allows producing maximal force in terms of joint angles.
In order to do that, we plot the same data as in Figure 5.7, but this time in terms of ψ_1 and ψ_2 measured during the plateau force production F_x. The figure 5.8 shows the dimensionless force $\frac{F_x}{F_{x,max}}$ as a function of ψ_1 for each player. $F_{x,max}$ corresponds to the maximal pushing force reached by each player.

In Figure 5.7, the two curves have different shapes and the optima are different. However, in Figure 5.8 the two curves are collapsing and show an optimum for $\psi_1 \sim 130 \pm 5°$. This means that both players have the same knee angle ψ_1 when they are maximizing their horizontal force. The optimal ψ_1 is represented with player 2 in Figure 5.8. We remark that

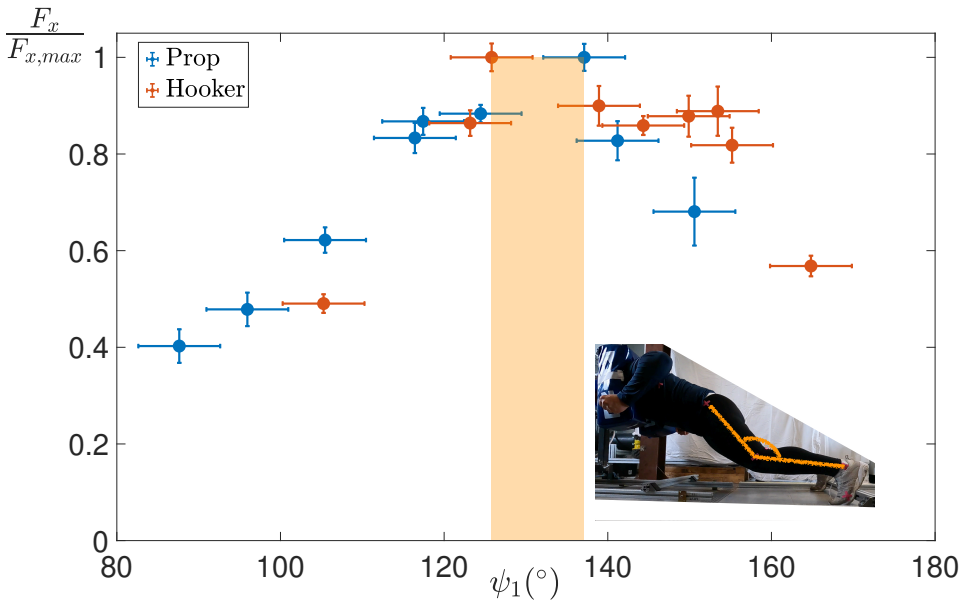


Figure 5.8: Dimensionless horizontal force $\frac{F_x}{F_{x,max}}$ versus knee joint angle ψ_1. Both players produce maximum force at $\psi_1 \sim 130 \pm 5°$. We illustrate this optimal ψ_1 with the picture of player 2 for his best trial.

this posture is more extended that the ones observed on real scrums in Figure 5.2. For this posture, ψ_2 is also quite high and implies a trunk that is slightly pushing upwards. The equivalent graph but with ψ_2 is given in Figure 5.9.

The same comment about the collapse of the two curves could be made. This time the maximum is approximately for a $\psi_2 \sim 153 \pm 5°$. We recall that the two angles are related to each other, more precisely, when l and ψ_1 is set, ψ_2 is imposed for a given player.
We do not give results in function of ψ_p because we already mentioned that the ground/shoe interface does not represent the field environment and this is one limit of our first study. The support bar has an effect of mobility reduction of players' ankles and they have a tendency to take all their support on the bar with sometimes no link between the end of the feet and ground in active phases for a few trials. This metallic bar is like a wall on which players can set their feet to produce maximal active forces without any problems of friction. In comparison, this same hooker produced maximal F_x at the "Atelier de la mêlée" (cf. 3.1.3) a little less than twice as low as the one observed in our scrum machine with the metallic bar. Moreover, the measure of ψ_p for large l should be read with caution because the distortion of the GoPro is more important at the edges.

5.4 Development of a Theoretical Model

We decide to develop a model in order to explain the evolution of the isometric force production with the joint angles adopted by a single player in a scrum posture for a maximal isometric effort. We use a biomechanic-inspired model of knee force production. In this part, we focus on the active part of the force F_a.

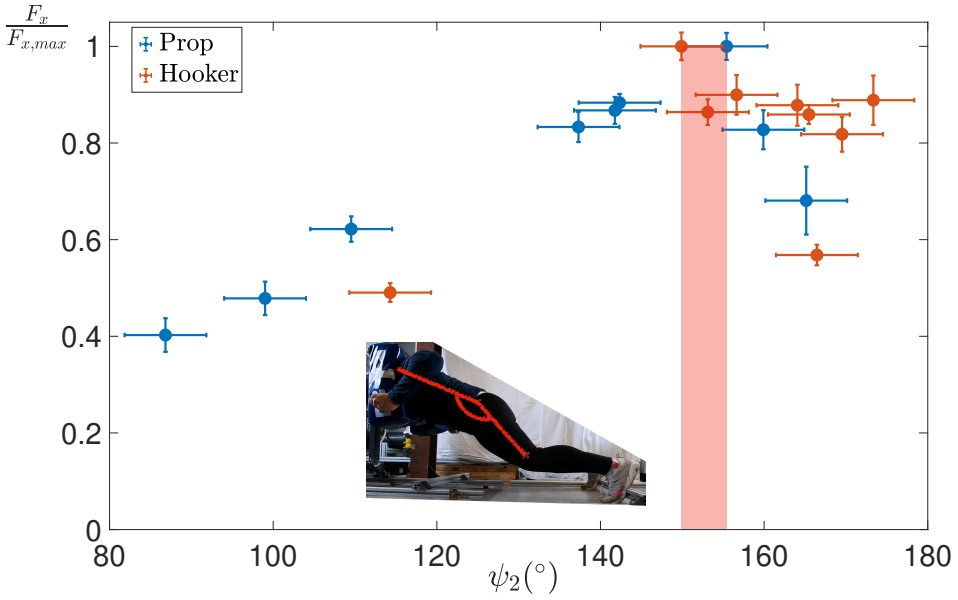


Figure 5.9: Dimensionless horizontal force $\frac{F_x}{F_{x,max}}$ versus knee joint angle ψ_2. Both players produce maximum force at $\psi_2 \sim 153 \pm 5°$. We illustrate this optimal ψ_2 with the picture of the best trial of player 2.

5.4.1 From the knee extensors to the hips

The global model we build consists of considering the player as a 2D stickman with three main segments- the trunk of length L_T, thigh of length L_C and leg of length L_M- and a feet segment- between external malleolus and metatarsophalangeal joints. To construct this model, we take into consideration the empirical knowledge of some coaches that we mentioned in 5.1.1.
The active force is produced at the lower limb level. We consider a maximal isometric torque Γ produced by the extensors muscles of each knee. We make the approximation that both legs are symmetric in terms of the production of torque Γ. This torque depends only on ψ_1 - the approximation that it is independent of ψ_2 is discussed in 5.5- and is represented in white in Figure 5.10.

For the majority of the male players of different playing levels we have tested, we can make the approximation that $L_C \simeq L_M$. We call L the length of such a lower limb segment.
In Figure 5.10, we determine the norm and direction of $\vec{F_{hip}}$ which is the force at the hip level produced thanks to the knee extensors muscles. We imagine the static situation of the stickman with a torque Γ that tends to extend the knee angle ψ_1. To keep a static situation, we draw an imaginary wire between the external malleolus and the greater tranchoter represented by a gray dashed line in Figure 5.10. The active force is then transmitted to the hips when we cut this wire. With this trick, we determine that:

$$F_{hip} = \frac{2\Gamma(\psi_1)}{L\cos\left(\frac{\psi_1}{2}\right)}. \tag{5.2}$$

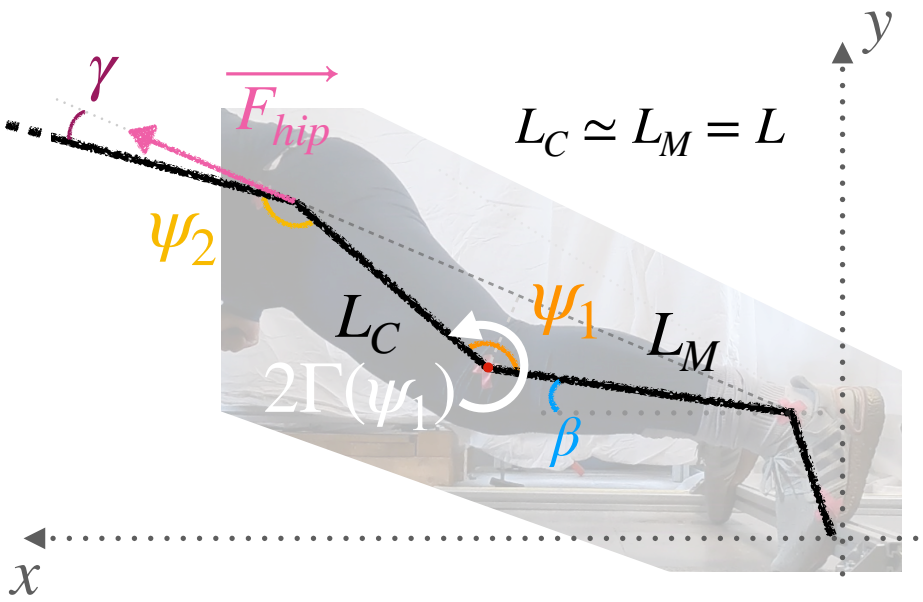


Figure 5.10: Stickman 2D model of individual isometric scrummaging with a focus on lower limb force production. Isometric knee extensors torque $2\Gamma(\psi_1)$ is produced by the quadriceps of the player. The tibia of length L_M has an angle β to the ground. Thigh length L_C is approximately equal to L_M in our example. γ is defined as the angle between the direction of $\vec{F_{hip}}$ and the midaxillary line of the player.

5.4.2 From the hips to the scrum machine

Then, the player needs to transmit the force produced through his back towards the opponent (here the scrum machine). We make the strong assumption that for our Academy players the active force produced by the lower limb is perfectly transmitted from their hips and backs to their shoulders thanks to their non-deformable and perfectly efficient backs. Contrary to the knee joint that we model with a torque, we make the choice to consider the hip joint as a weld between two non-deformable segments. Therefore, $\vec{F_{hip}}$ is transmitted as it is up to the shoulders. This is represented with the pink arrows in Figures 5.11a and b.
Then we investigate the relationship of $\vec{F_{hip}}$ with the active force $\vec{F_a}$ communicated to the scrum machine. We do not have a way of measuring the direction of F_a with this experimental setup version. We will see in subsection 6.3.3 (about active force direction measurements) that the $\vec{F_a}$ is directed along the main direction of the body defined between the metatarsophalangeal joints and the shoulders. We call θ the angle between the ground and this axis. It is represented in green in Figure 5.11a .

In order to establish $\vec{F_a}$, we project the $\vec{F_{hip}}$ on the axis defined by the direction of θ. Two cases are possible:

- If $\theta < \gamma + \alpha_{back}$, it means that $\vec{F_{hip}}$ is above the direction of the active force and so

$$F_a = F_{hip}\cos(\gamma - \theta + \alpha_{back}). \tag{5.3}$$

- Else, $\vec{F_{hip}}$ is below the direction of the active force and so

$$F_a = F_{hip}\cos(\theta - \gamma - \alpha_{back}). \tag{5.4}$$

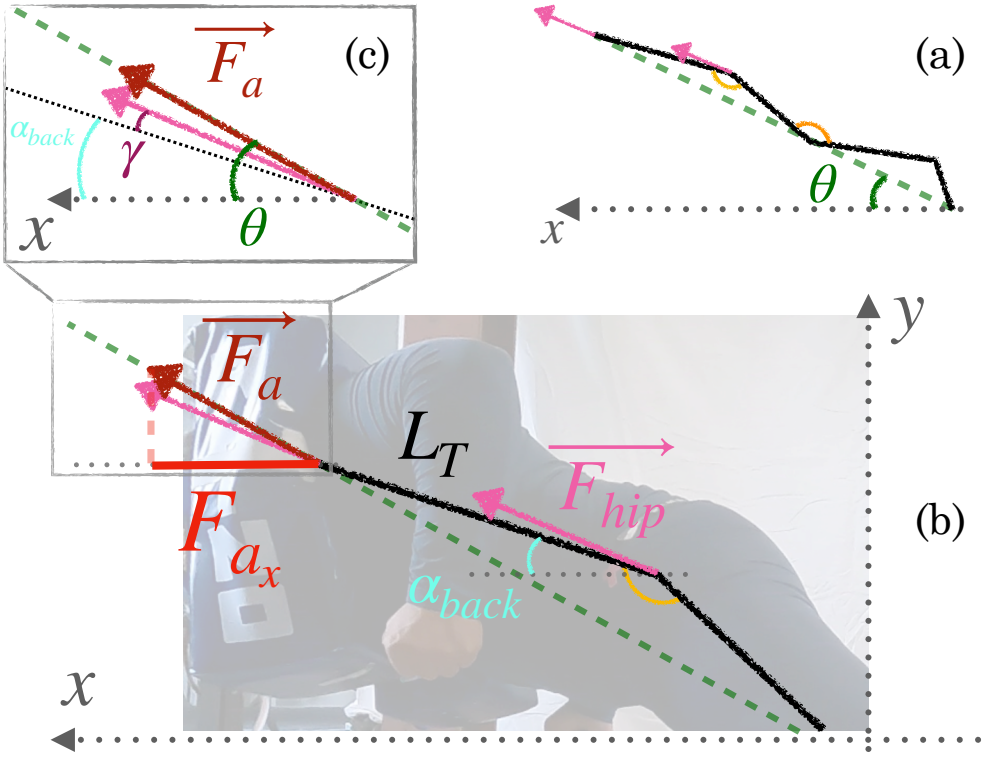


Figure 5.11: 2D stickman model of individual isometric scrummaging. (a) The complete schematic stickman with the angle θ and the pink arrows corresponding to the $\vec{F_{hip}}$ transmission. (b) Focus on the force transmission by the back. α_{back} is the back angle, and L_T is the trunk length. (c) We focus on force directions: $\vec{F_{hip}}$ has an angle equal to $\alpha_{back} + \gamma$ to the horizontal and $\vec{F_a}$ is directed along the axis defined by the angle θ.

In Figure 5.11c, $\vec{F_{hip}}$ is below the direction defined by θ (represented by the green dashed line). So, we have $\theta > \gamma + \alpha_{back}$.
Moreover, some geometrical considerations allow us to express γ as:

$$\gamma = \frac{\pi + \psi_1}{2} - \psi_2. \tag{5.5}$$

We also notice that we can link α_{back} with the joint angles and another intermediate angle β defined in Figure 5.10 as the angle of the tibia to the ground with the expression $\alpha_{back} = \psi_2 - \psi_1 + \beta$. We see that β and α_{back} can be seen as an echo of the instructions given by coaches to their players: keeping a flat back parallel to the ground means $\alpha_{back} = 0°$, and keeping the two tibias almost parallel to the ground means $\beta = 0°$.
But, in our model, we see that the way to be more efficient in the transition from $\vec{F_{hip}}$ to $\vec{F_a}$ is by aligning θ and the angle made by the axis external malleolus-great tranchoter (the imaginary wire of Figure 5.10).
So, from the equations (5.2) and (5.4), we express $\vec{F_a}$ norm as:

$$F_a(\psi_1, \psi_2, \theta, \alpha_{back}, L) = \frac{2\Gamma(\psi_1)}{L\cos\left(\frac{\psi_1}{2}\right)} \cos\left(\theta - \alpha_{back} + \psi_2 - \frac{\pi + \psi_1}{2}\right). \tag{5.6}$$

The last step consists on projecting $\vec{F_a}$ along the x-axis to obtain F_{a_x}. Thanks to Figure 5.11c, we obtain:

$$F_{a_x} = F_a(\psi_1, \psi_2, \theta, \alpha_{back}, L)\cos(\alpha_{back}). \tag{5.7}$$

Hence, we have a mathematical expression for the horizontal active force F_{a_x} that depends on the angles (ψ_1, ψ_2, α_{back},θ), the length L and the isometric torque $\Gamma(\psi_1)$. We note that the model does not formally take into account the ankle angle ψ_p. We then have to compare the experimental horizontal F_{a_x} obtained with player 1 to the results of the model applied to this player.
The angles are measured on side-view videos, and the lengths are measured directly on the body of the player. We only miss the information related to the knee torque to apply the model. To solve this issue, we decide to measure experimentally the isometric torque of knee extensors at the knee rotation center thanks to a CSMI Humac Norm Cybex® machine that belongs to Racing 92. Then, we develop a simple anatomical model of the knee joint during extension to understand the experimental curve shape and to obtain a mathematical form for $\Gamma(\psi_1)$,

5.5 Isometric Torque of the Knee Extensors

5.5.1 State of the art

Studies about the maximal isometric torque of knee extension have been already made. The authors use different experimental setups that measure forces produced with a motionless knee in extension and so equivalent torque at the knee rotation center level. Γ usually corresponds to a maximal isometric effort of three to five seconds. They all show common results.
First of all, when the knee is in full extension ($\psi_1 = 180°$) and in full flexion ($\psi_1 \longrightarrow 0°$)[2], it is difficult to produce isometric force with the quadriceps. Then, it seems that for every subject, the curve Γ versus ψ_1 shows a maximum between these two extreme cases. In [67], the maximum Γ is reached in $\psi_1 \sim 130°$, when in [68, 69] it is reached in $\psi_1 \sim 120°$.
Furthermore, in [70] we note that the isometric torque of the knee extensors is superior to the isokinetic [3] one for all ψ_1 on a sample of 25 male subjects between 17 and 37 years. The maximum Γ is obtained for an average $\psi_1 \sim 120 - 135°$. We observe similar results of optimal ψ_1 in [71].

In the article of Knapik *et al.* [72], 16 men and 15 women have been tested with a Cybex®, the majority of them are soldiers. In Figure 5.12, the peak torque is on average around $\psi_1 = 110 \pm 20°$ for men, and around $\psi_1 = 125 \pm 15°$ for women. We also see that in this trained population men have higher knee torque than women.
Last, but not least, we know that training influences the force-length relationship of the muscle [73]. When ψ_1 increases, the length of the quadriceps decreases, which then influences the force production. So the effect of training could also be seen on the curves of isometric torque of the knee extensors.
The playing level and the training influence the curves: even if there is always a maximum, there is no universal curve, the maximum could be reached for different optimal ψ_1, and the shape of the curve can change. Therefore, it is necessary to adapt $\Gamma(\psi_1)$ for each subject studied in the model.

[2] In reality, it exists a minimum angle ψ_1 for each of us which depends on the knee range of mobility due to factors like training, flexibility, past injuries...
[3] Torque produced at a constant angular velocity of the joint.

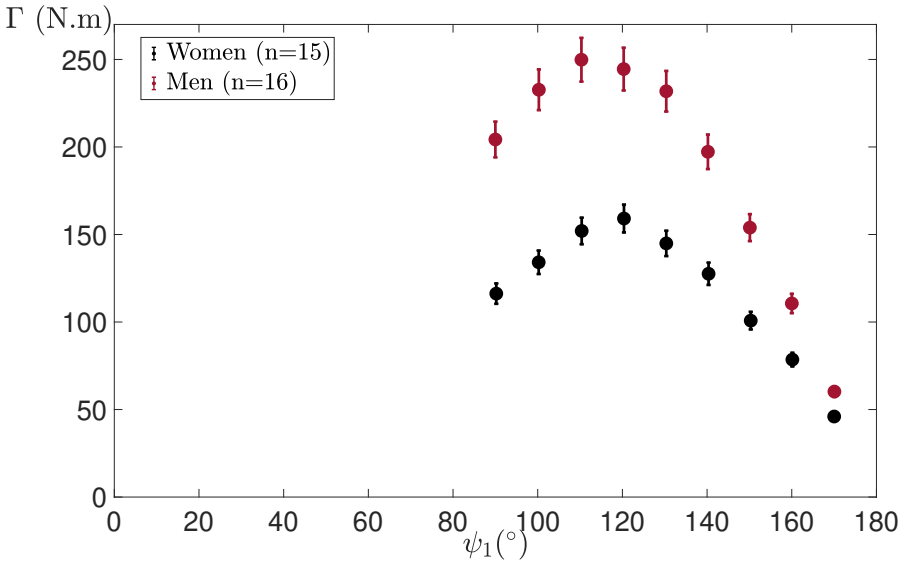


Figure 5.12: Isometric torque of the knee extensors extracted from [72]. The error bars we plot correspond to 5% of the values which are approximately what we observe in the article.

5.5.2 Experimental setup and results

We measure the isometric torque produced by the knee extensors with a CSMI Humac Norm Cybex® represented in Figure 5.13. The same kind of experiment was conducted a few years before by a master's student in the Sports Physics team under the supervision of Caroline Cohen and Christophe Clanet and could be found in Chapter 2 of [74].
We are applying a similar experimental protocol to determine $\Gamma(\psi_1)$ curves. A picture of the experimental setup is available in Figure 5.13. The subject is sitting with $\psi_2 \sim 90°$. One knee of the subject is aligned with the rotation center of the machine and the corresponding thigh is locked to the seat with a velcro strap. Then, above the malleolus of this same leg, the player is blocked at a distance d from the rotation center of the knee. The operator selects the different ψ_1 to test and for each of them, the subject applies a maximal isometric force on the support that blocked the leg for five seconds.

We start by measuring the curve of the right knee of player 1. For each angle ψ_1, the mean of the maximal plateau torque and the corresponding standard deviation is represented in Figure 5.13 with the orange points. For the sake of comparison, an amateur rugby player (male, 27 years, mass 83 kg and height 180 cm) and an untrained novice player (male, 25 years, mass 61 kg and height 176 cm) follow the same experimental protocol. We measure the curve on the left knee. Their results are represented in purple and in light blue respectively.

The Academy-level hooker is more trained and more powerful with his lower limb muscles compared to the other subjects. The curves of isometric torque confirm this assertion. The logic is respected with peak torques approximately equal to 350 N.m, 250 N.m, and 120 N.m for player 1, the amateur, and the novice player respectively. The three curves show a maximum for different ψ_1 with 105° for the novice, 100-110° for the amateur, and a flatter curve with a maximal plateau between 110° and 130° for the player 1. The amateur player has a curve similar to the cardinal red curve of Figure 5.12. We highlight the fact that the Academy-level hooker already has a force plateau in Figure 5.7 that shows his adaptability in terms of force production as a function of l.

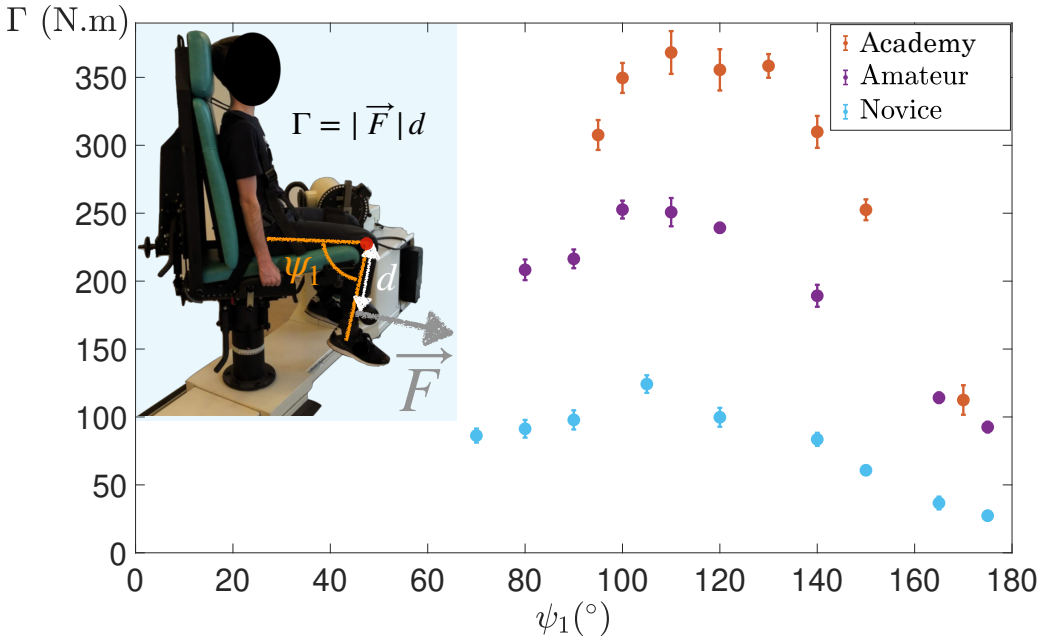


Figure 5.13: Maximal isometric torque of the knee extensors curves with the representation of the experimental setup used with the Novice player. For $\psi_1 = 80°$, he is applying a force $\vec{F}$ with a moment arm d. The results of player 1 are represented in orange, and the results of the amateur and the novice are represented in purple and light blue respectively.

The experimental results are obtained here with a fixed $\psi_2 \sim 90°$. But one can ask what is the influence of ψ_2 on $\Gamma(\psi_1)$. We repeat this experimental study with the novice player for ψ_2=70° and ψ_2=100°. No significant effect on $\Gamma(\psi_1)$ is noticeable in Figure 5.14. Indeed, we note that the maximal values of torques are all around 110-120 N. The optimal $\psi_1 = 110°$ is the same for the three curves and the curves are globally similar. For a wider variety of ψ_2, in [75] the authors observe a difference in the peak of torque value and location for $\psi_2 = 180°$ and $\psi_2 = 100°$.

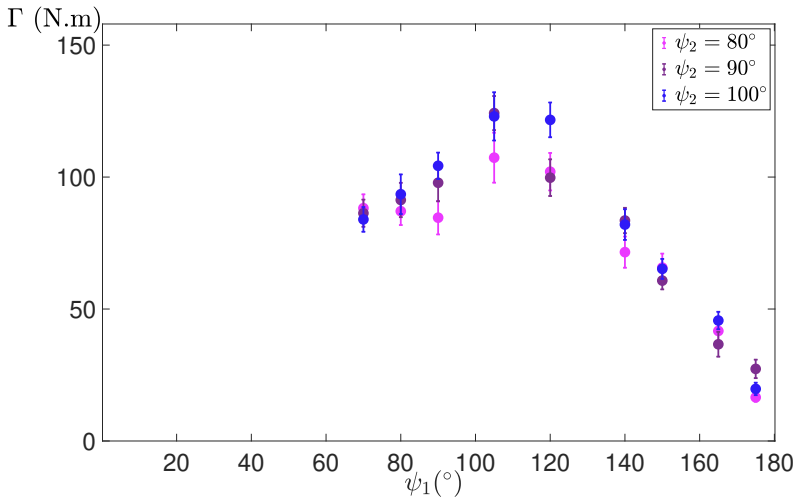


Figure 5.14: Maximal isometric torque of the knee extensors of the novice player for three different ψ_2.

Therefore, we keep the approximation that the torque of the knee extensors is a function of ψ_1 and not ψ_2. Further complete experimental studies could be lead to measure $\Gamma(\psi_1)$ for $\psi_2 \in [90; 180]°$.
Finally, we only conduct this experiment for one leg for each subject. In the model of Figure 5.10, we multiply Γ by two in order to obtain the complete torque produced by the two legs. However, we know that the performance of the lower-limb muscles is more or less symmetric in terms of force production [76, 77]. It would be interesting to measure the isometric torque of the knee extensors of each leg for a player in order to take into account this asymmetry in the model.

To explain the isometric torque curves, Herzog *et al.* [78] develop a theoretical cross-bridge model (cf. 6.5.1) extended for each muscle of the quadriceps. With this model, they recover a maximum in force production for ψ_1 around 100° and they observe a shift of the maximum towards 110° for $\psi_2 = 180°$.
The following model we develop to understand the isometric torque curves is in the spirit of the one developed in [79], but with the aim of introducing as few parameters as possible.

5.5.3 Knee model

Knee extension

Firstly, we need to understand how a knee extension movement is working and how the muscles of the lower limb can produce isometric forces.

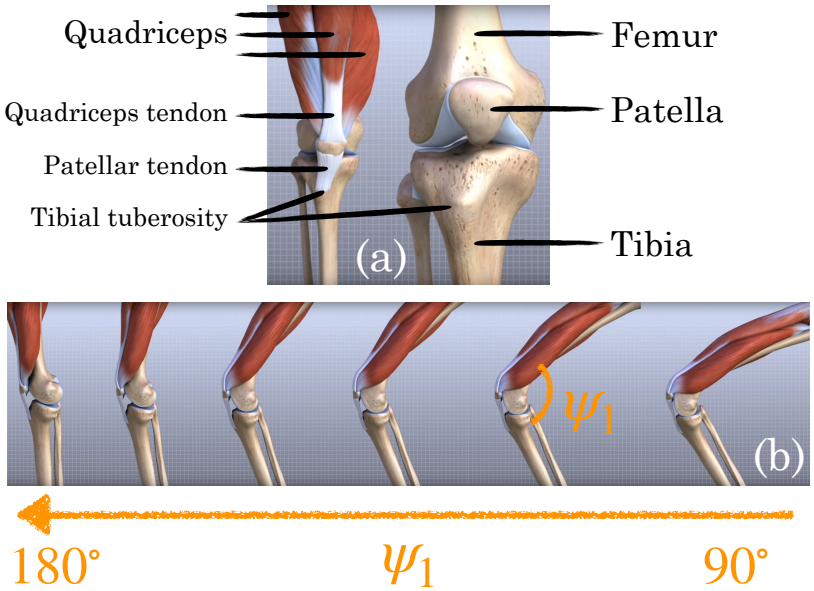


Figure 5.15: Knee schemes. Figure extracted from video [80]. (a) Bones and muscles that are involved in knee extension. (b) Extension of the knee. We observe the length reduction of the quadriceps and the singular movement of the patella during knee extension (from $\psi_1 = 90°$ to 180°.

Let us introduce the most important components of a knee that we consider in our model. All the presented information is taken from [81] where we have a complete presentation of the knee joint.
The muscles involved in knee extension are called the knee extensors and correspond to the quadriceps[4]. These muscles take their origins at the level of the femur head/greater

[4]Quadriceps muscles: rectus femoris, vastus lateralis, vastus medialis, vastus intermedius.

trochanter and have a common insertion at the level of the patella with the quadriceps tendon. Then, the patella is linked to the tibial tuberosity with the patellar tendon. All the bones and muscles evoked are presented in Figure 5.15a.

By contracting the quadriceps, the length of the muscle is reduced and this forces the patella to move towards the head of the femur. This action drives the patellar tendon by lengthening it and this leads to a rise of the tibia (cf. Figure 5.15b). In other words, this leads to a knee extension. With our convention, during a knee extension, ψ_1 increases[5]. $\psi_1 = 180°$ corresponds to the full extension of the knee where it is almost impossible to produce torque. For simplification purposes, we do not consider the antagonist hamstrings and gluteal maximus in the isometric force production process. We only consider an articulation with a single muscle that extends the knee to produce knee torque, and it is then perfectly (also for simplification purposes) transmitted to the back of the player.

Minimal physical model

Our one-knee model is composed of a femur, a tibia, and a patella. We connect the head of the femur with the tibial tuberosity through a single wire muscle by passing on the one-point patella. A schematic view of our model is given in Figure 5.16a where the wire muscle is drawn in red, the patella is represented with a gray circle and the red circle corresponds to the center of rotation of the knee. The femur and the tibia are represented in black lines.

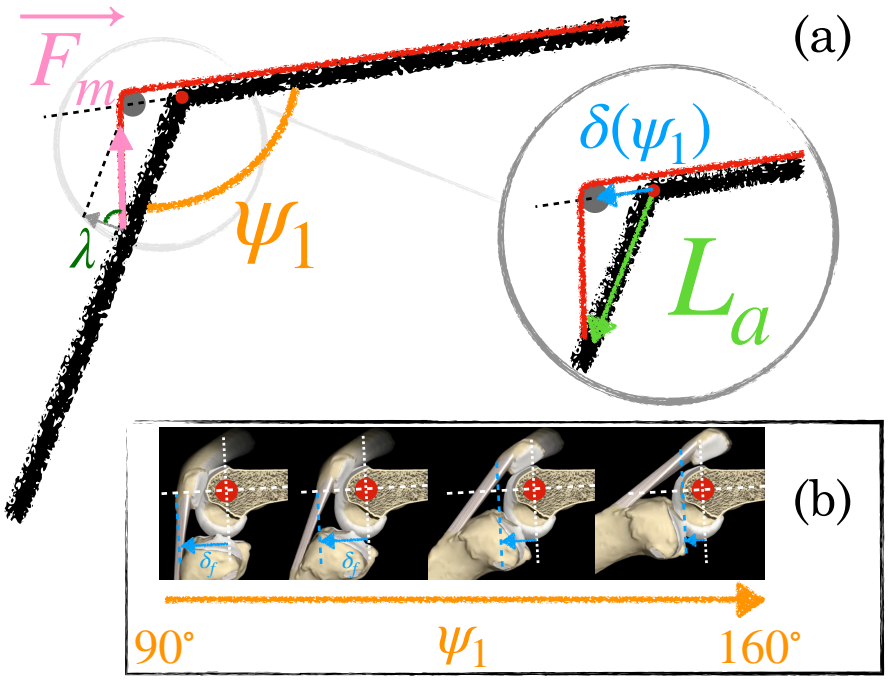


Figure 5.16: Model of the isometric torque of the knee extensors. (a) Scheme of the model with the patellar tendon force $\vec{F}_m$, the distance $\delta(\psi_1)$ between the center of rotation of the knee (marked with a red circle) and the patella position, and the length L_a between the center of rotation of the knee and the tibial tuberosity. (b) Patella displacement during the knee extension extracted from a video [82]. The evolution of the distance $\delta(\psi_1)$ is represented with the blue arrows.

By contracting the muscle, its length is shortened and it creates the muscular force $\vec{F}_m$ through the patellar tendon that lifts the tibia. We are interested in isometric force, which

[5]In literature about the knee joint angle, it is often characterized by the knee flexion angle which is the complementary angle of ψ_1 $(180° - \psi_1)$.

means ψ_1 is locked during force production. The torque $\Gamma(\psi_1)$ at the level of the knee rotation center is given by the product of the useful force $F_m \cos\lambda$ (represented with a gray arrow in Figure 5.16) to raise the tibia by the length L_a, the distance between the rotation center of the knee and the tibial tuberosity.
During extension, the patella does not have the same location for each ψ_1. Figure 5.16b shows the patella movement during a knee extension. When the knee is at a right angle, the patella is aligned with the femur axis and is at a distance δ_f of the rotation center represented in red. We call $\delta(\psi_1)$ the projected distance between the patella and the center of rotation of along the femur axis. For simplification of calculations, we only consider a 1D movement of the patella along this axis during the extension. We then observe, that when ψ_1 increases, at first δ is almost constant, and then δ decreases for ψ_1 around 120-130°.

We search to determine a mathematical expression of $\Gamma(\psi_1)$. Firstly, we need to express λ (cf. Figure 5.16a) in terms of ψ_1, L_a and δ. We apply the law of cosines formula[6] in the triangle defined by L_a, δ and the patellar tendon length L_{PT}. We obtain:

$$L_a L_{PT} \cos\left(\frac{\pi}{2} - \lambda\right) = L_a^2 + L_{PT}^2 - \delta^2(\psi_1). \tag{5.8}$$

Another application of Al-Kashi's theorem tells us that:

$$L_{PT}^2 = \delta(\psi_1)^2 + L_a^2 - 2\delta(\psi_1) L_a \cos(\pi - \psi_1). \tag{5.9}$$

By injecting equation (5.8) into equation (5.9), and noticing that $\cos(\pi - \psi_1) = \cos(\psi_1)$, we obtain an expression for $\frac{\pi}{2} - \lambda$. Then, Γ is equal to

$$\Gamma(\psi_1, L_a, F_m, \delta) = L_a F_m \cos\lambda = L_a F_m \sin\left(\frac{\pi}{2} - \lambda\right). \tag{5.10}$$

We get an isometric knee extensors torque which is determined by the following equation:

$$\Gamma(\psi_1) = F_m L_a \sin\left(\arccos\left(\frac{L_a + \delta(\psi_1)\cos\psi_1}{\sqrt{\delta(\psi_1)^2 + L_a^2 + 2\delta(\psi_1) L_a \cos\psi_1}}\right)\right). \tag{5.11}$$

We can simplify this expression by using $\forall x \in [-1;1], \sin\arccos(x) = \sqrt{1-x^2}$ and $\forall x \in [0;2\pi]$, $\sqrt{1-\cos^2(x)} = \sin(x)$. In the end, we find that:

$$\Gamma(\psi_1) = \frac{F_m L_a \delta(\psi_1)\sin(\psi_1)}{\sqrt{\delta^2(\psi_1) + L_a^2 + 2\delta(\psi_1) L_a \cos\psi_1}}. \tag{5.12}$$

We note that Γ depends on

- two geometrical parameters: δ, that depends on ψ_1, and L_a which is fixed.
- a muscular force of the patellar tendon $\vec{F_m}$ which is difficult to measure.

5.5.4 Application to player 1

We are going to apply this model to the data of the Academy-level hooker of Racing 92.

[6] Known as Al-Kashi's theorem in French

Geometrical parameters of the knee

Using x-rays of the knee, with the consent of the participant, we directly measure δ and L_a on the obtained medical images. However, we said that δ is not constant, so we need multiple positions of the knee at different ψ_1 if we want to apply this model.
In Figure 5.17a, we have a left knee x-ray image of player 1. This image is made on the same knee used for the isometric torque of Figure 5.13. In Figure 5.17a, the left knee is bent at an angle $\psi_1 \sim 100°$. We see the previously introduced components of the knee: the femur, the patella, and the tibia. X-ray images do not allow us to see the muscles and the tendons. But, we are able to measure the two geometrical parameters of the model: δ represented in blue and L_a represented in green. We measure $\delta = 5$ cm and $L_a = 9$ cm. The tibial tuberosity is recognizable thanks to two bumps on the edge of the tibia between which the patellar tendon hangs.
In Figure 5.17b, we have an equivalent x-ray image with $\psi_1 \sim 160°$. As we already mentioned, we see the displacement of the patella which is no longer in the femur prolongation. The corresponding projected δ is equal to 2.7 cm and L_a remains the same.

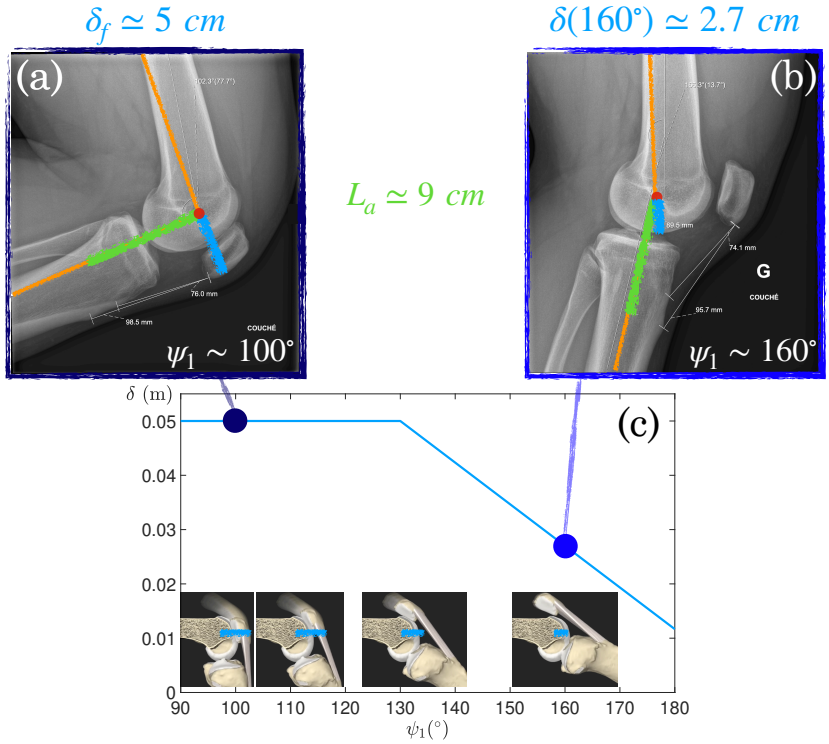


Figure 5.17: Measurement of the geometrical parameters δ and L_a for player 1. (a) X-Ray knee image for $\psi_1 \sim 100°$. (b) X-ray knee image for $\psi_1 \sim 160°$. X-ray images were obtained thanks to Quentin Vincent, a former member of the medical staff of Racing 92. (c) *delta* evolution with the patella displacement through the knee extension.

Then, as we see in Figure 5.17c, we track on a dimensionless video [82] the position of the patella during a knee extension. We observe that we can approximate the movement of the patella along the femur axis with two regimes:

- a constant regime where $\delta = \delta_f$ for ψ_1 between 90 and 130 °.
- a linear decrease regime for ψ_1 between 130 and 180 °.

After determining the existence of the two regimes on the video, we present the curve we have dimensioned with the values determined on X-ray images for player 1 in Figure 5.17c.

Obviously, this curve is adaptable for different subjects. We only need at least two reference values for sizing δ. Depending on the individual, there are probably many different displacements of the patella, and it likely modifies the transition value of ψ_1 between the two regimes.

Experimental fit of Fm

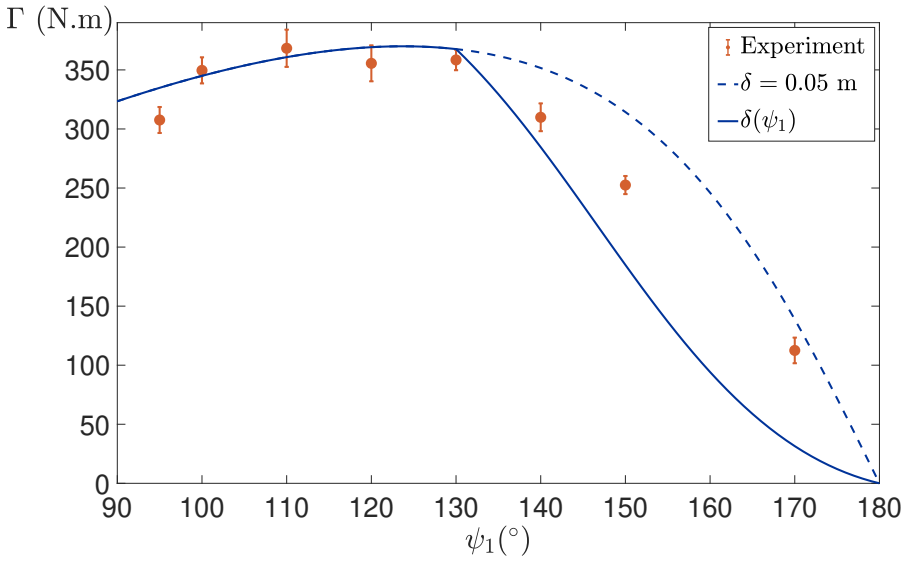


Figure 5.18: Comparison between the experimental data and the model results of the knee torque as a function of ψ_1. Experimental data are represented with orange dots. The solid blue line corresponds to the model with a constant δ, and the dashed line corresponds to the model obtained with the evolution of δ presented in Figure 5.17c.

The only unknown parameter left is F_m. We do not have any measurement techniques to determine it so we will deduce it from a numerical fit of the experimental data presented in Figure 5.13. We use a least-squares minimization on Matlab to fit the data and the mathematical expression of the equation (5.12). In the first place, we consider δ as a constant corresponding to the first regime of Figure 5.17c. The result is presented with a blue dashed line in Figure 5.18. The agreement with the experimental data is satisfying until $\psi_1 \simeq 130°$. The best fit is obtained with $F_m = 7400$ N.
In a second step, we consider the evolution of δ plotted in Figure 5.17c. The model curve obtained is represented in Figure 5.18 with the solid blue line. This consideration slightly improves the experiment-model agreement, especially for the two points between $\psi_1 = 130°$ and $\psi_1 = 150°$. This curve does not allow us to know if we need to consider the two regimes of the evolution of δ. But, we are going to see that it is essential to consider the dependence in ψ_1 for δ when we compare the result of the model with the experimental F_{a_x}.

5.6 Discussion

5.6.1 Comparison experiment/model

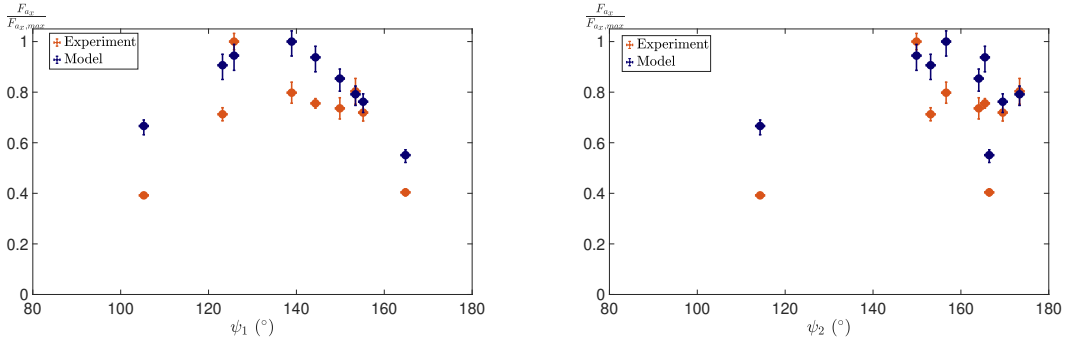
From equations (5.12), (5.6) and (5.7), we deduce the complete expression of F_{a_x}:

$$F_{a_x} = \frac{2F_m L_a}{L} f(\psi_1) \cos\left(\theta - \alpha_{back} + \psi_2 - \frac{\pi + \psi_1}{2}\right) \cos(\alpha_{back}), \tag{5.13}$$

with $f(\psi_1) = 2\sin\left(\frac{\psi_1}{2}\right) \frac{\delta(\psi_1)}{\sqrt{\delta^2(\psi_1) + L_a^2 + 2\delta(\psi_1) L_a \cos\psi_1}}$.
By measuring the angles on side-view videos (cf. Figure 5.6), and considering the previously determined parameters, we compare the experimental and model results for player 1.
The necessity to consider a decreasing δ with ψ_1 comes from the limit when $\psi_1 \to \pi$. Indeed, when the knee tends towards the full extension, we have:

$$\lim_{\psi_1 \to \pi} f(\psi_1) \to \frac{2\delta}{L_a - \delta}. \tag{5.14}$$

If we had considered $\forall \psi_1, \delta(\psi_1) = \delta^{ct}$, then it would have been problematical for our model because the horizontal active force would have tended toward a constant when $\psi_1 \to \pi$. But, we observe that F_{a_x} tends towards 0 when the player is fully extended.
By adding a second regime with a decreasing δ[7], we get closer to $F_{a_x} = 0$ when $\psi_1 = 180°$. With this consideration, we find back the results about optimal angles in Figure 5.19 and about optimal length l in Figure 5.20).



(a) **(b)**

Figure 5.19: Comparison between the experimental and the model dimensionless active force in terms of joint angles for player 1. (a) $\frac{F_{a_x}}{F_{a_x,max}}$ versus ψ_1. (b) $\frac{F_{a_x}}{F_{a_x,max}}$ versus ψ_2.

In Figure 5.19a, we plot the dimensionless active force as a function of ψ_1. The experimental data are represented in orange and the model results are represented in blue. We note a good-shape experiment-model agreement, with an optimal experimental active angle ψ_1 around 130 ° and a model optimal around $\psi_1 \sim 130 - 140°$. In the same way, Figure 5.19b shows us that the optimal trial corresponds to an angle $\psi_2 \simeq 150°$.

The obtained optimal angles are slightly superior to the ones seen in Figure 5.2 but they are similar to the different experimental results of the different articles cited in the state-of-the-art section.

[7] We notice in Figure 5.17c that $\delta(180°) \neq 0$, but it is enough to find a decrease in F_{a_x} from $\psi_1 = 140°$ in Figure 5.20

Finally, let us compare experimental and theoretical $F_{a_x}(l)$. In Figure 5.20, we keep the same color conventions as in Figure 5.19. In the results section, we said that the experimental optimal length $l^{exp}_{opt,h}$ for player 1 is between 103 and 108 cm. The model set a theoretical optimal length l^{th}_{opt} at 108 $\pm$1 cm.

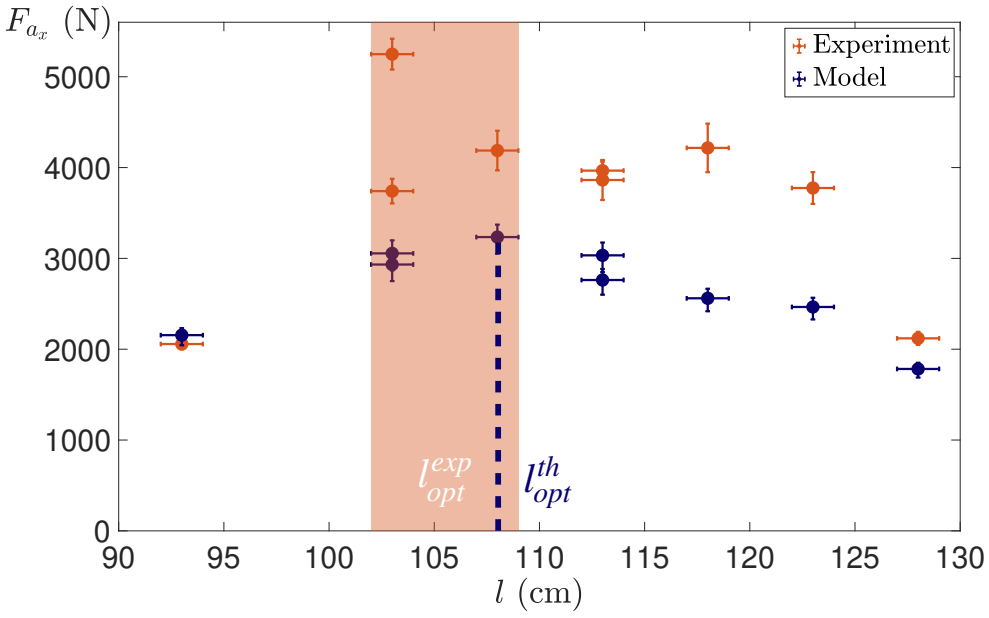


Figure 5.20: Comparison of the experimental (orange) and theoretical (blue) active force F_{a_x} as a function of l.

The shapes of the experimental and model curves are similar. However, we observe an underestimation of F_{a_x} by the model. On the force plateau between $l = 103$ cm and $l = 123$ cm, the difference between the experimental and the model F_{a_x} is of the order of magnitude of 1000 N (with a maximum difference of almost 2000 N). This order of magnitude corresponds approximately to the weight of the concerned player.
This difference could come from the approximations we made through the development of the model. For example, we consider a constant muscular force in the patellar tendon F_m whatever ψ_1. Indeed, even if in terms of order of magnitude the F_m we obtained makes sense [83][8], we still have a bad behavior of the evolution of the tendon length for the first regime we defined in Figure 5.17c. Another possible improvement is to take into account the patellar tendon force-elongation relationship [83, 84, 85].
But, this model is already very detailed and difficult to set up for only one individual. The minimum requirement to apply the model is to know the evolution of the isometric torque of the knee extensors during the knee extension, to measure the segments (L_T, L_C, L_M) of the player, and to have a side-view video of the experimental protocol on the scrum machine. Moreover, the mathematical model of the knee extension requires even more resources with X-ray images for different ψ_1. This is why, in the next chapter, we will develop simpler models to understand the individual optimal posture.

[8]The order of magnitude of the patellar tendon elongation $L_{PT} \simeq 4 - 5$ mm is also similar to the values of [83]

5.6.2 Experimental setup limits

The most likely reasons for this difference are surely related to our experimental setup. After this experimental session with academy-level players, we identified several experimental setup changes to implement:

- Foams are not rigid enough.
- The shoe-surface interaction is not representative of an ecological situation (cf. Figure 5.4). The players sometimes take all their feet support on the bar (no contact with the ground anymore), this is probably why the F_x measured are so important.
- It exists a height dependence of the force measurement due to experimental setup construction. These results are presented in the internship report of Baptiste Loire [66].
- We have an important barillet distortion with the side-view GoPro (cf. Figure 5.6).
- We need to measure the vertical forces in order to understand more precisely the postures adopted by the players.

The solutions adopted are outlined at the beginning of the next chapter.

Take home message of Chapter 5

We investigate the optimal individual scrummaging posture from the perspective of the optimal joint angles that maximize force production.

1. Optimal joint angles. In the laboratory environment, the joint angles that maximize the production of individual horizontal force are most of the time higher than the ones observed in real scrums. The posture adopted when the player is alone is not constrained by his/her teammates. The experimental setup in studies about scrums is most of the time static scrum machines that do not perfectly mimic what happens in a live scrum. The notion of stability is not included in our study but it has an important effect on the choice of the posture of the player. The optimal posture probably comes from the compromise of the optimal posture to maximize the production of force and the optimal posture to not lose equilibrium in a scrum.

2. A Knee model of production of force with the knee extensors was developed. This individual mechanical model is composed of two geometrical parameters identified on X-Ray images. This model allows us to compare experimental data of an Academy-level hooker of Racing 92 with the theoretical active force obtained with this 2D stickman representation of this player.

3. Experimental setup modifications have been highlighted through this study: the feet support bar enables players to produce a high amount of force as if they are pushing against a wall behind their feet and the force sensors location is not optimal.

6

Optimal Individual Scrum Posture on Grass

We present the modifications of the laboratory scrum machine setup and we use it to construct individual pushing force abacus.



Picture of a scrum during the Women's Six Nations match between Wales and Ireland in 2021. Credits: Catherine Ivill

Contents

6.1	Pushing Postures Observed in Other Sports	**92**
6.2	Updated Experimental Setup	**95**
6.3	Results	**99**
6.4	Model of the Passive Force $\vec{F_p}$	**112**
6.5	Model of the Active Force $\vec{F_a}$	**122**
6.6	The Total Force: Comparison Experiments/Model	**125**
6.7	Conclusion	**129**

This work has been done with Simon Giraud, Caroline Cohen, and Christophe Clanet.
A special thanks to Alice Boillet, Awa Dimel Sy, Antoine Garcia, Caroline Frot, Romain Labbé and Juliette Amauger.

In this chapter, we continue our study on optimal individual posture but we now measure biaxial forces (horizontal and vertical) and players have cleat shoes on a synthetic grass built in the laboratory. The new subjects follow a protocol where we vary the distance of the feet to the scrum machine l, and for one of them, we also vary the pushing height h in order to explore a complete range of posture. At the end of the chapter, we focus on the influence of the cleat size on force production.
A theoretical 2D model of the player as a single segment stickman is proposed to account for the experimental observations.

6.1 Pushing Postures Observed in Other Sports

To characterize the pushing, we consider here the main direction of the body of the player defined by the segment between the shoulders and the metatarsal joint. This segment allows us to define the angle θ with the ground. We represent in Figure 6.1 the typical range of θ that can be measured on side-view real scrums during the sustained phase.

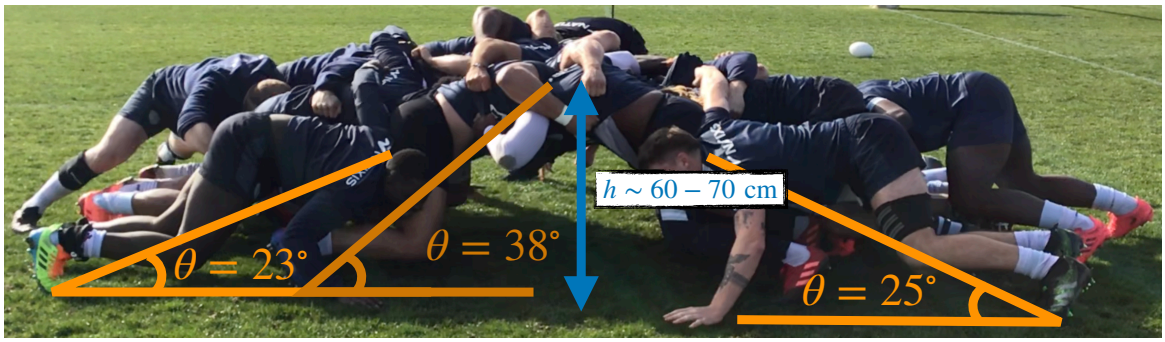


Figure 6.1: Example of a practice scrum with Racing 92 professional players. In orange, we define θ on different forwards. We remark that θ is smaller for third-row players than for first row players.

The observation of several real scrums reveals that the typical range of θ for front row players is 30-40 ° whereas it stands in the range of $\theta \sim 22 - 26°$ for flankers. We will compare those angles to the ones observed with the main subject of our study in this Chapter. We add that the typical pushing height h measured on practice scrums is around 60-70 cm.
Looking at players in this typical scrummage posture, we have been thinking about different sports that present similar individual or collective strength battles. Let us start with a comparison with the beginning of Sumo fights.
In Figure 6.2, we can see an example of the beginning of a Sumo fight. It is extracted from a recent event called Natsi Busho that takes place every year in May in Tokyo. A battle always starts with the two participants behind white lines that we can see in Figure 6.2a. The goal is to push the opponent outside of the playing area delimited by the white circle. After the authorization of the referee, the two players leap toward each other as fast as possible (cf. Figure 6.2b). Contrary to the scrum situation in Union Rugby, the player is not binding to each other before the "impact". When a player starts to touch the opponent with his arms (cf. Figure 6.2c), their typical θ are quite high compared to the ones observed in scrums. Then, they battle with angles θ of the order 50 to 65° in Figure 6.2d.

Obviously, this situation is a really dynamic one, it can recall the way scrums started 20-30 years ago with an important distance between the front rows to accelerate the body.
We are now going to measure θ in a collective battle situation closer to the Rugby Union Scrum: the line of scrimmage in American Football. This team sport is mostly played in North America. It probably has a common ancestor with the Union Rugby and the name

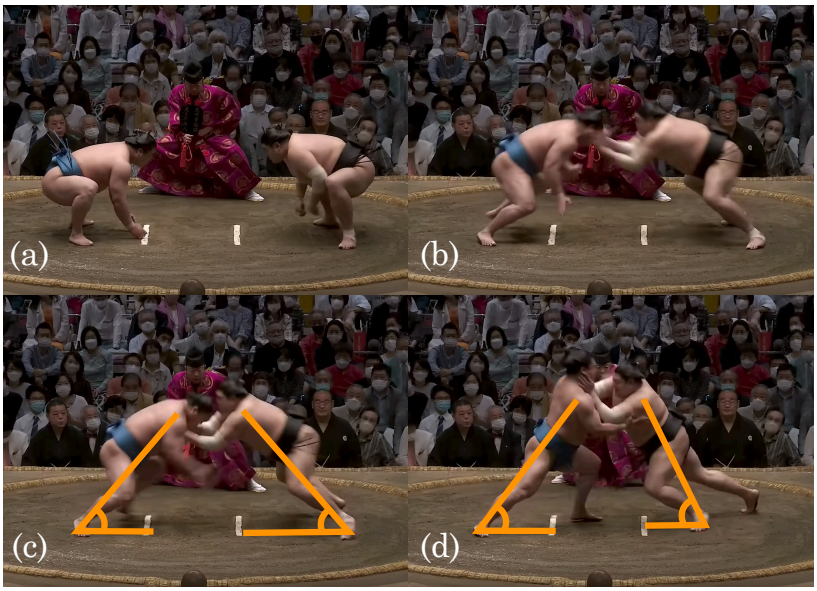


Figure 6.2: Chronophotography of Wakatakakage versus Abi fight at Natsi Busho 2022. Extracted from video [86]. (a) Sumo fighters are waiting to leap on the opponent. (b) They launch their body in a quasi-synchronous way toward the opponent. (c) and (d) Sumo fighters are touching their opponent, they are almost standing up and forcing with their legs to push the opponent outside of the dohyō.

scrimmage could be a marker of it [87, 88].

This very codified sport opposes two teams of eleven players: one is attacking in order to score a TouchDown[1] while the other one is defending. At each game launch, the two teams are organizing themselves in a way close to the one presented in Figure 6.3a. At least five players (the Center who has the ball, the Guards, and the Tackles) of the attacking team (in white in this figure) set themselves in position in front of the line of scrimmage (noted LS in Figure 6.3a) defined by the position of the ball. The Center (noted C in Figure 6.3b) is in charge to pass the ball to the quarterback (noted QB Figure 6.3a), and the other offensive linemen have to protect the quarterback while he is launching the ball (the trajectory of the ball is drawn in white dashed line in Figure 6.3d). Other players in this offensive line could be receivers and are eligible to receive the ball from the quarterback in order to score a touchdown.
The defensive linemen are starting to run when the Center starts his pass to the quarterback (cf. Figure 6.3b) and try to push the offensive linemen to reach and hinder the quarterback (cf. Figure 6.3c). We observe in Figure 6.3d, a collective strength fight composed of 1 vs 1 or 2 vs 1 fights. Once again, we can define the order of magnitude of the angle θ, even if it exists a bias due to the camera angle. Angles are probably close to 60-75 ° and are similar to the ones observed in Sumo fights. Once again, three different objectives in three different sports but it seems that strategies to produce force after a signal are similar in Sumo and American football, while in Rugby Union, players seem to use more of their body's natural weight to influence force production.

We also note that Sumo and American football show situations with players pushing with nonparallel feet, and this situation could be also seen in Rugby. Most of the forward players use quasi-parallel feet disposition in the scrum. In [62], in individual scrummaging the

[1]Reaching the End-Zone with the ball in a player's hands.

authors do not measure any significant difference on force production in function of feet configuration whereas Bayne *et al.* [65, 89] measure higher compression forces for parallel feet compared to nonparallel feet.
With the evolution of the rules of the scrum (cf. Chapter 2.2), the Rugby Union scrum is different from the launch of action in American football since speeds are lower and players are bound together. It seems that scrum is a more controlled situation that could help the players to put themselves in a better position to produce force.
Finally, the main difference between Sumo, American Football, and Rugby Union scrum is the applying force zone: forward rugby players transmit the forces towards opponents thanks to their cervical while Sumo and football players are using their chest and their arms.

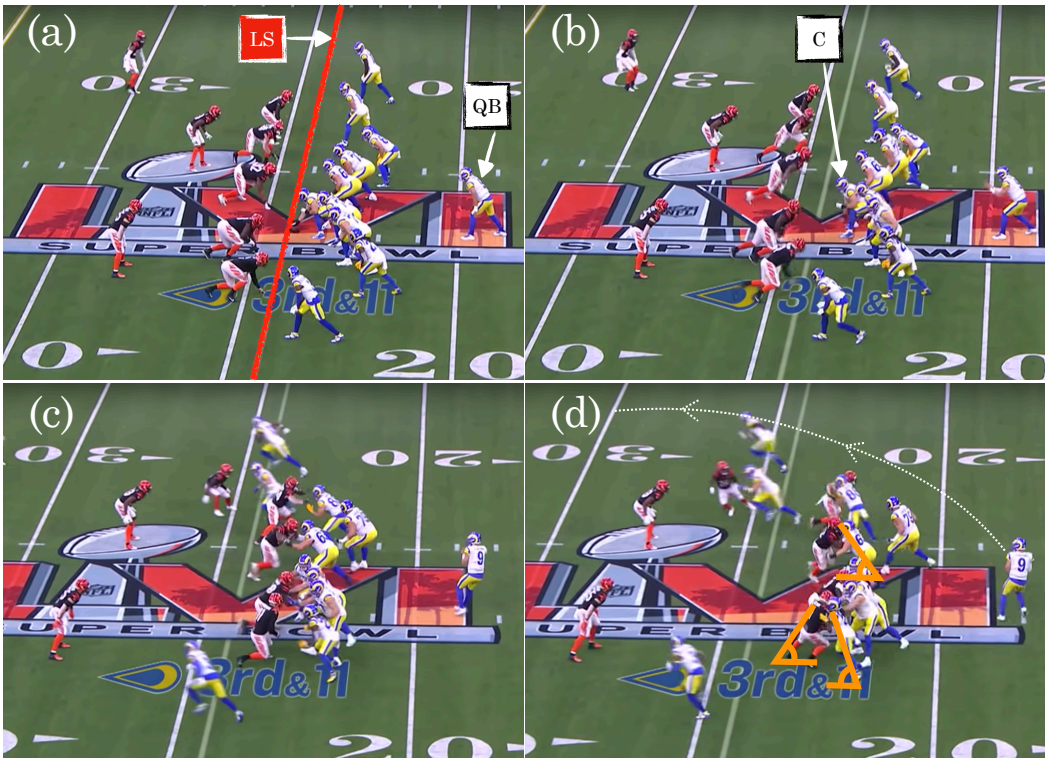


Figure 6.3: Chronophotography of a game launch at the LVI Super Bowl with Los Angeles Rams (white team) versus Cincinnati Bengals (black team). Extracted from [90]. (a) Line of scrimmage in red. Quarterback (QB) is organizing the offense. (b) The defending team in black is running towards the offensive line to charge the quarterback. The Center (C) passes the ball to the QB. (c) Offensive and defensive linemen are pushing each other to protect and disturb the quarterback respectively. (d) The fight between the two lines allows us to define θ pushing angles. The QB is about to throw the ball.

We study scrum posture at the individual level with the improved scrum machine device presented in section 5.2.1. We investigate a wider range of postures with our main subject and we develop a theoretical model to understand why players adopt this kind of postures in scrums.

6.2 Updated Experimental Setup

6.2.1 Modifications

After the previous experimental study, the pushing foams have been changed for stiffer ones with a Young Modulus ten times higher [66]. The force measurement was changed for a two components force platform designed by *Phyling* start-up[2] and screwed to the metallic plate attached to the L-shape structure and linked with a wooden plate to the new foams as we can see in Figure 6.4a. In Figure 6.4b, we present a top-view picture of force platforms and the new foams. The 2D force platforms measure the forces along the x and y axes.
In Figure 6.4c, we present the other major modification which is the construction of a 130×110 cm tub of synthetic grass for the foot support of the players. The bottom is made of a Medium Density Fiberboard panel and the surround is made of wood rafters. We then glued and stapled to the bottom the synthetic fiber turf mat of 55 mm height provided by Tarkett SPORTS®. We add a two centimeters layer of sand on top of it and another two-centimeter layer of SBR (Styrene Butadiene Rubber) aggregates coated with a green resin in which the cleats penetrate. We use this material in order to reproduce the artificial grass of Racing 92 practice field that is made by Tarkett SPORTS®.
The complete side-view scheme of the updated experimental setup is presented in Figure 6.4d.

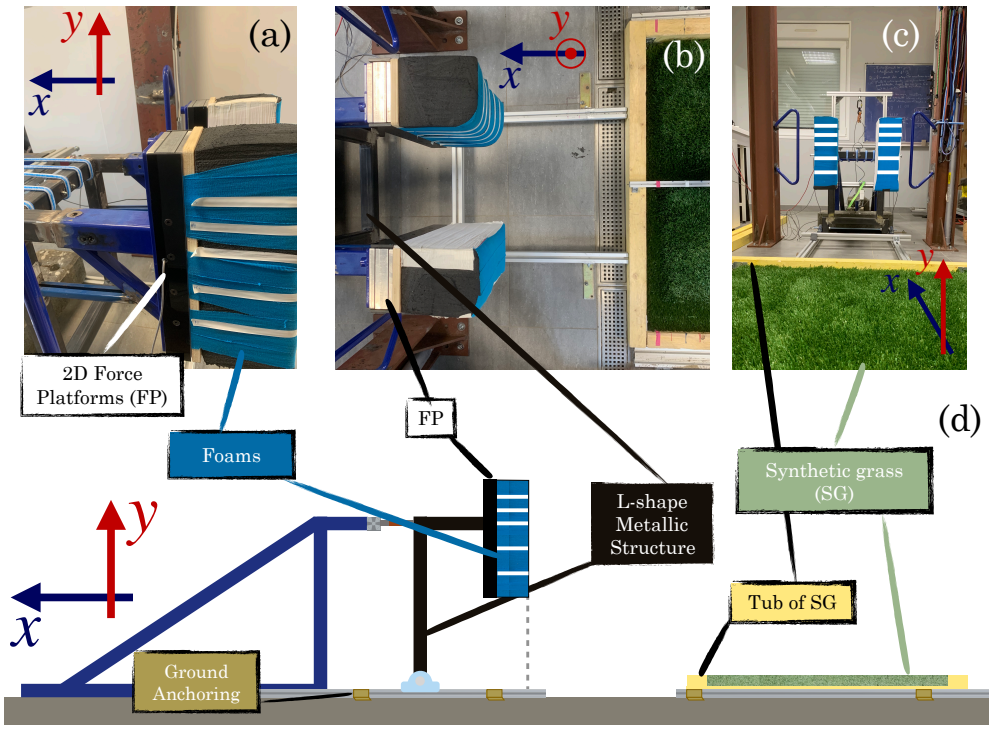


Figure 6.4: Updated version of the instrumented scrum machine. (a) Side-view picture of the new foams and the new 2D force platforms that measure F_x and F_y. (b) Top-view picture of the new foams and the tub of synthetic grass. (c) Front-view picture of the experimental setup with the white bands that mark the different pushing heights in the experimental protocol. (d) Side-view scheme of the experimental setup.

A side-view camera is synchronized with the force measurement device and it acquires images at 50 Hz with a wide-angle camera lens of a focal length of 10 mm. We use this camera

[2] *Phyling* website: `https://www.en.phyling.fr/`

lens in order to reduce barrel distortion while having a wide field of view. F_x and F_y are recorded at 1000 Hz.

6.2.2 Protocols

Participants

Three participants that we introduce in Table 6.1 took part in the new experimental study. The two novice players follow the same protocol as the one described in the previous chapter in subsection 5.2.1. Subject A follows the experimental protocol we are going to present below.

Player	Gender	Age (Years)	Mass (kg)	Height, $\mathcal{L}_{size}$ (cm)	Playing-level	Control parameters
A	M	22	75	185	Former amateur	h and l
B	F	24	61	176	Novice	l
C	M	26	61	176	Novice	l

Table 6.1: Age and anthropometrics of the three subjects involved in this study.

Subject A is a former amateur rugby player who used to play as a third-row forward. He is physically trained and practices basketball occasionally.
Subject B has never played Union Rugby, she is well physically trained, and she is an amateur swimmer practicing weightlifting several times a week.
Subject C has never played Union Rugby, he is not well trained physically compared to the two other subjects, but he has more opportunities to repeat the individual pushing scrum task on this scrum machine compared to subject B. He is practicing road cycling on a weekly basis.

Rugby Boots

The interaction between feet and ground is more realistic in this study because players are wearing cleat shoes.

The novice subjects B and C use the same pair of rugby shoes presented in Figure 6.5a. The model is Kaizen X 2.1 Power Rugby Boots with 8 studs from Gilbert® in size 7.5 (41 EUR). In Figure 6.5b, there is a picture of the pair of shoes used by subject A. The model is Agility V2 700SR SG from Kipsta® in size 10.5 (45 EUR).
In Figure 6.5, the presented pairs are equipped with 21 mm cleats on the front. The influence of cleats length on subject A performance is discussed in Chapter 7. We observe that the disposition of the cleats is not the same under the sole of each shoe model: 6 screw-in studs on the front for the left pair and 4 screw-in studs on the front for the right pair. But, it is important to notice that when novices are pushing against the scrum machine, there are only 4 studs by foot stuck in the ground. So, for all the subjects the number of cleats anchored in the ground is the same during the experiment.

Instructions

We ask subjects B and C to push at a constant height $h = h_{cmp} \sim 62$ cm and vary the control parameter l by imposing different distances between 87 and 127 cm in a randomized



Figure 6.5: Cleat shoes used by the three subjects. Both pairs are equipped here with 21 mm studs on the front of the shoes. (a) Shoes worn by subjects B and C. (b) Shoes worn by subject A.

order. We ask the players to align their metatarsal joints markers with the tested l. In post-process, we visualize the feet position of the subject and measure the exact l. We correct it if necessary.

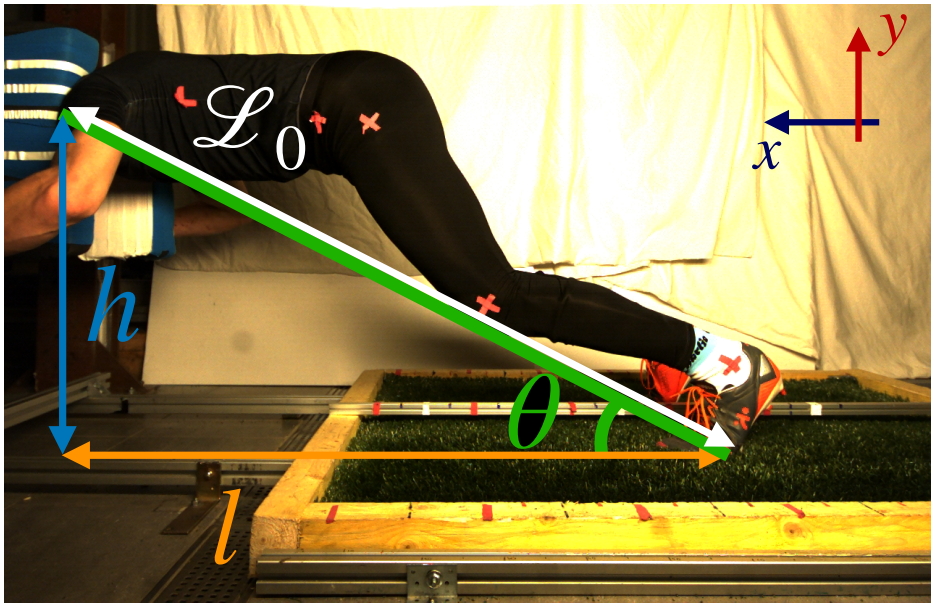


Figure 6.6: Example of an active push of the main subject at $l = 132$ cm and $h = 62$ cm. We define its elongation length $\mathcal{L}_0$ and the angle θ. The horizontal direction corresponds to the x-axis and the vertical direction to the y-axis.

For subject A, we add one more control parameter which is the pushing height h in order to investigate a wider range of players' postures. We investigate five heights between 47 and 70 cm and six lengths l between 90 and 132 cm. We notice in Figure 6.4 some white bands on the foams that we also see on the left of Figure 6.6. These white bands are here

to materialize the five heights tested for each distance l. They help the subject position his shoulders according to the instruction. The white band in the middle corresponds to h_{cmp}. For each trial, we measure the player elongation length $\mathcal{L}_0$ between shoulders and metatarsal joints marker defined in Figure 6.6. The maximal $\mathcal{L}_0$ that a player can reach in full extension is called $\mathcal{L}$. Thus, we define the dimensionless elongation factor as the ratio $\frac{\mathcal{L}_0}{\mathcal{L}}$. For subject A, we have $\mathcal{L} = 155$ cm. The angle θ corresponding to the angle of the segment $\mathcal{L}_0$ with respect to the ground is also measured. θ is related to h and l by the relation:

$$\theta = \arctan\left(\frac{h}{l}\right). \tag{6.1}$$

For each trial, we ask the player to produce a maximal isometric pushing force during 4-5 seconds and then the player is asked to stay on the scrum machine in a passive way for the same amount of time. Both phases are done without using arm strength.
In order to check the repeatability, several combinations of control parameters (h, l), were tested twice by subject A. We respect a resting time of at least two minutes between each trial and there are never more than 15 tests performed in 4 hours.

6.2.3 Range of postures

Subject A is experiencing extreme postures corresponding to lowest and highest heights h and lengths l. These positions are presented in Figure 6.7.

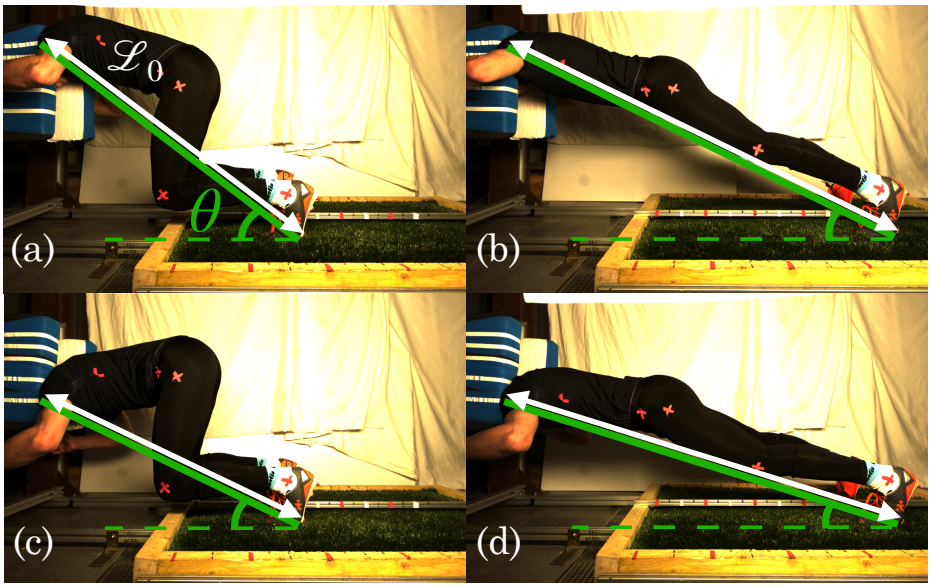


Figure 6.7: Example of pushing postures for $l = 92$ cm and $l = 132$ cm tested on the left and the right respectively. Postures adopted for $h = 70$ cm and $h = 48$ cm tested are at the top and the bottom respectively. (a) $\theta = 37°$, $\mathcal{L}_0 = 105$ cm. (b) $\theta = 26°$, $\mathcal{L}_0 = 140$ cm. (c) $\theta = 26°$, $\mathcal{L}_0 = 95$ cm. (d) $\theta = 18°$, $\mathcal{L}_0 = 135$ cm.

In Figure 6.7, we see that l has a bigger influence than h to change the posture of the player. The green line stands for the main axis of the player that characterizes his elongation and allows to measure the angle θ. In Figure 6.7a and c, we note that the player is compressed, especially when he is at the lowest height, it seems complicated to produce force in such

positions. In Figure 6.7b and d, the player is almost totally elongated with a body almost aligned with the main axis. In Figure 6.7a, subject A has an angle $\theta \simeq 37°$ and an elongation $\mathcal{L}_0 = 105$ cm. In Figure 6.7b and c, he has the same angle $\theta \simeq 26°$ but his elongation is different with $\mathcal{L}_0 = 140$ cm and $\mathcal{L}_0 = 95$ cm. In Figure 6.7d, the player is closer to the ground with $\theta \simeq 18°$ and $\mathcal{L}_0 = 135$ cm. The maximum length $\mathcal{L}_0$ that could be reached by a participant is called $\mathcal{L}$. We call the elongation factor the ratio $\frac{\mathcal{L}_0}{\mathcal{L}}$.

6.3 Results

6.3.1 Example of a 2D force signal

With the new force platforms, we now measure the horizontal and vertical forces produced by the player. An example of a force signal measured for Subject A subject at $l = 124$ cm and $h = 62$ cm is given in Figure 6.8.

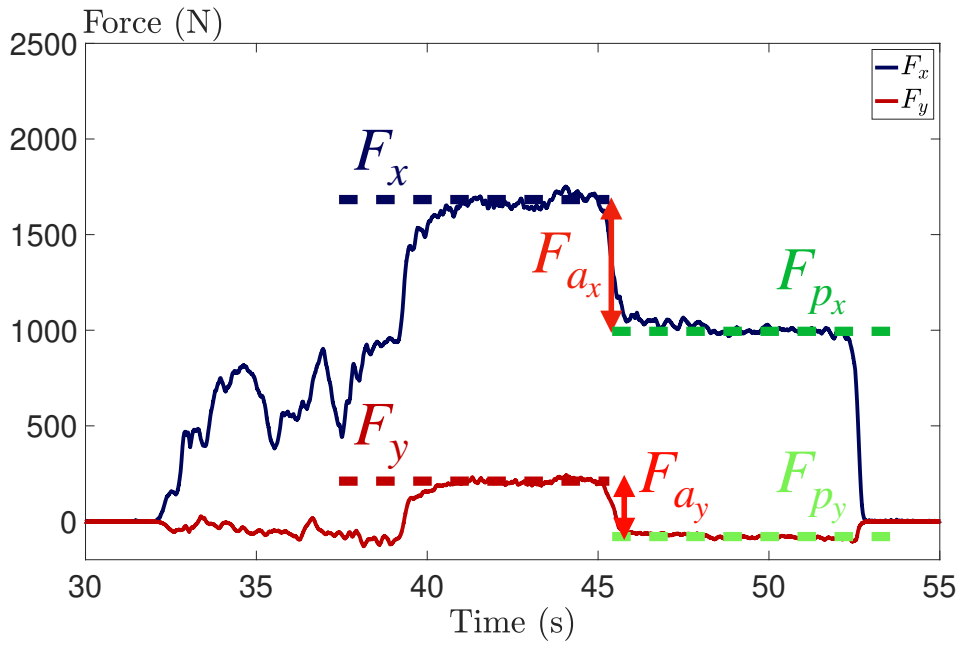


Figure 6.8: Example of force signal of subject A at the pushing height $h \simeq 62$ cm and length $l = 112$ cm. We decompose the total plateau force $\vec{F} = F_x\vec{e_x} + F_y\vec{e_y}$ with passive and active component: $F_x = F_{a_x} + F_{p_x}$ and $F_y = F_{a_y} + F_{p_y}$.

We keep the same definitions for the total horizontal force F_x composed of the passive force F_{p_x} and of the active force F_{a_x}. The horizontal force is represented with a dark blue line in Figure 6.8. We also measure the vertical force that has an average value of F_y during the active phase. We see in this example that the total vertical force is positive, meaning that the player is pushing upwards. We also decompose this component into the passive force F_{p_y} and the active force F_{a_y}. In this example, F_{p_y} is observed to be slightly negative. For each force measurement F_i, we calculate the uncertainties ΔF_i by taking the standard deviation of the temporal evolution of F_i over the averaging time.

6.3.2 Total forces: F_x and F_y

For the following results, in each subsection, we will first introduce subject A results and then we will compare them to subjects B and C results obtained for the fixed pushing height h_{cmp}. We also compare with subject C experiments with the feet support at fixed h_{cmp}.

Participant A

We have two control parameters for the main subject that allow us to present the results in a 2D space within abscissa the feet distance l and on the ordinate the pushing height h. In Figure 6.9a, we give values of F_x for each trial of the main subject. F_x decreases when h increases and is non-monotonic with l. Indeed, at fixed h, F_x increases from $l = 92$ cm to $l = 124$ cm and then decreases for $l = 132$ cm.

We then have an optimal pushing zone at low h and for $l = 124$ cm represented in orange in Figure 6.9a. The maximum horizontal forces reached by this player are around 2000 N, it represents 2.7 times his weight. And the lower F_x is around 950 N which is approximately 1.3 times his weight in the weakest pushing zone represented in light blue in Figure 6.9a. In Figure 6.9, we also show the side view snapshots during trials that correspond to posture that gives lower horizontal forces in Figure 6.9b and posture that allows him to perform his best F_x in Figure 6.9c.

In Figure 6.9b, we measure in green $\theta \simeq 20°$ and elongation factor $\frac{\mathcal{L}_0}{\mathcal{L}}$=0.85. We also measure the joint angles (ψ_p, ψ_1, ψ_2) represented in yellow, orange, and red respectively. We measure $\psi_p = 93°$, $\psi_1 = 84°$, and $\psi_p = 102°$. In Figure 6.9c, we measure $\theta \simeq 35°$ and $\frac{\mathcal{L}_0}{\mathcal{L}}$=0.65. We measure $\psi_p = 102°$, $\psi_1 = 152°$, and $\psi_p = 151°$.

F_x is the useful component of the force in order to push the opponent in a scrum. With this upgraded experimental setup, we also measure the F_y component which allows us to know the direction of the total force in the sagittal plane of the player. In Figure 6.10, we present the F_y map in the (l, h) plane. The maximal vertical forces are reached for higher pushing heights compared to the F_x optimal pushing zone of Figure 6.9a. F_y values range from 0 to 300 N and the higher values are found for l between 100 and 125 cm.

Comparison with subjects B and C at constant pushing height h_{cmp}

If we compare the total force obtained for the pushing height $h_{cmp} \sim 62$ cm corresponding to the one used in protocol with the two novice players (subjects B and C) wearing 21 mm cleat shoes, we obtain the curves $F_x(l)$ and $F_y(l)$ in Figures 6.11 and 6.12 respectively.

We recognize the curve shapes that allow us to define an optimal length l_{opt} corresponding to the maximum of different curves. We still notice that it exists different optimal lengths for the different subjects when they use cleats. Subject A has a higher optimal length ($l_{opt} \sim 124$ cm) than subjects B and C which seem to have approximately the same optimal length ($l_{opt} \sim 112$ cm). Once again, it is interesting to notice that subjects B and C have the same height of 176 cm (cf. Table 6.1). Subject A, which measures 185 cm, has an optimal length of approximately 10 cm higher than subjects B and C.

In Figure 6.12, we observe that the total vertical forces are always positive (one exception for the Novice M at $l = 122$ with a trial slightly under 0 N), which means that players always naturally push upwards when activating their muscles and trying to produce maximal isometric force. The higher vertical forces are reached for $l = 110 \pm 5$ cm for our three subjects.

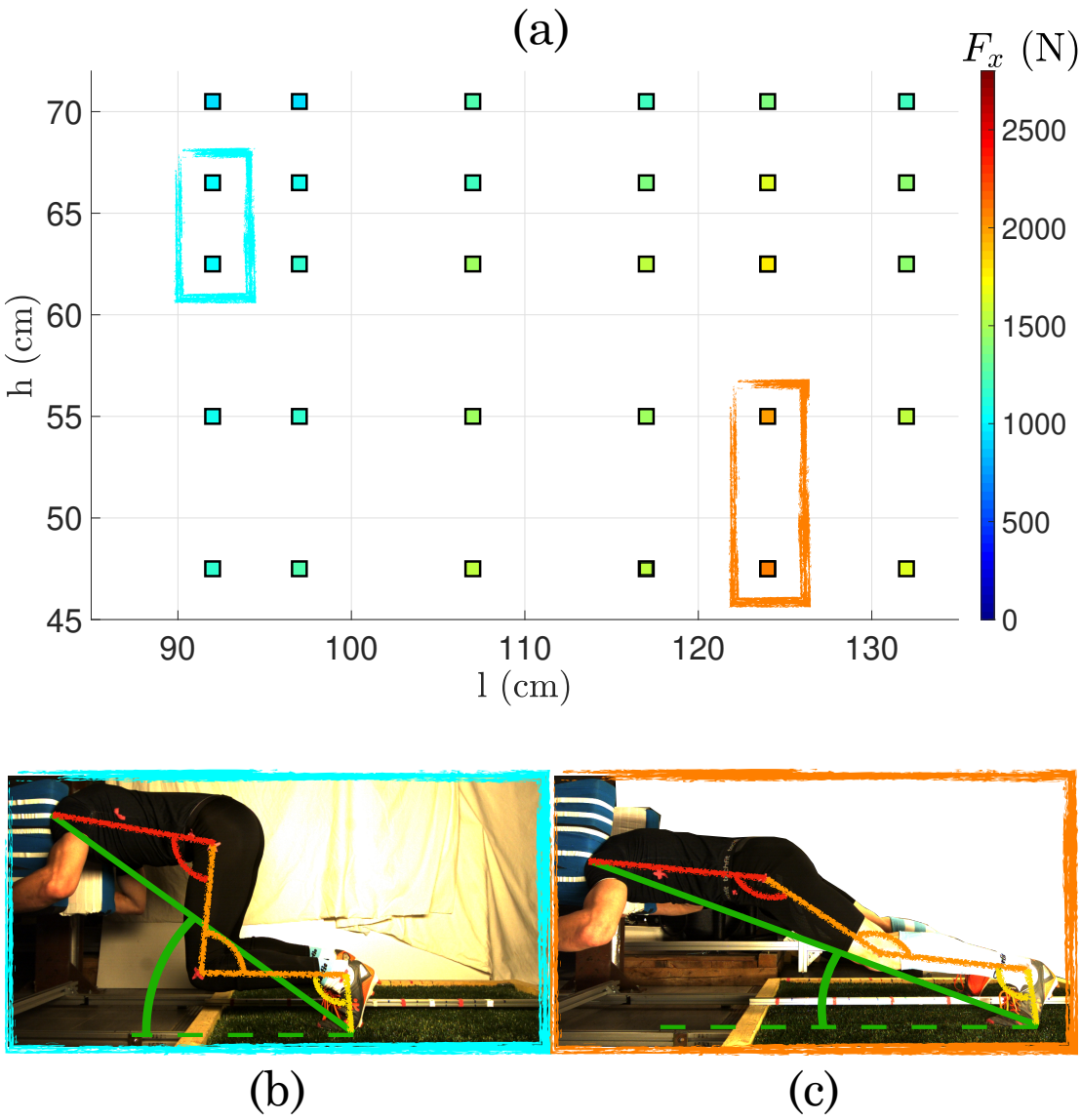


Figure 6.9: Horizontal forces F_x of subject A for the different (l, h) tested with examples of the worst and the best posture in terms of force production. (a) The orange rectangle corresponds to the optimal zone of pushing while the blue corresponds to trials where the subject was close to the lowest produced forces. (b) The worst posture corresponds to the light blue zone in (a). We measure $\theta = 35°$, $\psi_1 = 84°$, $\psi_2 = 102°$, and $\psi_p = 93°$. (c) Best posture corresponding to the orange zone in (a). We measure $\theta = 20°$, $\psi_1 = 152°$, $\psi_2 = 151°$, and $\psi_p = 102°$.

For our three subjects, we present pictures of their best postures at h_{cmp} in Figure 6.13. As we said, the feet distance for subjects B and C is equivalent but subject A has his feet 10 cm further.
Subject C has an optimal knee angle $\psi_1 = 130°$ and an optimal hip angle $\psi_2 = 156\circ$. His optimal joint angles are equivalent to the optimal joint angles measured for the Academy-level players of Racing 92 in Figures 5.8 and5.9. But, subjects A and B have higher and lower optimal angles respectively. We measure the optimal angles $\psi_1 = 110°$ and $\psi_2 = 135°$ for subject B. It is interesting to see that even if subjects B and C have the same l_{opt}, the same mass, and the same height, they have slightly different optimal joint angles. We measure the optimal angles $\psi_1 = 160°$ and $\psi_2 = 161°$ for subject A. This trial corresponds to $h = 62$ cm and $l = 124$ cm in Figure 6.9a.

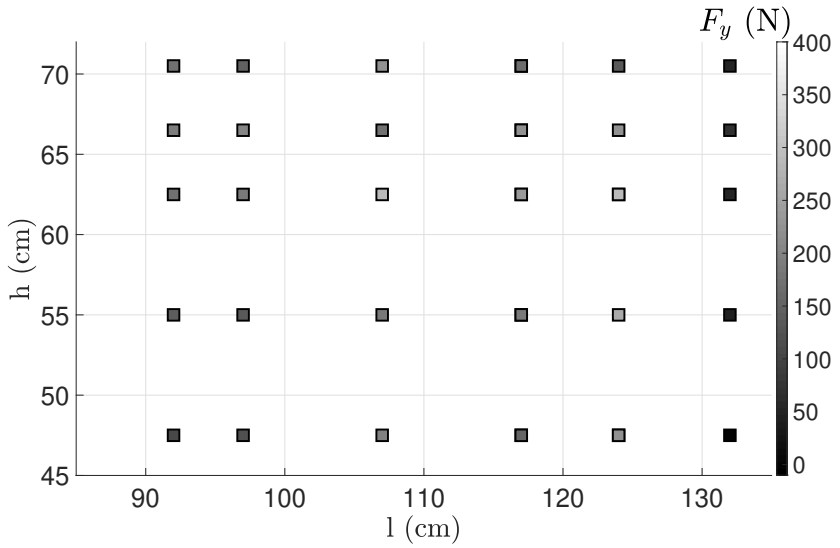


Figure 6.10: Vertical forces F_x of subject A for the different (l, h) tested.

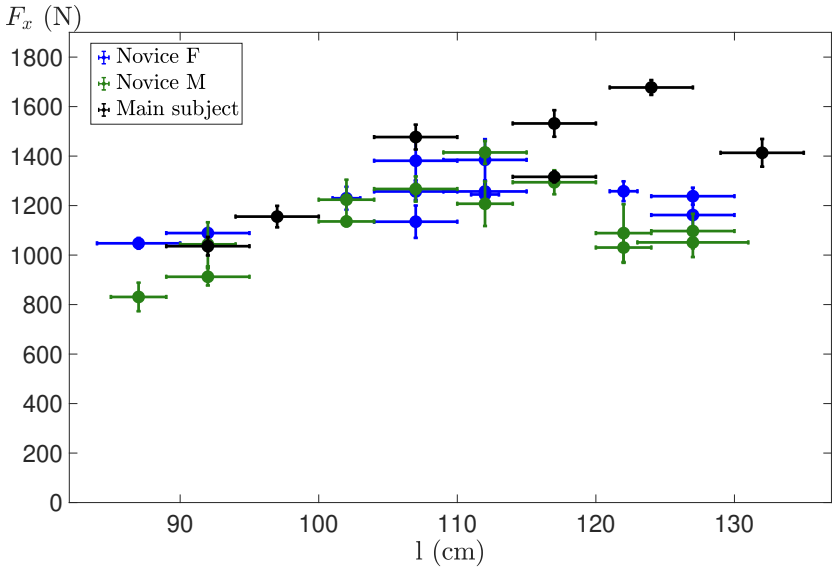


Figure 6.11: F_x as a function of l for the three subjects equipped with 21 mm cleats at pushing height $h \sim 62$ cm.

These differences in optimal joint angles could be linked to their gender differences, mass distribution differences, physical form, and sheathing quality. For example, Subject B is trained, she is an assiduous weightlifter and swimmer while subject C is less trained and he is a weekly road cyclist. However, he benefited from more training on this scrum machine than subject B. Interestingly, they develop an equivalent amount of force for the range of tested distance l in Figure 6.11.

At his optimal posture for h_comp, which is not his total optimal trial obtained for lower h, subject A adopts a $\theta \simeq 25°$ while the novices B and C have a $\theta \sim 27°$.

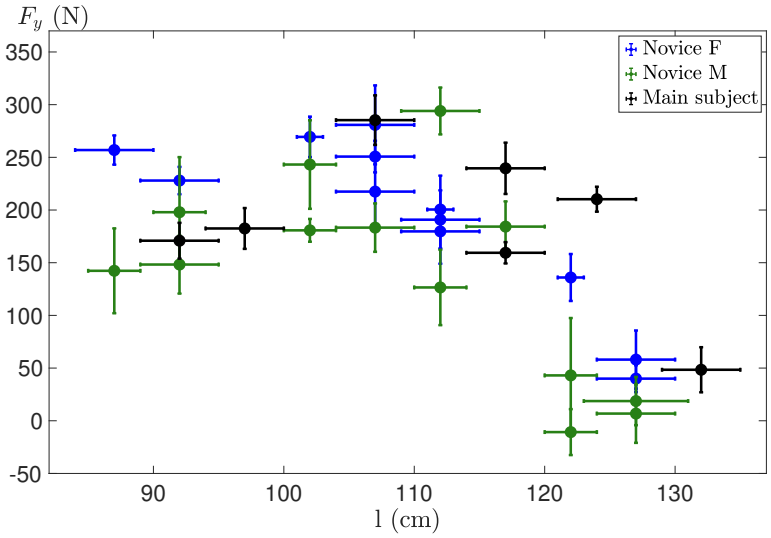


Figure 6.12: F_y as a function of l for the three subjects equipped with 21 mm cleats at pushing height $h \sim 62$ cm.

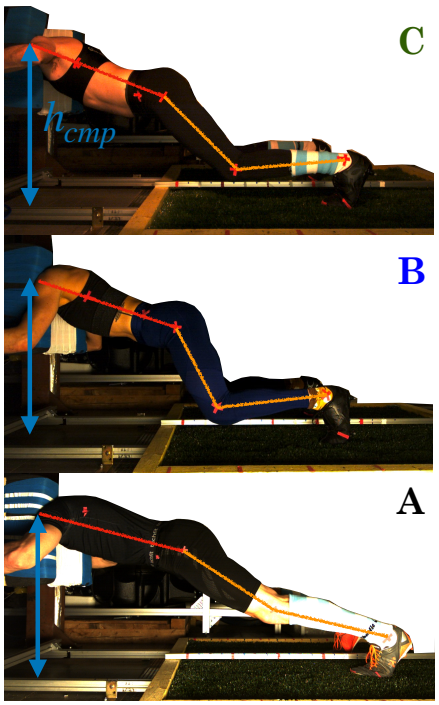


Figure 6.13: Snapshots of optimal postures for the three subjects at pushing height h_{cmp}. We measure the angles $\psi_1 = 160°$, $\psi_2 = 161°$ and $\theta = 25°$ for Subject A. We measure the angles $\psi_1 = 130°$, $\psi_2 = 156°$ and $\theta = 27°$ for Subject B. We measure the angles $\psi_1 = 110°$, $\psi_2 = 135°$ and $\theta = 27°$ for Subject C.

6.3.3 Active Force

Subject A

The active force is composed of two components F_{a_x} and F_{a_y} defined in Figure 6.8. In Figure 6.14, we present F_{a_x} and F_{a_y} obtained with subject A in the (l, h) plane.

The map of F_{a_x} is similar to the F_x map in Figure 6.9 in terms of dependence with l and h but with smaller force values. The optimal pushing zone is situated in the same area for

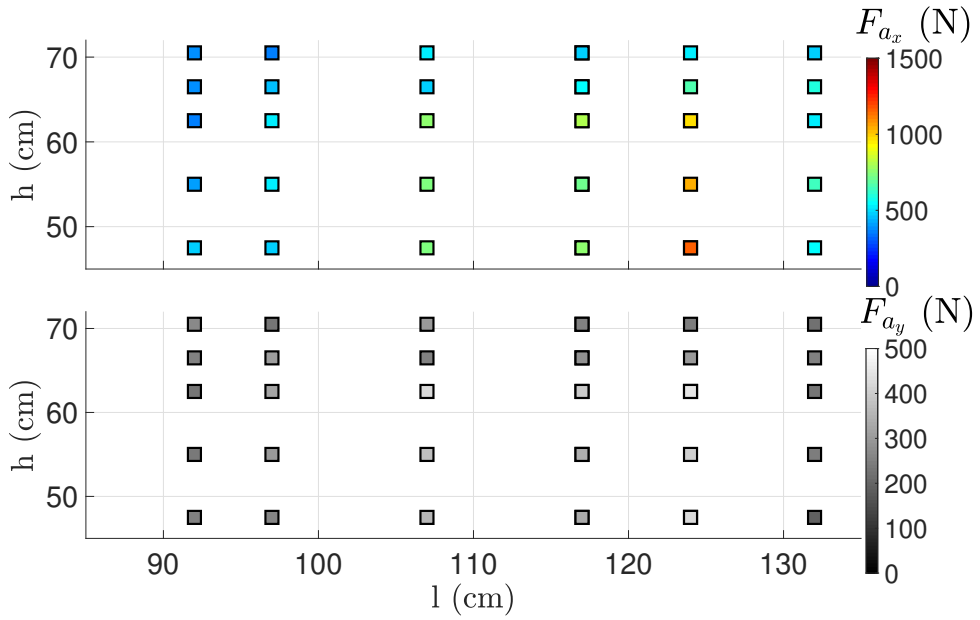


Figure 6.14: F_{a_x} and F_{a_y} as a function of (l, h) for subject A.

$l = 124$ cm and the lowest h tested. The F_{a_y} map is similar to the map of Figure 6.10 in terms of dependence with l and h with the higher forces reached for $h \simeq 70$ cm and an identical range of force values from 190 to 440 N.

Direction

The active force angle δ_a is defined in Figure 6.15a as:

$$\tan \delta_a = \frac{F_{a_y}}{F_{a_x}}. \tag{6.2}$$

We present the δ_a calculated on the subject A trials as a function of θ in Figure 6.15b. We have the active force angle that is equal to the angle θ whatever the kind of postures the main subject has. The higher θ, the more they will push actively upwards.

We plot δ_a as a function of θ for subjects A, B, and C at the pushing height h_{cmp}. In order to check the validity of equation (5.6) in subsection 5.4.2, we present the active force direction for experimental results obtained with subject C with 2D force sensors and the feet support in gray in Figure 6.15. We see that the angles δ_a as a function of θ are all aligned between the identity function in the blue dashed line and the $y = 0.9x$ function in the gray dashed line in Figure 6.16.

Whatever the subject, whether the subject is wearing cleat shoes with 21 mm cleats or pushing on foot support, the active part of the force is directed along the main direction of his-her body.

Intensity of the active force

After the direction, we study the intensity of the active force F_a. In Figure 6.17, we plot the norm of the active force F_a as a function of the elongation length $\mathcal{L}_0$ which we scale with the maximum length he could reach $\mathcal{L}$.

In Figure 6.15a, we present the results obtained for h between 47.5 cm and 62 cm. In Figure

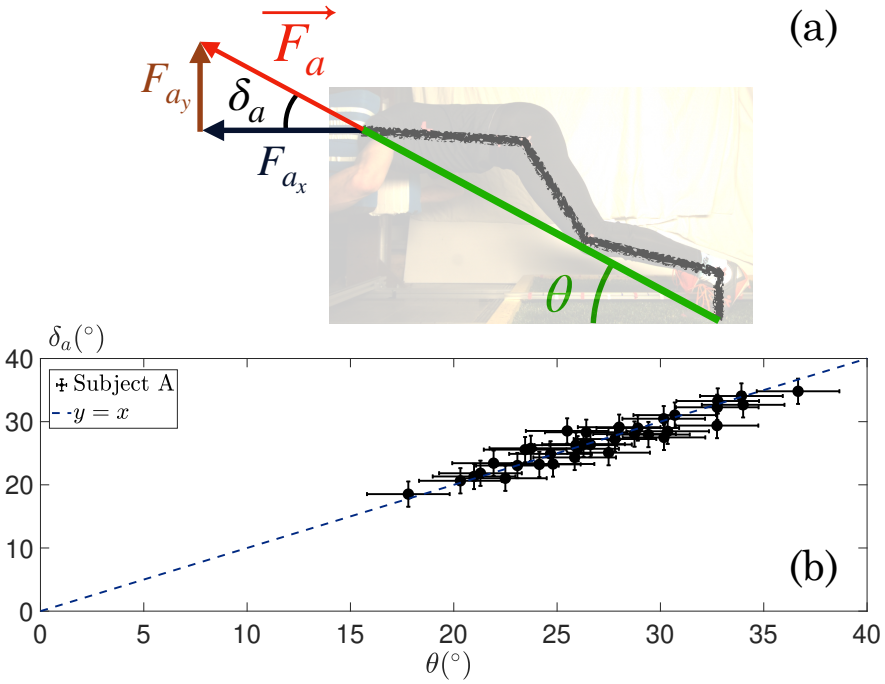


Figure 6.15: Active force angle δ_a as a function of θ. (a) Definition of the active force angle δ_a. (b) The black experimental points are aligned along the dashed line representing the identity function.

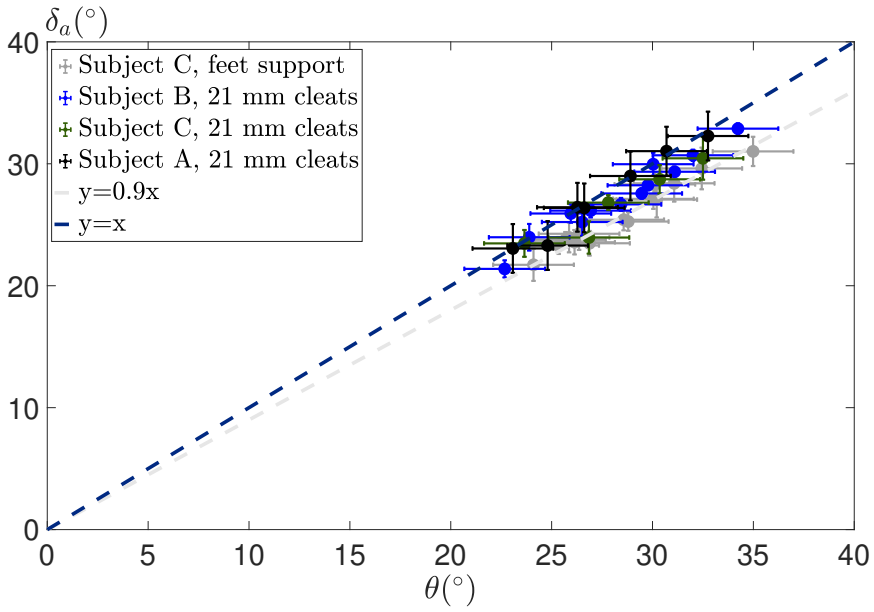


Figure 6.16: Active force angle δ_a as a function of θ for subjects A, B, and C with 21 mm cleats. The gray points correspond to the data of subject C on feet support. The blue and gray dashed lines are linear functions of θ with slopes of 1 and 0.9 respectively.

6.15b, we present the results obtained for h between 66 cm and 70.5 cm. We observe two types of behavior:

- The blue points in Figure 6.15a seem to show a maximum around $\frac{\mathcal{L}_0}{\mathcal{L}} = 0.8$
- The purple points in Figure 6.15b have a maximum in the 0.9-1 area even if like the blue points, it seems the force tends to decrease when $\frac{\mathcal{L}_0}{\mathcal{L}} \to 1$.

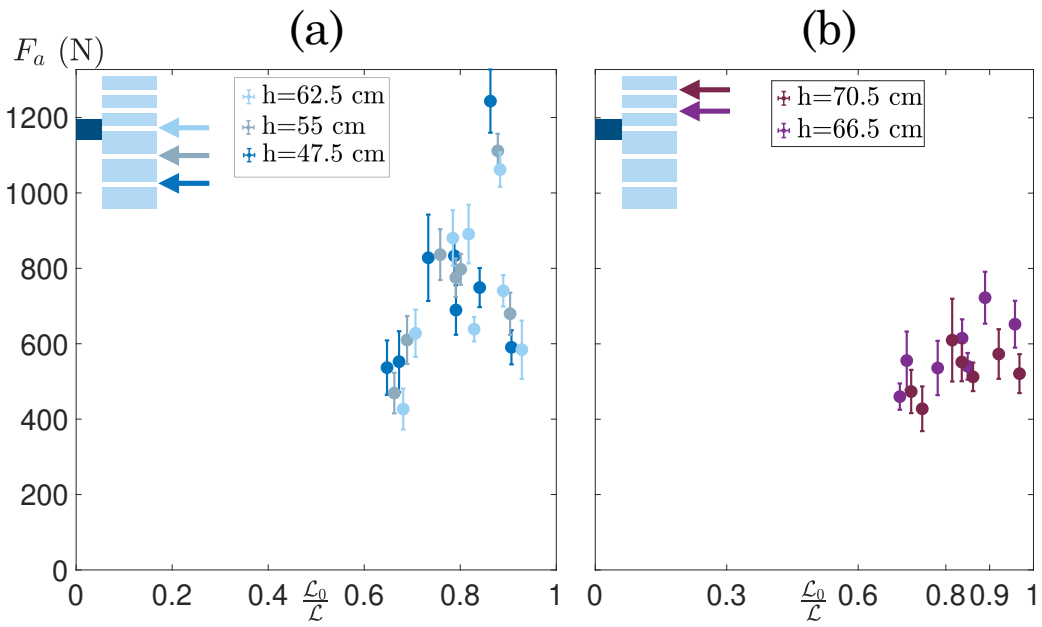


Figure 6.17: Norm of the active force F_a versus dimensionless elongation factor $\frac{\mathcal{L}_0}{\mathcal{L}}$ for subject A with 21 mm cleat shoes. (a) Active force norm for the three lowest pushing heights. (b) Active force norm for the two highest pushing heights.

Ch. 6

Moreover, it seems that the maximal active force decreases with h.
Let us compare the active force results of subject A with the results from subject B obtained for a constant pushing height h_{cmp}.

The intensity of the active force as a function of the elongation of the player seems to reach the maximum value at a similar elongation factor $\frac{\mathcal{L}_0}{\mathcal{L}} \sim 0.8$ for subjects A and C wearing 21 mm cleats in Figure 6.18. However, subject A develops more active force than subject C whatever the relative elongation.
We notice the shift in maximum location from 0.8 to 0.86 between the 21 mm cleats curve and the feet support curve of subject C. At elongation greater than $\frac{\mathcal{L}_0}{\mathcal{L}} > 0.75$, subject C produces more force thanks to the foot support. We discuss in subsection 6.7.1 the influence of optimal posture between these two situations for subject C.

6.3.4 Passive force

As for the active force, we present the results for the passive forces F_{p_x} and F_{p_y} obtained with subject A. We then study the direction and the intensity of the passive force $\vec{F}_p$.

Subject A

In Figure 6.19, we present F_{p_x} and F_{p_y} obtained with subject A in the (l, h) plane. The behavior of the passive components with l and h is different compared to the total forces (cf. Figures 6.9 and 6.10) and the active forces (cf. Figure 6.14).

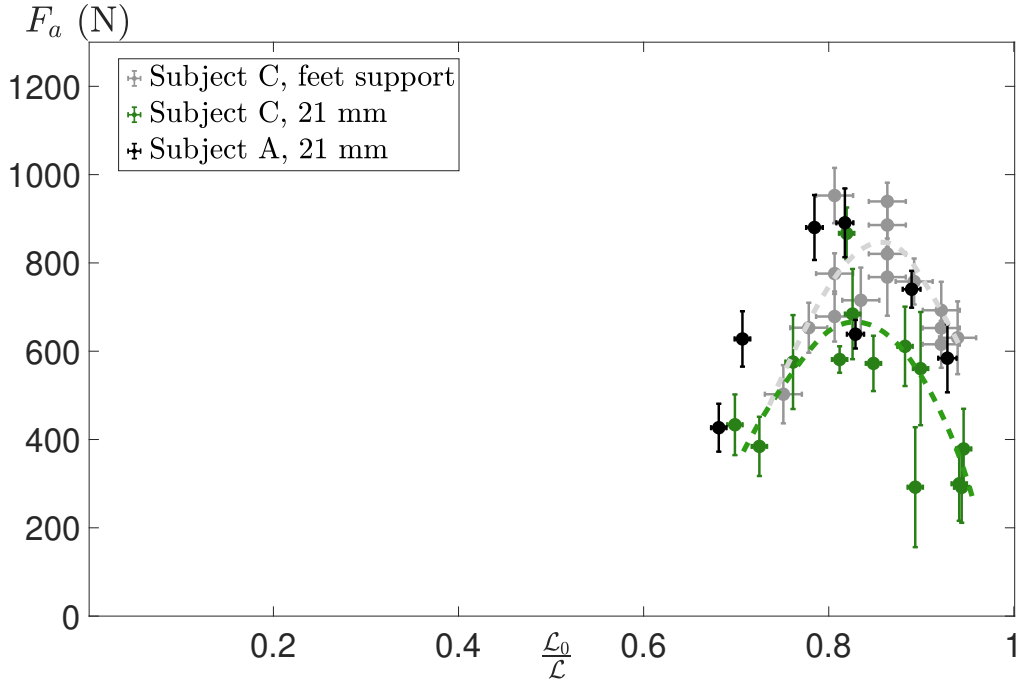


Figure 6.18: Intensity of the active force F_a versus dimensionless elongation factor $\frac{\mathcal{L}_0}{\mathcal{L}}$ for subject C with feet support and 21 mm cleats in gray and green respectively. The black points are results obtained with subject A at h_{cmp} wearing 21 mm cleats.

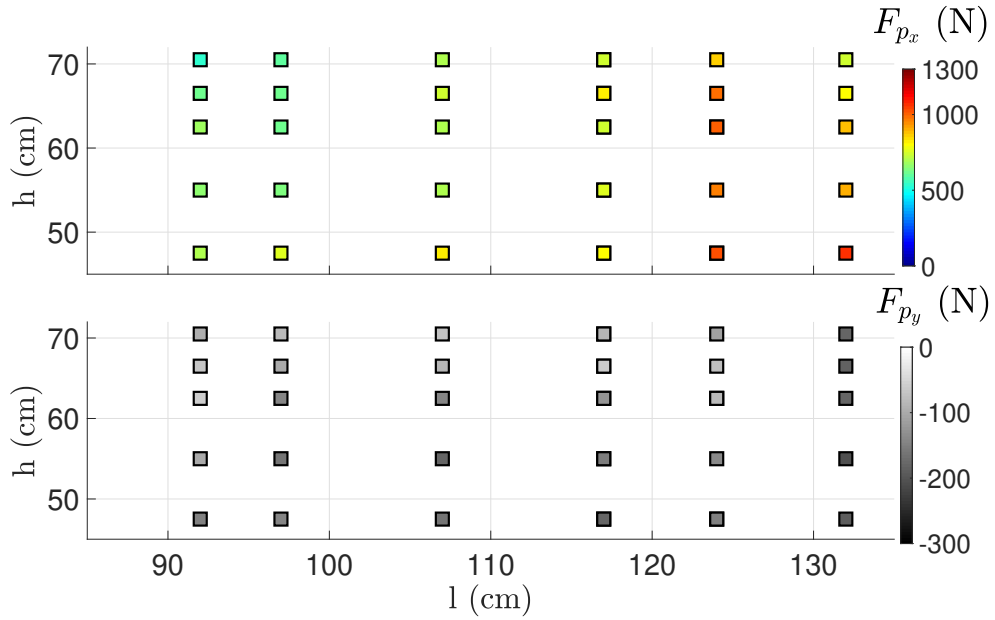


Figure 6.19: F_{p_x} and F_{p_y} as a function of (l, h) for subject A.

Indeed, the intensity of both components seems to increase with l and decrease with h. It signifies the posture of Figure 6.7a corresponds to the lowest values of passive forces with $F_{p_x} \simeq 540$ N and $F_{p_y} = -70$ N. And, the posture of Figure 6.7d corresponds to the highest values of passive forces with $F_{p_x} = 1060$ N and $F_{p_y} = -190$ N.
In Figure 6.20, we plot the opposite of F_{p_y} as a function of F_{p_x} obtained with subject A. We

note that all the experimental points are located under the blue dashed line which represents the linear function $-F_{p_y} = 0.25F_{p_x}$.

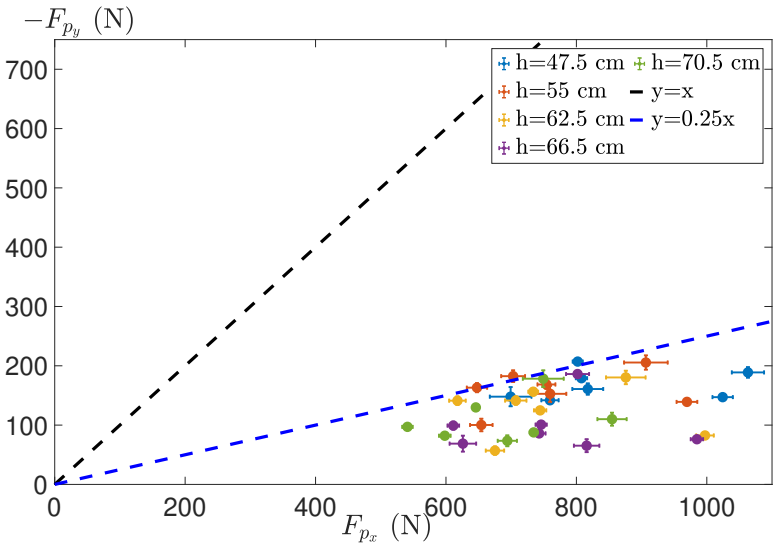


Figure 6.20: $-F_{p_y}$ as a function of F_{p_x} with colors corresponding to the different pushing heights. The black dashed line is the identity function. The blue dashed line is the linear function corresponding to $\frac{-F_{p_y}}{F_{p_x}} = 0.25$.

Ch. 6

Direction

The passive force angle δ_p is defined in Figure 6.21a as:

$$\tan \delta_p = \frac{F_{p_y}}{F_{p_x}} \tag{6.3}$$

We present the δ_p calculated on the subject A trials as a function of θ in Figure 6.21b.

Contrary to δ_a, there is no evident law of evolution between θ and δ_p. δ_p seems to range randomly between -15° and -4° for subject A.
The results are similar when we compare the δ_p angles calculated on subject C with the feet support experiments and the 21 mm cleats experiments at pushing height h_{cmp} in Figure 6.22. He obtains the same range of δ_p whatever the foot anchoring.

Due to the low values of δ_p, we focus on the intensity of the horizontal passive force behavior as a function of θ.

Intensity of the passive force

We present the reduced horizontal component of the passive force scaled with the weight of subject A as a function of θ in Figure 6.23.
F_{p_x} decreases with increasing θ. As θ changes from 18° to 36°, the horizontal passive force is divided by 2 from $1.5mg$ to $0.75mg$. Smaller θ are associated with an increase in F_{p_x}.

In Figure 6.24, we present $\frac{F_{p_x}}{mg}$ as function of θ at h_{cmp} for subject A (black points), and for subject C with 21 mm cleats (green points) and with the feet support (gray points). No clear difference is observed.

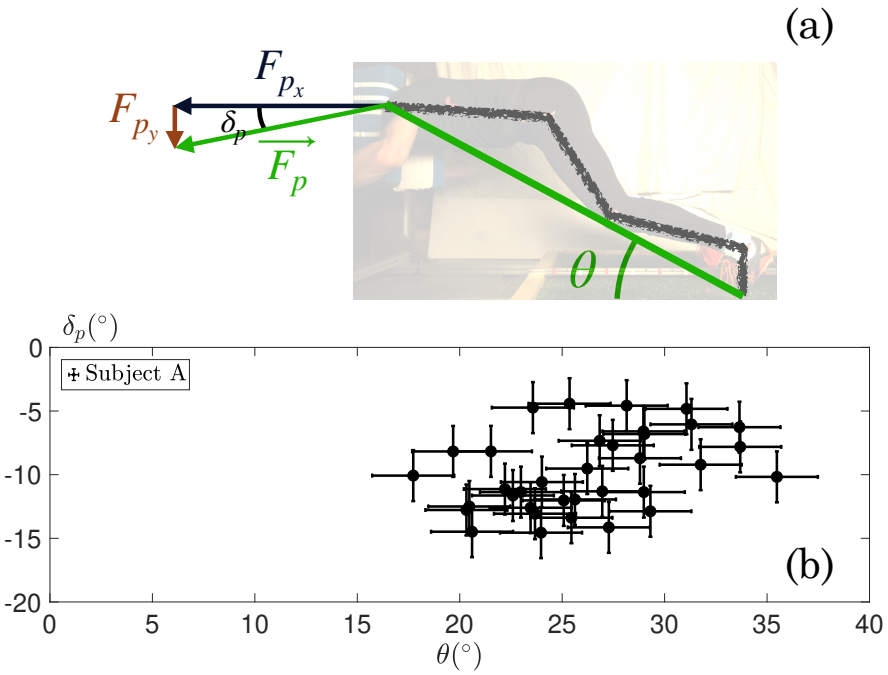


Figure 6.21: (a) Definition of the passive force angle δ_p. (b) δ_p as a function of θ for subject A.

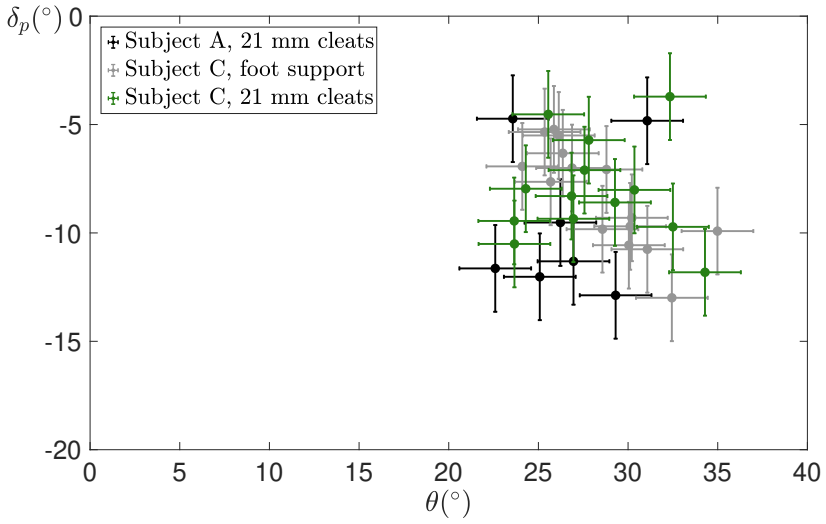


Figure 6.22: δ_p as a function of θ for subjects A and C at h_{cmp}.

We are presenting here dimensionless forces, so it does not mean that subject C develops more passive force than subject A. Indeed, in Table 6.1, we see that subject C weighs 61 kg while subject A weighs 75 kg.

6.3.5 Ratio between the active force and the passive force

We study the ratio between the intensity of the passive force $F_p = \sqrt{F_{p_x}^2 + F_{p_y}^2}$ and the intensity of the total force $F = \|\vec{F_a} + \vec{F_p}\| = \sqrt{F_x^2 + F_y^2}$. Figure 6.25 presents the ratio $\frac{F_p}{F}$ as a function of the player's elongation $\mathcal{L}_0$ that we scale with $\mathcal{L}_{size}$ (cf. Table 6.1). The further to the right on the x-axis you go, the more extended the player is.

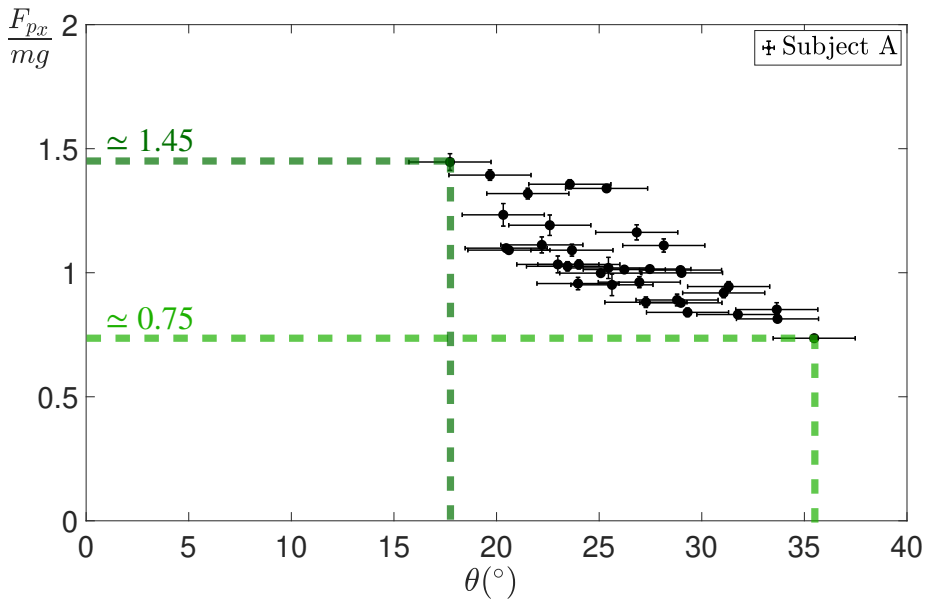


Figure 6.23: Dimensionless horizontal passive force $\frac{F_{p_x}}{mg}$ versus θ for subject A.

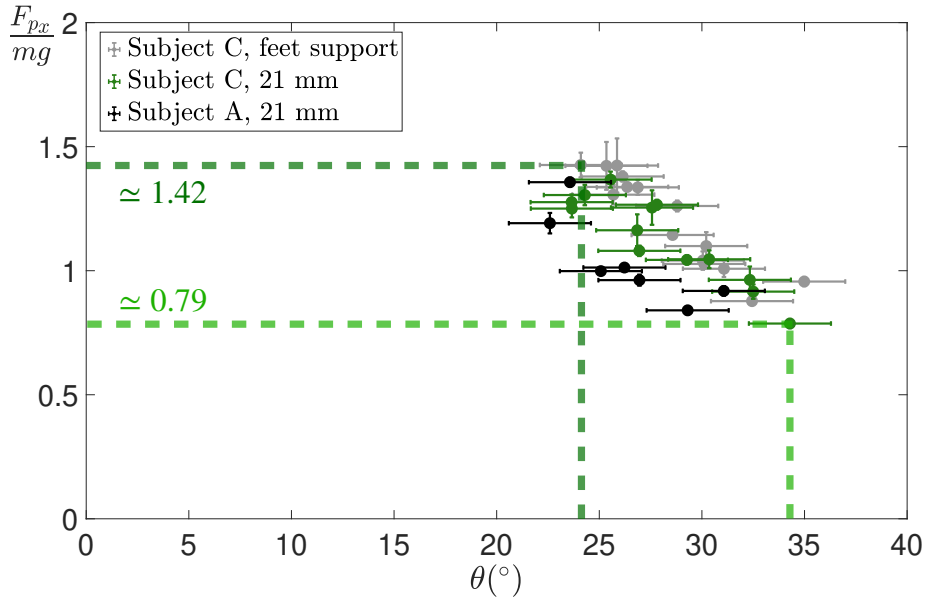


Figure 6.24: Dimensionless horizontal passive force $\frac{F_{p_x}}{mg}$ versus θ for subjects A and C at h_{cmp}.

The results of subject B are presented with blue dots, and the results of subject C are in green for the cleat shoes and in gray for the feet support. Finally, the results of subject A with 21 mm cleats at pushing height h_{cmp} are presented with black dots.

The green zone corresponds to $\frac{F_p}{F} > 0.5$ meaning that the passive force is more important than the active force. The red zone below the black dashed line shows the domination zone of the active force. The first observation is that F_p is the most important force on average,

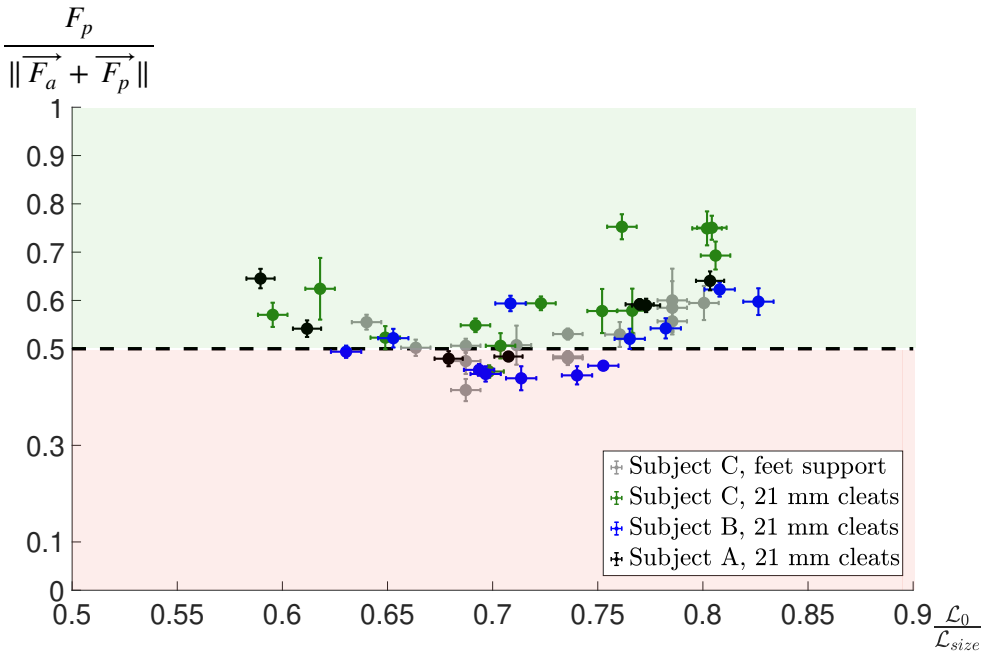


Figure 6.25: Evolution of the ratio $\frac{F_p}{F}$ as a function of a dimensionless elongation of the players $\frac{\mathcal{L}_0}{\mathcal{L}_{size}}$. The red zone corresponds to F_a domination and the green zone corresponds to F_p domination.

representing 60 to 80% of the total force for a large range of postures. More quantitatively, we have:

- for $\frac{\mathcal{L}_0}{\mathcal{L}_{size}} < 0.66$, the passive force represents 50 to 65% of the total force for all the subjects
- for $0.66 < \frac{\mathcal{L}_0}{\mathcal{L}_{size}} < 0.75$, F_a dominates. For every subject, the part of F_p never goes below 40% of F.
- for $\frac{\mathcal{L}_0}{\mathcal{L}_{size}} > 0.75$, the passive force dominates again and for the most extended position of Novice M with 21 mm cleats it reaches 75% of the total force.

The main message from Figure 6.25 is that passive force is important in a scrum. Most of the time it is larger than the active contribution.

6.3.6 Slip

Slip occurs with the main subject with 21 mm cleats during some trials in extreme positions close to the one of Figure 6.7(d). In Figure 6.26, we give an example with three snapshots of a slip and the corresponding force signal.
In Figure 6.26a, subject A is in the first phase of the protocol and applying his maximal isometric force on the scrum machine. This point is the beginning of the plateau but after one second, F_x and F_y suddenly drop because the player loses grip (cf. Figure 6.26d) and he starts to slip as we can see on the snapshot at t_2 in Figure 6.26.

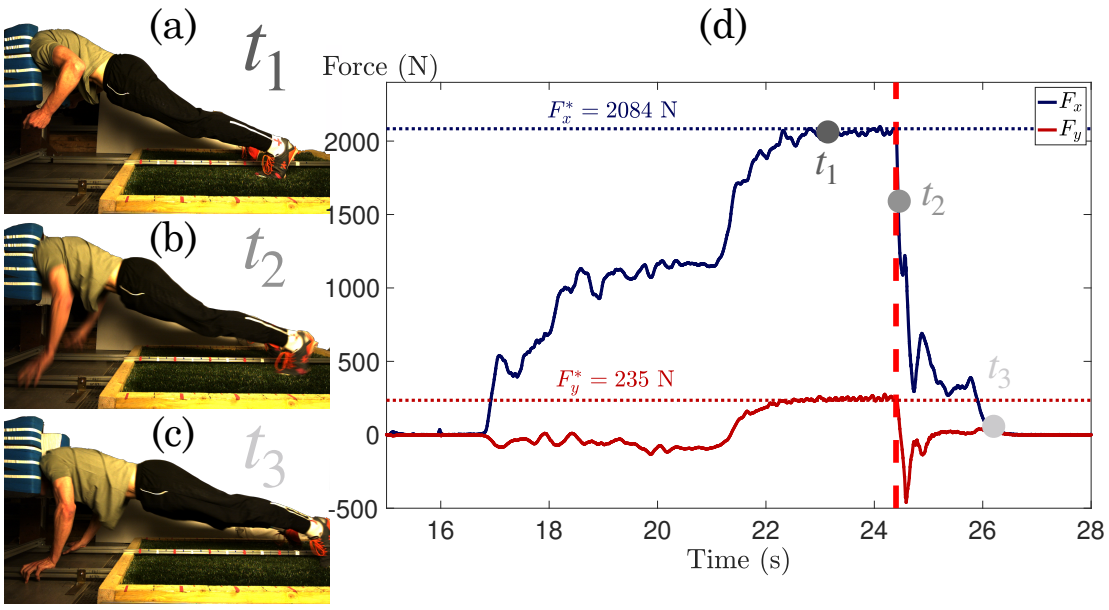


Figure 6.26: Example of slip for subject A with 21 mm cleats. (a) Snapshot of the player at t_1 when he is pushing actively on the scrum machine. (b) Snapshot of the player at t_2 when he starts to slip. (c) Snapshot of the player at t_3 when catches his fall using his arms. (d) Force signal during the slip. We note F_x^* and F_y^* the critical horizontal and vertical forces respectively corresponding to the maximal force player can reach in this configuration with these shoes.

In Figure 6.26c, subject A catches his fall using his arms and his shoulders do not touch the foams anymore: the force drops to 0 N.

F_x^* and F_y^* stand for the critical force components corresponding to a loss of adherence for the main subject with this pair of shoes equipped with 21 mm cleats. Here, $F_x^* = 2084$ N and $F_y^* = 235$ N.

6.4 Model of the Passive Force $\vec{F_p}$

We develop models to account for the different results exposed in the previous section. Let us start with the modeling of the passive force. The passive force $\vec{F_p}$ measured on the scrum machine is written as:

$$\vec{F_p} = F_{p_x}\vec{e_x} + F_{p_y}\vec{e_y} \tag{6.4}$$

with $F_{p_x} > 0$ and $F_{p_y} < 0$ (cf. subsection 6.3.4).

6.4.1 The pure horizontal limit

We first introduce the classic model of the homogeneous stick standing on a perfect wall. We then adapt it to the passive player on a scrum machine in the pure horizontal limit of

the passive force.

Homogeneous stick problem

In Figure 6.27, we consider a homogeneous stick of mass m standing on a perfect wall represented. The angle between the ground and the stick is θ and the length of the stick is $\mathcal{L}_0$. The stick is experiencing its own weight $m\vec{g}$, the ground reactions F_{g_x} and F_{g_y} and the force from the perfect wall F_{p_x}.

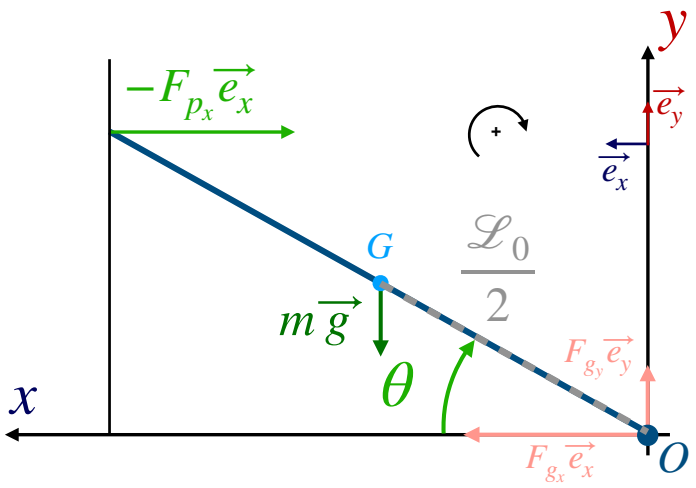


Figure 6.27: Scheme of a homogeneous stick of length $\mathcal{L}_0$ and mass m standing on a perfect wall with an angle θ.

Since the stick is homogeneously distributed, its center of mass G is in the middle. In the static limit, the balance of torques around O along the z-axis writes:

$$F_{p_x}\mathcal{L}_0 \sin\theta = mg\frac{\mathcal{L}_0}{2}\cos\theta. \tag{6.5}$$

This equation leads to the expression of the force:

$$F_{p_x} = \frac{1}{2}\frac{mg}{\tan\theta}. \tag{6.6}$$

Equation (6.6) implies that large mass and low θ both induce higher F_{p_x}.

Non-homogeneous stick

We transpose the problem of the homogeneous stick to the passive player set on the scrum machine at a given height h and whose feet are at a distance l from the scrum machine (cf. Figure 6.28a).

In a first step, we start with the simplest model by doing two strong hypotheses:

- F_{p_y} is negligible compared to F_{p_x}: in Figure 6.29, we observe that $\epsilon = -\frac{F_{p_y}}{F_{p_x}} \sim 0.17 \pm 0.05$ for subject A.
- The center of mass is located on the stickman at a distance $\alpha\mathcal{L}_0$ from the feet with $\alpha \in]0;1[$.

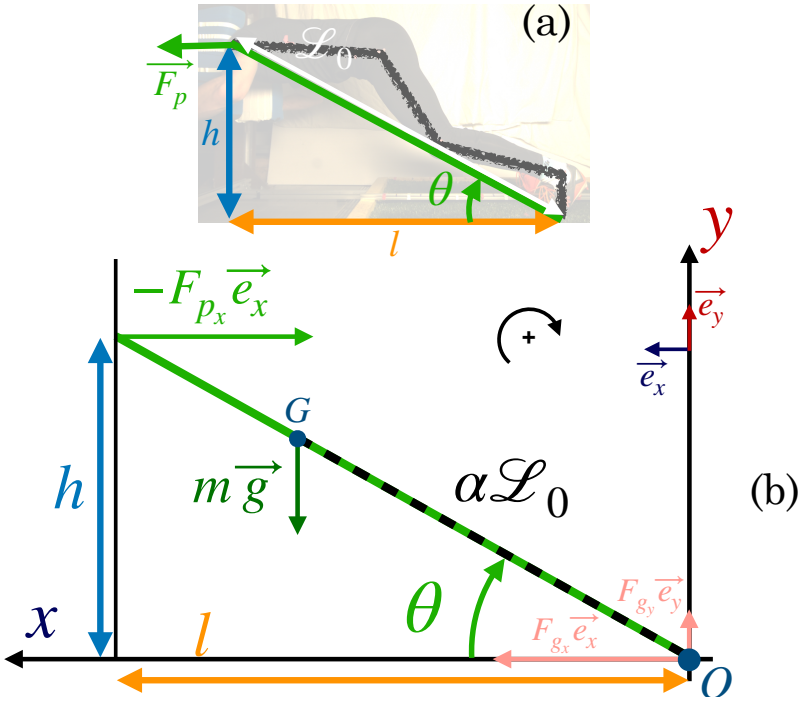


Figure 6.28: Non-homogeneous stick on a perfect wall model. (a) Example of an individual on the instrumented scrum machine. (b) Scheme of the inhomogeneously distributed stick of center of mass G at a distance $\alpha\mathcal{L}_0$ from O standing on a wall. The passive force is purely horizontal.

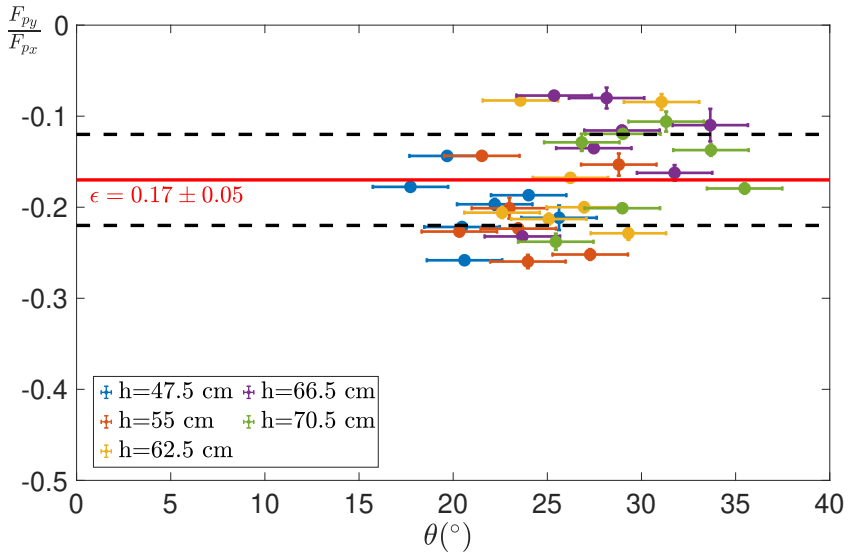


Figure 6.29: Ratio of F_{p_y} over F_{p_x} depending on θ for subject A.

The length $\mathcal{L}_0$ is not constant and varies with h and l. $\mathcal{L}_0$ is defined between the second metatarsal and the player's shoulder and is drawn in green in Figure 6.28a. In Figure 6.28b, the balance of torques at point O leads to:

$$F_{p_x} = \alpha \frac{mg}{\tan(\theta)} = \alpha \frac{mgl}{h}. \tag{6.7}$$

F_{p_x} increases with the mass of the player m and decreases with the angle θ. In terms of distances, it signifies that the passive force is higher when l is longer and h is lower.

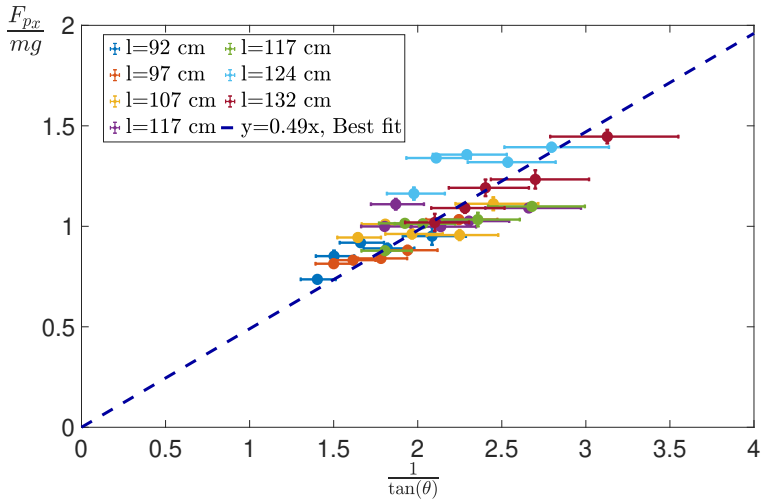


Figure 6.30: Dimensionless horizontal passive force $\frac{F_{p_x}}{mg}$ ordered by l as a function of $\frac{1}{\tan(\theta)}$. The blue dashed line corresponds to the model best fit with $\alpha \simeq 0.5$.

Equation (6.7) can be rewritten $\frac{F_{p_x}}{mg} = \alpha \frac{1}{\tan(\theta)}$ which implies that if we plot the dimensionless passive force as a function of $\frac{1}{\tan(\theta)}$, the result should be a straight line of slope α.
For the subject A, the experimental data are shown in Figure 6.30.
The experimental data is sorted by length l and we can see that the lower θ were obtained for the longest l. The horizontal error bars are due to measurement uncertainties on θ where the accuracy is $\pm 2°$. We note that experimental data is quite aligned along a line. The best fit obtained with equation (6.7) is obtained for $\alpha \simeq 0.5$. This value of α is true for this subject. In Figure 6.39 of subsection 6.4.3, we will see that the best fit α is different for subject C.

6.4.2 The non-horizontal case

Here, we take into account the dependency of the Center of Mass (CoM) location with the posture of the player and we also take into account the finite value of F_{p_y}.
The modified scheme of the situation is presented in Figure 6.31b. The CoM, G, is no longer on the stick man and needs to be measured thanks to side view images of the subject. Then, the reaction force of the scrum machine is equal to the opposite of $\vec{F_p}$ defined in equation (6.4).
We are first going to introduce the method we use to determine CoM location on side-view videos and we will then develop the calculus with these new elements.

Determination of the position of the center of mass, G, with anthropometric tables

As we see in Figure 6.6, subject A has pink markers on anatomical points. We detailed the placement of these points in section 5.1.1. Using side views, we measure directly the location of markers during the active pushing phase. This allows us to determine the CoM by using anthropometric tables. We divide the body into the trunk, thigh, and leg segments as shown in Figure 6.32a. With the 2D situation considered, we add the arms' mass to the segment of the trunk.

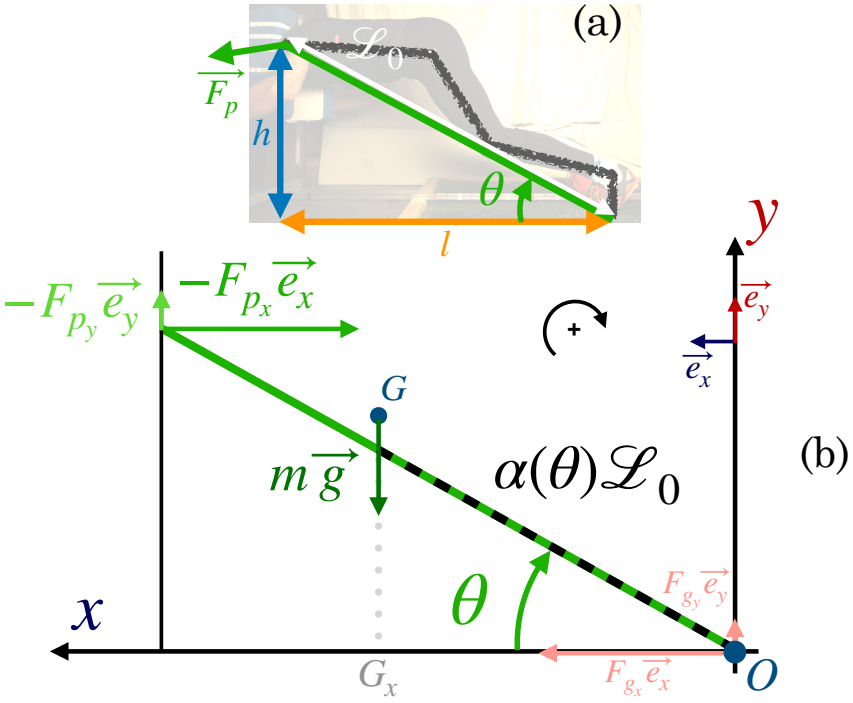


Figure 6.31: Complete model of a passive player on a scrum machine. (a) Example of a passive individual on the instrumented scrum machine. (b) Scheme of the inhomogeneously distributed stick of center of mass (Com) G. The Com is at a projected distance G_x from the origin O on the x-axis. The passive force is non-horizontal.

Anthropometric tables gather the position of CoM of the different segments defined by anatomical points (cf. Figure 6.32a). We use the parameters given in the book of David Winter [91] calculated from Dempster (DEM) *et al.* data [92]. Winter values of mass distribution of each segment as well as the segment's center of mass are given in Figure 6.32b and a respectively. We specify here that other anthropometric tables exist with slightly different coefficients for mass distribution and for the location of CoM for each segment. For example, for the trunk segment, the Zatiorsky's adjustments (ZAT) of De Leva anthropometric tables [93] have a relative mass of 43% compared to the total mass of the body M_{tot} when Winter [91] has a relative mass of 50%.

Furthermore, ZAT tables propose small differences between male and female coefficients. Indeed, Chambers *et al.* [94] show experimentally that obesity and gender influence the mass distribution and location of CoM coefficients. So, the choice of the anthropometric tables influence the position of the CoM [95].
Virmavirta *et al.* [96] compare the application of ZAT and DEM anthropometric tables to determine the CoM on different groups of physically active people. They use a reference experiment presented in Figure 6.33a to compare the results. this experimental setup is a high-accuracy reaction board (RB). The subject lies down on the RB, the balance of the torque between the torque applied on the force transducer at a distance L of the pivot connection and the weight of the subject at a distance x of the pivot connection enables calculating the location of CoM. The authors express the location of CoM along the longitudinal axis of the body relative to the height of the subject. In Figure 6.33b, they compare the results they obtained with the RB experiment and with the ZAT and DEM calculations for different gender. For males, they obtain a higher CoM on the longitudinal axis with DEM coefficients, and lower ZAT coefficients compared to the determination of the location of CoM with RB. The agreement between anthropometric tables and the results of RB is less satisfactory for female subjects.

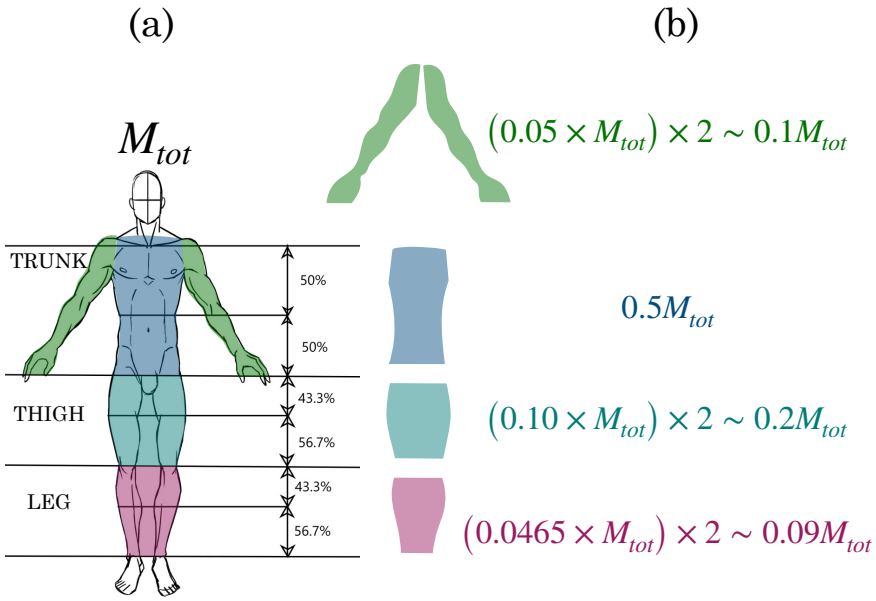


Figure 6.32: Anthropometric data extracted from [91]. (a) Center of mass position over the total length of segments. (b) Segment weights over the total body weight. The arms represent 10 % of the total mass M_{tot} of the player M_{tot}, the trunk is half the total mass and finally the lower limb segments represent approximately 30% of M_{tot} without taking into account the mass of the feet.

In Figure 6.33c, the authors present the location of the body's CoM determined by RB, ZAT, and DEM for different groups of male athletes: high jumpers (HJ), gymnasts (GYM), throwers (THR), ice hockey players (IH) and ski jumpers (SJ). The male throwers and the IH are the groups of athletes who are the most similar to forwards in Rugby Union in terms of morphology in this study: the THR tested have a mean body mass of 123 kg and an average height of 192 cm, the IH tested have a mean body mass of 85 kg and an average height of 181 cm. For comparison, a study made on 530 elite male rugby players concluded that they have a mean body mass of 101 kg and an average height of 185 cm [97]. In Figure 6.33c, the agreement between DEM and RB is better than ZAT and RB for the two groups THR and IH combined. We think it is better to use DEM coefficients for rugby players, even though it would be to study with an equivalent experimental setup the match with DEM coefficients, with a differentiation between the forwards and the backs.

For the male subjects, there is approximately a 1% difference in the location of the CoM along the longitudinal axis compared to the height of the subject between ZAT and DEM coefficients in Figure 6.33b. We decide to use the DEM coefficients presented in Figure 6.32 in the following calculations for male subjects A and C.
We give an example of the application of determination of the location of the CoM in the sagittal plane in Figure 6.34 with trials corresponding to the variation of l on subject C. Each segment is represented in black dashed lines. The blue dashed line gives the main direction of the body that defines the angle θ. The location of the center of mass of each segment is represented in orange in Figure 6.34, while the CoM is represented with a red cross. If we do not take into account the mass of the arms, the location of CoM does change significantly.

We observe that the CoM is not located on the one-stick man approximation. We define an effective $\alpha(\theta)$ expressed with G_x, the x-coordinate of the CoM (cf. Figure 6.31). We use the geometric relation between $\alpha\mathcal{L}_0$ and G_x given by:

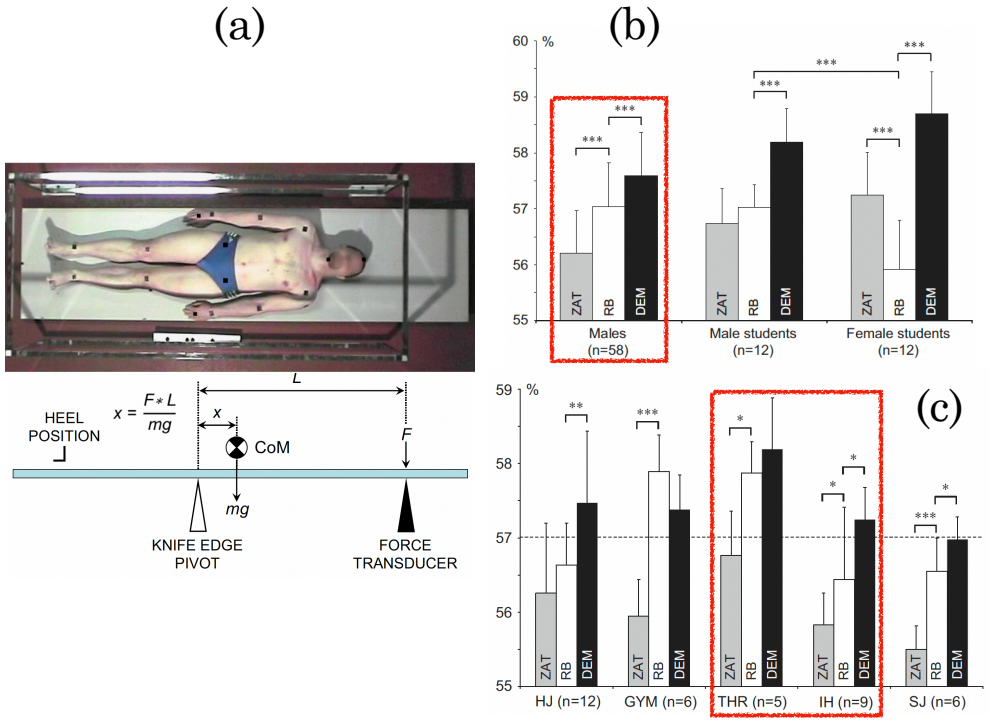


Figure 6.33: Experimental setup and results extracted from [96]. (a) Experimental setup used in the determination of the location of the CoM with the reaction board (RB). (b) Comparison between the

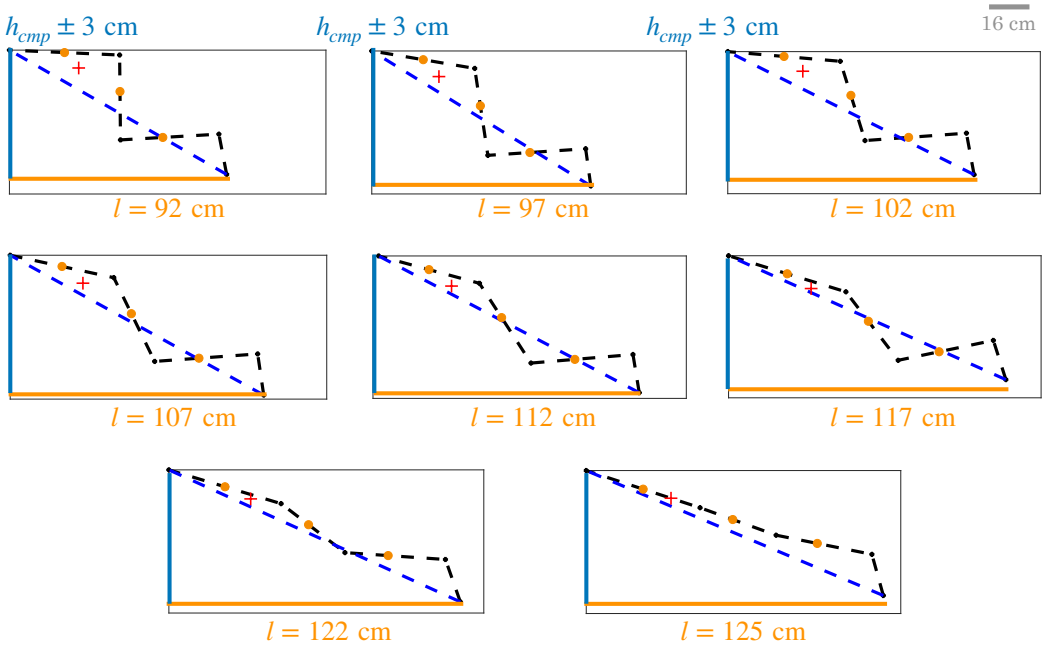
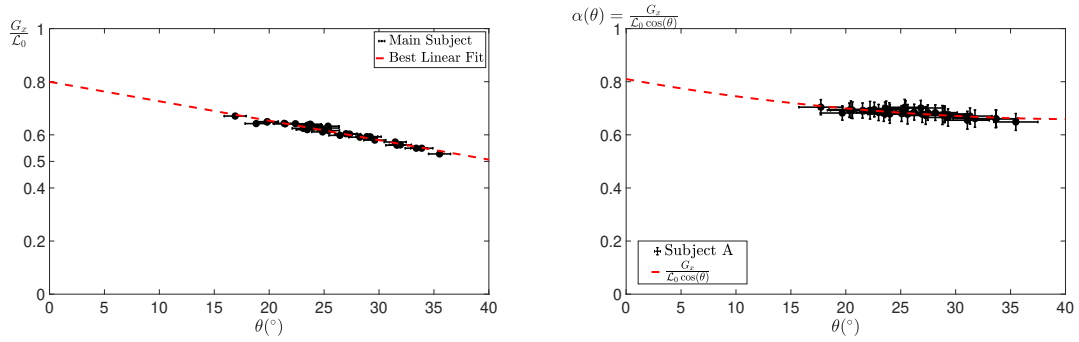


Figure 6.34: Examples of location of CoM in different postures for the subject C with foot support. The orange dots are the CoM of the different segments. The red cross is the CoM of the full body.

$$\alpha(\theta) = \frac{G_x}{\mathcal{L}_0 \cos(\theta)}. \tag{6.8}$$

Thanks to the measurements of G_x obtained with the method illustrated in Figure 6.34, we get the evolution of the ratio $\frac{G_x}{\mathcal{L}_0}$ for subject A in Figure 6.35a. We observe an affine relation of this ratio with θ (expressed in °), with an intercept of 0.8 and a slope of -8×10^3. Using equation (6.8), we plot the function $\alpha(\theta)$ in Figure 6.35b represented with a red dashed line.



(a) **(b)**

Figure 6.35: (a) Experimental ratio $\frac{G_x}{\mathcal{L}_0}$ with black points fitted by the red dashed line. (b) Function α against θ. The experimental values are presented with black points and equation (6.8) is drawn with a red dashed line.

We notice that $\alpha(\theta)$ is almost constant in the experimental region and takes a value around 0.7 for subject A.
Taking into account the location of the CoM and its evolution with the posture of the player is not enough. Indeed, the best fit for α was around 0.5 for subject A in Figure 6.30. Suppose we switch in equation (6.7) from $\alpha = 0.5$ to $\alpha(\theta)$, as presented in Figure 6.35b and with values around 0.7. In that case, one observes a worse result when comparing to the experimental data of subject A in Figure 6.30. We thus need to consider the passive force's vertical component.

With the vertical component

Thanks to the results plotted in Figure 6.29, we can make the approximation of a constant ratio between the two passive force components F_{p_y} and F_{p_x} such that

$$F_{p_y} = -\epsilon F_{p_x}. \tag{6.9}$$

We measured the average $\epsilon = 0.17 \pm 0.05$ for subject A. We use this equation in order to close the problem and to have the possibility to write an expression for F_{p_x}. Using the balance of torques in the situation of Figure 6.31, we get:

$$\frac{-F_{p_y}}{mg} + \frac{F_{p_x}}{mg} \tan(\theta) = \alpha(\theta). \tag{6.10}$$

Combining equations (6.9) and (6.10), we obtain:

$$\frac{F_{p_x}}{mg} = \frac{\alpha(\theta)}{\tan(\theta) + \epsilon}. \tag{6.11}$$

The comparison between the experimental data of subject A and the two different models of equations (6.7) and (6.11) is presented in Figure 6.36.

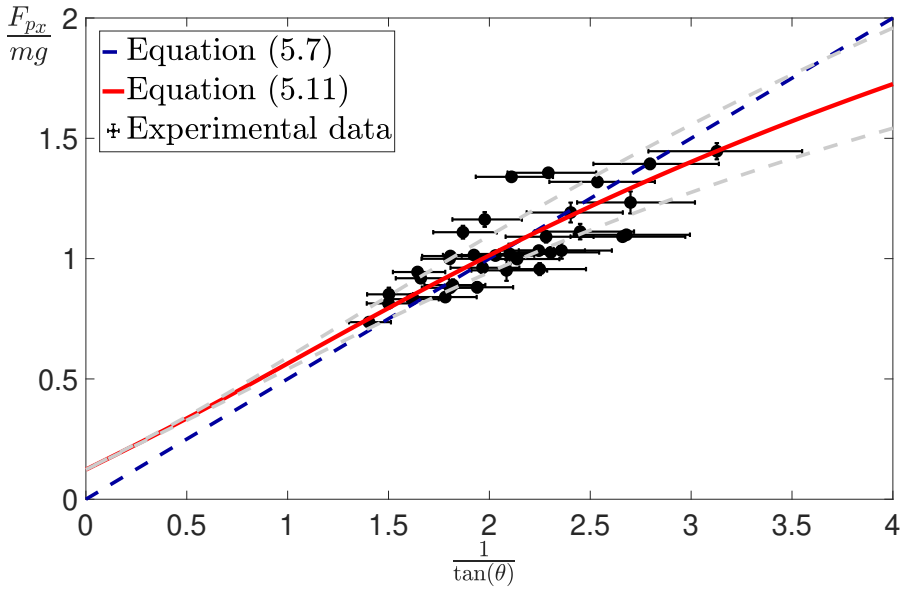


Figure 6.36: Comparison between the experimental data of subject A and the two models (equations (6.7) and (6.11)) for $\frac{F_{px}}{mg}$ as a function of $\frac{1}{\tan\theta}$. The experimental data of subject A is presented with black points. The blue dashed line is the model from equation (6.7) with $\alpha = 0.5$. The red solid line is the model from equation (6.11) using $\epsilon = 0.17$. The gray lines are the model from the same equation but using $\pm 30\%$ uncertainties on ϵ.

Ch. 6

The model corresponding to the equation (6.11) is presented in a solid red line, and the previous model (equation (6.7)) is shown in a blue dashed line. The error bars do not allow us to discriminate between the two models. It seems that the precision we add is going in the right direction, but the first model is quite sufficient to capture the physics of the passive force.

The model of the passive force with no approximations

Finally, we can also verify the complete model without approximation on F_{p_y}. Combining equations (6.8) and (6.10), we get:

$$-\frac{F_{p,y}}{mg}\cos\theta + \frac{F_{p,x}}{mg}\sin\theta = \frac{G_x}{\mathcal{L}_0} \tag{6.12}$$

Let $f(\theta) = -\frac{F_{p,y}}{mg}\cos\theta + \frac{F_{p,x}}{mg}\sin\theta$. In Figure 6.37, we compare the experimental $f(\theta)$ obtained for each trial of subject A. We compare it with the ratio depending on the location of the CoM $\frac{G_x}{\mathcal{L}_0}$ of Figure 6.35a represented with the black dashed line as function of θ.

The experimental results are aligned with the $\frac{G_x}{\mathcal{L}_0}$ ratio. Thus, equation (6.12) is verified but we cannot have an expression of F_{p_x} independent of F_{p_y} with this model.

We conclude that we understand quite well the physics behind the passive force of an individual player. For subject A, the pure horizontal limit model is sufficient to explain the experimental data.

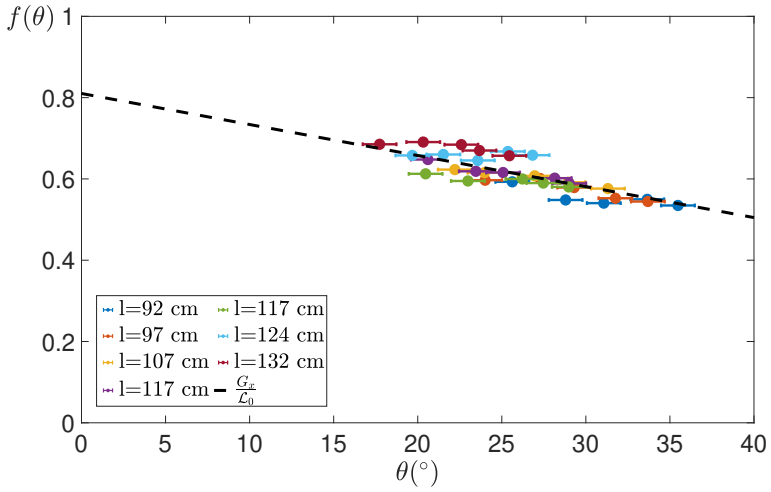


Figure 6.37: Verification of equation (6.12) without any assumption on F_{p_y}.

6.4.3 Comparison with subject C

We are doing here the same work using the data of subject C. In Figure 6.38, we plot the ratio $\frac{F_{py}}{F_{px}}$ as a function of θ. The average ϵ obtained with 21 mm cleats on synthetic grass (green points) is equal to $\epsilon_g = 0.14 \pm 0.04$. We have a similar $\epsilon_s = 0.15 \pm 0.04$ for feet support experiments (gray points).

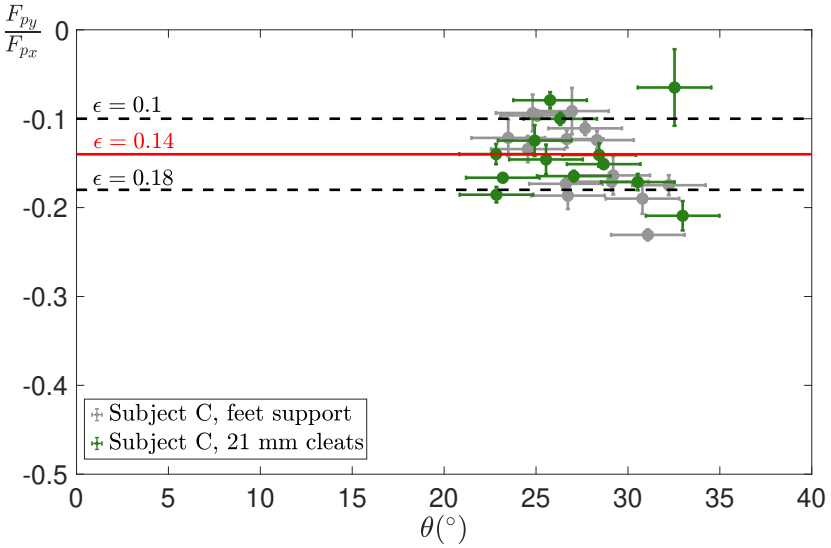


Figure 6.38: $\frac{F_{p_y}}{F_{p_x}}$ versus θ for Novice M experiments. Green points correspond to 21 mm cleats data and gray points correspond to feet support data.

If we apply the pure horizontal model of equation (6.7) on the dimensionless passive force data of subject C in Figure 6.39, we obtain the best fit $\alpha_g = 0.57$ for 21 mm cleats data and the best fit $\alpha_s = 0.62$ for feet support data. On average, it gives $\alpha \simeq 0.6$ for subject C which is presented in Figure 6.39 with a dashed blue line.

For the model with constant $\frac{F_{py}}{F_{px}}$ ratio presented with the red line, we measure the position of the CoM along the x-axis G_x (corresponding to Figure 6.34) and we take into account the value of ϵ_g. Using equation (6.8), we plot the experimental values of α for the feet support

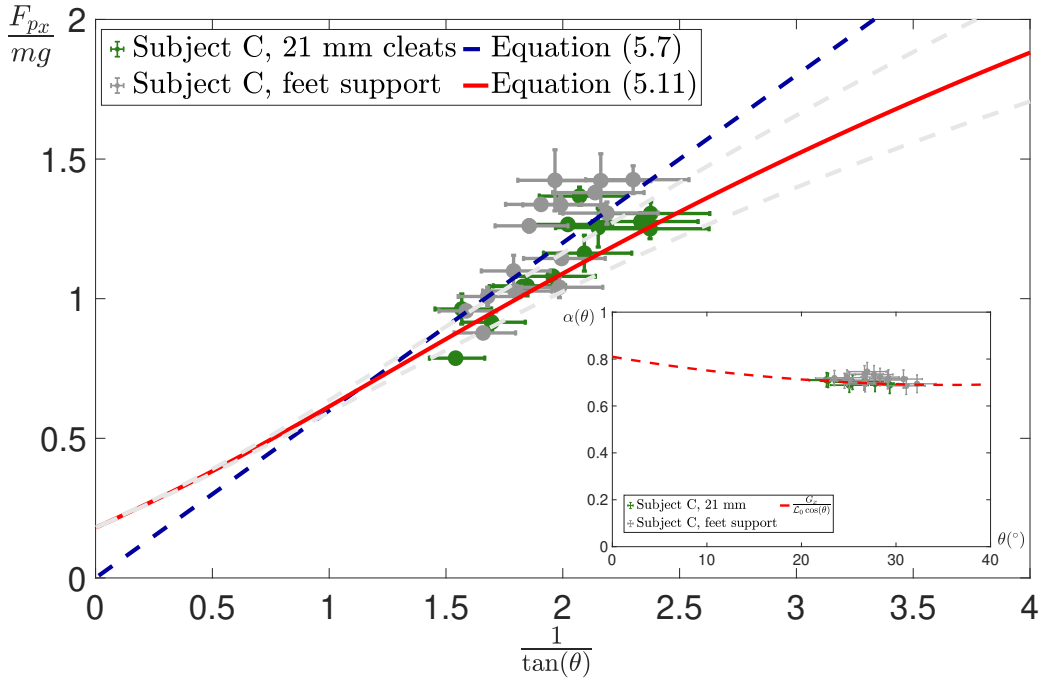


Figure 6.39: Dimensionless $\frac{F_{px}}{mg}$ as a function of $\frac{1}{\tan\theta}$ for subject C. Comparison between the experimental results and the passive models of equations (6.7) and (6.11). Data corresponding to 21 mm cleats are presented with green points and data corresponding to feet support with gray points. The blue dashed line is the pure horizontal model of equation (6.7). The red solid line is the model from equation (6.11) using $\epsilon = 0.14$. The gray lines are the model from the same equation but using $\pm 30\%$ uncertainties on ϵ. The inset presents the graph of $\alpha(\theta)$ for subject C.

and 21 mm cleats data in the inset of Figure 6.39 in green and gray respectively. We observe that $\alpha(\theta)$ is almost constant around 0.7.

We notice that the values of α for feet support are slightly above the values obtained with 21 mm cleats. This result is consistent with the pure horizontal model which gives a higher slope for the feet support. It means that when subject C is pushing against the aluminum profile bar, his CoM is slightly closer to his shoulders than when he is using cleat shoes with 21 mm cleats.

6.5 Model of the Active Force $\vec{F_a}$

The active force $\vec{F_a}$ is directed along the direction defined by the angle θ (cf. Figure 6.16). We want here to be able to explain the behavior of the intensity of F_a as a function of the elongation factor $\frac{\mathcal{L}_0}{\mathcal{L}}$ presented in Figure 6.18.

6.5.1 Sarcomere

According to the experimental results, the model needs to have a force production that tends to 0 when the player is totally elongated (corresponding to knee angle in full extension) and also when the player is fully compressed $\left(F_a\left(\frac{\mathcal{L}_0}{\mathcal{L}} \to 0\right) = 0\right)$. Moreover, F_a shows

a maximum around the elongation factor of 0.8 in Figure 6.18.

Such behavior makes us think about the force production mechanism of striated skeletal muscle. Caroline Cohen in her Ph.D. [98] details the physiology and physics of muscle contraction. In particular, thanks to the kinetic model of Descherevskii [99] for muscle contraction, she recovers the macroscopic dynamics of bench press experiments.

The basics of muscle contraction come from the contraction of elementary units called sarcomeres of typical length 3μm. The series of these units form a myofibril. The parallel myofibril clusters of typical length 10 cm and diameter of 1μm are forming a muscular fiber, which are themselves the components of fiber bundles that make up the muscle. All these elements are presented in Figure 6.40. Contracting each sarcomere unit implies the contraction of the whole muscle, even if it is an isometric contraction (thanks to tendons). The principle of sarcomere contraction is explained on top of Figure 6.41. Each sarcomere is composed of myosin and actin filaments. Myosin heads are pulling on actin filaments and this is the source of force and contraction. Thus we understand that the force produced by a muscle depends on its length [100, 101]. The relationship between tension and length of a sarcomere is given in Figure 6.41 extracted from [102].

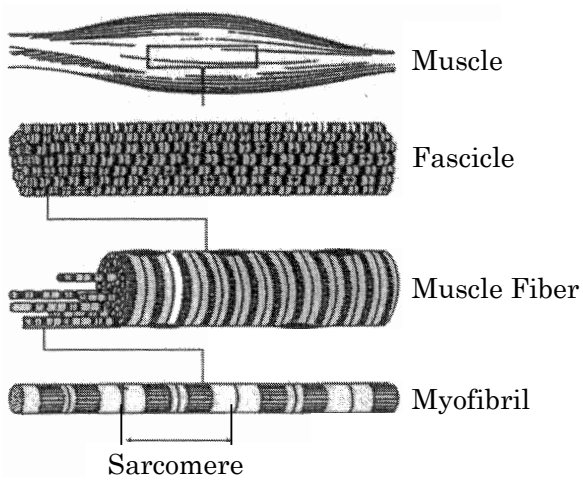


Figure 6.40: Structural organization of the muscle from the macroscopic to the microscopic level. Extracted and adapted from [103].

At the muscle level, the active part of the muscular force has an equivalent tension-elongation curve as in Figure 6.41b. The relation between elongation and force is asymmetrical: the force tends to zero when it is completely elongated and compressed. Here, we are not looking for the biomechanical explanation to link the mechanics of muscle contraction to the active force F_a on the scrum machine, but this description of molecular force production helps to build the mathematical equation for $F_a\left(\frac{\mathcal{L}_0}{\mathcal{L}}\right)$:

$$F_a\left(\frac{\mathcal{L}_0}{\mathcal{L}}\right) = F_{a_0}\left(\frac{\mathcal{L}_0}{\mathcal{L}}\right)^{m_1}\left(1-\frac{\mathcal{L}_0}{\mathcal{L}}\right)^{m_2}. \tag{6.13}$$

When the player tends to be totally compressed ($\frac{\mathcal{L}_0}{\mathcal{L}}=0$)) or totally extend ($\frac{\mathcal{L}_0}{\mathcal{L}}=1$)), this expression is equal to 0. Then, the parameters m_1 and m_2 are the ones that set the position of the maximum. Finally, F_{a_0} indicates the ability of the player to produce a large force.

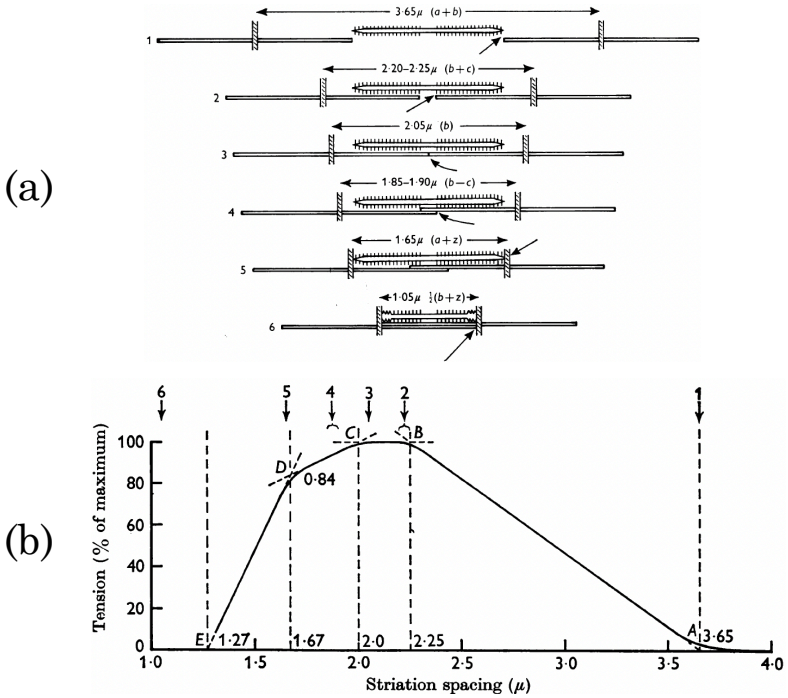


Figure 6.41: Sarcomere contraction extracted from [102]. (a) Diagram of actin-myosin contraction in a sarcomere. (b) Corresponding tension-length relation at the sarcomere level. The numbers given on the left of each step are reported on the curve.

6.5.2 Comparison between the experiments and the model.

Subject A

We decide to perform a nonlinear least-squares regression on the experimental data of subject A presented in Figure 6.17. We use MATLAB to execute this regression by using the expression of equation (6.13) and adjusting the three parameters m_1, m_2, and F_{a_0}. The results for these regressions at fixed h are shown with dashed lines in Figure 6.42.

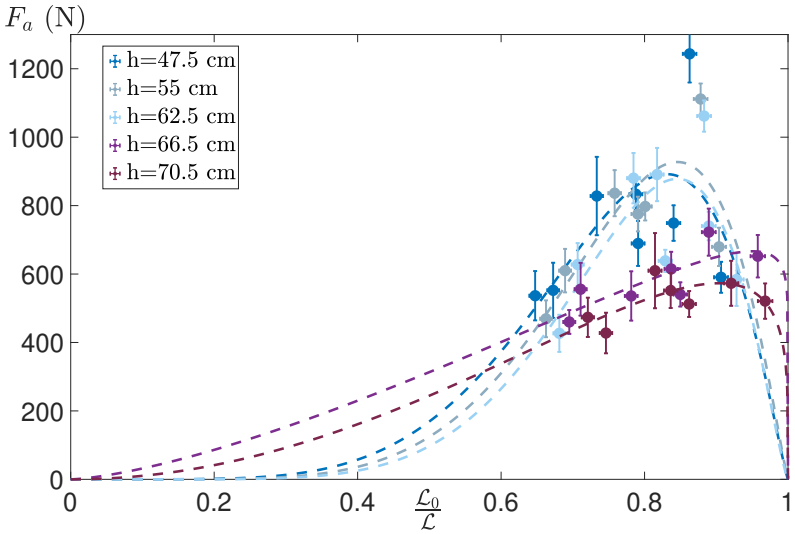


Figure 6.42: Active force F_a as a function of the elongation factor. Data are sorted by pushing heights and the nonlinear fits are done for this different fixed h. Two families of points are well captured by the nonlinear regression with two main groups of curves.

The two groups of curves described in Figure 6.15 give two main fitting results that correspond to the blue points and the purple points. The regression curves are presented with dashed lines with colors that correspond to the set of data fitted. The best coefficients determined by the regressions are gathered in Table 6.2.

Pushing height (cm)	m_1	m_2	$F_{a_0}(N)$
47.5	5.8	1.2	2.1×10^4
55	6.5	1.2	2.5×10^4
62.5	7	1.3	3.2×10^4
66.5	1.5	0.1	1×10^3
70.5	2	0.3	1.5×10^3

Table 6.2: Best parameters obtained with the non-linear least-squares regression on the intensity of the active force for subject A.

m_1 and m_2 are the parameters that influence the asymmetry of the curve: if $m_1 = m_2$, the curve is symmetrical around $\frac{\mathcal{L}_0}{\mathcal{L}} = 0.5$. The parameters of Table 6.2 lead to a maximum situated on elongation factor $\frac{\mathcal{L}_0}{\mathcal{L}} = 0.83$ for the lowest heights represented in blue in Figure 6.42. And, they lead to a maximum active force located in $\frac{\mathcal{L}_0}{\mathcal{L}} = 0.9 - 0.95$ for the highest pushing heights represented in purple. The two groups of curves correspond to the set of parameters $m_1 \simeq 6.5$, $m_2 \simeq 1$, and $F_{a_0} \simeq 2.5 \times 10^4$ N for the lowest pushing heights, and the set of parameters $m_1 \simeq 2$, $m_2 \simeq 0.1$, and $F_{a_0} \simeq 1 \times 10^3$ N for the highest pushing heights.

Comparison with subject C

We also use the non-linear regression on the data of subject C with 21 mm cleats. In order to compare subjects A and C, we determine the values of the coefficient obtained for all the data of the three lowest pushing heights for subject A presented with blue dots in Figure 6.43. Then, we fix the m_1 and m_2 values obtained, and we proceed to a regression on the data of subject C with F_{a_0} as the only free parameter. Thus, F_{a_0} reflects player performance.
In Figure 6.43, the dashed blue curve is achieved for $m_1 = 6.37$, $m_2 = 1.22$ and $F_{a_0} = 2.56 \times 10^4$ N. This set of parameters corresponds to the best fit of blue points. Then, for fixed m_1 and m_2, we obtain $F_{a_0} = 1.74 \times 10^4$ for the data of subject C. The corresponding curve is presented in a green dashed line in Figure 6.43.

Contrary to the passive model in subsection 6.4.3, the active force curve with feet support is really different from the 21 mm cleats curve. We show and discuss this point in the next Chapter 7.

6.6 The Total Force: Comparison Experiments/Model

6.6.1 Friction

To sum up, we design a model divided into two sources of force: the horizontal passive force and the active force acting along in the player's main direction θ (cf. Figure 6.44a). The

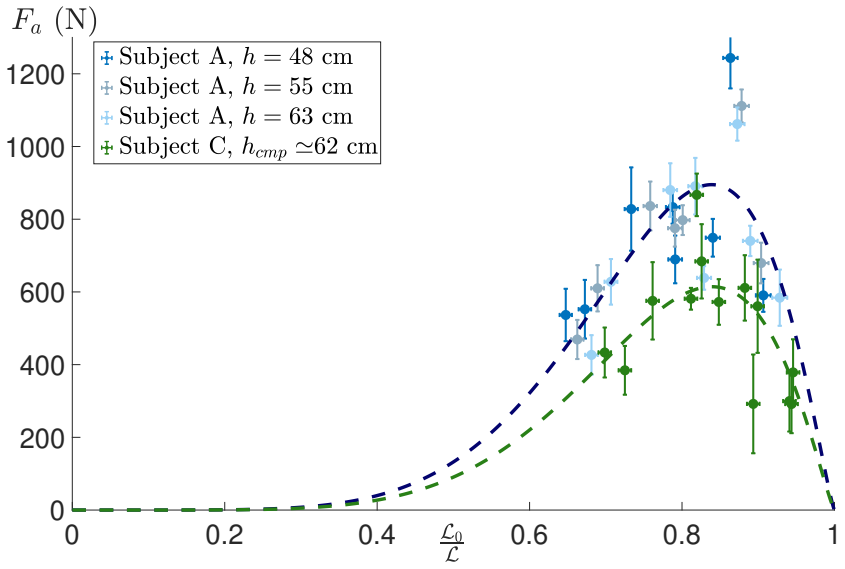


Figure 6.43: Intensity of the active force F_a versus the elongation factor. The experimental data of subjects A and C are represented with blue and green points respectively. The dashed lines are obtained with equation (6.13) by using non-linear regressions.

useful force to push the opponent can be written as:

$$F_x = \underbrace{\alpha \frac{mg}{\tan\theta}}_{F_{p_x}} + \underbrace{F_{a_0} \left(\frac{\mathcal{L}_0}{\mathcal{L}}\right)^{m_1} \left(1 - \frac{\mathcal{L}_0}{\mathcal{L}}\right)^{m_2} \cos(\theta)}_{F_{a_x}}. \tag{6.14}$$

If we consider the passive model with constant $\epsilon = \overline{\left(\frac{-F_{p_y}}{F_{p_x}}\right)}$, we obtain the following expression:

$$F_x = \alpha(\theta) \frac{mg}{\tan\theta + \epsilon} + F_{a_0} \left(\frac{\mathcal{L}_0}{\mathcal{L}}\right)^{m_1} \left(1 - \frac{\mathcal{L}_0}{\mathcal{L}}\right)^{m_2} \cos(\theta). \tag{6.15}$$

Furthermore, we need to take into account the possibility to slip on the synthetic grass as we saw in subsection 6.3.6. The friction ensures the support of the player and allows him to push the opponent. The no-slip condition imposes that the tangential component of the force of friction $F_T = F_x$ is smaller than the normal component of the force of friction $F_N = mg + F_y$ multiplied by μ (cf. Figure 6.44b).
In Figure 6.26d, when subject A slips, we observe a sudden drop in total force that happens when F_x and F_y reach critical values of forces F_x^* and F_y^*. We thus define the friction coefficient μ at the limit case when $F_T = \mu F_N$. We then obtain:

$$\mu = \frac{F_x^*}{F_y^* + mg}. \tag{6.16}$$

Using equation (6.16) with F_x^* and F_y^* of Figure 6.26, the friction coefficient of subject A wearing 21 mm cleats is $\mu \simeq 2.2$.
The horizontal pushing force F_x is thus limited by μ. The player needs to adapt the production of active force in order to avoid slipping on the grass. In the model, if the no-slip condition is not respected, then we set $F_x = \mu(F_y + mg)$ (cf. Figure 6.44b).

Using equation (6.14) or equation (6.15) modifies the no-slip condition: with equation (6.14), we get $F_y = F_{a_y}$; with equation (6.15), we get $F_y = -\epsilon F_{p_x} + F_{a_y}$.

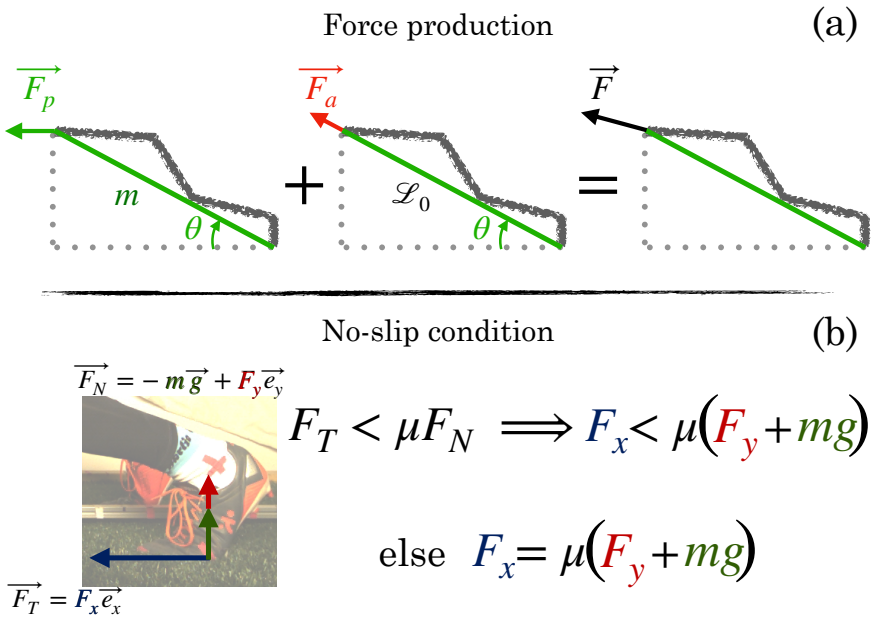


Figure 6.44: Model of the total force obtained with the sum of the passive force and the active force. To not slip, the no-slip condition needs to be respected. (a) Force production. (b) No-slip condition on the tangential component of the force of friction $F_T = F_x$ that has to stay below μF_N, with $F_N = mg + F_y$ the normal component of the force of friction.

6.6.2 Map

In Figure 6.45, we compare the experimental F_x (cf. Figure 6.9) obtained with subject A wearing 21 mm cleats with the model of equation (6.14) presented with colored isoforce curves. We consider here the sum of the pure horizontal passive model (cf. equation (6.7)) with the active force model fitted on lowest pushing heights (cf. Figure 6.43).

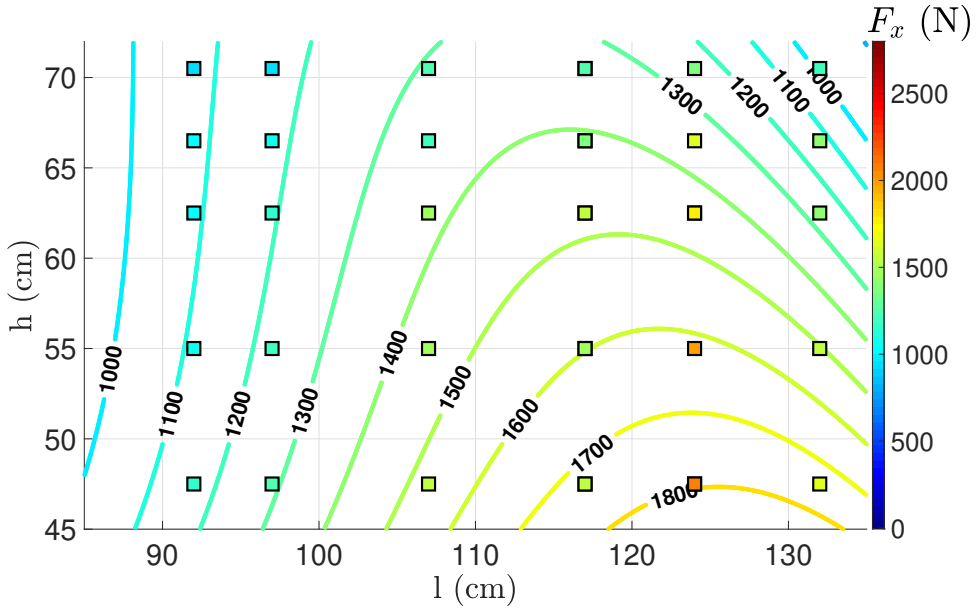


Figure 6.45: Total pushing force comparison F_x between the experimental data and the model of equation (6.14) for subject A with 21 mm cleats. The experimental data are represented with colorful squares and the model is presented with isoforce curves with the same color scale.

We notice a good match between the experiments and the model, in particular for the location of the optimal pushing zone for $l \sim 125$ cm and $h \sim 47$ cm. The pure horizontal passive model seems efficient to describe the behavior of the total compression force F_x with an overall good match in all the parts of the phase plan. But, looking into the details of the isoforce curves, we observe that the maximum of the model is outside of the presented limits in the (l, h) plane. However, it is experimentally impossible for subject A to push with $h < 45$ cm (cf. Figures 6.7c and d).
Moreover, subject A slips in the posture corresponding to the point at $l = 132$ cm and $h = 47$ cm. But, the model obtained with equation (6.14) is not limited by the friction in this area.

We do the same experiment-model comparison but using equation (6.15) -meaning that we consider the passive force with constant ϵ- in Figure 6.46. On this map, we plot the iso-θ curves in grayscale. The gray line corresponds to the limit of equation (6.16). Below this line, F_x is limited by μ: the player cannot produce his maximal force to if he does not want to slip.

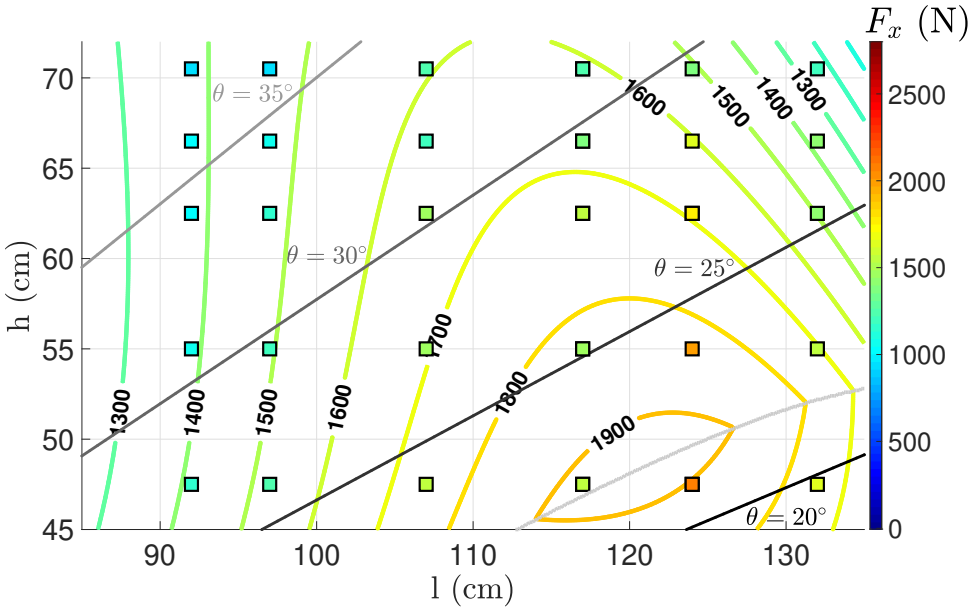


Figure 6.46: Total pushing force comparison F_x between the experimental data and the model of equation (6.15) for subject A with 21 mm cleats. The experimental data are represented with colorful squares and the model is presented with isoforce curves with the same color scale. The iso-θ curves are presented with lines in shades of gray.

We notice a good match between the experiments and the model, once again in particular for the location of the optimal pushing zone, even if the force intensity F_x is a little bit overestimated in this zone. But, with this model of equation (6.15), the experimental point at $l = 132$ cm and $h = 47$ cm is in the zone where the no-slip condition is not respected anymore. The player is here limited by friction in his production of force. Still, we can say that friction is not an important limit for 21 mm cleats: it only forbids the postures with very low h and elongated subjects that are really rare to find in real scrums.

In Figure 6.46, the agreement between experiments and model is less satisfying for $h > 60$ cm and $l < 100$ cm.
For the zone corresponding to the higher pushing heights h, the difference could be explained by the coefficients of the active force. They are calculated with a fit on the data of intensity

of F_a for $h < 65$ cm (cf. Figure 6.43).
For the zone corresponding to the lower feet distances l, the difference could be understood thanks to Figure 6.36. As a matter of fact, the lower l, the lower $\frac{1}{\tan\theta}$ is. We see in Figure 6.36 that model of equation (6.11) overestimates F_{p_x} for the lower values of $\frac{1}{\tan\theta}$.

6.7 Conclusion

In order to conclude, we assimilate an individual player pushing on a scrum machine as a single segment defined by the support points of the subject: shoulders on the scrum machine and feet on the ground. Thanks to the model of the passive force inspired by the classic model of a stick standing on a wall, we understand that F_{p_x} is linearly increasing with the mass m of the player. The heavier the forward player, the higher F_{p_x} is applied to the opponent. This is why first-row players are the most massive in a Rugby Union team: they naturally maximize their F_{p_x}, and then by lowering their pushing height (as seen in [60]) or by increasing the feet distance, they also increase F_{p_x}. All the comments made here about F_{p_x} are applicable at the collective scale.
In our experimental setup, we also measured a vertical passive component F_{p_y} that could be linked to the elasticity of the foams. Some measurements of F_{p_y} in live scrums would be interesting to study, and it will bring an answer about the interest of the model of the passive force with $F_{p_y} \neq 0$.

Then, we suggest a mathematical model- inspired by the mechanics of muscle contraction- describing the evolution of F_a as a function of the elongation factor of the subject. Further experiments need to be done with more subjects in order to validate the universal characteristic of the $F_a\left(\frac{\mathcal{L}_0}{\mathcal{L}}\right)$. Nevertheless, we are confident in the experimental results of the direction of the active force aligned with θ. We do this observation whatever the gender, the playing level of Rugby, and physical fitness.
So, to maximize the intensity of the active force, the player should lower their pushing heights. However, when it is advantageous to be as extended as possible for maximizing F_{p_x}, it is not exactly the case for F_a. It exists an optimal l that enables to have an elongation factor of $\frac{\mathcal{L}_0}{\mathcal{L}} \simeq 0.8$ and that maximizes F_a for the lower pushing heights. It is more complicated to generalize the comments made about F_a at the collective level.

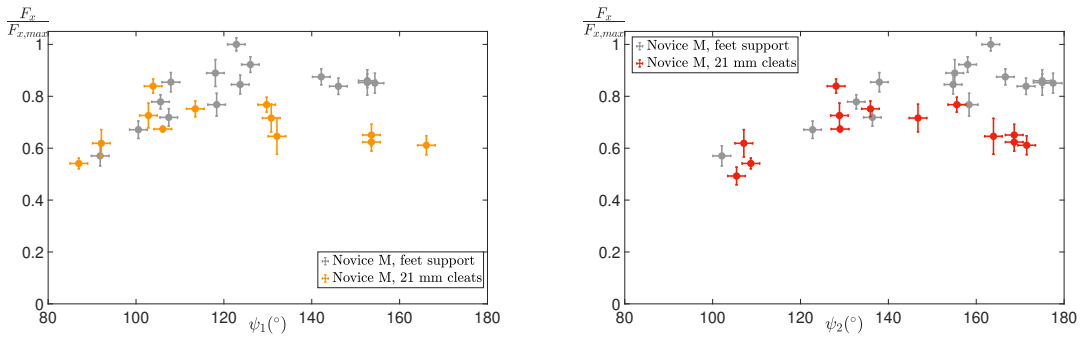
The maximization of the total compression force F_x corresponds to the maximization of the sum of $F_{p_x} + F_a\cos\theta$. We saw in the previous paragraphs that the player has an interest in lowering h (F_{p_x} and F_a increase), having a $\frac{\mathcal{L}_0}{\mathcal{L}}$ close to 0.8 (F_a is maximal and F_{p_x} increases with l) but we he can also maximize the $\cos\theta$ by lowering θ as much as possible. But, we do not have to forget about the friction governed by the no-slip condition. We will discuss that in Chapter 7. The comparison between the model and the experiments of subject A identifies the same optimal pushing zone at the lower height h and a length l that corresponds experimentally to an elongation factor of $\frac{\mathcal{L}_0}{\mathcal{L}}$=0.85, while the model predicts a slightly lower optimal extension.
This optimal posture of subject A (cf. Figure 6.9c) corresponds to an angle θ slightly above 20° and for an elongation factor $\frac{\mathcal{L}_0}{\mathcal{L}} \simeq 0.83$ corresponding to the maximal intensity of F_a (cf. Figure 6.43). However, we observed in Figure 6.1 that first-row players are more close

to $\theta \sim 30°$ rather than 20°. But, this optimal posture is closer to the postures adopted by the flankers in this same figure.

It would be interesting to conduct further experiments on collective scrums to study how the binding with teammates and the dynamics influence the optimal individual posture.

6.7.1 Influence of feet support on optimal angles for subject C

Finally, foot anchoring seems to have an important influence on individual force production. In Chapter 5, the Academy-level players adopted a similar optimal posture in terms of joint angles (cf. subsection 5.1.1) but they were pushing against a fixed feet support.
In order to compare the influence of the ground anchoring, subject C follows the experimental protocol with 21 mm cleats and with foot support (cf. Figure 6.7.1). In Figure 6.47, we plot the dimensionless horizontal forces $\frac{F_x}{F_{x,max}}$ as a function of knee angle $\psi 1$ and hip angle ψ_2 obtained with subject C with foot support in gray and with 21 mm cleats on the synthetic grass in colored points. $F_{x,max}$ is defined as the higher horizontal force obtained with the foot support. In Figure 6.47a, we find that the optimal ψ_1 is around 135-140° and in Figure 6.47b we observe that the optimal is $\psi_2 \sim 160°$ with the feet support. These angles are close to the optimal angles obtained with the academy level in Chapter 5.



(a) **(b)**

Figure 6.47: Dimensionless horizontal force re-scaled by the maximal horizontal force $F_{x,max}$ obtained with subject C as a function of joint angles. The gray data correspond to the experiments with the foot support. The orange and red data represented the experiments with 21 mm cleats. (a) $\frac{F_x}{F_{x,max}}$ versus knee angle ψ_1. (b) $\frac{F_x}{F_{x,max}}$ versus hip angle ψ_2.

We compare with the results obtained with cleats in orange in Figure 6.47a and in red in Figure 6.47b. We see that it changes the shape of the curves:

- The optimal angles are smaller, with an optimal $\psi_1 \sim 115 - 120°$ and a ψ_2 around 140-145 °.
- For angles smaller than the optimal, the forces are similar to the feet support trials. But a difference is observed at large angles when the player can produce 80 to 90% of his maximal force with foot support. He cannot exceed 70% of his maximal strength with cleat shoes.

The lack of space in the experimental room leads to a choice of a wide-angle lens on the side-view camera to film the player. It induces a barrel distortion on the images which is most problematic when we measure angles and distances on very elongated postures of the subjects (cf. Figure 6.7d). Furthermore, we measure the joint angles in the sagittal plane

with a 2D simplification of the player. To go further, the installation of a motion capture system around this experimental setup would allow precise measurements of the joint angles with markers. It would also allow the study of the player in 3D which could be interesting to investigate asymmetry of force production along the transverse axis of the player.

Take home message of Chapter 6

1. The passive force produced by a single player on a scrum machine is similar to the force applied by a stick standing on a wall. The vertical component of the passive force could reach 25% of the horizontal passive force value on our scrum machine. But, even if we neglect it, the model of the stick captures the physics of the situation and allows us to say that the horizontal passive force increases with the mass of the player and the distance from shoulders to feet along the compression axis. However, the horizontal passive force decreases when the pushing height is increased.

2. The active force is directed along the main axis of the player that passes through the metatarsal joint of the feet in contact with the ground and the shoulders of the player. When the player is elongated, the horizontal active force increases until an optimal elongation of the body.

3. The optimal individual posture on synthetic grass seems different from the optimal posture obtained with the foot support. For subject A, the optimal posture obtained with 21 mm cleats corresponds to a low pushing height of 45 cm and an elongated posture with a distance of l ∼120 cm. This optimal posture is close to the one adopted by professional flankers in real scrums. They are the players that have the fewer mechanical constraints imposed by other players with no teammate pushing behind them and no opponent pushing against them in direct contact.

4. Synthetic grass is installed on the individual scrum machine setup to get closer to ecological conditions. Friction seems to play an important role in force production. This is why we study the influence of the choice of cleats on force production in the next chapter.

7

Influence of Cleats Length on Optimal Posture

We study the influence of the size of cleats on the force production of subject A defined in Chapter 6. We measure the evolution of the friction coefficient and the evolution of the passive and active forces produced on the laboratory scrum machine depending on the lengths of the cleats. Finally, we compare the results to understand the influence of cleat length on individual posture.



Boots of the New Zealand rugby player Colin Meads in 1967. Picture extracted from [104].

Contents

7.1 The friction Coefficient **134**
7.2 Experimental Studies **136**
7.3 Results **138**
7.4 Comparison of the Total Force $\vec{F}_x$ **141**

This work has been done with Simon Giraud, Caroline Cohen and Christophe Clanet.

7.1 The friction Coefficient

7.1.1 Friction in sports

Friction is playing a key role in sports and it is important to characterize its value in order to optimize performances illustrated in Figure 7.1. The goal is either to reduce friction as much as possible, as in road cycling [105] where solid friction is involved in the tire rolling resistance but also in air resistance (cf. Figure 7.1a). Or it is to understand the frictions in order to adapt gestures or chemicals used to improve the sliding as in ice skating and curling [106, 107] or on snow [108] (cf. Figures 7.1b, c, and d).

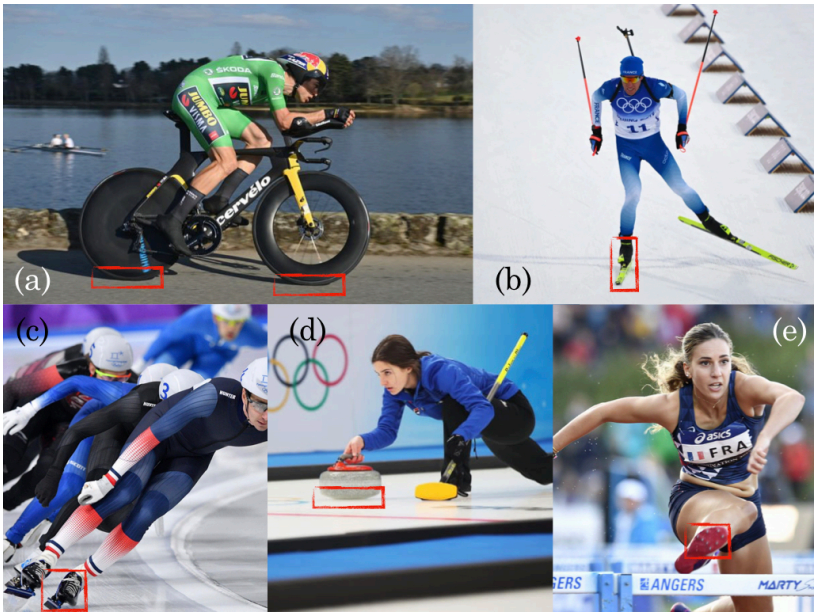


Figure 7.1: Illustrations of the role of friction in different sports: in road cycling with the reduction of rolling resistance (a), in cross-country skiing with wax adaptation (b), in ice skating with blade settings adaptation (c), in curling with the need for sliding precision (d), and in track and field races with spikes shoes for force restitution (e).

We focus here on cleat-grass friction [109]. Contrary to road cycling or ice skating, the role of cleats is to maximize the friction at the shoe-turf interface in order to increase the production of compression force in scrums.
The choice of the size of cleats and their number is a compromise between players' safety [110, 111, 112, 113] and targeted performance [114, 115]. Many studies focus on the characterization of the cleat-grass interface in terms of traction and rotation for natural and synthetic turf [116, 117, 118].
In Rugby Union, the shapes of cleats changed over the years in order to prevent injuries, in particular during rucks. In terms of performance, the goal is to maximize the compression force produced in the scrum but forwards also need to perform a number of different tasks presented in Figure 7.2. Indeed, the forwards push in the scrums (cf. Figure 7.2a), they must be able to run as fast as possible and to change direction quickly with the ball (cf. Figure 7.2b), they protect the ball in rucks (cf. Figure 7.2c) and finally they jump or lift their teammates in lineouts (cf. Figure 7.2d).

In Rugby Union, the shoes can be molded-cleat shoes or screwed-in cleats shoes. The cleat lengths vary from 8 mm to 21 mm. If we just consider the maximization of force production in scrums, mauls, or ball protection in rucks we would like to have cleats as long as possible. But, the longer the cleats, the more they become a hindrance to the running actions and



Figure 7.2: Different tasks accomplished by forwards in modern Rugby Union. (a) Scrummaging. (b) Running. (c) Protecting and contesting the ball in the rucks. (d) Lifting teammates during lineouts.

quick changes of direction that are also part of the forward's role. In Sylvain Blanchard's Ph.D. thesis [110], one finds on page 157 the table -adapted below (cf. Table 7.1)- that gathers results from a survey about the size of cleats that the professional and academy-level players of Racing 92 wear depending on the field type: natural grass, greasy natural grass, and synthetic turf. The survey was made in 2017. It was completed by 60 players including 37 professional players and 23 academy-level players. 31 players were forwards.
If we focus on forwards, we see that most of them are playing with screwed-in cleats whatever the type of surface. They use longer cleats than the average of the team whatever the surface. The backs tend to wear longer cleats at the front of their shoes, whereas the forwards have the tendency to wear homogeneous cleat sizes. In Table 7.1, we give the minimal, maximal, and mean values of cleats size used by forward players for the different ground conditions.

Position	NG (mm)		Greasy NG (mm)		Synthetic turf (mm)	
	Fr	Ba	Fr	Ba	Fr	Ba
All-team	14 (8-21)	15 (10-21)	16 (8-21)	17 (10-21)	15 (8-21)	16 (10-21)
First-row	18 (16-21)	18 (16-21)	20 (16-21)	20 (18-21)	18 (16-21)	18 (16-21)
Second-row/ Third-row	15 (10-18)	16 (12-18)	18 (10-21)	18 (12-21)	15 (10-18)	16 (12-18)
Backs	12 (8-14)	13 (10-17)	13 (8-16)	15 (10-17)	12 (8-13)	13 (10-15)

Table 7.1: Results of the survey about cleat lengths used by Racing 92 players. The results are given in mm. For each position, we give the average value following between parenthesis by the minimum and the maximum length of cleats used. NG stands for Natural Grass. Fr and Ba stand for the Front and Back of the shoes respectively. Extracted and adapted from [110].

We also observe in Table 7.1 that first-row players wear the longest cleats: whatever the surface, they have 18 mm cleats on average, with some players that are always using 21 mm cleats.
In order to rationalize the choice of cleat size, we develop an experimental protocol to quantify the friction at the sole ground interface.

7.2 Experimental Studies

7.2.1 Cleats tested for friction coefficient

Subject A (defined in Chapter 6) stands on the grass equipped with his cleat boots (cf. Figure 6.5b) and pushes on the scrum machine presented in Figure 6.4. The compression force F_x and the vertical force F_y are time recorded up to the point where the subject starts to slide (cf. Figure 7.6a).
The different cleats tested are presented at in Figure 7.6b: their length ranges from $L_C = 8$ mm to $L_C = 21$ mm. We also calculate the friction coefficient for a standard tennis shoe pair without studs to represent the limit $L_C = 0$ mm. Screwed cleats from $L_C = 13$ mm to $L_C = 21$ mm have a similar truncated cone shape with $D_C = 12$ mm at the tip and a diameter of 17 mm at the base.

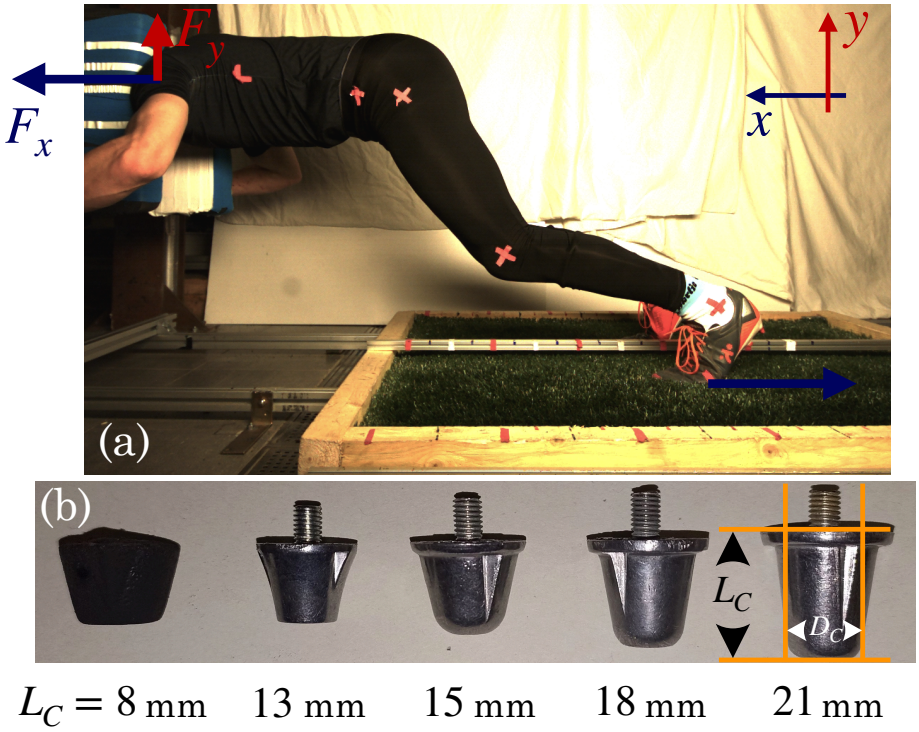


Figure 7.3: Experimental study of the influence of the length of cleats L_C on the friction coefficient. (a) Subject A pushes on the instrumented scrum machine and we measure F_x and F_y until he slips. (b) Picture of the different cleats used in the experiments.

The molded cleats shoes used by subject A are presented in Figure 7.4. The disposition of cleats is different from the screwed cleats boots (cf. Figure 6.5b). So, in a scrummaging posture, the player has 10 cleats anchored in the ground contrary to 8 for L_C=13 mm to 21 mm. This remark is critical because we know that cleat-grass friction is driven by the number of cleats sunken in the grass and their size [119]. The molded studs are slightly different in shape: they have a circular shape with a diameter of 10 mm and are crossed by a plane. The apparent length L_C of molded cleats is 8 mm.

7.2.2 Cleats tested for the maps of force

Subject A follows the experimental protocol presented in subsection 6.2.2 where we time recorded F_x and F_y with varying the posture of the subject with l and h (cf. Figure 7.5a).



Figure 7.4: Molded-cleat shoes used by subject A.

The total force $\vec{F}$ is composed of the passive force $\vec{F_p}$ and the active force $\vec{F_a}$ (cf. Chapter 6).

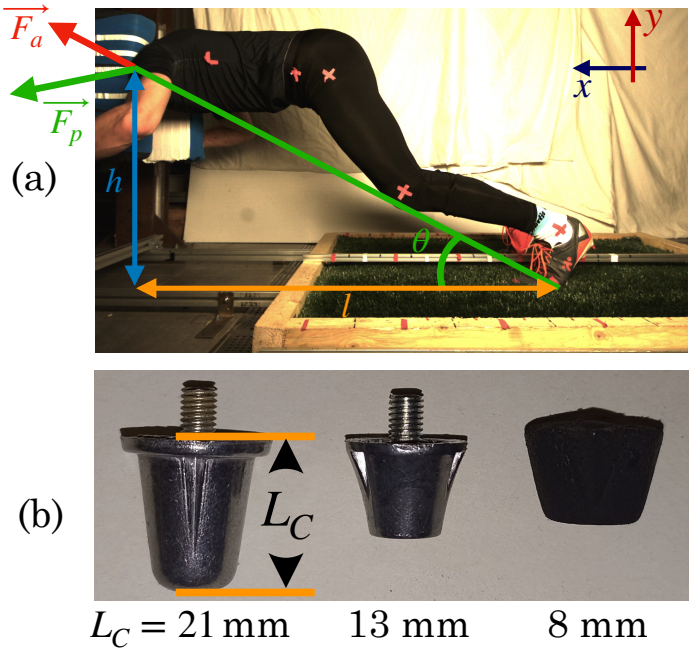


Figure 7.5: Experimental study of the influence of the length of cleats L_C on the forces in the phase plane (l, h). (a) Subject A pushes on the instrumented scrum machine. (b) Picture of the three different cleats used in the experiments.

In chapter 6, we already measure the force maps for $L_C = 21$ mm (cf. Figures 6.9 and 6.10). Here, we repeat this protocol with the length of cleats $L_C = 13$ mm and $L_C = 8$ mm (cf. Figure 7.5b). Finally, subject A is following the same protocol using the foot support (cf. Figure 5.3) that corresponds to the limit $\mu \to = +\infty$.

7.3 Results

7.3.1 Evolution of μ

In Figure 6.26d, subject A slips on the synthetic grass with cleats of $L_C = 21$ mm. The equivalent curves are obtained for cleats from $L_C = 8$ mm to $L_C = 18$ mm. For each of them, we define the vertical forces F_x^* and F_y^* which correspond to the limit of the no-slip condition (cf. subsection 6.6.1). The equation (6.16) tells us $\mu = \frac{F_x^*}{F_y^* + mg}$ with m mass of the subject.
In Figure 7.6, we present μ as a function of L_C for a fixed number of cleats, $N_C = 4$ under each foot, except for $L_C = 8$ mm where $N_C = 5$ under each shoe. $\mu(0)$ corresponds to the limit case with the tennis shoes.

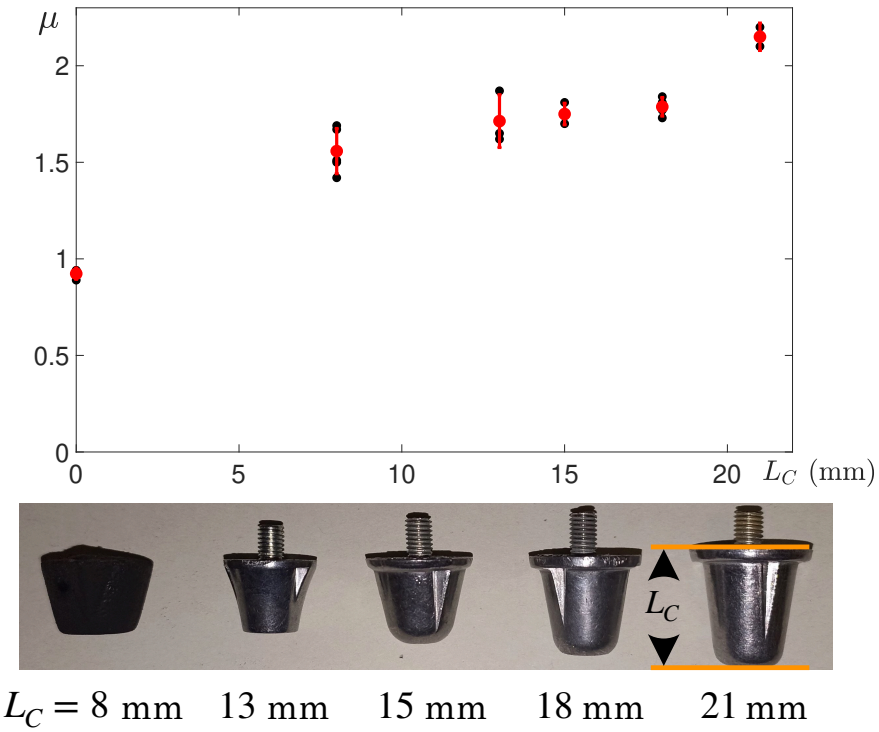


Figure 7.6: Friction coefficient as a function of the length of the cleats L_C.

The black points represent all the trials made for different postures of subject A by changing l and h. For $L_C > 10$ mm, these postures were elongated ones (cf. Figure 6.7d) with $l > 115$ cm and $h < 60$ cm. For the postures with an important pushing height or the postures with a smaller l, subject A is not able to slip.
For $L_C = 8$ mm, there is a wider range of postures for which the subject slips with $h < 65$ cm and $l > 105$ cm. For $L_C = 0$ mm, subject A is not able to activate his muscles to produce the active force without slipping in most of the postures. The friction coefficients are thus obtained for compressed postures with pushing heights $h > 60$ cm (cf. Figure 6.7a).
The red points are the average μ for fixed L_C, with the error bars that correspond to the standard deviation of the black points.

Without any cleats, we measure $\mu = 0.93$. This value increases to $\mu = 1.56$ with $L_C = 8$ mm and reaches a maximum value of $\mu = 2.15$ with $L_C = 21$ mm.

7.3.2 Passive force

The horizontal passive force F_{p_x} measured for the different size of cleats shown in Figure 7.5b are presented in Figure 7.7. The passive force is scaled with the weight of subject A mg and is plotted as a function of θ. Moreover, the black points represent the results obtained with the foot support.

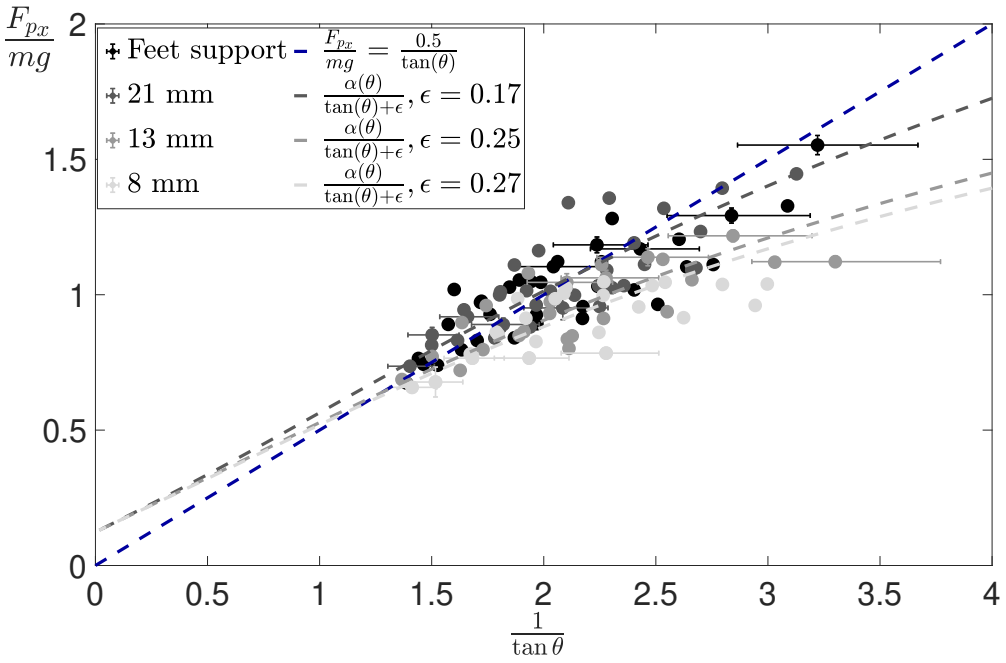


Figure 7.7: Dimensionless $\frac{F_{p_x}}{mg}$ as a function of $\frac{1}{\tan\theta}$ with L_C =8 mm (very light gray), L_C = 13 mm (light gray), L_C = 21 mm (dark gray) and foot support (black). The blue dashed line represents the pure horizontal passive model of equation (6.7). The dashed lines in shades of gray represent the model with a constant $\epsilon = \frac{-F_{p_y}}{F_{p_x}}$ of equation (6.11).

For the sake of clarity, we show the error bars just on a few points. The horizontal error bars correspond to the measurement uncertainties of $\pm 2°$ for θ. The vertical error bars correspond to the dimensionless standard deviation of F_{p_x} calculated on the passive force plateau (cf. Figure 6.8). The blue dashed line corresponds to equation (6.7) with the passive force purely horizontal and $\alpha = 0.5$. The other dashed lines represent the model of equation (6.11) where we fix the average of the ratio $\epsilon = \frac{-F_{p_y}}{F_{p_x}}$ calculated on each set of data ($L_C = 8$ mm, $L_C = 13$ mm, and $L_C = 21$ mm). In this model, we also measure the position of the CoG of subject A with side view images (cf. subsection 6.4.2).

We observe a good match between the pure horizontal model and the experimental data with the foot support and $L_C = 21$ mm.
We note that the average ratio $\epsilon = \frac{-F_{p_y}}{F_{p_x}}$ increases with L_C: $\epsilon = 0.17$ with $L_C = 21$ mm (cf. Figure 6.29), $\epsilon = 0.25$ with $L_C = 13$ mm and $\epsilon = 0.27$ with $L_C = 8$ mm. It signifies that when the player is in a passive posture on the scrum machine, with (l, h) fixed, wearing the 8 mm molded-cleats shoes, he tends to produce a higher F_{p_y} than when he is wearing 21 mm cleats. It should be linked to a compensating effect of the lack of grip at the shoe-turf interface. We notice that the model with constant ϵ and CoG calculated on each posture (equation 6.11) depicts the dropout of $\frac{F_{p_x}}{mg}$ compared to the dashed blue line for the smaller

θ. The higher ϵ, the larger the dropout is. Nevertheless, the dropout in the model results is less important than what we observe in the experimental data.

7.3.3 Active force

Figure 7.8 shows the evolution of the norm of active force F_a as a function of the elongation factor $\frac{\mathcal{L}_0}{\mathcal{L}}$. The same color scale as Figure 7.7 is used to discriminate the data with foot support and the different length of cleats.

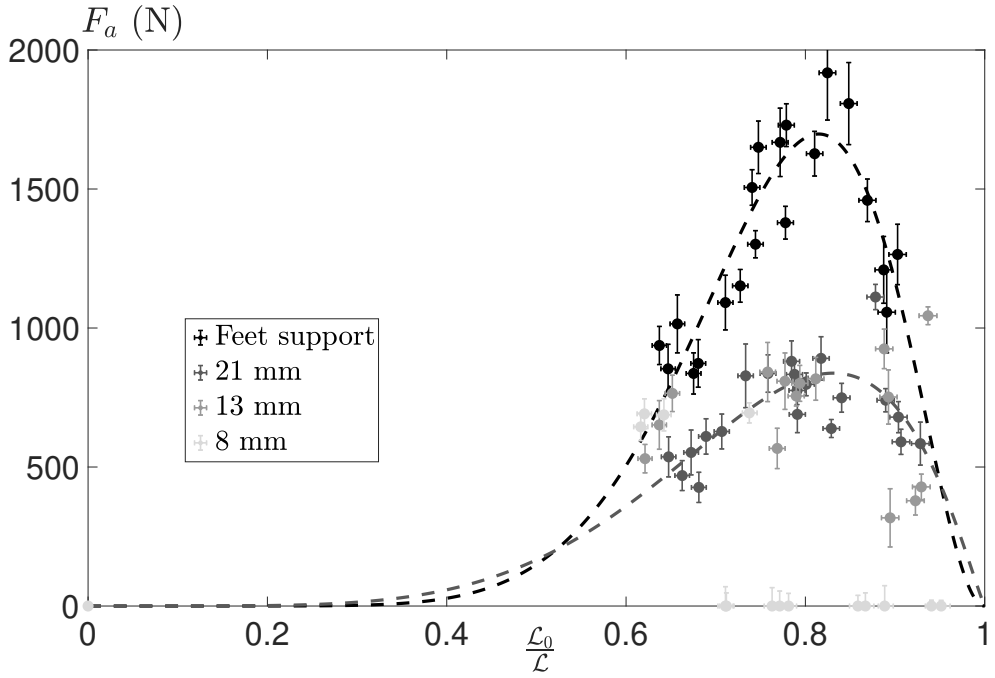


Figure 7.8: Intensity of the active force as a function of the elongation factor $\frac{\mathcal{L}_0}{\mathcal{L}}$ with L_C =8 mm (very light gray), L_C = 13 mm (light gray), L_C = 21 mm (dark gray) and foot support (black). The dashed line in gray represents the model of equation (6.13) fitted on experimental data with L_C = 21 mm. This curve correspond to the one presented in Figure 6.43 for subject A.

We present here the active force obtained for $h < 65$ cm as we did in Figures 6.18a and 6.43. We observe that the intensity of the force F_a is twice as large with the foot support as with the cleat shoes whatever the elongation factor. Indeed, the dashed line model (from equation (6.13)) fitted on the black data reaches a maximum value of approximately 1700 N at $\frac{\mathcal{L}_0}{\mathcal{L}}$=0.8. Whereas the gray dashed line model fitted on the data with L_C = 21 mm reaches its maximum value of approximately 850 N at $\frac{\mathcal{L}_0}{\mathcal{L}}$=0.83. The set of parameters obtained with the non-linear regression for the black dashed line is $m_1 = 9.2$, $m_2 = 2.1$ and $F_{a_0} = 3.9 \times 10^5$ N (cf. Table 6.2).
The gray dashed line satisfyingly describes the experimental data obtained with L_C=13 mm. However, we observe that the behavior of the experimental data with L_C = 8 is different. For $\frac{\mathcal{L}_0}{\mathcal{L}} \in [0.6; 0.7]$, the few experimental points follow the gray dashed line but then, for $\frac{\mathcal{L}_0}{\mathcal{L}} > 0.7$ the active force drops to 0 N. The player is not able to activate his muscles after he set himself on the scrum machine with L_C = 8 mm. If he starts to produce an active force for $\frac{\mathcal{L}_0}{\mathcal{L}} > 0.7$, subject A slips.

7.4 Comparison of the Total Force $\vec{F}_x$

7.4.1 Foot support

We compare the horizontal force F_x of subject A obtained experimentally with the complete model presented in Figure 6.44. We start here by presenting the comparison for the experiments with the foot support.

In Figure 7.9, the experimental data F_x are presented with squares of colors corresponding to the values of F_x. The model is presented with the colored isoforce curves. The total force of the model is calculated by adding the results of the pure horizontal passive model (equation (6.7)) and the active force model presented in the black dashed line in Figure 7.8. With the feet support, there is no limit imposed by the friction coefficient μ: we are in the limit where $\mu \to +\infty$[1].

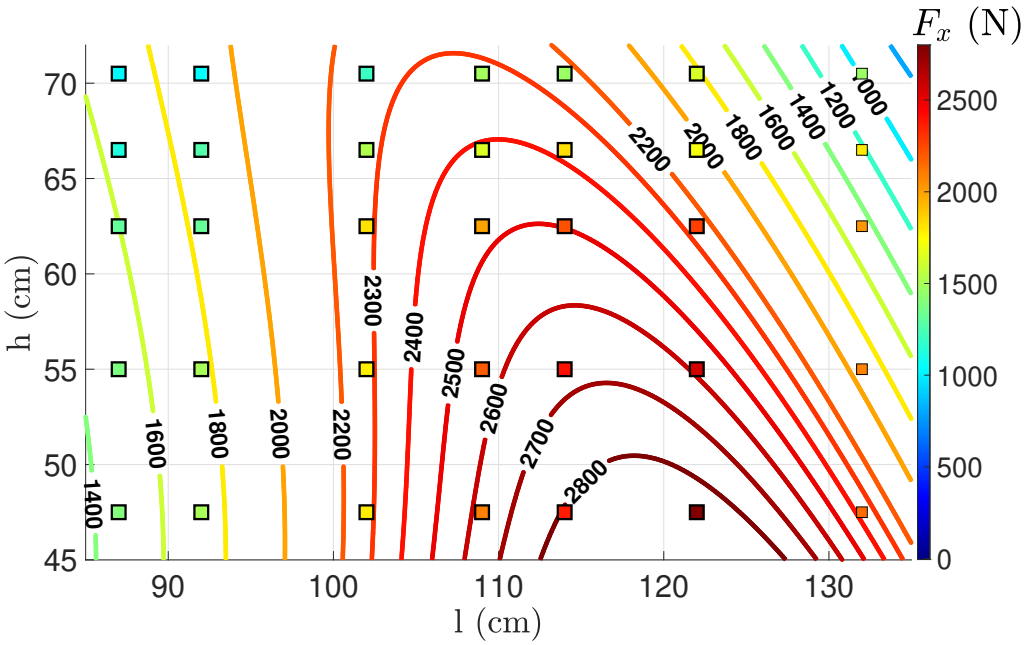


Figure 7.9: Total pushing force comparison F_x between the experimental data and the model of equation (6.14) for subject A with foot support. The experimental data are represented with colorful squares and the model is presented with isoforce curves with the same color scale.

Compared to the 21 mm F_x maps of F_x (cf. Figures 6.45 and 6.46), subject A reaches pushing forces that are 1.6 times larger in the equivalent optimal pushing zone ($l \simeq 122$ cm and $h \simeq 47$ cm). Subject A is not limited by the friction for very extended postures, he then reaches $F_x = 2150$ N for $l = 132cm$ and $h = 48$ cm.
The matching of the location of the optimal pushing zone between the model and the experiments is really good. The values of force between the experiments and the model are similar in the zone of low $h < 60 - 65$ cm. This remark echoes what we already said about Figure 6.46: the active model is fitted on experimental data obtained with $h < 65$ cm (cf. Figure 7.8).
The optimal posture of subject A remains equivalent to the one obtained with 21 mm cleats in terms of l and h.

[1] We numerically take $\mu = 20$.

7.4.2 $L_C = 13$ mm and $L_C = 8$ mm

For the experiments obtained with, $L_C = 21$ mm, $L_C = 13$ mm and $L_C = 8$ mm, we use the model of the total force of equation (6.15) which is composed of the the passive model that considers the vertical component F_{p_y} (cf. equation (6.11) and Figure 7.7) and the active model corresponding to the gray dashed line of Figure 7.8. We already showed the results of the comparison with $L_C = 21$ mm in Figure 6.46. Moreover, the value of μ in the model is set for each L_C thanks to Figure 7.6.

Figure 7.10 presents the F_x comparison between experimental data and the model for $L_C = 13$ mm with $\mu(L_C = 13) = 1.7$.

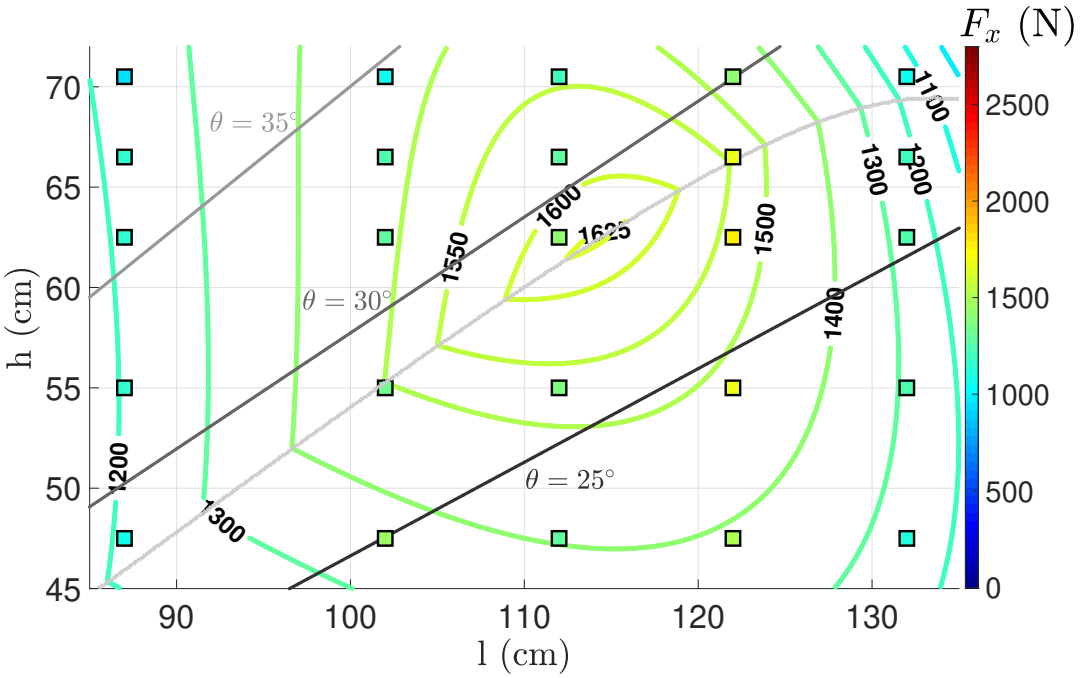


Figure 7.10: Total pushing force comparison F_x between the experimental data and the model of equation (6.15) for subject A with $L_C = 13$ mm. The experimental data are represented with colorful squares and the model is presented with isoforce curves with the same color scale. Iso-θ curves are presented with lines in shades of gray.

Figure 7.11 presents the F_x comparison between experimental data and the model for $L_C = 8$ mm with $\mu(L_C = 8) = 1.5$. We use the same active model for $L_C = 8$ mm as the one used for $L_C = 13$ mm and $L_C = 21$ mm, but the no slip-condition is here to limit the production of active force in the model.

The comparison between the experiments and the models is qualitatively satisfying. The longer the cleats, the lower the optimal pushing height is, and also the larger the forces F_x are. For 21 mm cleats, the experimental maximum $F_x = 2080$ N is reached for $l = 124$ cm and $h = 48$ cm. For 13 mm cleats, the experimental maximum $F_x = 1770$ N is reached for $l = 122$ cm and $h = 62$ cm. For 8 mm cleats, the experimental maximum $F_x = 1230$ N is reached for $l = 122$ cm and $h = 67$ cm.
Thus, the optimal posture of subject A wearing 13 mm cleats is obtained with $\theta = 26°$ and elongation factor $\frac{\mathcal{L}_0}{\mathcal{L}} = 0.89$. The optimal posture of subject A wearing 8 mm molded-cleats is obtained with $\theta = 28 - 29°$ and elongation factor $\frac{\mathcal{L}_0}{\mathcal{L}} = 0.9$. We recall that the optimal posture with 21 mm cleats was obtained with $\frac{\mathcal{L}_0}{\mathcal{L}} = 0.83$ and $\theta = 20°$ (cf. Figure 6.46).

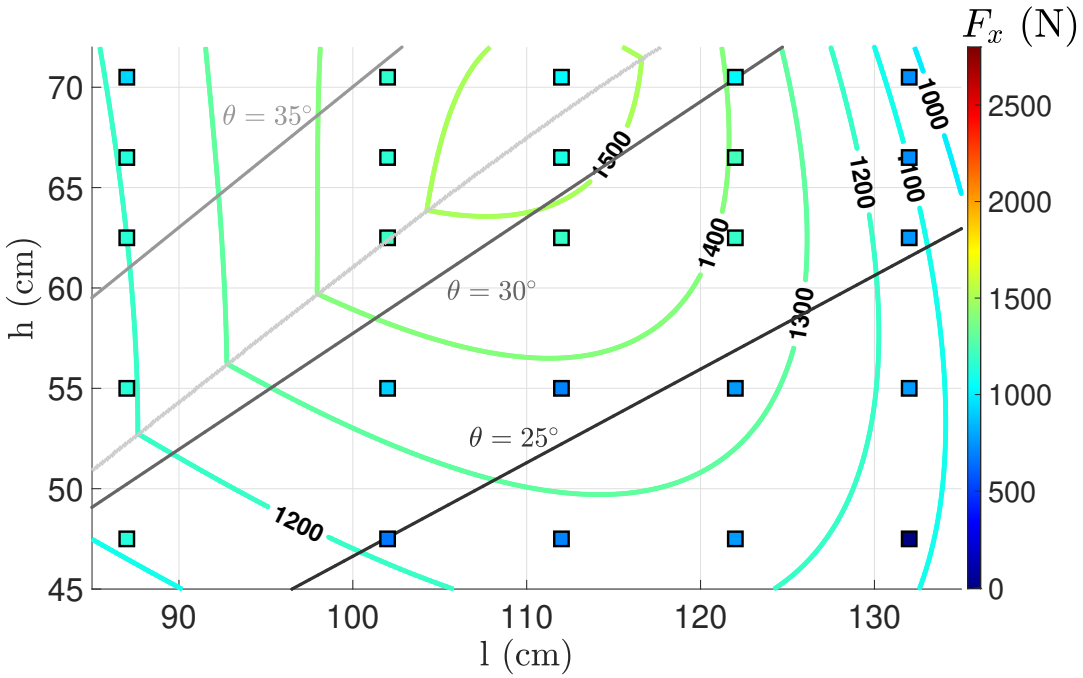


Figure 7.11: Total pushing force comparison F_x between the experimental data and the model of equation (6.15) for subject A with $L_C = 8$ mm. The experimental data are represented with colorful squares and the model is presented with isoforce curves with the same color scale. Iso-θ curves are presented with lines in shades of gray.

7.4.3 Conclusion and perspectives

The size of the cleats L_C influences the anchoring to the ground of the players. In doing so, the length of the cleats influences the individual force production and the individual optimal posture. This last point is reflected in the models we developed with the displacement of the optimal pushing zone towards higher pushing heights h and lower foot distance l when L_C increases.

Here, we only tested three different L_C to build the F_x maps (cf. Figures 6.46, 7.10 and 7.11). $L_C = 21$ mm and $L_C = 13$ mm are mounted on the same pair of screwed-cleats boots, $L_C = 8$ mm is tested with another pairs of molded-cleat boots (cf. Figure 7.4).
If we only compare $L_C = 21$ mm and $L_C = 13$ results, we have a 20% raise in the maximum value of F_x with the longer cleats. These maximal pushing forces are not reached for the same postures. But, if we consider a fixed posture that is close to the postures observed in a real scrum for front-row players (cf. Figure 6.1), the gain between $L_C = 13$ mm and $L_C = 21$ mm is no longer as important for subject A. Indeed, for θ of the order of 30° and a pushing height of approximately h ∼70 cm, subject A produces a total pushing force $F_x \sim 1280$ N ($h = 67$ cm and $l = 112$ cm) with $L_C = 13$ mm, and a total pushing force $F_x \sim 1360$ N ($h = 67$ cm and $l = 117$ cm) with $L_C = 21$ mm. It corresponds to a raise of 6% in horizontal force production. However, we point out that 13 mm studs are short compared to the ones used by professional first-row players (cf Table 7.1). How much force subject A would win in this typical front-row posture with 21 mm cleats compared to 18 mm cleats? It will be inferior to a 5% raise. Furthermore, this posture is not limited in the zone limited by friction. So, it would be interesting to study it experimentally in order to rationalize the choice of the length of the cleats and see whether the player really benefits from choosing 21 mm studs instead of 18 mm studs.
An experimental study about the optimal number of cleats N_C under the shoes can also be

conducted with keeping in mind that this distribution should not interfere with the ability of the forwards to perform a wide variety of tasks during rugby games.

Take home message of Chapter 7

The size of the cleats L_C modifies the optimal individual posture. The longer the cleats, the higher the pushing force is. Nevertheless, for a set of parameters h and l corresponding to the ones observed on front-row players in real scrums, the difference in production of compression force between 21 mm cleats and 13 mm is less important than the difference in production of force for the respective maximal F_x. the experimental protocol exposed here could help players to rationalize their choice of length of cleats by knowing the benefits in force production in their postures adopted during rugby games from 21 mm cleats compared to 18 mm cleats for example. This experimental study could be adapted to natural grass or a different type of synthetic grass to work on the adaptation of the length of the cleats with the type of field.

PART III

COLLECTIVE EFFECTS AND DYNAMICS

We have conducted collective experiments at "Atelier de la mêlée" (cf. 3.1.3) with the professional players of Racing 92 in order to study transmission issues. Indeed, in the two previous parts, we studied the impact and sustained push phases at the individual level in order to discuss force production. But when the force is produced by each player, it does not mean that the total force applied to the opponent is equal to the sum of the individual performances (Chapter 8). And, the stability of the structure is not acquired as when a player pushes individually against a scrum machine (Chapter 9).

8

Transmission Losses in a Pack

We conduct an experimental study with professional players of Racing 92 in order to characterize the transmission of forces within a pack. We compare the scrum with another force battle: the tug of war, in order to understand the sources of transmission losses.



LHOTE André, *Rugby*, 1917, huile sur toile, 127,5 x 132,5 cm, Paris, Centre Pompidou.

Contents

8.1 State of the Art **150**
8.2 Experimental Study **151**
8.3 Postures and Positions **156**
8.4 1D Analogy: Tug of War **157**
8.5 Passive and Active Components **160**
8.6 Synchronization **163**

This work has been done with Sylvain Blanchard, Christophe Clanet, and Caroline Cohen thanks to a collaboration with Julien Piscione, Olivier Chaplain, and Didier Retière.
A special thanks to Laurent Travers, Patricio Noriega, and all the professional and academy Racing 92 players who participated in the tests.

8.1 State of the Art

In the study of Quarrie *et al.* [61], the authors compare the collective force achieved during the sustained phase of scrum and the sum of individuals. The total number of participants formed eight packs, producing mean forces ranging from 6210 to 9090 N. The table of results extracted from [61] is presented in Table 8.1.

		Team scrummaging force (N)					
Team	Pack weight (N)	Trial 1	Trial 2	Trial 3	Mean ± s	Sum of individual forces (N)	Pack force/sum of individual forces
1	8230	9100	9140	9020	9090 ± 70	12 380	0.73
2	7840	7580	8250	9340	8390 ± 890	11 310	0.74
3	7290	6600	7860	8100	7520 ± 810	10 360	0.73
4	7450	6700	6310	6350	6450 ± 210	9 370	0.69
5	7370	6390	6150	6320	6290 ± 120	11 380	0.55
6	7530	6660	5660	6390	6240 ± 520	11 950	0.52
7	7290	6680	5960	6000	6210 ± 400	9 940	0.62
Mean ± s	7570 ± 350	7100	7050	7360	7170 ± 1180	10 960 ± 1100	0.65

Table 8.1: Team and individual scrummaging force extracted from [61].

The second observation is that some teams achieve forces greater than the pack weight (Teams 1,2,3) while the weakest teams produce forces equivalent to 82% to 86% of the pack weight.
Looking at the sum of individual performance, it is systematically larger than the mean average force of the pack. We call losses in force transmission in the pack the percentage of force that miss to the collective force in order to reach the sum of individual forces. From the data of Table 8.1, we obtain the percentage of losses gathered in Table 8.2.

Team	Losses (%)
1	27
2	26
3	27
4	31
5	45
6	48
7	38
Mean ± std	35 ± 8

Table 8.2: Losses obtained with the packs in [61].

The losses are not the same for every pack. The ones that produce the larger force seem to have the lower losses. We note that the authors obtain losses of 35% on average for forwards of seven teams in the Dunedin Premier Rugby competition. The three teams with the best efficiencies correspond to the three teams able to generate more than their own total weight.

In the study by Milburn *et al.*, the authors test two Rugby Union packs without measuring the individual forces. However, they test different configurations in order to understand the contribution of sub-units in collective force production and transmission. We note N the number of players in a sub-unit. For example, the front-row plus the second-row configuration ($N = 5$) obtains an average sustained pushing force of 3790 N, the full scrum minus the flankers ($N = 7$) obtains 3830 N while the full scrum ($N = 8$) produced 4610 N. They observe a non-linearity between the number of players in the configurations and the pushing force produced on the scrum machine for both University first-grade packs.

Finally, the authors refer to a book from Hodge *et al.* [120] in which they test eight different binding or scrum formation techniques. They conclude that the difference in force production between a full pack and a pack minus the flankers is 28% lower. Then, removing the Number-eight, to reduce the number of players to $N = 5$, does not reduce the force produced. This means that the role of the Number-eight in a pack is not associated to force production but more probably with strategy.

8.2 Experimental Study

We decide to conduct our own experimental study to quantify losses of transmission in the professional pack and sub-unit configurations with the Racing 92 team in order to understand the physical origins of the inefficiency of collective force.

8.2.1 Material and methods

Subjects

Eleven male forwards of the professional team of Racing 92 agreed to take part in the experimental study. This testing session was included in the training schedule as a scrum practice session.
The mass, height, age, and role of each subject are detailed in Table 8.3.

Identifier	Role	Mass (kg)	Height (cm)	Age	Pack number
1A	Loosehead Prop	116	183	28	1
1B	”	108	183	28	2
2A	Hooker	99	181	35	2
2B	”	116	178	35	1
3	Tighthead Prop	143	189	37	1 and 2
4	Lock	112	198	34	1 and 2
5A	”	122	206	27	1
5B	”	147	197	25	2
6	Flanker	114	195	23	1 and 2
7	”	106	201	25	1 and 2
8	Number eight	108	191	34	1 and 2

Table 8.3: Mass, height, age, role, and pack number of the subjects.

We form two packs with these eleven players in order to study the repeatability and the influence of players' turnover. The last column of Table 8.3 gives the number of the pack they belong to. Five of them took part in two different versions of the packs.

Experimental setup

We use the M-Rex scrum machine of "Atelier de la mêlée" in Marcoussis that we described in subsection 3.1.3. The performance and research pole of the French Federation of Rugby welcomed us and helped us to use the machine.
The scrum machine is set with a stiffness along the pushing axis equivalent to k_{61} (cf. subsection 4.2). Moreover, there are lower unquantified resistances along the y and z axes

(transversal and vertical axes respectively). The initial height of the scrum machine and all the settings are identical for all the trials presented here.
The sequences are video recorded with a zenith camera and two side-view cameras at 25 fps. The players wear their usual studded boots and underfoot conditions are dry synthetic grass. The players perform a warm-up protocol led by physical trainers of the club just before the experimental session.

Protocol

We limit the total number of trials achieved by one player to 10 and the players are taking part in the experimental study in a randomized order that allows them to have at least one minute of rest between each trial. These precautions are used in order to minimize the impact of fatigue in the results [121, 122].

The different tested configurations are presented in Figure 8.1.
For the individual trials, the front-row players push on the scrum machine at the position corresponding to their role: the loosehead prop does an individual trial on the left of the scrum machine (cf. subsection 3.1.3) with only one shoulder as if he was in a complete pack. For the locks and the back-row players, we ask them to push in the place most representative of their usual role in a pack. The flankers push on the left of the scrum machine with the right shoulder on the force sensor A of Figure 3.2a. The locks and the number-eight push in the position between the force sensors B and C.
Then, the second-row configuration pushes against the mannequins representing the opposing hooker and loosehead prop. For the collective trials from 1R to 1R+2R+8, the players are setting themselves as if they are pushing in a pack configuration.

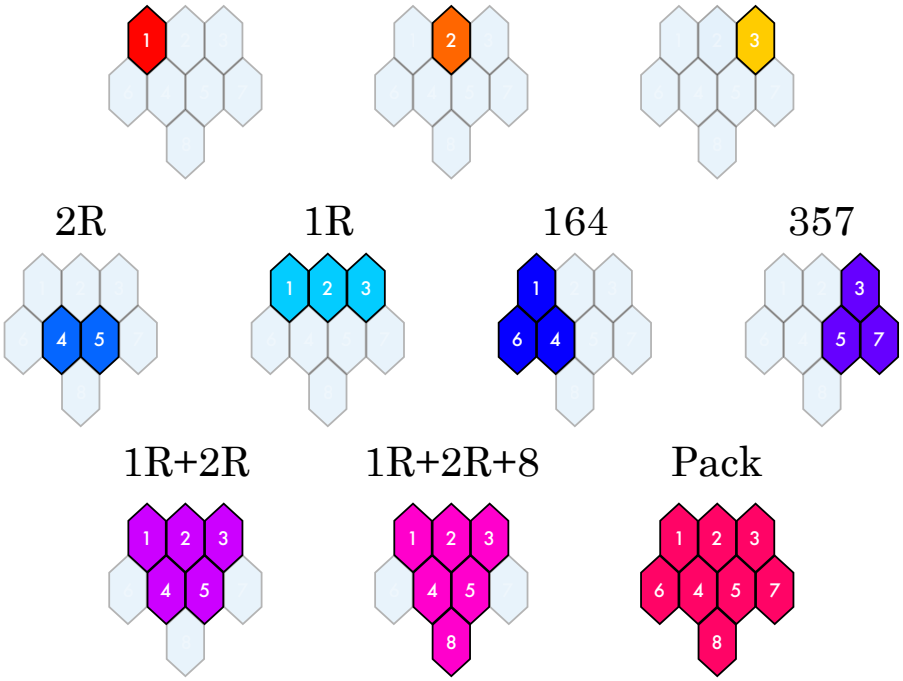


Figure 8.1: Configurations tested in the experimental study.

Each player is first invited to do his individual trial, and then each configuration represented in Figure 8.1 is tested for both pack versions.
Each trial, individual or collective, is composed of an impact (that we studied in Chapter 3) and a sustained push phase of 3-4 seconds. We ask the player to generate as much force

as possible during the sustained phase and it is triggered by a voice signal given by the scrum captain. This voice signal corresponds to the one used in the real scrum by the pack of Racing 92 in order to synchronize the collective push after the ball introduction. The players are loudly vocally encouraged by the forward coach during their trials.

8.2.2 Results

Examples of force signals

We study pushing forces F_x defined by the x-component of the total force F. We give some compression force F_x signals in Figure 8.2.

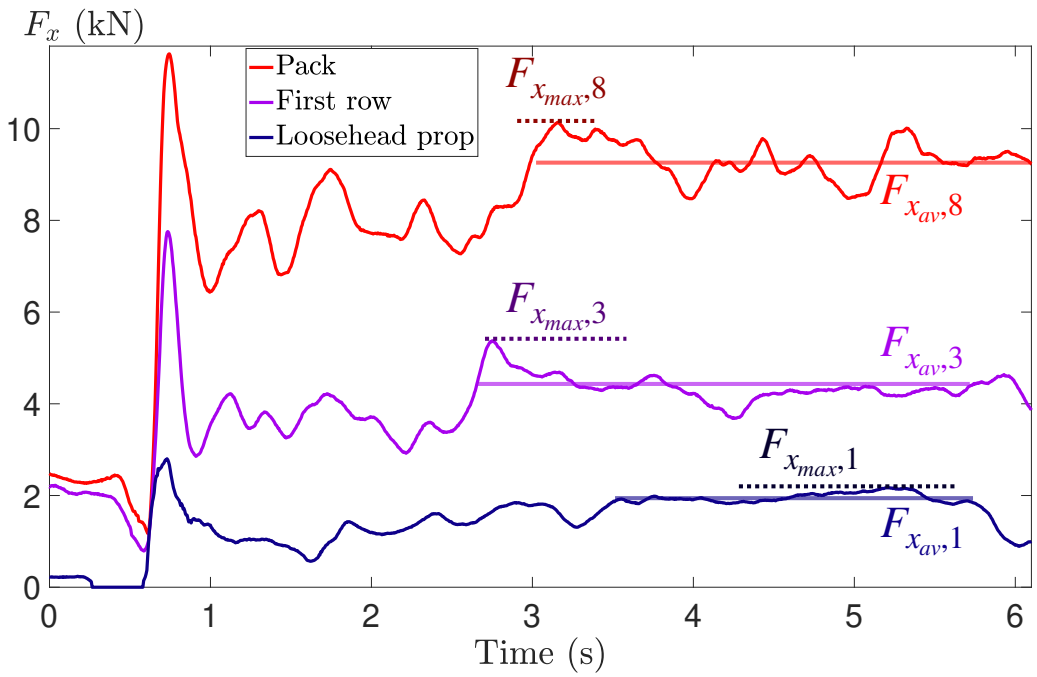


Figure 8.2: Time evolution of the compression force for different configurations. The blue line corresponds to 1B trial, the purple line corresponds to 1R V_2 trial and the red line corresponds to the full pack V_2 trial.

We define $F_{x_{av},i}$ as the average force produced during the sustained phase for 2 to 3 seconds by a configuration composed of i players. $F_{x_{max},i}$ is the maximal compression force reached during the plateau force generated by a configuration composed of i players. $F_{x_{max},i} - F_{x_{av},i}$ is an indicator of force production stability during the sustained phase.

The minimum value of the ratio $\frac{F_{x_{av}}}{\|\vec{F}_{av}\|}$ among the collective trials during the sustained phase is 0.97 while the minimum ratio $\frac{F_{x_{av}}}{\|\vec{F}_{av}\|}$ among the individual trials is 0.91.

The blue solid line shows the evolution of F_x for subject 1B. In Table 8.4, we show the individual forces $F_{x_{max},1}$ and $F_{x_{av},1}$ obtained with the subjects of Table 8.3. We observe that a player is able to produce forces around 2000 N

The purple solid line corresponds to the time evolution of F_x for the 1R version 2 (V_2) trial and the red curve corresponds to the full pack V_2 trial. The loosehead prop 1B participates in

Identifier	$F_{x_{av},1}$ (N)	$F_{x_{max},1}$ (N)
1A	1620	1820
1B	1990	2170
2A	1970	2240
2B	1970	2270
3	1640	1780
4	2040	2200
5A	1950	2080
5B	1870	2080
6	1240	1420
7	2260	2410
8	1760	2130

Table 8.4: Individual performance of all the subjects.

the three trials presented in Figure 8.2. When we compare the compression force produced to the respective weight of configurations, we obtain $\frac{F_{x_{max},1B}}{m_{1B}g} = 2$, $\frac{F_{x_{max},1R,V_2}}{(m_{1B}+m_{2A}+m_3)g} = 1.5$ and $\frac{F_{x_{max},Pack,V_2}}{\left(\sum_i^8 m_i\right)g} = 1.1$. In all the configurations tested, they are able to push more than the total weight of the configuration.

We already observe here that the evolution of $F_{x_{max}}$ and $F_{x_{av}}$ is not linear with the number of players. Indeed, we have $F_{x_{max},1B} = 2170$ N, $F_{x_{max},1R,V_2} = 5380$ N and $F_{x_{max},Pack,V_2} = 10140$ N.
As it was done in [61], we compare the collective forces of a given configuration to the sum of individual forces of the players that compose the configuration. We find $\frac{F_{x_{max},1R,V_2}}{\sum_{i=1}^3 F_{x_{max},i}} = 0.87$ and $\frac{F_{x_{max},Pack,V_2}}{\sum_{i=1}^8 F_{x_{max},i}} = 0.62$. If we execute the same calculation on $F_{x_{av},i}$ we obtain 0.76 and 0.63 respectively. We notice that for the full pack we obtain a similar result to the one obtained on average in [61].

Ch. 8

Configuration efficiencies

We define $L^m_{\%}$ of a configuration as the percentage of losses of maximal collective compression force $F_{x_{max}}$ compared to the sum of individual performances $\sum_{i=1}^{N} F_{x_{max},i}$ as

$$L^m_{\%} = \left(1 - \frac{F_{x_{max}}}{\sum_i^N F_{x_{max},i}}\right) \times 100. \tag{8.1}$$

In Table 8.5, we gather the collective forces, the sum of the individual forces, and the $L^m_{\%}$ for each trial made with subjects of pack V_1 and subjects of pack V_2.

We can do the same calculation on average forces rather than $F_{x_{max}}$ by calculating $L^{av}_{\%}$, that we obtain by substituting $F_{x_{max}}$ with $F_{x_{av}}$ in equation (8.1). We obtain approximately the same results at $\pm 3\%$ except for 1R trials with $L^{av}_{\%} = 20\%$ and $L^{av}_{\%} = 24\%$ for V_1 and V_2 respectively.

Configuration	N	Sub-unit force (N)		Sum of individual forces (N)		$L^m_{\%}$ (%)	
		V_1	V_2	V_1	V_2	V_1	V_2
2R	2	4156	4140	4280	4280	2.8	3.3
1R	3	5196	5376	6025	6170	14	13
164	3	4021	3490	5440	5790	26	40
357	3	4144		6270		34	
1R+2R	5	7778	7440	10310	10450	30	29
1L+2L+8	6	8680	7860	12440	12580	30	37
Pack	8	10392	10140	16270	16410	36	38

Table 8.5: $L^m_{\%}$ obtained for the different configurations. N is the number of players in the configuration.

We observe in Table 8.5 that the losses increase with the number N of forwards in a configuration. However, for the same N, V_1 and V_2 packs obtain similar results for a given configuration. Except for the 164 configuration where V_1 is more efficient than V_2.
The same kind of experiment has been conducted before with eight players of the amateur-level Rugby Club of Versailles[1] on the same instrumented scrum machine. The individual $F_{x_{max}}$obtained were on average smaller than the professional ones with $\overline{F_{x_{max},1}} = 1661$ N. In Table 8.6, we gather the $L^m_{\%}$ measured for the amateur pack from Versailles.

Configuration	N	$L^m_{\%}$(%)
2R	2	3
1R	3	22
1-6-4	3	38
3-5-7	3	30
1R+2R	5	34
Pack	8	45

Table 8.6: $L^m_{\%}$ obtained for the different configurations of the amateur pack of Versailles. N is the number of players in the configuration.

Except for the first configuration with $N = 2$ players, we note that the losses $L^m_{\%}$ obtained with amateurs are higher than the ones obtained with professionals.

In Figure 8.3, we plot $F_{x_{max},i}$ as a function of N for experiments performed with Racing 92 players. The black dashed line is the linear function that represents the sum of the forces of the average individual performance $N.\overline{F_{x_{max},1}}$.

We notice an increase of losses with N thanks to the deviation from the linear mean curve, and similar results for V_1 and V_2 for a given configuration. For $N = 3$, we have three configurations tested with 1R (V_1 and V_2), 164 V_1 and V_2 and 357 V_1. We clearly see that the configurations with only one player in direct contact with the scrum machine (164,357) are less efficient than the first-row trials (1R).

In the next sections, we would like to investigate qualitatively and with complementary experiments the reasons why we observe these losses in the collective structure of a scrum.

[1] Unknown masses of the players.

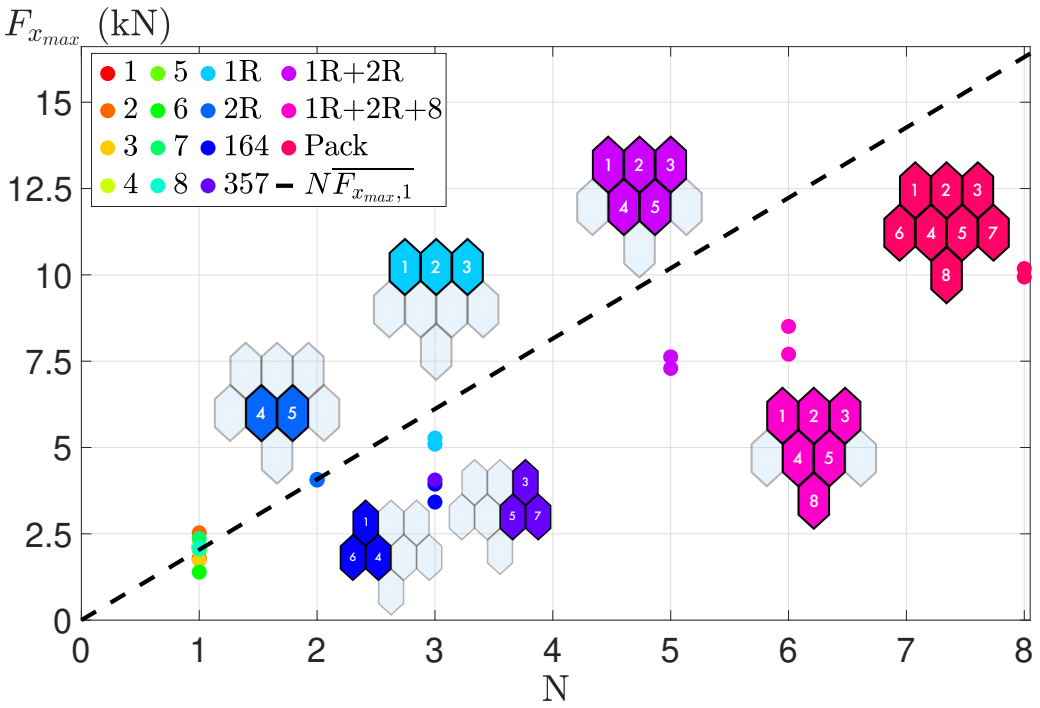


Figure 8.3: Maximal compression force reached during the sustained phase by the different individuals and configurations. Experimental data are represented with color dots. The black dashed line corresponds to the linear function of N with a slope equal to the average of individual $N.\overline{F_{x_{max},1}}$.

8.3 Postures and Positions

The first explanation for losses is associated with the difference in the posture of the player when he/she is pushing alone on the scrum machine compared to the postures adopted in a collective configuration.
Indeed, in Figure 8.4, we give two examples with the flanker 7. In Figure 8.4a, we have a side-view of his individual trial and in Figure 8.4b, we have a side-view picture of a full pack trial in which he takes part. We see that he adopts two different postures, on the individual trial his pushing height is slightly higher, his back is directed upwards and his knee angle is bigger than the one he has in the collective trial where his trunk direction is more aligned with the ground. But, we have seen in the two previous chapters that all postures are not equivalent and the force produced by a player is strongly correlated with pushing height and joint angles. In addition, this player does not push with the same shoulder during his individual trial and during the collective trials. We thus understand that in collective trials, the players could not adopt the posture they want and they will not necessarily produce the same amount of force as in the free single trial.

These posture constraints are imposed by the position of the player in the scrum. For instance, the first-row players cannot extend their legs as much as they want since they must define a contact zone for the flankers and locks with their gluteal muscles.

To this first explanation for losses linked to force production, we can add a second linked to transmission: it is not the same to push directly on the scrum machine or to push on a player that is pushing against the scrum machine. Indeed, all the force produced by a player at the level of his shoulder is transmitted to the scrum machine foams when the

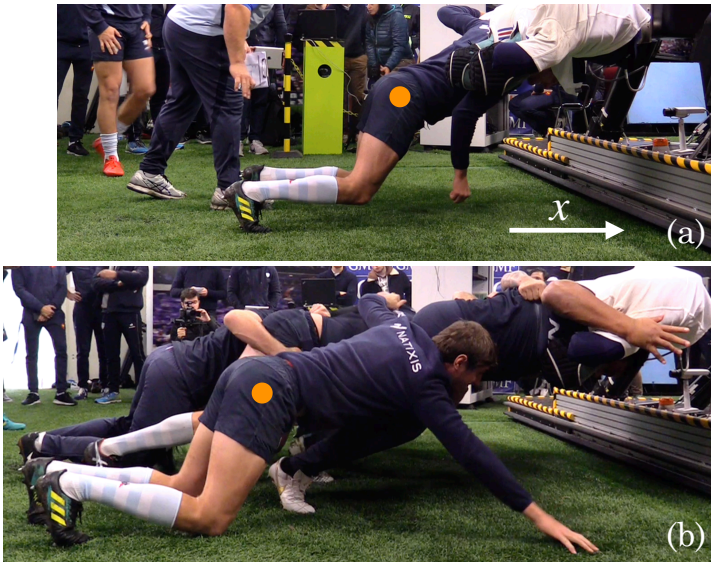


Figure 8.4: Side view pictures of the individual trial of subject 7 and the collective trial of full pack V_2.

subject is alone. When the subject is pushing on a player, some force could be lost in player deformation or in the direction of the force applied. Moreover, this action of one player can lead to a decrease in the force produced by the player who is forward.
We understand the different phenomena evoked previously:

- When we add a number eight to a 1R+2R configuration, the force is approximately equivalent to the 1R+2R despite subject 8 being able to produce $F_{x_{av}} = 1760$ N individually (cf. Table 8.4). For instance, for V_2 players we have a 5% increase with the addition of the number eight.
- 1R is more efficient than 164 or 357. In 1R, the three players apply directly their force on the scrum machine whereas in the triangle configurations (164 and 357) only one prop is pushing on the scrum machine. The core qualities of this player and the stability are the key factors to transmitting the lock and the flanker forces.

Another origin of the losses could be linked to the bindings with the teammates, which also modify the posture of each player and then the efficiency of pushing. For example, the arms positions during an individual trial could help to stabilize the subject but in a collective trial, the flankers are sometimes obliged to put a hand on the ground to balance themselves and thus inevitably lose force to transmit to the players on the front.

8.4 1D Analogy: Tug of War

When we deal with collective force production, one has to refer to the work of the French agronomist Maximilien Ringelmann [123] who studied human agricultural work in fields by measuring and estimating forces needed to move different agricultural machinery. In [123], he introduces an experimental study of humans pulling a rope in a 1D situation. This experimental study is close to the Olympic sport of tug of war introduced between 1900 and 1920.

Tug-of-war contests consist of two opposing teams pulling a rope in order to attract the opponents towards them. In Figure 8.5, we have a picture taken by Jules Beau during the 6 vs 6 Tug-of-war contest of the 1900 Summer Olympics in Paris. The official in the middle of the picture holds a stick that symbolizes the imaginary line not to cross.
For the record, this contest took place between two mixed teams. One was composed of Scandinavians with men from the Danish and the Swedish Olympic teams, the other team was composed of sportsmen from Racing Club de France. This team was composed of five French and one Colombian. Three of the French players were playing Rugby Union in Racing Club de France, the former name of Racing 92: Jean Collas, Charles Gondouin, and Émile Sarrade. They were also part of the French Rugby Union team who won the 1900 Olympic tournament. Unfortunately, the mixed French/Colombian team lost against the Scandinavians in the tug-of-war contest, and it was the only official tug-of-war battle of the tournament.



Figure 8.5: Tug-of-war contest between Racing Club de France and the Scandinavian team at the 1900 Summer Olympics. Picture from Jules Beau, extracted from [124].

Seventy-four years after, Alan G. Ingham would have said that they partly lost because of social laziness: individuals would tend to produce less force when they are in a group than when they are alone.
In 1913, Ringelmannn [123] conducted an experimental study where he increased the number of pullers in a rope-pulling task from 1 to 6. He also observed an increase in force losses with the number of participants as we made for the sub-units of the scrum. Moreover, he observed an almost linear evolution of losses with N as we can see in Figure 8.6. He presented his results by dividing the force measured by the number of participants N and by comparing it with the mean individual performance of a puller. Thus, he defined an average pull efficiency defined as

$$P_{eff} = \frac{F_{meas}}{N.F_{meas,ind}}. \tag{8.2}$$

P_{eff} quantifies the losses and is equivalent to the ratio $\frac{F_{x_{max}}}{\sum_{i=1}^{N} F_{x_{max},i}}$ obtained with the experimental study we made. We present the values of the ratio as a function of N with colorful points in Figure 8.6.

Contrary to the Ringelmann losses (black dashed line), the losses of the sub-units of scrum are not linear with N (visual guide of the red dashed line in Figure 8.6). The efficiencies of the triangular configurations are way worst than the three pullers of Ringelmann. The six pullers of Ringelmann's study have 37% of losses compared to the sum of the individual forces. This value corresponds to the losses $L^m_{\%}$ observed in the full pack configuration ($N = 8$, cf. Table 8.5).
In 1974, Ingham *et al.* [125] studied the Ringelmann effect by doing two studies of rope-pulling tasks in a more controlled way in order to compare their results with those of Ringelmann. We also present their results in Figure 8.6 with the dashed gray line. The authors underline that the losses are not linear with the number of participants. The six pullers of Ingham's study have 21% of losses.
In the first study, which corresponds to the one presented in the dashed gray line in Figure 8.6, Ingham *et al.* randomly increase the number of pullers from 1 to 6. They wonder if the increasing output loss is due to synchronization problems of members or if it results from a reduction in personal performance with the increase of individuals in the group: the social loafing theory [126, 127]. This is why they designed a second study where the participants are blindfolded. Then the authors make the blinded pullers believe that some pullers are added to help them. In this second study, they observe that until $N = 3$ the individual behaved like the imaginary mean puller of the first study and he was reducing his force production in the same way. For a larger number of fake participants N, there was stagnation in his individual force production. Ingham *et al.* conclude that the group size may have an impact on individual motivation to produce force. Nevertheless, we can doubt this conclusion because the experimental setup is not described in detail in Ringelmann's study, and some examples of force signals are not given in both studies.

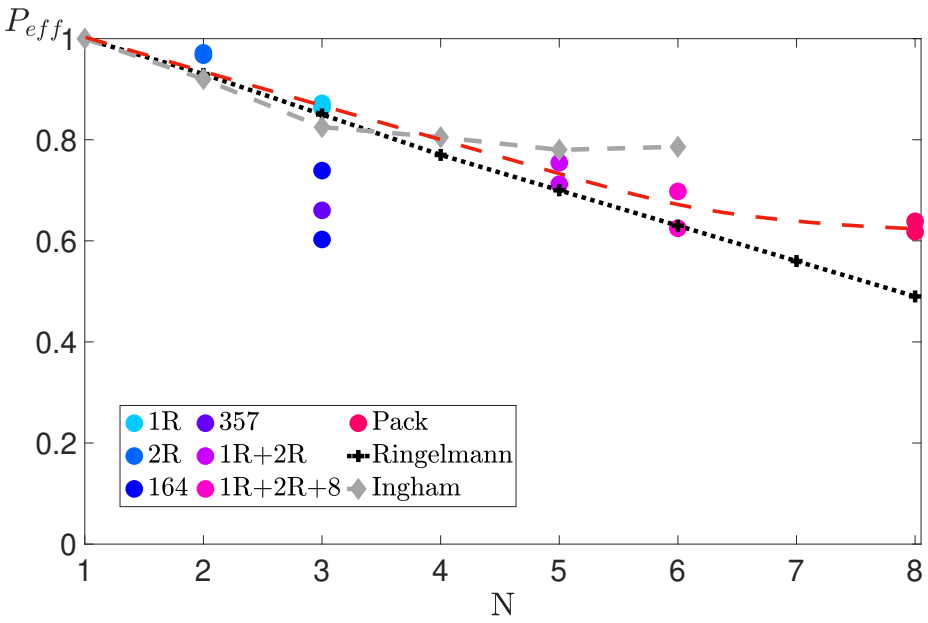


Figure 8.6: Average individual pull efficiency P_{eff} defined in equation (8.2) in the tug of war experimental studies (black and gray dashed lines) and the ratio of force produced over the sum of individual performances in sub-units scrum configurations (colored data) as a function of the number of participants N. The black dashed line is extracted from [123] and the gray dashed line is extracted from [125].

Even if the lack of motivation is hard to measure, the Ringelmann effect is interesting to study and a group of students from École Polytechnique conducted a tug-of-war study [128]

supervised by Christophe Clanet and Caroline Cohen. A rope was attached to a wall with a force sensor that measure a 1D force F_x (cf. Figure 8.7a). The number of pullers varies from 1 to 10. In Figure 8.7b, the time evolution of their signals of force are similar to the force signals of scrums in Figure 8.2 and allow them to define $F_{x_{av},i}$ and $F_{x_{max},i}$. We note that there is no impact at the beginning of the plateau of force contrary to the force signals of sub-units of the scrum.
In Figure 8.7c, $F_{x_{av},i}$ is presented in black dots as a function of the sum of individual forces $\sum_{i=1}^{N} F_{x_{av},i}$. The same thing is made with $F_{x_{max},i}$ as a function of $\sum_{i=1}^{N} F_{x_{max},i}$ in blue triangles. The supervisors obtain a linear behavior of $F_{x_{av},i}$ with N, however they observe losses in $F_{x_{max},i}$ with an almost constant $L^m_{\%} = 20\%$ for $N \geq 3$. This is a important difference with the experimental study about scrum where we obtained similar results when we calculate the percentage of losses $L^m_{\%}$ with $F_{x_{max},i}$ and $L^{av}_{\%}$ with $F_{x_{av},i}$ (cf. subsection 8.2.2).

In Figure 8.7d, we superimpose the ratio $\frac{F_{x_{max},i}}{\sum_{i=1}^{N} F_{x_{max},i}}$ obtained by Cohen *et al.* on Figure 8.6. These results seem to confirm the results obtained by Ingham *et al.* even if Ingham does not precise if he uses the average force or the maximal force to do the calculations.

The students of École Polytechnique [128] made complementary experiments in order to explain the additivity of mean forces $F_{x_{av},i}$ by decomposing the force in different components:

- The additive component of passive force $F_{p_x,i}$, corresponding to the pullers just using their weight to exert some force.
- The additive component of active force $F_{a_x,i}$, corresponding to the muscular synchronized force of the N pullers.

The sum of $F_{p_x,i}$ and $F_{a_x,i}$ gives the additive force $F_{x_{av},i}$. But, we observe in Figure 8.7b that there are some variations of force: $F_{x_{max},i} - F_{x_{av},i} \neq 0$. $F_{x_{max},i} - F_{x_{av},i}$ is called the impulse force $F_{x_{imp},i}$ and it is not additive with N (because $F_{x_{max},i}$ is not additive with N). The impulse force corresponds to the different lack of synchronization between pullers and their parasitic movements.
It appears that there is no problem with the transmission of force in the tug of war because each player is pulling the rope whereas, in scrums, the players are bound to each other.
And finally, we observe that the sub-units configurations of scrum are different from tug-of-war situations because we obtain similar losses for $F_{x_{av}}$ and $F_{x_{max}}$.

8.5 Passive and Active Components

To investigate the additivity of active and passive force components in a scrum, we conduct an experimental study on the Racing 92 scrum machine presented in Figure 4.5 in subsection 4.3. We measure $F_{x_{av}}$ for individual trials and for 1R, 1R+2R, and full pack configuration with thirteen players from the academy-level team of Racing 92 forming two packs versions. The experimental protocol was similar to the one presented in subsection 8.2.1 with the difference that we ask the players to previously set their body passively on the scrum machine to measure the passive horizontal force F_{p_x} of each player and configurations. We then ask them to activate their muscles in order to measure the active part of the force. This is illustrated in Figure 8.8c on the force signal with the first plateau corresponding to F_{p_x} and the second plateau corresponding to $F_{x_{av}} = F_{p_x} + F_{a_x}$. We show snapshots of the individual

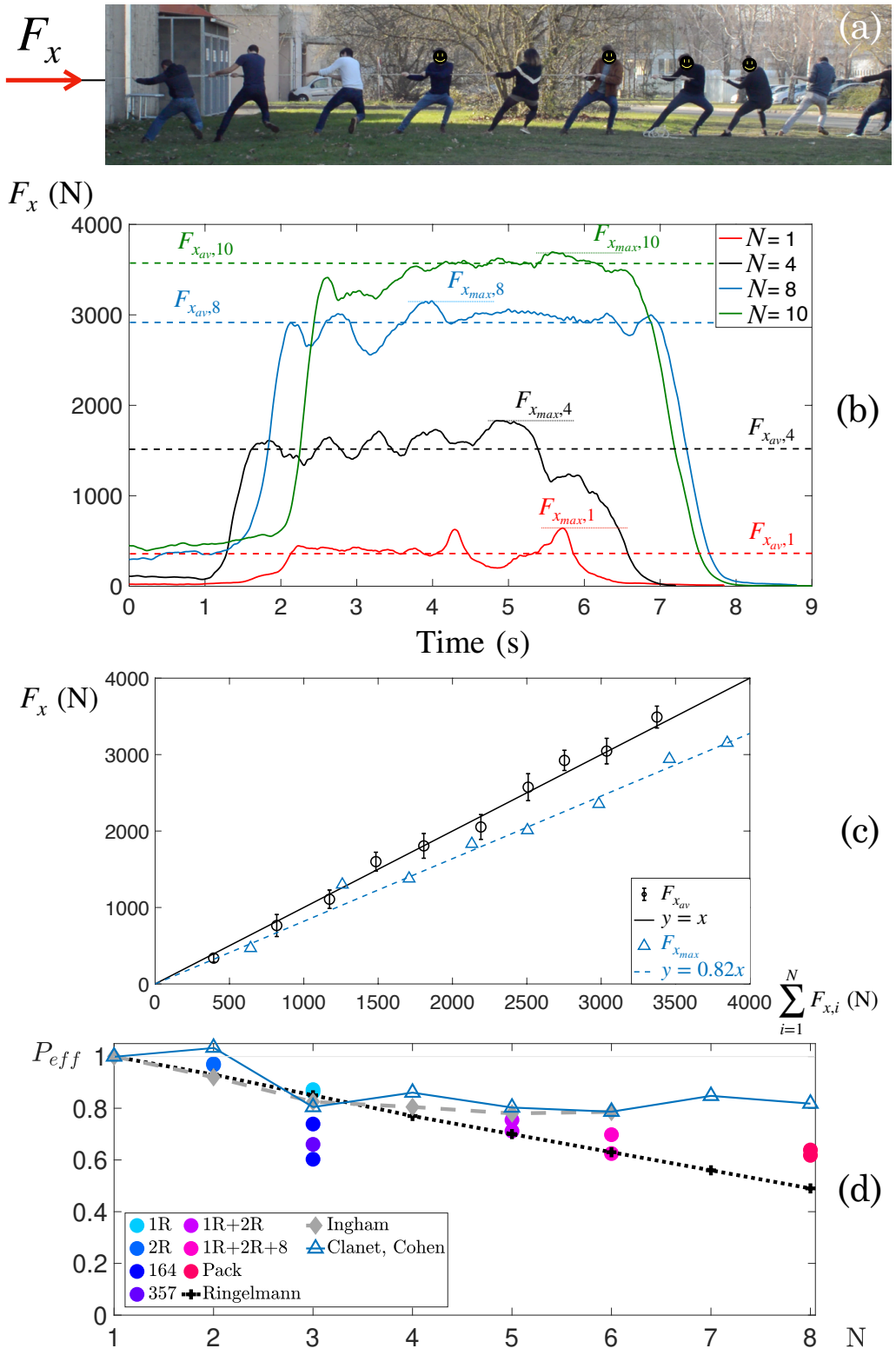


Figure 8.7: Experimental study of the tug-of-war contest. (a) Experimental setup with a force sensor that measures the force F_x produced by N pullers. (b) Examples of force signals. Adapted from a graphic of Caroline Cohen. (c) Average and maximal values of the collective forces as a function of the sum of the individual forces. The black points stand for $F_{x_{av},i}$ and the blue triangles stand for $F_{x_{max},i}$. (d) $\frac{F_{x_{max},i}}{\sum_{i=1}^{N} F_{x_{max},i}}$ and P_{eff} (equation (8.2)) as a function of N. The blue triangles represent the results of Caroline Cohen and Christophe Clanet. The other data is presented in Figure 8.6.

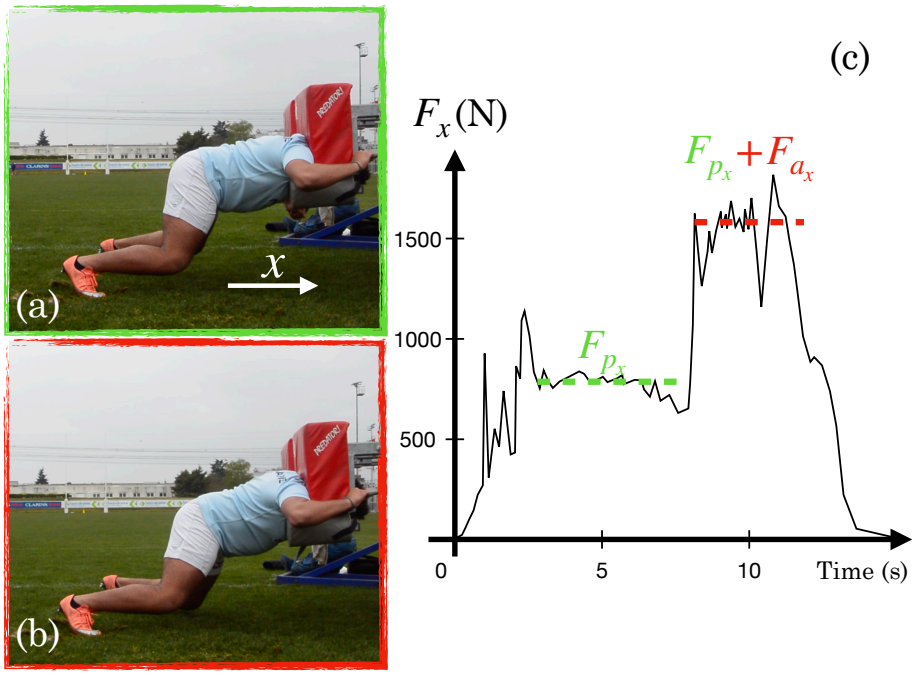


Figure 8.8: Academy-level loosehead prop pushes on the Racing 92 scrum machine. (a) Snapshot of the active phase of push. (b) Snapshot of the passive phase of push. (c) Time evolution of the compression force.

prop pushing on the scrum machine during the passive phase in Figure 8.8a and during the active phase in Figure 8.8b.

We obtain similar percentage of losses $L^{av}_{\%}$ than the professionals (cf. Table 8.5) for the configurations tested in Table 8.7, except for the 1R V_1 trial which was particularly inefficient with $L^{av}_{\%} = 25\%$.

Ch. 8

Configuration	N	F_{p_x} (N)	F_{a_x} (N)	$L^{av}_{\%}$(%)
1R V_1	3	2620	1950	25
1R V_2	3	1970	3350	5
1R+2R V_1	5	4410	4120	13
Pack V_1	8	5940	4630	27
Pack V_2	8	5790	3000	34

Table 8.7: $L^{av}_{\%}$ obtained for the different academy-level configurations. N is the number of players in the configuration.

In Figure 8.9, we decompose $F_{x_{av}}$ in passive and active components with green and red experimental data respectively, in order to understand the force losses observed.

On one hand, we observe that passive force seems additive like in the study of the tug of war made at École Polytechnique [128]. On the other hand, the active force data is not additive and we can thus explain the losses observed for the total force.
To this active force lack of transmission, we have to add the desynchronization between players in activation of their muscles and also with parasitic movements that are also bringing efficiency losses.

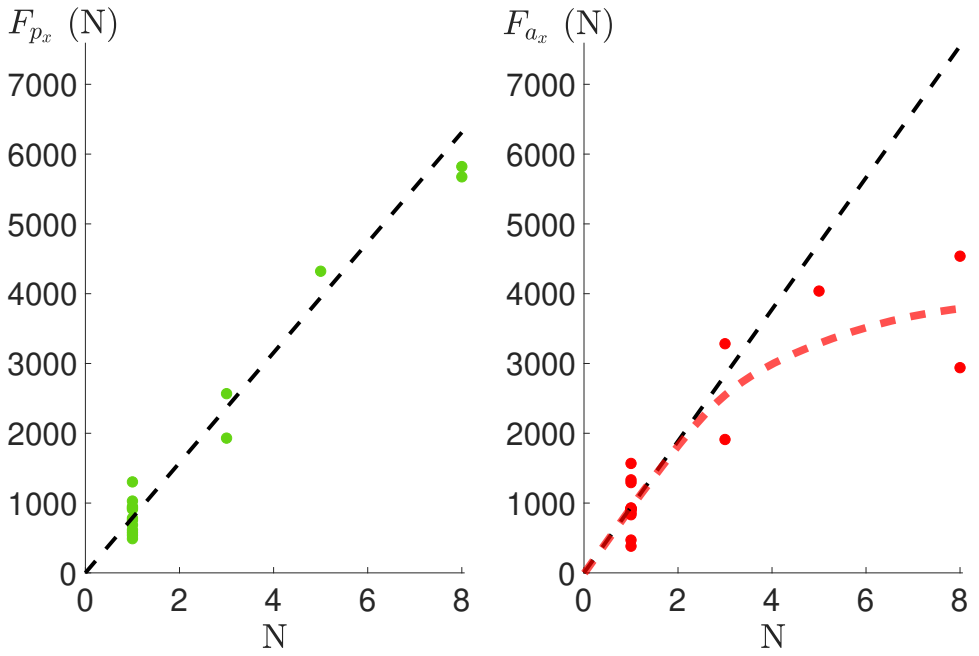


Figure 8.9: Passive and active force as a function of number of participants N. The black dashed line represents the linear evolution of slope corresponding to the mean individual performance in passive and active force.

8.6 Synchronization

Synchronization plays a key role in collective force efficiency in the scrum. Professional rugby players are already aware of the crucial issue of pushing at the same time and most professional teams have a referent player that is in charge of giving a vocal signal in order to synchronize the collective push after the introduction of the ball. It echoes the proposition of Ringelmann in [123] consisting of making the workers sing on a determined rhythm in order to synchronize their efforts. An example of tug of war synchronization is given in the video [129] where the athletes are synchronizing their support recoveries.
In the following, We use a numeric method of image analysis borrowed from Fluid Mechanics in order to determine the velocity vector field of a fluid flow thanks to colloids dispersed in a fluid. This technique is called Particle Image Velocimetry (PIV) [130, 131, 132] and we apply it qualitatively on top-view videos of scrum in order to characterize the synchronization of players.

8.6.1 PIV basic principle

PIV is not designed to describe the deformation of solid structures but it is designed to describe the complex movements of an important number of particles in a flow. For example, if you put a bike with a mannequin that mimics the cyclist in a wind tunnel, one can use an experimental setup to capture the flow of the particles moving in the airflow around the cyclist. One obtains some images as the one in Figure 8.10. By describing the movement of the particles in the flow, one describes the movement of the flow.

PIV algorithms evaluate the displacements of the particles by dividing the images into

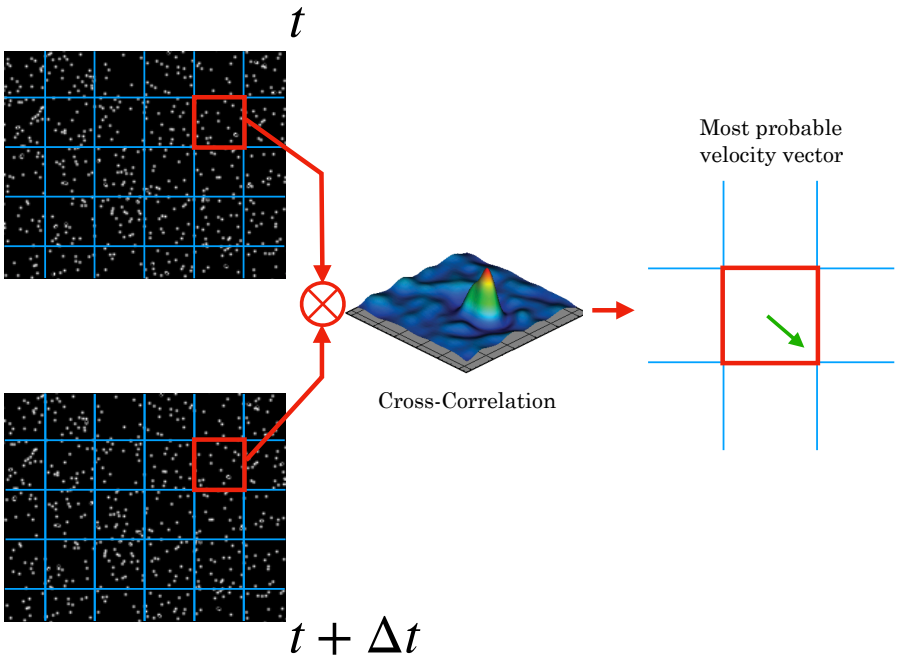


Figure 8.10: Principle of PIV analysis. Two pictures, at the instant t and $t+\Delta t$, of the particles in the airflow are divided into squares called Interrogation Areas (IA). Each of them is cross-correlated with each other and one calculates the spatial distribution of the cross-correlation for each IA. The maximum of this 2D function corresponds to the most probable displacement of an IA and one determines the vector velocity of the flow in each IA by dividing by Δt.

Interrogation Areas (IA) that we represent with the blue lines in Figure 8.10. Then, for two consecutive images at instant t and $t+\Delta t$, the IA are cross-correlated with each other, pixel by pixel. This cross-correlation provides a spatial signal with a peak that identifies the most probable common displacement of the particles in each IA. One needs to finally divide by Δt in order to obtain the velocity for each IA[2] represented by a green arrow. The length of the arrow reflects the intensity of the velocity and the direction of the arrow gives the direction of the velocity. We obtain a field of velocity vectors on the complete image at each time t.

Ch. 8

8.6.2 Application on the scrums and on the sub-units of the scrums

In Figure 8.11, we present snapshots of the different top-view videos we use for the PIV analysis. The first step of the video analysis is to correct the barrel distortion that deforms the straight lines. After the calibration and the choice of the size of the IA, we process the images with a toolbox of Matlab called PIVlab[3].
We present the final results of the PIV analysis of the 2R V_2 configuration in Figures 8.12a to d. We observe the green arrows corresponding to the field of velocity vectors.

Synchronization of the PIV analysis with the signal of compression force

The 2R V_2 trial is interesting because the signal of compression force measured at the "Atelier de la mêlée" (cf. Figure 8.12e) shows a diversity of situations: after the impact, both players maintain a stable force around 3500-3800 N; then, there is an unstable event with

[2] More details about PIV could be found in [133]
[3] `https://fr.mathworks.com/matlabcentral/fileexchange/27659-pivlab-particle-image-velocimetry-piv-tool-with-g`



Figure 8.11: Top view snapshots of sub-units configurations used for PIV analysis.

the force that drops to 2400 N.

In Figure 8.12a, the lock in blue is called player 1, and the lock in red is called player 2. The different quantities have an index i to specify the player we are talking about. In Figure 8.12f, we plot a quantity proportional to the individual time derivative of the momentum in order to quantify the disruptive desynchronization in collective trials. We consider the total mass of each player m_i and multiply it by an acceleration a_i that we calculate by space-averaging the speed values in the different colored squares v_{x_i} and by dividing it by Δt.
At the time t_1, the players exercise a quasi-constant force on the scrum machine without moving. Indeed, we do not observe green arrows in Figure 8.12a at t_1.In Figure 8.12f, both of the players have an average acceleration $a_i \sim 0$ m.s^{-2} so the total quantity $m_i a_i$ is close to 0 N.
However, in Figure 8.12b, player 1 is moving his right foot in order to bring it closer to his center of mass. We observe an induced movement at the level of the trunk which also has an immediate consequence on the force applied in Figure 8.12e. The movement of player 1 implies an oscillation of the quantity $m_1 a_1$ in Figure 8.12f while this quantity stays stable at that time for player 2. Finally, in Figure 8.12c, player 2 feels the need to reposition himself after the movement of his teammate by lifting his left foot which he rests at time t_4 (cf. figure 8.12d. We observe that the compression force drops in Figure 8.12e and that $m_2 a_2$ increases (red curve in Figure 8.12f) between t_3 and t_4.
We observe that the signal of force (cf. Figure 8.12e) of these two professional players is almost constant after t_4. The variations around $F_{x_{av},2}$.

We note that loss of support is detected by looking at the movements of the trunks of the player. Thus, for more complex configurations, such as the 1R+2R or the complete pack, we cannot see the feet of the first-row players on the top view video. But, we can identify the parasitic foot movements by identifying the movements at the level of the trunk. And thus explain why F_x drops in the collective signal of force. This result is known by the coaches: in [55], on page 99, the author advises the forwards to have a steady foot position after the engagement and specifies: "Not having to adjust the feet after the engagement precludes

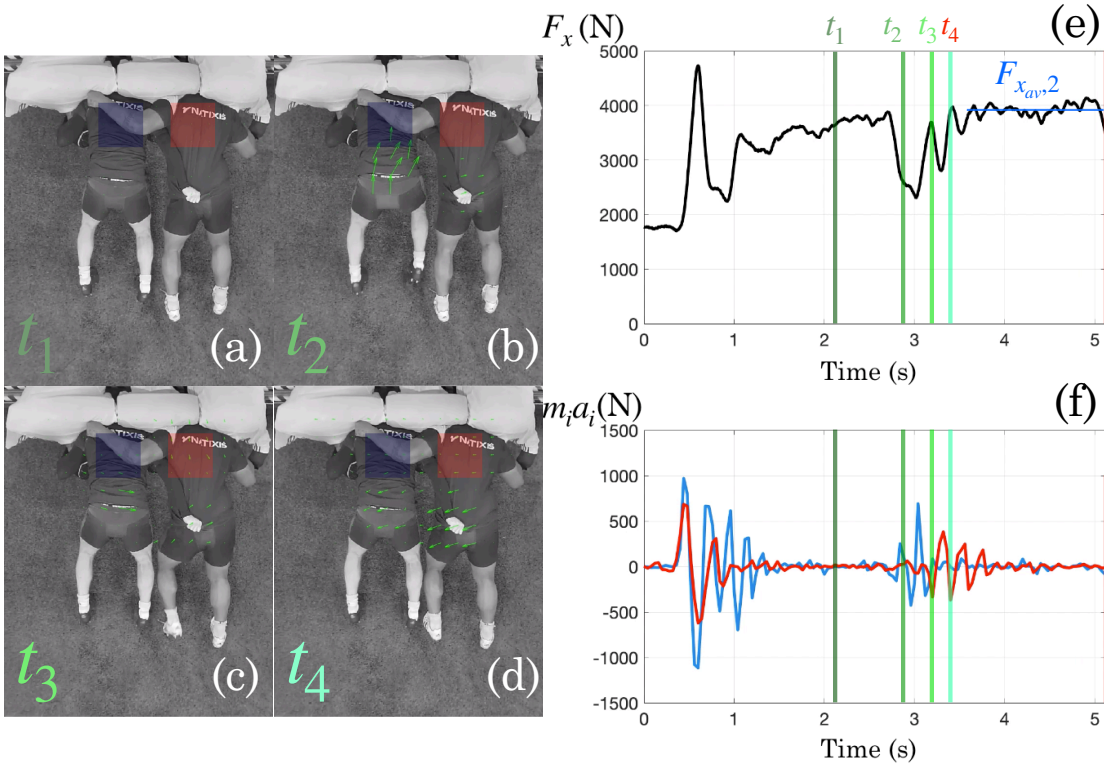


Figure 8.12: Example of PIV analysis on the 2R V_2 trial. (a) Top view snapshot with the field of velocity vectors represented with the green arrows. The areas that correspond to the speed-averaging of $m_i a_i$ are presented in blue and in red for players 1 and 2 respectively. (b) Player 1 lifts his right foot. (c) Player 2 lifts his left foot. (d) Player 2 rests his left foot. (e) Time evolution of the compression force F_x. (f) time evolution of the $m_i a_i$ quantity for both players synchronized with the signal F_x.

any loss of pressure".
The PIV technique cannot help us to determine of the values of the active and the passive force components. But, it provides information about the impulsion forces due to the dynamical collective effects.

Ch. 8

Impact estimation

The force at impact is mainly due to the setting in motion of a mass towards the scrum machine (cf. Chapter 3). Thus, it is almost purely an impulsion force. In Figure 8.13, we plot on the same graph the data of Figure 8.12e and 8.12f. The solid black line corresponds to the compression force F_x measured by the scrum machine and the red and blue lines correspond to the momenta-like quantities $m_i a_i$ for each player of Figure 8.12a.

In Figure 8.13, we observe that $F_{peak} \simeq 4700$ N but the initial force does not start from 0. The force difference ΔF is equal to the difference of F_{peak} minus the initial force exerted by the two players with their arms on the scrum machine. Here, we have $\Delta F = 3032$ N. Furthermore, we measure $\Delta \mathrm{m}_1 a_1 = 2085$ N and $\Delta \mathrm{m}_2 a_2 = 1306$ N.
The sum $\sum_i^2 m_i a_i$ is approximately equal to ΔF. We do these measurements for some individual and collective trials, and we compare the sum of the lookalike momentum of each player $\sum_i^2 m_i a_i$ with ΔF in Figure 8.14.

The experimental points are almost aligned with the black dashed line which represents the identity function. We note that this technique may be an interesting way to approximate

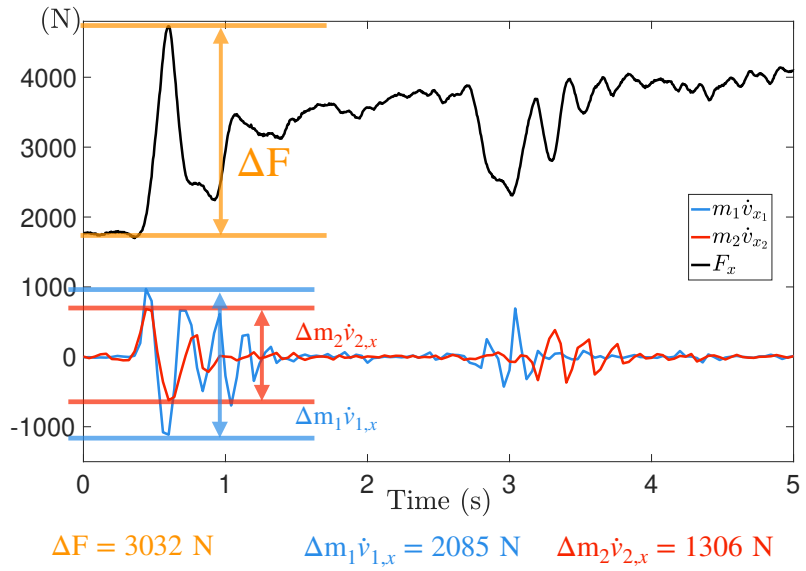


Figure 8.13: Time evolution of the compression force with the results from the PIV analysis. These signals are the same as the ones presented in Figure 8.12e and f. We measure the amount of impulse force ΔF at the impact and we compare it to the sum of the $m_i a_i$ determined with the PIV analysis.

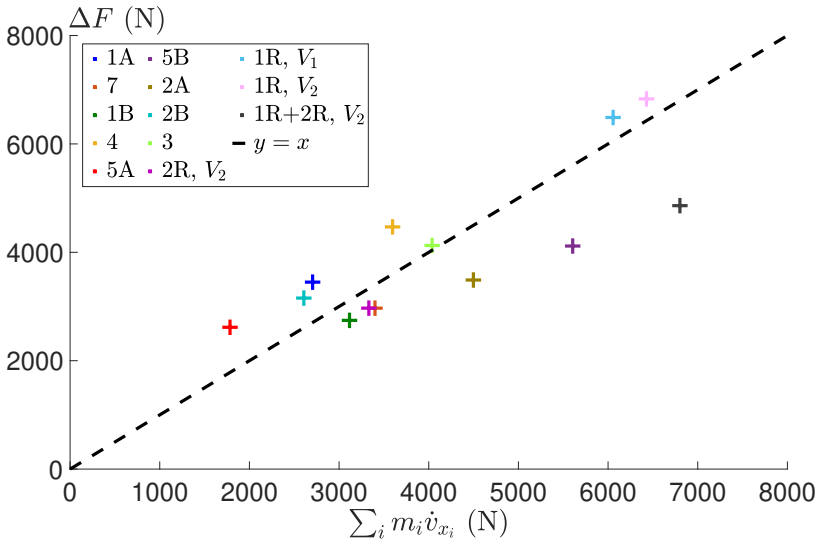


Figure 8.14: Individual and collective impulse forces ΔF at the impact as a function of $\sum_i^2 m_i a_i$. The black dashed line represents the identity function.

the forces at impact.
However, this technique cannot evaluate the initial value of the force before the "Set" referee call. It can only determine the impulse force ΔF. Furthermore, this short study gives less precise agreement when the number of players is higher than 5 in the sub-unit of the scrum, so the technique is not ready yet to estimate the forces at the impact of a real scrum:

- One of the limits is linked to the acquisition frequency of the top camera in the "Atelier de la mêlée" which is equal to $f_e = 25$ Hz. It signifies that there is a point every 40 ms which implies that we have typically 5 points to describe the rising of the impact force signal (cf. Figure 2.1).
- we developed an experimental study about the losses during the sustained push phase.

This is still an issue during an impact. Even if the players are quite well synchronized, the momentum generated by the number eight will be difficult to transmit to the opponent.

- in Chapter 2.2, we saw that F_{peak} depends on the impactor but also the impacted.

Live Scrum Application

Even if we cannot estimate the forces at impact, we use the PIV analysis to track the centers of mass of the players (or other points of interest) during a live scrum. In Figure 8.15, we show an example of chronophotography of a scrum video captured with a drone during a training session of Racing 92. The field of the velocity vectors obtained with the PIV analysis is represented with yellow arrows.



Figure 8.15: Application of the PIV treatment on a top view video during a practice of Racing 92 professional team. (a)

First of all, it is a non-invasive method to study synchronization and the players are used to being filmed by drones during their practice sessions. This is a qualitative tool to highlight the lack of coordination between players. In 8.15a, the two packs just impacted and the scrum half is about to introduce the ball. The yellow arrows are quite important, and they convey the fact that the pack on the right wins the impact phase and we observe a short backward movement of the left pack thanks to the PIV arrows. We also notice that the arrows are present on the immobile grass, this is probably due to the spatial finite nature of the two packs whereas PIV algorithms are used to study the flows occupying the entire image. The red squares on each player are approximately located at the level of their center of mass. We wrote an algorithm that allows us to select these points on the first image of the video and then track them on each image with the PIV analysis. Indeed, by using the

results of the Eulerian field of velocity vectors, the algorithm determines the Lagrangian movement of each point through the video.
In Figure 8.15b, the two packs are stabilizing after the throw-in of the ball. In Figure 8.15c, a perturbation appears at the level of the loosehead prop 1. It seems that players 1, 2, and 6 are not pushing towards the compression axis of the scrum anymore. In Figure 8.15 where we see that the scrum has turned and all the structure is moving in the transverse direction. This tool identifies the dynamic events that could affect the stability of a scrum and could help to objectify the cause of an infringement in the scrum.

A tool to quantify the parasitic movements in the scrums would be a way to optimize the synchronization in order to optimize the collective forces. The lack of synchronization is one of the sources of the losses, the other sources are the lack of transmission of the active forces due to the elasticity of the players (the first rows are not perfect transmitters of the force produced behind them) and the postures adopted in the collective player are constrained by their teammates which could imply a loss of production of the individual forces.

Take home message of Chapter 8

We conducted an experimental study on the efficiency of collective force production in scrums.

1. Pack efficiency is defined as the ratio between the collective force produced by the entire pack and the sum of the individual forces. For the professional pack of Racing 92, we obtain a ratio of 0.65 and for the amateur pack of Versailles, we obtain 0.55 which means that they are less efficient in the forces they transmit. The playing level and the frequency of training sessions are probably important parameters to optimize the efficiency of the collective force of a rugby pack. We identify several key parameters that explain these losses: individual postures for optimal force production, core qualities for force transmission, bindings, and synchronization with teammates for force production and transmission.

2. A comparison with the tug of war is presented in order to see what could be the similar reasons that explain the collective losses. A student experimental study does not confirm the results of the literature and claims that the passive and active components of forces produced by the rope-pullers are completely additive. The problem of synchronization is the main creator of losses in tug-of-war battles. However, in scrum situations, a quick experimental study we conducted shows that individual passive forces seem additive but the active component loses efficiency in a complete scrum.

3. Synchronization plays also a key role to reduce the scrum collective losses in force transmission. We started to develop a tool using Particle Image Velocimetry to exhibit the lack of synchronization by determining the velocity vector field on top-view videos of scrums. We link the evolution of impulse force with the parasitic movements in the pack

9

Scrum Instabilities

We present the different scenarios of the scrum. We measure the movements of the contact line between the two first rows made on stable, rotated, and moving forward scrums. We use those measurements to design an experimental protocol at the "Atelier de la mêlée".



Raised scrum during a France-England game. Extracted from coachxv.com [134]

Contents

9.1 An Instable Structure **172**
9.2 Dynamics of the Contact Line of Scrums **175**
9.3 Dynamical Experimental Study **179**

This work has been done with Caroline Cohen and Christophe Clanet thanks to a collaboration with Olivier Chaplain and Julien Piscione.

9.1 An Instable Structure

We have studied the scrum during the two main phases: during the impact with a dynamical experimental study on a passive scrum machine with a fixed stiffness and during the sustained push phase with quasi-static experimental studies on a motionless scrum machine. Nevertheless, we saw in Chapter 8 that even during the sustained push phase, the scrum structure is constantly moving and quite unstable and that exhibit a limit of our experimental study. In this chapter, we want to present how we designed an experimental study in which we impose displacements at the level of the first row in order to observe dynamical collective effects.

We choose to classify the types of scrums into six categories: the stable scrums, the moving forward or backward along the pushing axis scrums, the collapsed scrums, the raised scrums, the turned scrums, and the moving in the transversal direction scrums.
The two first categories generally respect the rule of providing a push " straight and parallel to the ground " [3]. In particular, the second category corresponds to the scrums that are clearly won by a pack. The last four categories of scrums lead to a penalty or a reset of the scrum.

9.1.1 The stable or stationary scrum

A scrum is called stable when the two packs give the impression of not moving after the ball introduction (cf. Figure 1.9). In this case, both packs produce approximately the same amount of pushing force, but there is an intense battle between the two first rows: there is a movement of a few centimeters of the contact line that we will measure in subsection 9.2.2.

9.1.2 The moving forward or backward scrum

If a pack is taking advantage of the other by producing a greater force, the other one starts to move backward. In Figure 9.1, we have a chronophotography of a scrum during a men's game between Fiji (white team) and Tonga (red team).

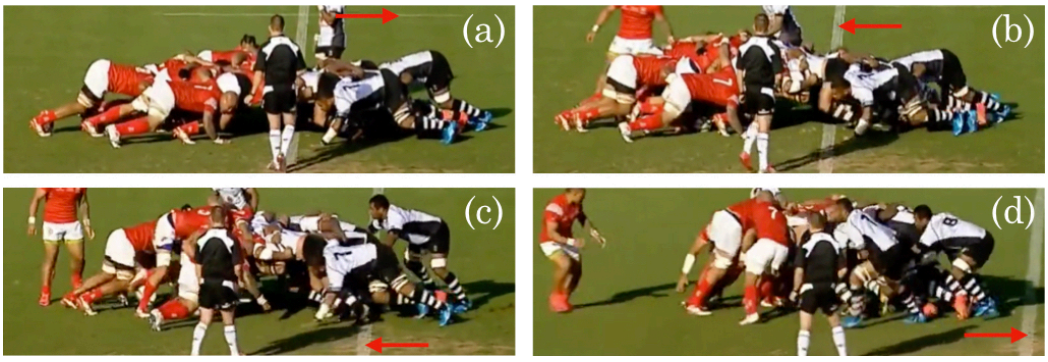


Figure 9.1: Example of a moving forward scrum during a Fiji vs Tonga international men's Rugby Union game. This chronophotography is extracted from [135].

In Figure 9.1a, the ball is introduced by the Tongan scrum-half. We identify one of the marked lines as a reference on each frame with a red arrow. Thus, in Figures 9.1b and c, the Tongan pack is cornered. In Figure 9.1d, this pack lost almost 5 meters and will be hindered in the release of the ball.

9.1.3 The collapsed scrums

This is a dangerous type of scrum illustrated in Figure 9.2 where the structure collapses under its own weight. It can be due to some of the first rows that are not pushing parallel to the ground anymore or a player destabilized by the opponent and that loses control of the core of the trunk. An important part of the new rules that are constantly introduced to have safer scrums (cf. Chapter 2.2) tend to reduce the risks of collapsed scrums which are more likely to cause major injuries (as for example spine injuries [27]) at professional and community level [136, 137].



Figure 9.2: Side-view picture of a collapsed scrum in a men's Rugby Union international game between Australia and England. It has been extracted from [138].

9.1.4 The raised scrums

This is another instability along the vertical axis, this time it happens when players are pushing upwards and could also be dangerous for the spinal cord. We give an example of a lifted scrum in Figure 9.3.

In Figure 9.3a the English scrum-half throws the ball under her loosehead prop. But the English pack undergoes the push of the French pack and in Figure 9.3b, the two first-rows rise up. In this case, the referee must blow the whistle to reset the scrum except if the ball leaves the structure while it is rising up.

9.1.5 The turned scrum

A rotated scrum is another type of scrum that involves a team turning the scrum. If the scrum is rotated more than 90 degrees by the will of a pack, it must be reset.
We show an example of a rotated scrum during Racing 92 practice in Figure 9.4. The offensive pack is on the left and the defensive pack is on the right. In Figure 9.4a, the red line symbolizes the central axis that defines the initial compression axis of the scrum that we then report in the other pictures. The scrum-half is going to introduce the ball. But, he sees that the situation is not stable enough in Figure 9.4b and refrains from doing so. We observe that the scrum has turned compared to the initial central axis of the scrum. Finally, in Figure 9.4c, the scrum-half is finally introducing the ball but it is too late because the scrum has completely turned. During an official game, the referee would have blown the whistle.

In subsection 9.2.3, we will quantify the typical angular speeds of the line between the two front rows on training wheeled scrums.

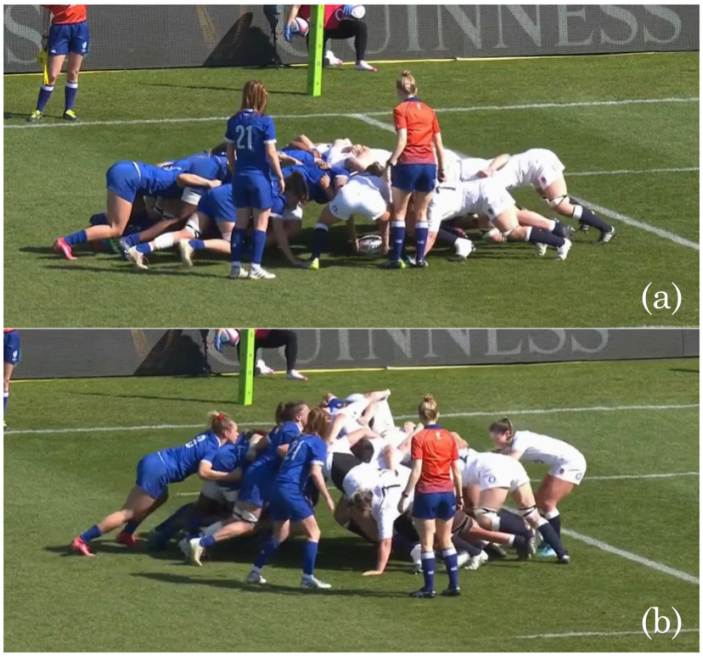


Figure 9.3: Snapshots of a lifted scrum during an international women's Rugby union game between England and France. These pictures are extracted from [139].

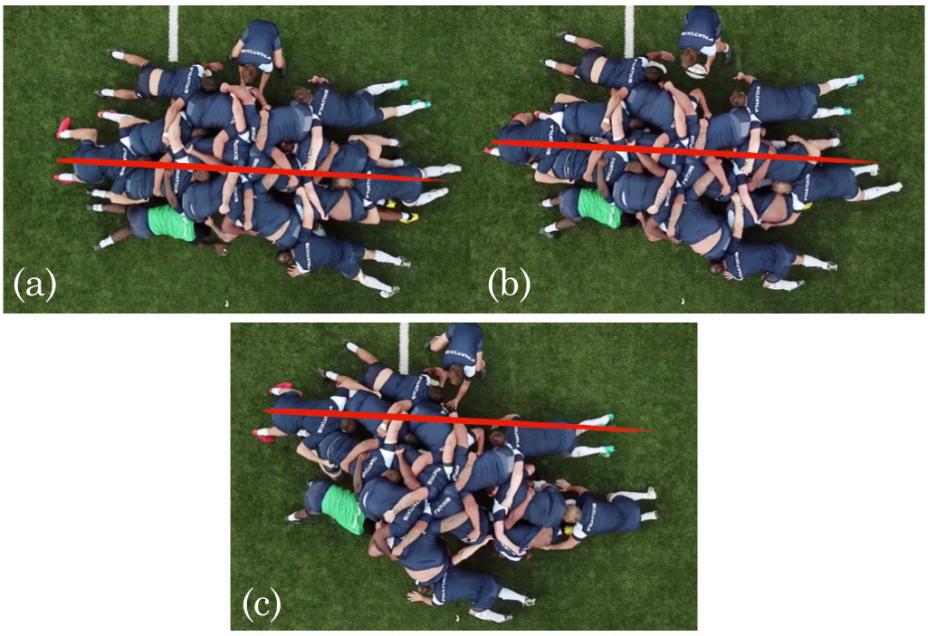


Figure 9.4: Turned scrum during a training session of Racing 92. (a) The scrum-half is about to introduce the ball. The red line represents the initial direction of the compression axis. (b) The scrum-half does not introduce the ball because the scrum starts to turn around the vertical axis. (c) The scrum practically turned almost 90°.

9.1.6 The moving in transversal direction scrum

Finally, the last category we identify corresponds to a rare case of a scrum moving in the lateral direction (cf. Figure 8.1).
The example given in Figure 9.5 is another practice scrum of the professional men's team of

Racing 92. In Figure 9.5a, the scrum-half introduces the ball under the offensive loosehead. We notice in Figure 9.5b, that the direction of the offensive loosehead starts to deviate from the initial compression axis. It implies a collective movement along the lateral axis in Figure 9.5c. The scrum finally ends up outside of the video capture field in Figure 9.5d.

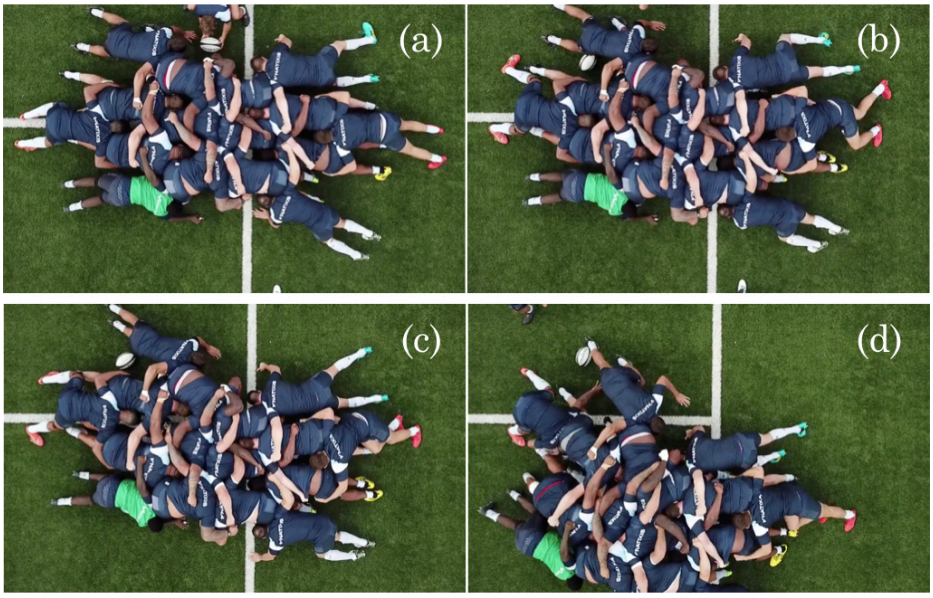


Figure 9.5: Top view chronophotography of a training scrum of Racing 92 team. The scrum moves laterally compared to the main axis of the scrum and the referee would have to blow the whistle if such a scrum happens in an official game.

9.2 Dynamics of the Contact Line of Scrums

We decide to focus on three types of scrums and quantify the dynamics of the contact line of the first rows defined by the points of contact between the players of the two opposite front rows.

9.2.1 Moving forward scrums

In Figure 9.6a, we show a training scrum of Racing 92, with the scrum-half that introduces the ball under the offensive pack on the left. The different colored crosses symbolize the points defining the contact line between the first rows. The pink cross corresponds to the left shoulder of the offensive loosehead prop. The blue and cyan crosses correspond to the left and right shoulder of the offensive hooker respectively. And the green cross corresponds to the right shoulder of the offensive tighthead prop.
On each video studied the initial time t_0 corresponds to the time where the cut video starts before the throw-in. The compression axis of the scrum is initially aligned with the x-axis represented with a red arrow in Figure 9.6a. We focus on the 1D displacement of the scrum along this axis. In Figure 9.6c, we give the time evolution of the displacement of each cross x_i along the x-axis compared to their initial location x_{0_i} at t_0. The time t_1 corresponds to the throw-in at the scrum and is illustrated with the snapshot of Figure 9.6a.

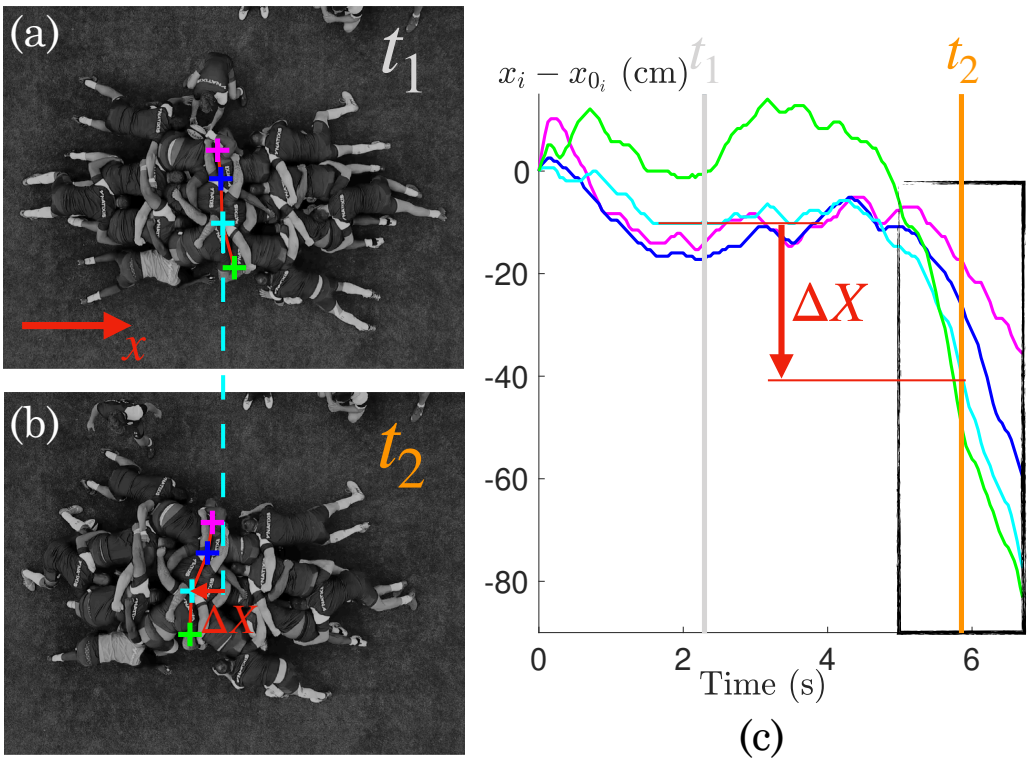


Figure 9.6: Example of a scrum during the practice of Racing 92 moving along the x-axis. (a) Top view picture at time t_1. We follow the displacements of the colored crosses along the x-axis. (b) Top view picture at time t_2. (c) Time evolution of the crosses displacements x_i compared to their initial positions x_{0_i}.

We notice a half-second stagnation of the cross displacements before t_1 which is consistent with the official scrum law that stipulates that when "both sides [of the scrum] are square, stable and stationary, the scrum-half throws in the ball"[3]. Then, both packs may start to push. We note that until $t = 5$ s, the scrum is quite stable and the points are slightly oscillated (cf. next subsection). After that, we see in the black rectangle of Figure 9.6c that the offensive pack is losing the scrum and it goes backward. At time t_2, the scrum moved along the x-axis and the corresponding top view picture is shown in Figure 9.6b. $\Delta X \sim 30$ cm corresponds to the cyan cross displacement between t_1 and t_2 that reflects the decline of the offensive pack. We can see that the players from the defensive pack are more extended that the one of the offensive pack.

In Figure 9.7, we focus on the black rectangle zone of Figure 9.6c. The same convention of color is used for the identification of the displacement of the crosses. We note that the blue and cyan curves have similar dynamics because they follow the left and right shoulder of the same player. We give as visual guides dashed straight lines that correspond to speeds along the x-axis from 17 to 60 cm.s^{-1}.

We can consider that contact line has a constant speed along the x-axis between $t = 5.4$ s and $t = 6.4$ s of the order of magnitude of 30-40 cm.s^{-1}.
The compressed postures of the offensive pack that is going backward reflect that the offensive forwards players lost this scrum. Moreover, at the end of the video at $t = 6.7$ s the scrum collapses, meaning that the last high speeds of the contact line correspond to maximal speeds that could be dangerous for first-rows.

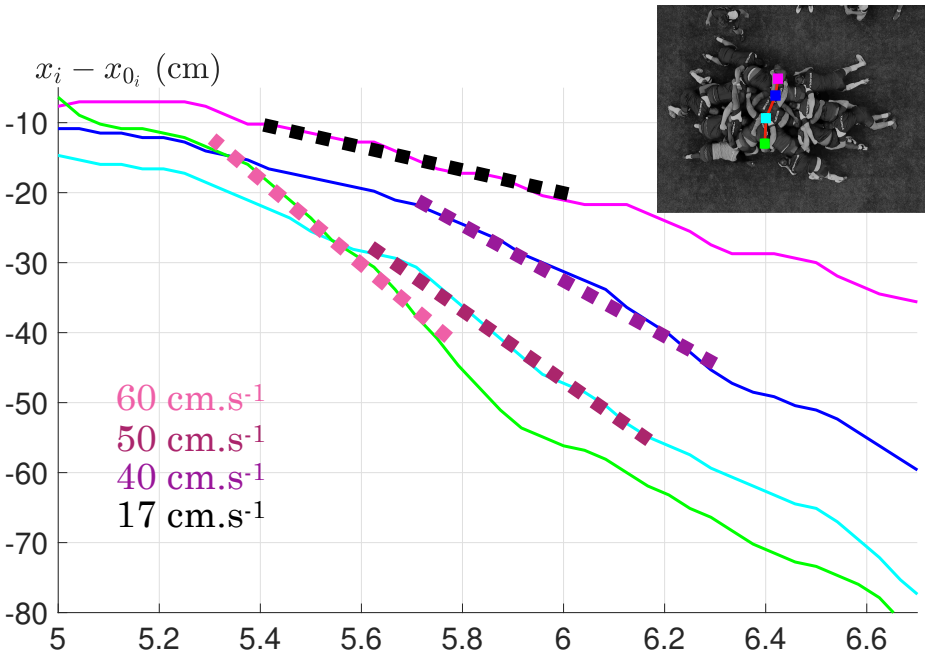


Figure 9.7: Zoom on time evolution of the crosses displacements x_i compared to their initial positions x_{0_i} of Figure 9.6c.

9.2.2 Stable

We can see in Figure 9.6 that the scrum is quite stable before one of the team takes the lead and starts to move forward along the compression axis (cf. Figure 9.7). Even if the scrum is stable, we observe some oscillations of the contact line between the first rows along the x-axis. In order to have a more detailed example, we perform the same analysis on a scrum that remains stable in Figure 9.8. This example is representative of scrums that give the macroscopic feeling of not moving (cf. subsection 9.1.1).
In Figure 9.8a, we set the initial position of the crosses -that represent the same landmarks as before- at t_0 just after the impact. We can see on a later snapshot at t_1 (cf. Figure 9.8b) that the scrum is almost at the same location as at t_0. But, the colored crosses are not distributed in the same order along the x-axis.

These little displacement of the contact line are quantified in Figure 9.8c where we plot the time evolution of $x_i - x_{0_i}$. We observe some oscillations in the position signals that we characterize with the time period T and the spatial amplitude A.

In Figure 9.8c, we note that there are rarely more than 3 distinct oscillations in a row. We can still measure T for those oscillations. The typical value we obtain is of the order of magnitude of 1 or 2 s. For instance, the left shoulder of the left pack hooker has two oscillations between $t = 4$ s and $t = 7$ corresponding to $T = 1.5$ s. The amplitudes A are of the order of magnitude of the centimeter. We exhibit some A measurements with the green arrows in Figure 9.8c on the left shoulder of the left pack loosehead prop signal. We obtain $A \simeq 2 - 3$ cm.

We do the same kind of measurement on other stable scrums and we deduce that the typical frequencies of oscillations of the contact line are between 0.5 to 2 Hz and that amplitudes are of the order of two-three centimeters.

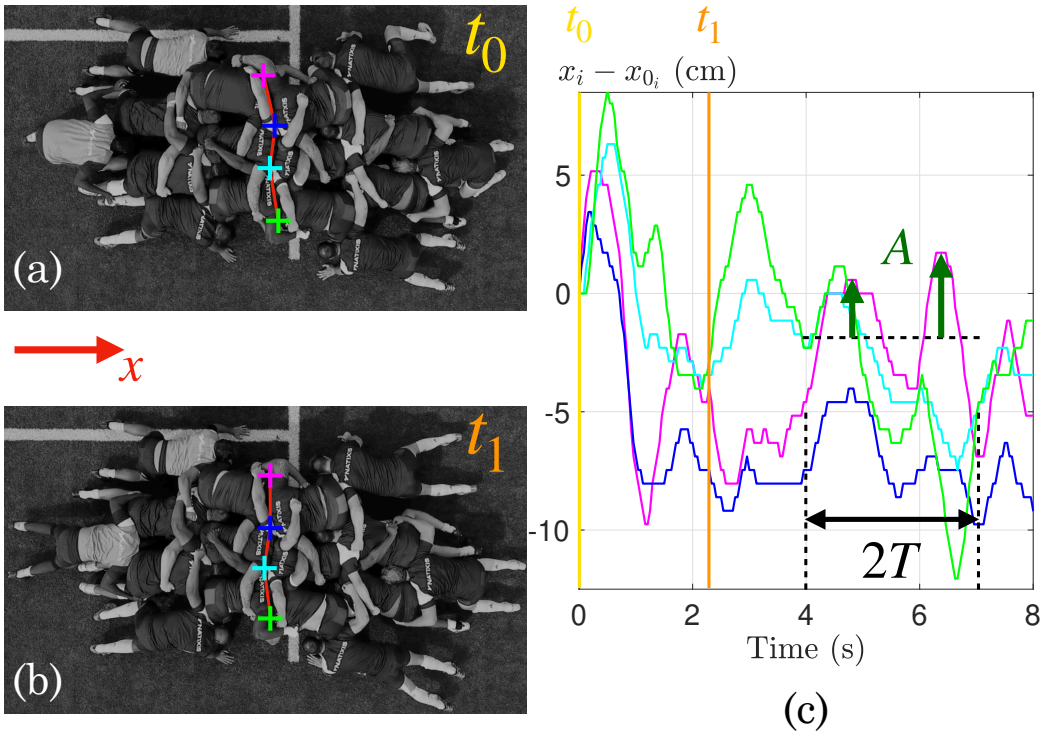


Figure 9.8: Measurement of the displacement of the contact line on a stable scrum of Racing 92. (a) Top-view picture of the scrum at the initial time t_0. Each cross of color corresponds to a point we track. (b) Top-view picture at t_1. (c) Displacement $x_i - x_0$ of the crosses along the x-axis as a function of time. The color of the solid line corresponds to the displacement of the cross of the same color.

9.2.3 Rotated scrums

Finally, with the same technique, we also characterize the scrums presented in subsection 9.2.3. However, this time we look at the time evolution of the angular speed of the linear approximation of the contact line. This linear approximation is defined in Figure 9.9a with the yellow line by connecting the pink cross with the green cross. We see that the scrum-half throw-in the ball and he is located at the bottom of Figure 9.9a. It means that the offensive pack is this time the pack on the right of the picture.
As a matter of reference, the red line given is aligned along the perpendicular of the x-axis at each instant t. It allows us to define the angle φ between the yellow and red lines as shown in Figure 9.9b. It allows us to follow the rotation of the scrum.

Figure 9.9c gives the time evolution of φ. At time t_0 (cf. Figure 9.9a), the yellow axis is almost aligned with the perpendicular of x-axis. But, from $t = 0.5$ s, the defensive pack is starting to push not along the compression axis with a little transverse angle. It implies a rotation of the scrum with a drop of the angle φ into the negative values.
We define the angular speed of the scrum along the vertical axis by

$$\omega_s = \dot{\varphi}. \tag{9.1}$$

In Figure 9.9c, we give two linear approximations of φ evolution with the yellow and pink dashed lines that correspond to angular speeds of $\|\omega_s\| = 29°s^{-1}$ and $\|\omega_s\| = 40°s^{-1}$.

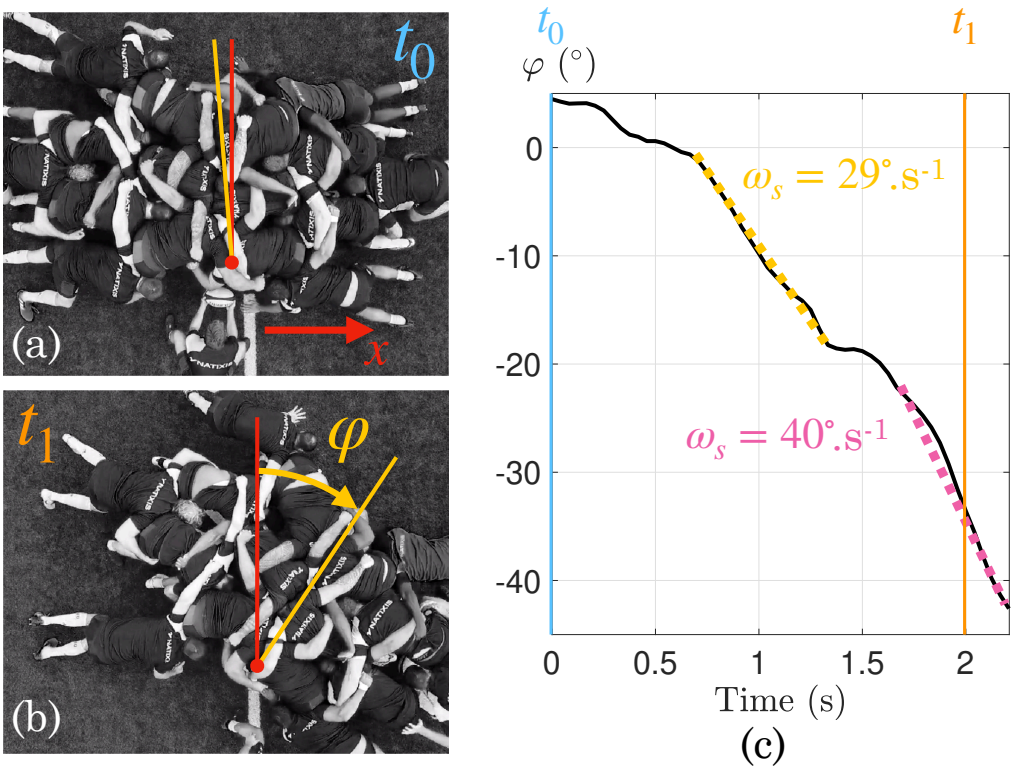


Figure 9.9: Measurement of the rotation of the contact line on a rotated scrum of Racing 92. (a) Top-view picture of the scrum at the initial time t_0. The red line is perpendicular to the x-axis. The yellow line is the linear approximation of the contact line. (b) Top-view picture at t_1. We define φ the angle between the red line and the yellow line at each instant t. (c) Time evolution of the angle φ.

9.3 Dynamical Experimental Study

9.3.1 Experimental setup and subjects

In Chapter 3, we presented an experimental study about individual impact on a quasi-static scrum machine. Here, we use the same scrum machine that belongs to the French Federation of Rugby but we use it in the active mode (cf. 3.1.3) with settings that we have chosen to be close to the measurements made in section 9.2.
We focus on two types of scrum instabilities: the oscillations of the stable scrums (cf. subsection 9.2.2) and the constant speed movement along the compression axis (cf. subsection 9.2.1).
For this experimental study, the subjects are 8 academy-level players and 8 professional players of Racing 92.
The academy-level players form a pack of mass $m_{pack} = 802$ kg. We ask the pack to push on the scrum machine with infinite stiffness. Then, these players are tested collectively with dynamic settings in order to mimic the moving forward scrum. The scrum machine is set to move backward -the players push and move forward- for three different constant speed along the compression axis: $v_5 \simeq 5$ cm.s^{-1}, $v_{10} \simeq 10$ cm.s^{-1} and $v_{15} \simeq 15$ cm.s^{-1}. These speeds are voluntarily sub-maximal compared to those measured in Figure 9.7 for the safety of the players. The movement of the scrum machine is triggered when the force produced by the pack is higher than 8 kN.

The professional pack has a mass of $m_{pack} = 924$ kg. We test them individually and

collectively on a completely static scrum machine. Then, we set the scrum machine to produce oscillations to mimic the stable situation. We approximate the total movement of the contact line as a sinusoidal displacement for 4-5 s. The scrum machine is set to excite the pack at frequencies $f_1 = 1$ Hz and $f_2 = 2$ Hz and with amplitudes $A \sim 1$ cm. The movement of the scrum machine is triggered when the force is superior to 1.5 kN for individual trials and superior to 8 kN for collective trials.
Thus, we ask the players not to impact the scrum machine in order to not trigger the programmed movement during the impact phase. There is the first part of stabilization and then the players activate the collective push to trigger the movement.

9.3.2 Results

Constant speed

In Figure 9.10a, we show a top view picture of the academy-level pack on the moving scrum machine. Figures 9.10b, c, and d present the force signals for the three different speeds with the blue solid lines. The associated displacement $\Delta X = x - x_0$ of the scrum machine along the x-axis is plotted in an orange solid line. x_0 corresponds to the position of the scrum machine when the players do not apply any force on it.

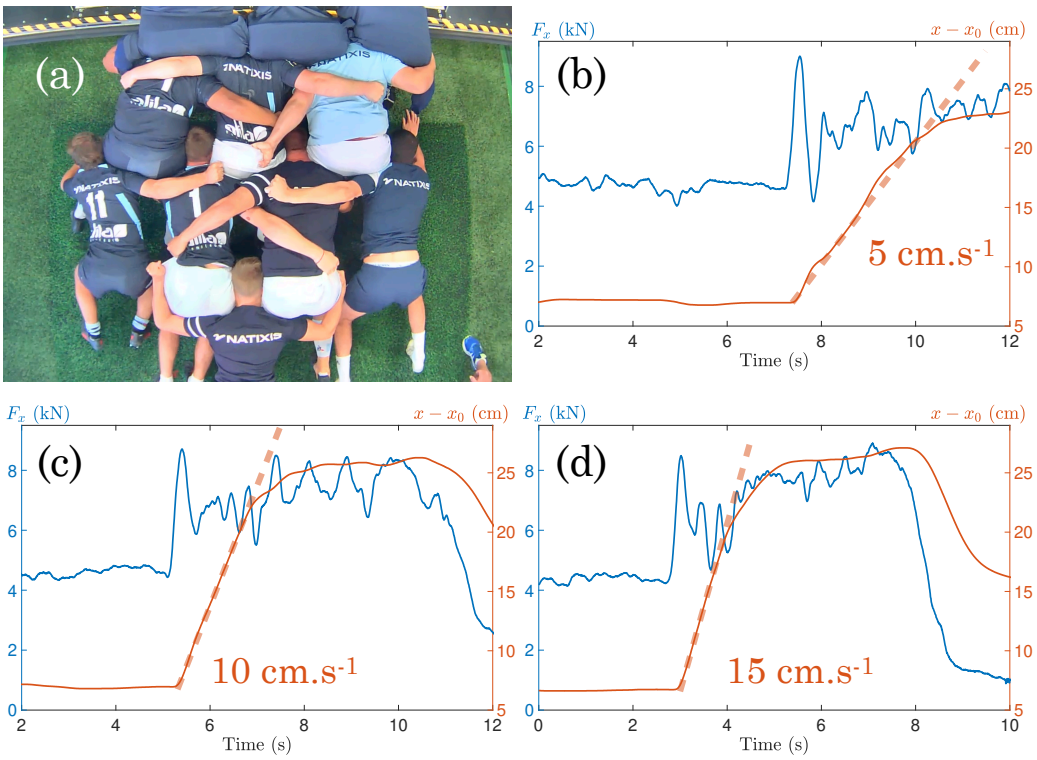


Figure 9.10: Constant speed trials on the scrum machine of the "Atelier de la mêlée" with the academy-level pack of Racing 92. (a) Top-view picture. (b) Time evolution of the compression force F_x (blue solid line) and the displacement $x - x_0$ (orange solid line) of the scrum machine along the x-axis for the trial at a constant speed of 5 cm.s^{-1}. (c) Time evolution of F_x and $x - x_0$ for the trial at a constant speed of 10 cm.s^{-1}. (d) Time evolution of F_x and $x - x_0$ for the trial at a constant speed of 15 cm.s^{-1}.

In Figure 9.10b, we observe the first phase of movement of the pack along the x-axis at the constant speed v_5 represented with the dashed straight line. Then, the scrum machine

reaches the programmed displacement limit. Figures 9.10c and d have the same time evolution of $x - x_0$ but with constant speeds v_{10} and v_{15} respectively. For the time evolution of the forces, we observe that the mean force developed during the movement is smaller than the force during the motionless phase. Furthermore, during the moving phase, we can see numerous drops of force that are the signature of the change of position of the feet while the scrum machine is moving (cf. subsection 8.6.2).
In the case of the static trial shown in Figure 9.11, the academy-level pack produced $F_{x_{av}} \simeq 7.9$ kN and $F_{x_{max}} \simeq 9.4$ kN (cf. Figure 8.2 for the definitions). The displacement of the scrum machine is lower than 1 cm.

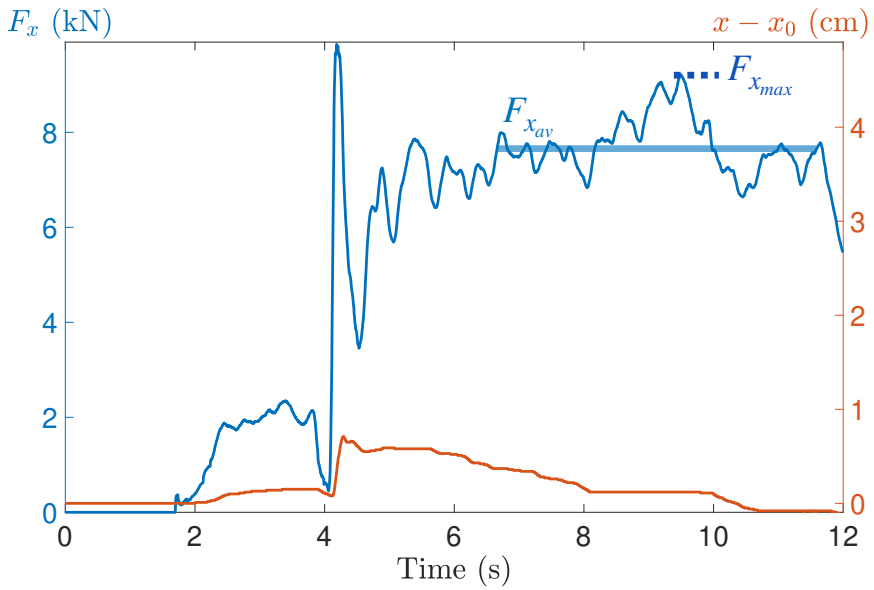


Figure 9.11: Time evolution of F_x and $x - x_0$ for the trial on a completely static scrum machine with the academy-level pack.

In Table 9.1, we present the mean $F_{x_{av}}$ and maximal $F_{x_{max}}$ forces obtained during the trials of Figure 9.10 in order to compare with the values observed in the static situation.

Speed	Moving phase		Quasi-static phase	
	$F_{x_{av}}$ (kN)	$F_{x_{max}}$ (kN)	$F_{x_{av}}$ (kN)	$F_{x_{max}}$ (kN)
v_5	6.4	7.8	7.2*	8.1*
v_{10}	6.8	7	7.7	8.5
v_{15}	6	6.9	7.9	8.9

Table 9.1: $F_{x_{av}}$ and $F_{x_{max}}$ forces reached by the academy-level pack in the trials of Figure 9.10.

We observe that the $F_{x_{av}}$ and $F_{x_{max}}$ measured during the movement of the scrum machine are lower than the ones we observe in a static situation. Then, during the second phase of the trials presented in Figure 9.10b, c, and d, the forces are similar to the ones observed in Figure 9.11.

Sinusoidal

Figure 9.12 presents the force of the professional pack and displacement obtained for the static case. The blue solid line corresponds to the compression force produced on the scrum machine and the orange solid line is the displacement $x - x_0$ along the x-axis of the scrum

machine. We measure $F_{x_{av}}$= 10.6 kN and $F_{x_{max}}$=11.8 kN for the professional pack on the motionless scrum machine.

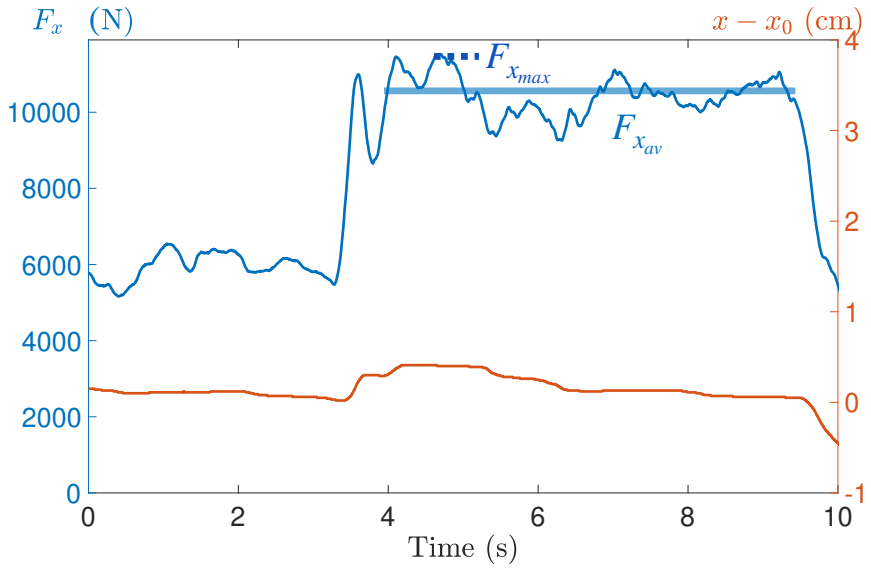


Figure 9.12: Time evolution of F_x and $x - x_0$ for the trial on a completely static scrum machine with the professional pack.

Then, the same pack shown in Figure 9.13a push on the scrum machine that oscillates at 1 Hz (cf. Figure 9.13b) and at 2 Hz (cf. Figure 9.13c).

This time, the scrum machine is moving during the sustained push phase. In Figure 9.13b, during the time T, we have approximately one period of the signal of displacement meaning that it corresponds to f_1. The amplitude A is slightly smaller than 1 cm. We remark that the sinusoidal displacement of the scrum machine is not perfect and that it is modulated by another slower displacement linked to the force-displacement relationship of the scrum machine (cf. subsection 4.2.2). In Figure 9.13c, we observe two periods of the signal during $T = 1$ s, which corresponds to f_2, and the typical amplitude A is approximately half a centimeter.
In terms of force production, we measure $F_{x_{av}}$=8.0 kN and $F_{x_{max}}$=9.5 kN in Figure 9.13b. These values are lower than the ones observed in the static situation. We measure $F_{x_{av}}$=10.1 kN and $F_{x_{max}}$=11.7 kN in Figure 9.13c. The values of force produced in the f_2 trial are similar to the one observed in Figure 9.12.

However, we clearly observe some differences in the patterns of force between Figure 9.13c and Figure 9.12. In Figure 9.12, the variations of force seem randomly distributed around $F_{x_{av}}$ whereas there is a periodic pattern of the force in Figure 9.13c. Indeed, the force signal looks like a sinusoidal signal of a temporal frequency of 2 Hz. And, we can also see a slight tripling of the frequency of the force signal with a very low amplitude between $t = 7$ s and $t = 10$ s.

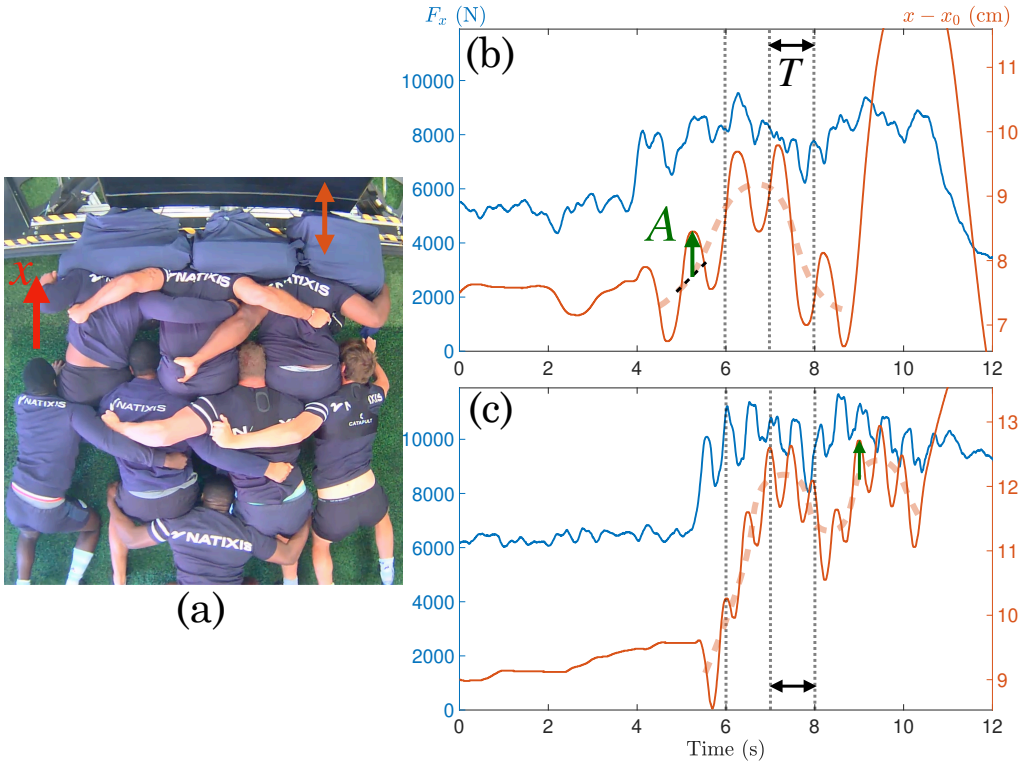


Figure 9.13: Dynamical sinusoidal trial of the professional pack. (a) Top view picture of the pack. (b) Time evolution of the compression force F_x (blue solid line) and the displacement $x - x_0$ (orange solid line) of the scrum machine along the x-axis for the f_1 trial. (c) Time evolution of F_x and $x - x_0$ for the f_2 trial.

We also observe this phenomenon in the individual force signals obtained on the oscillating scrum machine. In Figure 9.14, we present the time evolution of the force signal obtained individually for the hooker (cf. Figure 9.14a) of the professional pack (age 28 years, height 183 cm, mass 107 kg) for the f_1 trial in Figure 9.14b and f_2 trial in 9.14c. The amplitude A is approximately equal to 1 cm in Figure 9.14b and the time T corresponds to the time period of the $x - x_0$ signal. In Figure 9.14c, there are two time periods during the time T (which corresponds to a frequency of 2 Hz) and the amplitude is lower by approximately half a centimeter. We observe that the sinusoidal displacement is clearer during the individual trial than in the collective oscillating trial.

In Figure 9.15, we present the time evolution of the force F_x and the displacement of the scrum machine $x - x_0$ for the static trial of the professional hooker. We observe less variation around the plateau of force than in the oscillating trials of Figures 9.14b and c. We measure $F_{x_{av},stat}$=2250 N and $F_{x_{max},stat}$=2350 N.

While on the f_1 trial of Figure 9.14b, we have F_{x_{av},f_1}=2390 N and F_{x_{max},f_1}=2540 N. And, in Figure 9.14c, F_{x_{av},f_2}=2570 N and F_{x_{max},f_2}=2860 N. Contrary to the observations made at the collective scale, here the forces of the hooker increase with the frequency. However, this is true for only two players studied. The other players of the pack studied have lower F_{x_{av},f_1} and F_{x_{max},f_1} than in the static case. And, they obtain equivalent or slightly lower F_{x_{av},f_2} and F_{x_{max},f_2} than in the static case.

In Figure 9.14c, the tripling of the frequency is more pronounced than in Figure 9.13c. When we proceed to a Fourier analysis on the different individual signals, we observe that there are no particular peaks of frequency in the Spectral Power Density[1] (SPD) in Figure 9.15.

[1]Distribution of power into frequency components that compose the signal treated. It is proportional to

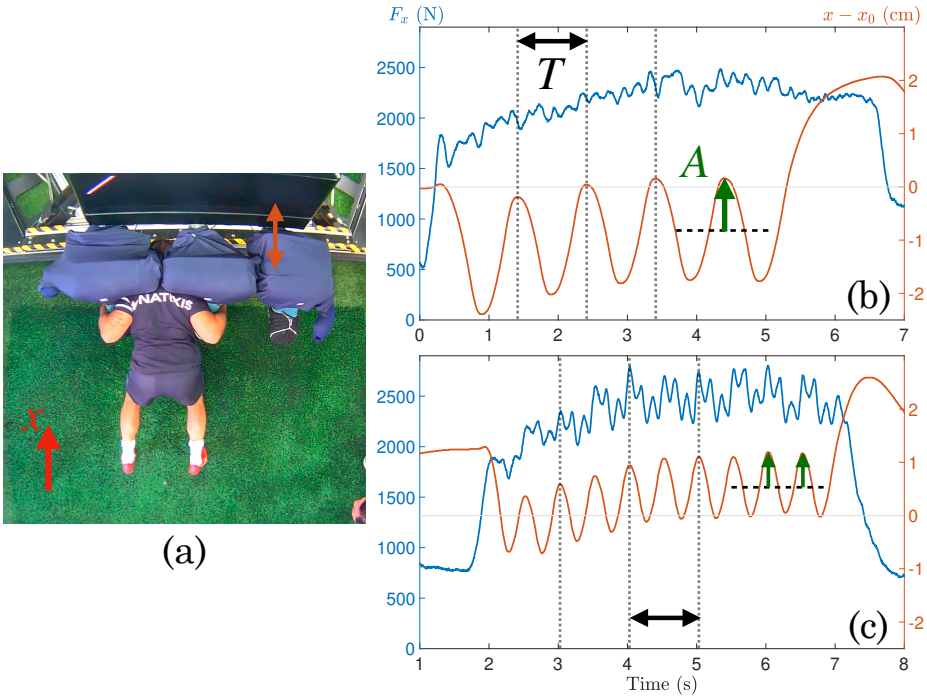


Figure 9.14: Dynamical sinusoidal trial of the professional hooker. (a) Top view picture of the hooker on the moving scrum machine. (b) Time evolution of the compression force F_x (blue solid line) and the displacement $x - x_0$ (orange solid line) of the scrum machine along the x-axis for the f_1 trial. (c) Time evolution of F_x and $x - x_0$ for the f_2 trial.

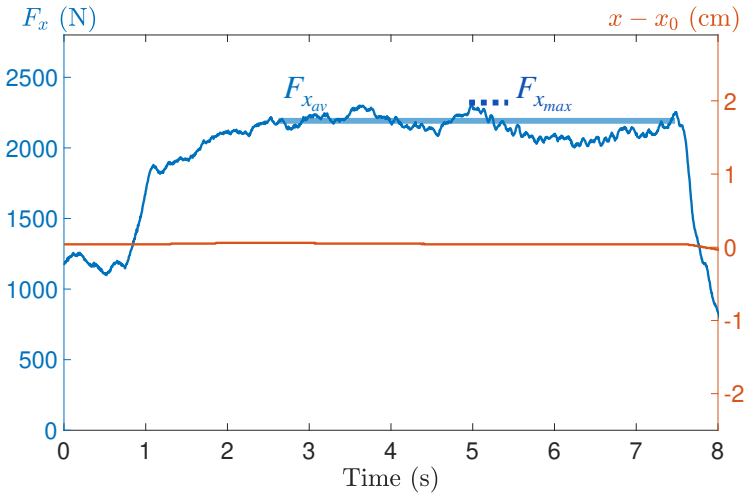


Figure 9.15: Time evolution of F_x and $x - x_0$ for the hooker on a static scrum machine.

It means that the variations of force on the static case do not show any particular periodic pattern. However, when applying the same analysis to the force signal of Figure 9.14, we obtain a peak at $f = 5$ Hz (we can count approximately 5 temporal periods of the variations of the force during T). Finally, we also observe peaks in the DSP for the signal of the force during the 2 Hz oscillations in Figure 9.14c. There are localized in $f = 2$ Hz and $f = 6$ Hz. It corresponds to the tripling frequency phenomenon observed. It could be interesting to link the typical frequencies observed with microscopic or macroscopic properties of muscular

the Fourier transform of the signal squared

force production.

We observe typical responses of the force signals to sinusoidal displacements at the individual and collective scale. Further experimental studies should be conducted in order to determine the equivalent of a transfer function of the pack which has the displacement of the scrum machine as an input and the force produced as an output. This function could help to build a model of the pack by analyzing the Bode Diagrams of packs and by comparing them to Bode diagrams of simpler physical systems. Such analysis would be possible if the amplitude of displacement of the scrum machine is fixed for each trial and by varying the frequencies of excitation from 0.5 Hz to 8 Hz for example.

Take home message of Chapter 9

1. Scrum is an unstable structure where a lot of instabilities occur. Even if the scrum is called stable, we can observe some movement of the contact line between the two packs during the sustained push phase.

2. Dynamical experiments were conducted at the "Atelier de la mêlée" where we programmed the simplified displacements of the scrum machine thanks to measurements made on real scrums. The sinusoidal displacements and the displacement at constant speed put a strain on the players and they develop less force on average than in static situations. Further experiments need to be conducted to study the effect of dynamics on pack force production in order to optimize it.

CONCLUSION

We have seen that scrum is at the heart of the history of Rugby Union and this gives it a special place in today's games. This is a battle of force between the forwards of each team that we describe in two main phases in terms of force production. The first phase is a dynamic phase of collision between the two packs characterized by a quick rise of the compression force. The second phase is the one following the introduction of the ball by the scrum-half which is recognizable by the production of a plateau of force during a few seconds.

Impact

The safety of the players is an important issue during the impact. During the last three decades, the masses of forward players increased at the professional level. We have described the evolution of rules that control the progress of scrums. This evolution led to the reduction of the space between the front rows to reduce the engagement speed of each pack. Thus, we have seen that the peak force is linear with the engagement speed, which implies a reduction of the peak force.
We have conducted an individual experimental study to go further in understanding the physics of the impact. This study allows us to define a parameter to quantify the quality of an impact, that could be generalized to the collective scale in future works. The development of a phase plane exhibit the difference in impact force signals between a novice player and a professional group of player and could help to detect the dangerousness of some impacts. Finally, we have noticed that the scrum machine used in an experimental protocol influences the curves of the force signals. The physics of the impact depends on the system that is impacting, and the ones that are impacted. Then, it is important to keep the same physical characteristics of the scrum machine during an experimental protocol. And because each experimental setup is unique, we must be careful when comparing results from different studies about forces at impact.
In the future, to get rid of the mechanical properties of the scrum machines, it would be interesting to conduct such experimental studies with force pads on the front-row shoulders in live scrums.

Sustained Push

The idea of a scrum is to push the opponent as much as possible along the compression axis. So, to optimize the performance of a scrum after the introduction of the ball (the moment when the packs are authorized to start the pushing phase) we have conducted some experimental studies about the postures that maximize the force produced by each player. We were interested in the optimal values of the joint angles to develop a maximum force. We observed that the professional players that participated in our experimental protocol adopted the same knee and hip angles when they maximize their force production. The orders of magnitudes of these angles were coherent with the literature. But we have seen that the foot anchoring system of the experimental setup plays a key role.
We conducted a study on synthetic turf and it shows that the postures adopted by the flankers in real scrums are the ones closer to the optimal postures we obtained. If the front-row players would like to produce a higher force, they would have to adopt postures close to the ground but the experimental study we conducted was static. The more elongated postures being the less stable postures, there is probably an optimal posture to find between

the optimum of stability and the optimum of force production. This study must be repeated a significant number of times with professional or academy-level players to validate the model we developed to explain the physics of the individual optimal posture.
Finally, we observed that the length of the cleats influences the individual force production and also the optimal posture of force production. The work done about the influence of the cleats could be used to develop a method to help the forward players select the optimal length of cleats to maximize their pushing forces during the scrums, without being a hindrance to the other tasks they need to accomplish.

Collective effects

After the individual experimental studies about force production during the two main phases of the scrum, we studied some issues at the collective scale. We have seen that the sum of the individual forces of the players of a pack is higher than the collective force produced by the pack. These losses could be explained by the different postures of each player that are constrained by their teammates, by the loss in transmission of the active muscular force in the deformable structure of a scrum, and probably mainly by the problem of synchronization of force production between each player.
We have finished by presenting a last collective experimental study with a moving scrum machine that imposed displacements on the players. The force produced was impacting and the models presented in the manuscript could be adapted in future works in order to understand the physics behind the impact of the dynamic on collective force production.

Bibliography

[1] Beka and Poupard. *Les rugbymen - : Les Rugbymen - Les Règles du Rugby 2020 - 2021*. Bamboo Édition, 2020. **Cited in page 2**

[2] Antoine Kneblewski. *Analyse biomécanique de la performance en rugby professionnel : optimisation du lancer en touche et prise en charge des commotions cérébrales.* PhD thesis, École Nationale Supérieure des Arts et Métiers, 2022. Thèse de doctorat dirigée par Rouch, Philippe Biomécanique (AM) Paris, HESAM 2022. **Cited in page 3**

[3] World Rugby. Règles du jeu par numéro: 19 la mêlée ordonnée. `https://www.world.rugby/the-game/laws/law/19`, 2021. Accessed: 2022-03-25. **Cited in pages 3, 9, 172, and 176**

[4] Jonathan McCormick. Revolutionising rugby – a statistical analysis on how the game has evolved. `https://www.statsperform.com/resource/revolutionising-rugby-a-statistical-analysis-on-how-the-game-has-evolved/`. Accessed: 2022-07-15. **Cited in pages 4 and 8**

[5] Tony Collins. The evolution of the scrum. `http://www.tony-collins.org/rugbyreloaded/2012/8/12/the-evolution-of-the-scrum`, 2012. Accessed: 2022-04-27. **Cited in page 4**

[6] Tony Collins. The past, present and future of the scrum. `http://www.tony-collins.org/rugbyreloaded/2016/1/30/the-history-of-the-scrum`, 2016. Accessed: 2022-07-27. **Cited in page 5**

[7] RCF Rugby. Notre histoire. `https://www.racing92.fr/page/notre-histoire`. Accessed: 2022-04-25. **Cited in page 5**

[8] Ron Palenski. Rugby union - the changing game. `https://teara.govt.nz/en/interactive/40044/the-2-3-2-scrum`, 2013. Accessed: 2022-04-25. **Cited in page 6**

[9] Archives New Zealand. Rugby football in new zealand: British isles tour (1950). `https://www.youtube.com/watch?v=8gktEJLnRaE`. Accessed: 2022-07-26. **Cited in page 7**

[10] Le Rugbynistère (Credits: USA Sevens Rugby). L'évolution de la mêlée depuis les années 50. `https://www.dailymotion.com/video/x51my0u`. Accessed: 2022-07-26. **Cited in page 7**

[11] Barbarian F.C. Official. Rugby gold, wales 24-31 barbarians 1990 - extended highlights. `https://www.youtube.com/watch?v=YRaHrxqoakI`. Accessed: 2022-07-26. **Cited in page 7**

[12] RugbyBack. France - angleterre 1998 (tournoi des 5 nations) 1ere mi-temps. `https://www.youtube.com/watch?v=jxBqvJLnEtg`. Accessed: 2022-07-26. **Cited in page 7**

[13] Kenneth L Quarrie and Will G Hopkins. Changes in player characteristics and match activities in bledisloe cup rugby union from 1972 to 2004. *Journal of sports sciences*, 25(8):895–903, 2007. **Cited in page 8**

[14] Colin W Fuller, John HM Brooks, Rebecca J Cancea, John Hall, and Simon PT Kemp. Contact events in rugby union and their propensity to cause injury. *British journal of sports medicine*, 41(12):862–867, 2007. **Cited in pages 8 and 18**

[15] Riaan Schoeman and Robert Schall. Comparison of match-related performance indicators between major professional rugby competitions. *International Journal of Sports Science & Coaching*, 14(3):344–354, 2019. **Cited in page 9**

[16] J H M Brooks, C W Fuller, S P T Kemp, and D B Reddin. Epidemiology of injuries in english professional rugby union: part 1 match injuries. *British Journal of Sports Medicine*, 39(10):757–766, 2005. **Cited in page 18**

[17] AT Scher. Rugby injuries to the cervical spinal cord. *South African Medical Journal*, 51(14):473–475, 1977. **Cited in page 18**

[18] Merrick J. Wetzler, Toks Akpata, William Laughlin, and Andrew S. Levy. Occurrence of cervical spine injuries during the rugby scrum. *The American Journal of Sports Medicine*, 26(2):177–180, 1998. PMID: 9548109. **Cited in page 18**

[19] Ramesh Swaminathan, Jonathan M Williams, Michael D Jones, and Peter S Theobald. A kinematic analysis of the spine during rugby scrummaging on natural and synthetic turfs. *Journal of sports sciences*, 34(11):1058–1066, 2016. **Cited in page 18**

[20] Peter D Milburn. Biomechanics of rugby union scrummaging. *Sports Medicine*, 16(3):168–179, 1993. **Cited in page 18**

[21] Peter D Milburn. The kinetics of rugby union scrummaging. *Journal of sports sciences*, 8(1):47–60, 1990. **Cited in pages 18, 20, 29, 48, and 53**

[22] Ezio Preatoni, Keith Stokes, M England, and Grant Trewartha. The influence of playing level on the biomechanical demands experienced by rugby union forwards during machine scrummaging. *Scandinavian journal of medicine & science in sports*, 23, 01 2013. **Cited in pages 18 and 20**

[23] Colin W. Fuller, Aileen E. Taylor, John H. M. Brooks, and Simon P. T. Kemp. Changes in the stature, body mass and age of english professional rugby players: A 10-year review. *Journal of Sports Sciences*, 31(7):795–802, 2013. PMID: 23244349. **Cited in page 19**

[24] Tim Olds. The evolution of physique in male rugby union players in the twentieth century. *Journal of sports sciences*, 19:253–62, 05 2001. **Cited in page 19**

[25] Neil E Hill, Sian Rilstone, Michael J Stacey, Dimitri Amiras, Stephen Chew, David Flatman, and Nick S Oliver. Changes in northern hemisphere male international rugby union players' body mass and height between 1955 and 2015. *BMJ Open Sport & Exercise Medicine*, 4(1), 2018. **Cited in pages 19 and 20**

[26] F Maso and A Robert. Évolution anthropométrique des joueurs de l'élite du rugby français. *Science & sports*, 14(6):301–304, 1999. **Cited in page 19**

[27] Grant Trewartha, Ezio Preatoni, Michael E England, and Keith A Stokes. Injury and biomechanical perspectives on the rugby scrum: a review of the literature. *British Journal of Sports Medicine*, 49(7):425–433, 2015. **Cited in pages 20, 56, and 173**

[28] ESPN. 1973 rugby union test match: Ireland vs new zealand all blacks (highlights). `https://www.youtube.com/watch?v=hwcpVNFdSBs`. Accessed: 2022-05-12. **Cited in page 20**

[29] John Winter. What do referees say in the scrum? (rugby scrum calls explained). `https://rugbydome.com/what-do-referees-say-in-the-scrum-rugby-scrum-calls-explained/`. Accessed: 2022-05-09. **Cited in page 20**

[30] World Rugby. France v argentina rwc 2007. https://www.youtube.com/watch?v=M3K2EPMvfus&t=1298s. Accessed: 2022-05-12. **Cited in page 21**

[31] S Gianotti, P A Hume, W G Hopkins, J Harawira, and R Truman. Interim evaluation of the effect of a new scrum law on neck and back injuries in rugby union. *British Journal of Sports Medicine*, 42(6):427–430, 2008. **Cited in page 22**

[32] Ezio Preatoni, Keith A Stokes, Michael E England, and Grant Trewartha. Engagement techniques and playing level impact the biomechanical demands on rugby forwards during machine-based scrummaging. *British Journal of Sports Medicine*, 49(8):520–528, 2015. **Cited in pages 22, 48, 53, and 56**

[33] Serge Couvet, Didier Retiere, Pierre Paul Vidal, and Julien Piscione. Training deice for rugby, 2015-07-20. **Cited in page 27**

[34] Dario Cazzola, Benjamin Stone, TP Holsgrove, Grant Trewartha, and Ezio Preatoni. Spinal muscle activity in simulated rugby union scrummaging is affected by different engagement conditions. *Scandinavian journal of medicine & science in sports*, 26(4):432–440, 2016. **Cited in pages 42 and 67**

[35] Adrien Cerrito, Peter Milburn, Clair Alston-Knox, and Kerrie Evans. Cervical spine kinematics during machine-based and live scrummaging. *Journal of Sports Sciences*, 37(13):1551–1559, 2019. **Cited in page 42**

[36] K Geary, BS Green, and E Delahunt. Effects of neck strength training on isometric neck strength in rugby union players. *Clin J Sport Med.*, 24(6):502–508, 2014. **Cited in pages 42 and 44**

[37] R Naish, A Burnett, S Burrows, W Andrews, and B Appleby. Can a specific neck strengthening program decrease cervical spine injuries in a men's professional rugby union team? a retrospective analysis. *J Sports Sci Med*, 12(3):542–550, 2013. **Cited in pages 42 and 44**

[38] DM Salmon, PJ Handcock, SJ Sullivan, NJ Rehrer, and BE Niven. Reliability of repeated isometric neck strength and endurance testing in a simulated contact posture. *J Strength Cond Res*, 29(3):637–646, 2015. **Cited in pages 42 and 44**

[39] Unknown. Milton high school. http://www.oldmiltonians.com/sportsaction/rugby.html. Accessed: 2022-07-29. **Cited in page 47**

[40] Dario Cazzola, Ezio Preatoni, Keith A Stokes, Michael E England, and Grant Trewartha. A modified prebind engagement process reduces biomechanical loading on front row players during scrummaging: a cross-sectional study of 11 elite teams. *British Journal of Sports Medicine*, 49(8):541–546, 2015. **Cited in page 48**

[41] Gianpietro del Piero and Giampiero Pampolini. On the visco-elastic properties of open-cell polyurethane foams. In *6th International Congress of the Croatian Society of Mechanics*, pages cd–rom, 2009. **Cited in pages 49 and 50**

[42] Anindya Deb and ND Shivakumar. An experimental study on energy absorption behavior of polyurethane foams. *Journal of reinforced plastics and composites*, 28(24):3021–3026, 2009. **Cited in pages 49 and 50**

[43] Daniel Whisler and Hyonny Kim. Experimental and simulated high strain dynamic loading of polyurethane foam. *Polymer Testing*, 41:219–230, 2015. **Cited in pages 49 and 50**

[44] JV Mane, S Chandra, S Sharma, H Ali, VM Chavan, BS Manjunath, and RJ Patel. Mechanical property evaluation of polyurethane foam under quasi-static and dynamic strain rates-an experimental study. *Procedia engineering*, 173:726–731, 2017. **Cited in pages 49 and 50**

[45] Tom Allen, Jonathon Shepherd, TAM Hewage, Terry Senior, Leon Foster, and Andrew Alderson. Low-kinetic energy impact response of auxetic and conventional open-cell polyurethane foams. *physica status solidi (b)*, 252(7):1631–1639, 2015. **Cited in page 50**

[46] Eva Kasparek, Uwe Zencker, Robert Scheidemann, Holger Völzke, and Karsten Müller. Numerical and experimental studies of polyurethane foam under impact loading. *Computational materials science*, 50(4):1353–1358, 2011. **Cited in page 50**

[47] Ali Taherkhani, Mojtaba Sadighi, Ali Sadough Vanini, and Mohsen Zarei Mahmoudabadi. An experimental study of high-velocity impact on elastic–plastic crushable polyurethane foams. *Aerospace Science And Technology*, 50:245–255, 2016. **Cited in page 50**

[48] AK Maji, HL Schreyer, S Donald, Q Zuo, and D Satpathi. Mechanical properties of polyurethane-foam impact limiters. *Journal of engineering mechanics*, 121(4):528–540, 1995. **Cited in page 50**

[49] Griselda Lyn and NJ Mills. Design of foam crash mats for head impact protection. *Sports engineering*, 4(3):153–163, 2001. **Cited in page 50**

[50] Svein Kleiven. A parametric study of energy absorbing foams for head injury prevention. In *The 20th International Technical Conference on the Enhanced Safety of Vehicles Conference (ESV), Lyon, France*, pages 18–21, 2007. **Cited in page 50**

[51] Purvi SD Patel, Duncan ET Shepherd, and David WL Hukins. Compressive properties of commercially available polyurethane foams as mechanical models for osteoporotic human cancellous bone. *BMC musculoskeletal disorders*, 9(1):1–7, 2008. **Cited in page 51**

[52] Ezio Preatoni, Dario Cazzola, KA Stokes, Michael England, and Grant Trewartha. Pre-binding prior to full engagement improves loading conditions for front-row players in contested rugby union scrums. *Scandinavian journal of medicine & science in sports*, 26(12):1398–1407, 2016. **Cited in page 56**

[53] Tristan Sharp, Mark Halaki, Andrew Greene, and Benedicte Vanwanseele. An emg assessment of front row rugby union scrummaging. *International Journal of Performance Analysis in Sport*, 14(1):225–237, 2014. **Cited in pages 66 and 67**

[54] Brian P. O'Shea. Level i coaching manual. Technical report, Australian Rugby Union, 2003. **Cited in page 66**

[55] Enrique TOPO Rodríguez. *Rugby: The Art of Scrummaging: A History, a Manual and a Law Dissertation on the Rugby Scrum.* Meyer & Meyer Verlag, 2015. **Cited in pages 66 and 165**

[56] D. Marks and T. Burkett. *Australian Rugby Union National Coaching Scheme. Rugby Forward Play.* Smithfield: National Library of Australia, 1998. **Cited in page 66**

[57] A Green, Y Coopoo, J Tee, and W McKinon. A review of the biomechanical determinants of rugby scrummaging performance. *South African Journal of Sports Medicine*, 31(1), November 2019. **Cited in page 66**

[58] E. Martin and G. Beckham. Force production during the sustained phase of rugby scrums: a systematic literature review. *BMC Sports Science, Medicine and Rehabilitation*, 12, 2020. **Cited in page 66**

[59] Svein Mensaert, Tristan Sharp, and Benedicte Vanwanseele. Influence of playing level on the kinematics and kinetics of the rugby scrum. In *ISBS-Conference Proceedings Archive*, 2015. **Cited in page 66**

[60] Andrew Green, Samantha Kerr, Chloe Dafkin, Benita Olivier, and Warrick McKinon. A lower body height and wider foot stance are positively associated with the generation of individual scrummaging forces in rugby. *International Journal of Performance Analysis in Sport*, 17(1-2):177–189, 2017. **Cited in pages 66, 67, and 129**

[61] Ken L. Quarrie and Barry D. Wilson. Force production in the rugby union scrum. *Journal of sports sciences*, 18:237–46, 04 2000. **Cited in pages 66, 150, and 154**

[62] Wen-Lan Wu, Jyh-Jong Chang, Jia-Hroung Wu, and Lan-Yuen Guo. An investigation of rugby scrimmaging posture and individual maximum pushing force. *Journal of strength and conditioning research*, 21(1):251—258, February 2007. **Cited in pages 67 and 93**

[63] J.A. Burns, E. Seminati, D. Cazzola, E. Preatoni, and G. Trewartha. Poster: Machine scrummaging does not mimic the head/neck load experienced in live scrummaging. In *World Rugby Science Network*, Bath, England, 2016. **Cited in page 67**

[64] Mostafa Yaghoubi, Sally D Lark, Wyatt H Page, Philip W Fink, and Sarah P Shultz. Lower extremity muscle function of front row rugby union scrummaging. *Sports Biomechanics*, 18(6):636–648, 2019. **Cited in page 67**

[65] Helen Bayne and Cor-Jacques Kat. The influence of foot position on scrum kinetics during machine scrummaging. *Journal of Sports Sciences*, 36(24):2836–2842, 2018. PMID: 29790433. **Cited in pages 67 and 94**

[66] Baptiste Loire. Caractérisation d'un joug individuel de mêlée de rugby. Master's thesis, ENSTA, 2021. **Cited in pages 69, 89, and 95**

[67] D Haffajee, U Moritz, and GJAOS Svantesson. Isometric knee extension strength as a function of joint angle, muscle length and motor unit activity. *Acta Orthopaedica Scandinavica*, 43(2):138–147, 1972. **Cited in page 79**

[68] M WILLIAMS and L STUTZMAN. Strength variation through the range of joint motion. *The Physical therapy review*, 39(3):145–152, 1959. **Cited in page 79**

[69] O Lindahl, A Movin, and I Ringqvist. Knee extension: Measurement of the isometric force in different positions of the knee-joint. *Acta Orthopaedica Scandinavica*, 40(1):79–85, 1969. **Cited in page 79**

[70] Alf Thorstensson, Gunnar Grimby, and Jan Karlsson. Force-velocity relations and fiber composition in human knee extensor muscles. *Journal of applied physiology*, 40(1):12–16, 1976. **Cited in page 79**

[71] Gary L Smidt. Biomechanical analysis of knee flexion and extension. *Journal of biomechanics*, 6(1):79–92, 1973. **Cited in page 79**

[72] Joseph J Knapik, James E Wright, Roberta H Mawdsley, and Joanne Braun. Isometric, isotonic, and isokinetic torque variations in four muscle groups through a range of joint motion. *Physical therapy*, 63(6):938–947, 1983. **Cited in pages 79 and 80**

[73] DA Jones, OM Rutherford, and DF Parker. Physiological changes in skeletal muscle as a result of strength training. *Quarterly Journal of Experimental Physiology: Translation and Integration*, 74(3):233–256, 1989. **Cited in page 79**

[74] Yuliya Karanouskaya. Physical aspects of muscle contraction. Master's thesis, École Normale Supérieure, 2017. **Cited in page 80**

[75] Ryoichi Ema, Taku Wakahara, and Yasuo Kawakami. Effect of hip joint angle on concentric knee extension torque. *Journal of Electromyography and Kinesiology*, 37:141–146, 2017. **Cited in page 81**

[76] Darjan Smajla, Olivera M Knezevic, Dragan M Mirkov, and Nejc Šarabon. Interlimb asymmetries and ipsilateral associations of plantar flexors and knee extensors rate-of-force development scaling factor. *Symmetry*, 12(9):1522, 2020. **Cited in page 82**

[77] Darjan Smajla, Jure Žitnik, and Nejc Šarabon. Investigation of inter-limb symmetry in knee extensors using different strength outcome measures. *Diagnostics*, 11(10):1882, 2021. **Cited in page 82**

[78] Walter Herzog, Sheila K Abrahamse, and Henk EDJ ter Keurs. Theoretical determination of force-length relations of intact human skeletal muscles using the cross-bridge model. *Pflügers Archiv*, 416(1):113–119, 1990. **Cited in page 82**

[79] James G Andrews. The functional roles of the hamstrings and quadriceps during cycling: Lombard's paradox revisited. *Journal of biomechanics*, 20(6):565–575, 1987. **Cited in page 82**

[80] Randale Sechrest for eOrthopod.com. Knee anatomy animated tutorial. **Cited in page 82**

[81] Physopedia. Knee - physopedia. `https://www.physio-pedia.com/Knee`. Accessed: 2022-06-14. **Cited in page 82**

[82] Roy Wung. Patellofemoral joint motion and patellar tracking. **Cited in pages 83 and 85**

[83] Philip Hansen, J Bojsen-Moller, Per Aagaard, Michael Kjaer, and S Peter Magnusson. Mechanical properties of the human patellar tendon, in vivo. *Clinical Biomechanics*, 21(1):54–58, 2006. **Cited in page 88**

[84] Thomas D. O'Brien, Neil D. Reeves, Vasilios Baltzopoulos, David A. Jones, and Constantinos N. Maganaris. Mechanical properties of the patellar tendon in adults and children. *Journal of Biomechanics*, 43(6):1190–1195, 2010. **Cited in page 88**

[85] H-U Stäubli, L Schatzmann, P Brunner, L Rincon, and L-P Nolte. Quadriceps tendon and patellar ligament: cryosectional anatomy and structural properties in young adults. *Knee surgery, sports traumatology, arthroscopy*, 4(2):100–110, 1996. **Cited in page 88**

[86] NattoSumo. Sumo natsu basho 2022 day 15 may 22nd makuuchi all bouts. **Cited in page 93**

[87] Allen Guttmann. Civilized mayhem: Origins and early development of american football. *Sport in Society*, 9(4):533–541, 2006. **Cited in page 93**

[88] Adam Burns. From the playing fields of rugby and eton: The transnational origins of american rugby and the making of american football. *Sport History Review*, 52(2):315 – 331, 2021. **Cited in page 93**

BBl

[89] Helen Bayne and Cor Jacques Kat. Effect of foot position on the compression and lateral force production of a player in a rugby scrum. In *ISBS-Conference Proceedings Archive*, 2016. **Cited in page 94**

[90] beIN SPORTS France. Résumé nfl : Les rams remportent le super bowl face aux bengals ! **Cited in page 94**

[91] DA Winter. *Anthropometry*, chapter 4, pages 82–106. John Wiley & Sons, Ltd, 2009. **Cited in pages 116 and 117**

[92] Wilfred Taylor Dempster. Space requirements of the seated operator, geometrical, kinematic, and mechanical aspects of the body with special reference to the limbs. Technical report, Michigan State Univ East Lansing, 1955. **Cited in page 116**

[93] Paolo de Leva. Adjustments to zatsiorsky-seluyanov's segment inertia parameters. *Journal of Biomechanics*, 29(9):1223–1230, 1996. **Cited in page 116**

[94] April J Chambers, Alison L Sukits, Jean L McCrory, and Rakié Cham. The effect of obesity and gender on body segment parameters in older adults. *Clinical biomechanics*, 25(2):131–136, 2010. **Cited in page 116**

[95] Robert D Catena, Szu-Hua Chen, and Li-Shan Chou. Does the anthropometric model influence whole-body center of mass calculations in gait? *Journal of biomechanics*, 59:23–28, 2017. **Cited in page 116**

[96] Mikko Virmavirta and Juha Isolehto. Determining the location of the body's center of mass for different groups of physically active people. *Journal of biomechanics*, 47(8):1909–1913, 2014. **Cited in pages 116 and 118**

[97] Shane M Heffernan, GK Stebbings, Liam P Kilduff, RM Erskine, Stephen H Day, CI Morse, JS McPhee, CJ Cook, B Vance, William J Ribbans, et al. Fat mass and obesity associated (fto) gene influences skeletal muscle phenotypes in non-resistance trained males and elite rugby playing position. *BMC genetics*, 18(1):1–9, 2017. **Cited in page 117**

[98] Caroline Cohen. *La physique du sport.* PhD thesis, École polytechnique, 2014. **Cited in page 123**

[99] VI Deshcherevskii. Two models of muscle contraction. *Biofizika*, 1968. **Cited in page 123**

[100] Thomas J Burkholder and Richard L Lieber. Sarcomere length operating range of vertebrate muscles during movement. *Journal of Experimental Biology*, 204(9):1529–1536, 2001. **Cited in page 123**

[101] Robert W. Ramsey and Sibyl F. Street. The isometric length-tension diagram of isolated skeletal muscle fibers of the frog. *Journal of Cellular and Comparative Physiology*, 15(1):11–34, 1940. **Cited in page 123**

[102] AM Gordon, Andrew F Huxley, and FJ Julian. The variation in isometric tension with sarcomere length in vertebrate muscle fibres. *The Journal of physiology*, 184(1):170–192, 1966. **Cited in pages 123 and 124**

[103] Francis Goubel and Ghislaine Lensel-Corbeil. *Biomécanique: éléments de mécanique musculaire.* Masson, 2003. **Cited in page 123**

[104] Jack Gregson. The evolution of rugby boots. `https://www.sutori.com/en/story/the-evolution-of-rugby-boots--hD3dPAKuSUyHTNndb2jesbUG`. Accessed: 2022-07-18. **Cited in page 133**

[105] Caroline Cohen, Emmanuel Brunet, Jérémy Roy, and Christophe Clanet. Physics of road cycling and the three jerseys problem. *Journal of Fluid Mechanics*, 914, 2021. **Cited in page 134**

[106] Anne-Marie Kietzig, Savvas G Hatzikiriakos, and Peter Englezos. Physics of ice friction. *Journal of Applied Physics*, 107(8):4, 2010. **Cited in page 134**

[107] Harald Nyberg, Sara Alfredson, Sture Hogmark, and Staffan Jacobson. The asymmetrical friction mechanism that puts the curl in the curling stone. *Wear*, 301(1-2):583–589, 2013. **Cited in page 134**

[108] Samuel C Colbeck. A review of the friction of snow skis. *Journal of sports sciences*, 12(3):285–295, 1994. **Cited in page 134**

[109] I Martin Levy, Mary Louise Skovron, and Julie Agel. Living with artificial grass: A knowledge update: Part 1: Basic science. *The American journal of sports medicine*, 18(4):406–412, 1990. **Cited in page 134**

[110] Sylvain Blanchard. *Influence des caractéristiques techniques de la chaussure à crampons sur l'interface terrain-joueur.* PhD thesis, Aix-Marseille, 2020. **Cited in pages 134 and 135**

[111] TJ Serensits and AS McNitt. Comparison of rotational traction of athletic footwear on varying playing surfaces using different normal loads. *Applied Turfgrass Science*, 11(1):1–10, 2014. **Cited in page 134**

[112] Robert S Heidt JR, Stephen G Dormer, Patrick W Cawley, Pierce E Scranton JR, Gary Losse, and Mark Howard. Differences in friction and torsional resistance in athletic shoe-turf surface interfaces. *The American journal of sports medicine*, 24(6):834–842, 1996. **Cited in page 134**

[113] Jan Ekstrand and Benno M Nigg. Surface-related injuries in soccer. *Sports medicine*, 8(1):56–62, 1989. **Cited in page 134**

[114] A Thomson and D Rennie. Evolution of natural grass playing surfaces for elite football. *Aspetar Sport. Med. J*, 5:322–327, 2016. **Cited in page 134**

[115] S. Blanchard and M. Behr. Functional field protocol to optimize the choice of footwear on synthetic turf in rugby. *Science & Sports*, 36(3):e69–e79, 2021. **Cited in page 134**

[116] Steph Forrester and Paul Fleming. Traction forces generated during studded boot-surface interactions on third-generation artificial turf: A novel mechanistic perspective. *Engineering Reports*, 1(5):e12066, 2019. **Cited in page 134**

[117] Dara M Twomey, Monique Connell, Lauren Petrass, and Leonie Otago. The effect of stud configuration on rotational traction using the studded boot apparatus. *Sports Engineering*, 16(1):21–27, 2013. **Cited in page 134**

[118] K Douglas Bowers and R Bruce Martin. Cleat-surface friction on new and old astroturf. *Med Sci Sports*, 7(2):132–135, 1975. **Cited in page 134**

[119] Bruce Barry and Peter Milburn. Tribology, friction and traction: understanding shoe-surface interaction. *Footwear Science*, 5(3):137–145, 2013. **Cited in page 136**

[120] Ken Hodge. *Spinal injuries in rugby scrums*. University of Otago, School of Physical Education, 1980. **Cited in page 151**

[121] B Morel and CA Hautier. The neuromuscular fatigue induced by repeated scrums generates instability that can be limited by appropriate recovery. *Scandinavian Journal of Medicine & Science in Sports*, 27(2):209–216, 2017. **Cited in page 152**

[122] Darryl J Cochrane, Keegan Harnett, Nicolas Lopez-Villalobos, and Jeremy Hapeta. The effect of repetitive rugby scrummaging on force output and muscle activity. *Sports Medicine International Open*, 1(03):E89–E93, 2017. **Cited in page 152**

[123] Max Ringelmann. Recherches sur les moteurs animés: Travail de l'homme. *Annales de l'Insitut National Agronomique*, 12:1–40, 1913. **Cited in pages 157, 158, 159, and 163**

[124] Jules Beau. *Photographie spotive-reportage photographique*. Jules Beau, 1900. **Cited in page 158**

[125] Alan G Ingham, George Levinger, James Graves, and Vaughn Peckham. The ringelmann effect: Studies of group size and group performance. *Journal of Experimental Social Psychology*, 10(4):371–384, 1974. **Cited in page 159**

[126] Ashley Simms and Tommy Nichols. Social loafing: A review of the literature. *Journal of Management*, 15(1):58–67, 2014. **Cited in page 159**

[127] Robert Liden, Sandy Wayne, Renata Jaworski, and Nathan Bennett. Social loafing: A field investigation. *Journal of Management*, 30(2):285–304, 2004. **Cited in page 159**

[128] Jean-Baptiste ANGLEYS, Julien LAVALLEY, Louis LOCQUEVILLE, and Hugo SERRES. Étude de l'efficacité de la mêlée au rugby. Master's thesis, Ecole polytechnique, 2018. **Cited in pages 159, 160, and 162**

[129] Stéphanie Langlet Ethno Travels. Fêtes de sare, tir à la corde. `https://www.youtube.com/watch?v=q_wMXYg6M7M`. Accessed: 2022-07-11. **Cited in page 163**

[130] Ronald J Adrian and Jerry Westerweel. *Particle image velocimetry*. Cambridge university press, 2011. **Cited in page 163**

[131] Ian Grant. Particle image velocimetry: a review. *Proceedings of the Institution of Mechanical Engineers, Part C: Journal of Mechanical Engineering Science*, 211(1):55–76, 1997. **Cited in page 163**

[132] Ronald J Adrian. Twenty years of particle image velocimetry. *Experiments in fluids*, 39(2):159–169, 2005. **Cited in page 163**

[133] Daniel Edgington-Mitchell. Particle image velocimetry. `http://daniel.edgington-mitchell.com/how-it-works/particle-image-velocimetry/`. Accessed: 2022-07-13. **Cited in page 164**

[134] COACHXV. Quel est l'avenir pour la mêlée ? `https://www.coachxv.com/analyse-jeu/quel-avenir-pour-la-melee/`. Accessed: 2022-07-11. **Cited in page 171**

[135] Habi Aftabi. Fiji repeatedly puts pressure on the tonga scrum. `https://www.youtube.com/watch?v=YdRBHJA2r6I`. Accessed: 2022-07-16. **Cited in page 172**

[136] Aileen Taylor, Simon Kemp, Grant Trewartha, and Keith Stokes. Scrum injury risk in english professional rugby union. *British journal of sports medicine*, 48, 03 2014. **Cited in page 173**

[137] Simon P Roberts, Grant Trewartha, Mike England, and Keith A Stokes. Collapsed scrums and collision tackles: what is the injury risk? *British Journal of Sports Medicine*, 49(8):536–540, 2015. **Cited in page 173**

[138] Rex features. England v australia: Jones "taking heat off england scrum" says cheika. `https://www.bbc.com/sport/rugby-union/38173794`. Accessed: 2022-07-16. **Cited in page 173**

[139] Rugby Interview. Xv de france : Angleterre v france : La super poussée des filles en mélée. `https://www.youtube.com/watch?v=ZsdmAEsj36M`. Accessed: 2022-07-15. **Cited in page 174**

ECOLE
DOCTORALE

Titre : Physique de la mêlée

Mots clés : Mêlée, Impact, Position optimale de poussée, Production de force, Efficacité collective

Résumé : La mêlée est un élément primordial d'un match de rugby à XV. Elle consiste en une remise en jeu du ballon se déroulant sous la forme d'une opposition de force entre deux packs de 8 avants chacun. Chaque pack est organisé en 3 rangées avec 3 joueurs en premières lignes, 4 joueurs derrière eux et un dernier joueur en troisième rangée. La mêlée est orchestrée par les commandements de l'arbitre qui ont changé au fil de l'Histoire du Rugby afin de protéger l'intégrité physique des joueurs. Ceci étant, en terme de production de force par chacun des deux packs, nous pouvons diviser la mêlée peut en deux phases distinctes: une phase d'impact pendant laquelle chaque pack accélère et entre en collision avec l'autre, suivie d'une phase de poussée continue après l'introduction du ballon sous l'édifice pendant laquelle les joueurs de chacun des packs essaient de se synchroniser pour produire la plus grande force collective. Cette thèse CIFRE, financée par le club professionnel de Rugby du Racing 92, s'intéresse à ces deux phases avec des études expérimentales menées à l'échelle individuelle afin de comprendre les mécanismes de production de force. Dans un premier temps, grâce à une machine d'entraînement à la mêlée équipée de capteurs de force appelée l'Atelier de la mêlée et appartenant à la Fédération Française de Rugby, nous avons caractérisé individuellement les joueurs à afin de construire un espace des phases qui permet de quantifier la qualité d'un impact d'entrée en mêlée. Ensuite, grâce à une machine de mêlée individuelle que nous avons développé au laboratoire -équipée elle aussi de capteurs de forces- nous avons conduit des études expérimentales permettant de rechercher la position individuelle de poussée qui maximiser la force produite par un joueur. Nous avons de plus mené une étude qui regarde l'influence de la taille des crampons sur la force produite par un joueur sur un gazon synthétique. Le travail de thèse s'est finalement dirigé à l'échelle collective afin de comprendre les mécanismes de transmission des forces dans un pack professionnel grâce à l'Atelier de la mêlée. L'objectif sportif étant d'améliorer les performances en mêlée grâce à l'identification des variables physiques traduisant la synchronisation d'un pack et son efficacité de poussée.

Title : Scrum Physics

Keywords : Scrum, Impact, Individual optimal posture, Force production, Collective efficiency

Abstract : The scrum is an essential element of a Rugby Union game. It consists of the ball being put back into play in opposition of strength between two packs of 8 forwards each. Each pack is organized in 3 rows with 3 players in the first row, 4 players behind them, and a last player in the third row. The scrum is orchestrated by the referee's calls which have changed over the history of Rugby to protect the physical integrity of the players. We can divide the scrum into two distinct phases in force production: an impact phase during which each pack accelerates and collides with the other, followed by a continuous pushing phase after the throw-in of the ball under the scrum. During the sustained push phase, the players of each pack try to synchronize to produce the greatest collective force. This thesis, financed by the professional rugby club of Racing 92, focuses on these two phases with experimental studies conducted at the individual level in order to understand the mechanisms of force production. First, using a scrum training machine equipped with force sensors called the « Atelier de la mêlée » and belonging to the French Federation of Rugby, we characterize individual players in order to construct a pusher phase space that allows us to quantify the quality of a scrum impact. Then, thanks to an individual scrum machine that we developed in the laboratory -also equipped with force sensors- we conducted experimental studies to find the individual scrummaging posture that maximizes the force produced by a player. We have also led a study that looks at the influence of the size of the cleats under the shoes on the force produced by a player on synthetic turf. The thesis work finally aims at the collective scale to understand the mechanisms of force transmission in a professional pack thanks to the « Atelier de la mêlée ». The performance objective is to improve the performance in scrums through the identification of physical variables translating the synchronization of a pack and its efficiency of pushing.

Institut Polytechnique de Paris
91120 Palaiseau, France